

University of Nottingham

UK | CHINA | MALAYSIA

EFFECT OF REWINDING TWIST ON PROPERTIES OF BRAIDED COMPOSITES

BETHANY GRIMES

MENG (HONS)

Thesis submitted to the University of Nottingham
for the degree of Doctor of Engineering

March 2024

Abstract

State-of-the-art braiding simulation and processing capabilities use tow geometry approximations built on generalised assumptions. This results in discrepancies between the key process variables such as cover factor and braid thickness of the designed braid and manufactured preform. The challenge in predicting the properties of braided composites is one of the primary reasons for the limited application of braiding in composite manufacturing processes. Localised variations in braid architecture are detrimental to the final quality of the manufactured preform. This coupled with variance in key process metrics such as braid angle and cover factor between simulated and manufactured preforms leads to inaccuracies in the predicted mechanical properties. One of the ways tow widths can be influenced is by adding twist to fibre during the rewinding stage of the process.

It is accepted that the tow rewinding stage of the braiding process is critical to the resultant product quality. An additional measured level of twist can be added to fibres during the rewinding process, this is a technique used by some industry leaders to improve fibre processability. As the number of twists increases, a more compact tow structure is also produced resulting in a reduction in the degree of tow spread. This has a significant impact on the cover factor and braid thickness of a preform.

The main objective of this study to develop the understanding of the inclusion of a rewinding twist to braid architecture and the resulting impact on mechanical properties.

To address this objective a series of studies are presented, aiming to initially understand the influence of rewinding twist on the mechanical behaviour of braided composites. A higher variability in failure strength was observed with untwisted coupons in comparison to twisted coupons, which resulted in a high A-basis allowable for twisted coupons. Different stress-strain behaviour was observed. Untwisted coupons failed instantaneously with brittle failure, where twisted coupons saw an initial failure point but then continued to take on load before final failure occurred.

Braid architecture variability as a result of the inclusion of rewinding twist has been investigated through the braiding of cylindrical mandrels at different levels of rewinding twist between 0-10 twists per metre. The inclusion of 5 twists per metre was seen to reduce the tow width by 28% with the reduction in tow width resulting in an increase in tow thickness. This has been used to develop approximations for tow width and thickness as a result of rewinding twist, along with developing the understanding of the influence of rewinding twist on key process variables. Additionally, images of the braided preforms along with manufacturing observations indicate an increase in fibre damage as a result of braiding with untwisted fibres due to an increase in friction between yarns. This results in process interruptions and machine down time.

In addition to this, mandrel complexity has been investigated with the inclusion of converging and diverging frusto-conical sections to the mandrel. Observations demonstrate a significant impact in braid architecture variability and stability as a result of the introduction of a cross-sectional change. Braiding on diverging conical sections demonstrate the largest deviation in braid angle from predicted braid angle due to the effective reduction in stabilisation length. Whereas minimal angle deviation was noted when braiding on converging conical cross-sections. This angle deviation appeared to be independent of the level of rewinding twist on fibres. However, the addition of rewinding twist to fibres did reduce tow spread when braiding on a geometry of changing cross-section in either converging or diverging orientation.

These studies have enabled the investigation of the scale of the braiding machine using a 48-carrier and 192-carrier braider. Investigations into braid architecture including tow width and braid angle for both braiders on both circular and conical mandrels have showed minimal differences between the braiders. This is significant as it enables results from small scale trials and pre-production models to be used to approximate full-sized components. This reduces the requirements for expensive manufacturing trials and large-scale set-ups.

Acknowledgements

The completion of this EngD has been a journey shaped by the most extraordinary circumstances; multiple changes to industrial supervision, a global pandemic, and a medical emergency to name a few. As always there are far too many people to thank.

Firstly, I have to thank my academic supervisor, Professor Nick Warrior, at the University of Nottingham along with the wider EPSRC Future of Composite Manufacturing Research Hub. Your wealth of knowledge and insight has been invaluable, and your support and advice has empowered me to complete this thesis. The same goes for my industrial supervisor Pete Giddings who has become a mentor alongside supporting my work through thought-provoking discussion and advice. I would like to express my gratitude to the Industrial Doctorate Centre in Composites Manufacturing, in particular Ivana Partridge and Janice Barton. The IDC has provided an exciting and interesting environment for me to develop as engineer but also offered the opportunity for unique life experiences which has shaped me as person and professional.

I would also like to thank the National Composites Centre for funding my research and providing the opportunity to contribute to industrial challenges in a way I couldn't have imagined. Thank you to the many colleagues that have supported me throughout my work over the years, in particular; Matt Scott, Ruth Courtney and Pete Whitton who have been there from the start! To my 3D Textiles/ Complex Deposition team colleagues I can only say thank you. I could not have finished this without your constant support and ability to listen to my incessant braiding chat. To all my fellow EngD and PhD students that I have had the pleasure of sharing this journey with, your camaraderie has got me to this point. Special thanks to Matthew Thompson for sharing my enthusiasm in the world of braiding!

Last but not least, thank you to my family. I could not have made it to the end of this EngD without them. I cannot thank my parents enough for their constant encouragement and for never doubting me even when I doubted myself. A special mention to my grandparents whose unwavering support has been constant throughout my academic career. We sadly lost my grandma just after I submitted my thesis- she always used to say that I got my brains from her- so this one is for you Grandma!

And thank you to you for taking the time to read this thesis- I hope you enjoy reading the culmination of the 5-year journey that was my EngD!

Publications

Journals

B.Grimes, P.Giddings and N.Warrior " The influence of guide ring size on braid architecture", Journal of Plastics, Rubber and Composites, Pages 418-422, September 2022

Conferences

B.Grimes, M.Thompson, P.Giddings and N.Warrior, "The Influence of Twist on the Mechanical Properties of Braided Composites", presented at the ICCM23-The 23rd International Conference on Composite Materials, Belfast, 2023

B.Grimes, M, Thompson, P.Giddings, and N.Warrior, "Braiding Characterisation and Optimisation: Complex Geometries," presented at the ECCM20- The 20th European Conference on Composite Materials, Lausanne, 2022

M.Thompson, B.Grimes K.Rengaraj and N. Warrior, "Effect of Winding Twist on Multilayer Braided Composites", presented at the ACM5 2022, Bristol, UK, April 2022

B.Grimes, P.Giddings, and N.Warrior, " A computational and experimental analysis of the influence of guide ring size on fibre architecture in the braiding process," presented at the International Conference on Manufacturing of Advanced Composites, Online, 2021

B. Grimes, M. Thompson, T. Buns, F. Martin, N. Warrior, The Effect of Twist on Braid Architecture and Stability, SAMPE Europe 2021

T. Buns, M. Scott, B. Grimes and P. Giddings, "Large Braided Hydrofoil Development Approach," in *SAMPE Europe*, Nantes, 2018.

Table of Contents

Abstract i

Acknowledgements iii

Publications iv

Journals iv

Conferences iv

Table of Contents v

Equation List: ix

Table of Figures: x

Summary of Tables: xv

Nomenclature xvii

1 Introduction 1

1.1 History of Braiding 1

1.2 Research Environment 2

1.3 Thesis Outline and Project Aims 2

2 Introduction to the Braiding Process 4

2.1 The Braiding Process 4

2.1.1 Mechanical Braiding Process 4

2.1.2 Braid Architecture 11

2.1.3 Braiding Machine Type 12

2.1.4 Fundamentals of the Rewinding Process 15

2.2 Commercial Braided Components 28

2.3 Challenges in Braiding 30

3 Review of Literature related to Manufacturing Braided Composites 32

3.1 Key Process Variables for Braiding 32

3.1.1 Braid Angle 32

3.1.2 Cover Factor 33

3.1.3 Braid Thickness 35

3.2 Manufacturing of Braided Composites 38

3.2.1 Braiding of Complex Geometries 38

3.2.2 Guide Ring Studies 44

3.2.3 Process-induced fibre damage within braiding 48

3.2.4 Testing of Fibre Damage 51

3.2.5 Infusion of Braided Preforms 53

3.2.6 Characterisation of Mechanical Properties 56

3.2.7 Using Simulation to Determine Mechanical Properties 66
3.3 Process Simulation of the Overbraiding Process 68
3.3.1 Types of Computational Model 69
3.3.2 Tow Geometry Modelling 74
3.3.3 Yarn Modelling Assumptions 76
3.4 Conclusions and Research Needs 78
4 Methodology 81
4.1 Experimental Methodologies 81
4.1.1 Braiding 81
4.1.2 Mechanics of the Rewinding Process 96
4.1.3 Metrology 103
4.1.4 Composites Manufacturing 113
4.1.5 Mechanical Testing 121
4.2 Statistical Methodologies 124
4.2.1 Testing the Statistical Significance 124
4.2.2 A-Basis Design Allowable 125
4.3 Discussion 126
4.4 Conclusion 127
5 Effect of Rewinding Twist on Mechanical Properties of a Braided Composite 128
5.1 Background and Aim 128
5.2 Impact of Twisting on Fibre Processability 128
5.2.1 In-Process Fibre Damage 128
5.2.2 Indication of Fibre Damage 130
5.3 Tensile Properties of Braided Composites 134
5.3.1 Failure Type Analysis 134
5.3.2 Stress-Strain Data 138
5.3.3 Ultimate Tensile Strength (UTS) 142
5.3.4 Failure Strength 145
5.3.5 Tensile Modulus 146
5.3.6 Tensile Strain at Failure 147
5.3.7 Poisson's Ratio 148
5.4 Discussion 149
5.5 Conclusions 150
6 Effect of Rewinding Twist on Braided Fibre Architecture of Cylindrical Preforms 151
6.1 Background and Aim 151

6.2 Braid Architecture Variability Induced by Process Parameters 151
6.2.1 Machine Speeds 151
6.2.2 Application of Guide Ring 155
6.3 Braid Architecture Variability as a Result of Twisting 160
6.3.1 Influence of Twisting on Tow Width 161
6.3.2 Influence of Twisting on Tow Geometry 162
6.3.3 Validation of Assumptions with Different Material 168
6.3.4 Influence of Twist on the Variability of Key Process Variables 170
6.3.5 Single Layer Preform Summary 173
6.4 Braid Architecture Variability of a Multilayer Preform 173
6.4.1 Tow Width Variability of a Multilayer Preform 174
6.4.2 Maximum Layer Thickness Variability of a Multilayer Preform 175
6.4.3 Braid Angle Variability of a Multilayer Preform 176
6.4.4 Multilayer Preforms Summary 177
6.5 Braid Architecture Variability Induced by Machine Size 177
6.5.1 Experimental Methodology 178
6.5.2 Preform Stabilisation 178
6.5.3 Influence of machine size on tow width variability 180
6.5.4 Machine Size Summary 180
6.6 Triaxial Braid Architecture 180
6.6.1 Braid Architecture of Single Layer Triaxial Preforms 181
6.6.2 Summary of Conclusions for a Triaxial Preform 185
6.7 Conclusions 186
7 Effect of Rewinding Twist on Axisymmetric Non-Prismatic Geometries 189
7.1 Background and Aim 189
7.2 Effects of Part Gradient on Braid Architecture Variability 189
7.2.1 Effect of part gradient on braid angle in single layer preforms 190
7.2.2 Effect of part gradient on tow width in single layer preforms 194
7.2.3 Effect of Part Gradient on the layer thickness in a single layer preform 195
7.3 Influence of Twist on Braid Architecture Variability for Complex Preforms of different part gradients. 199
7.3.1 Influence of Rewinding Twist on the Braid Angle of Components With Different Part Gradients 199
7.3.2 Influence of rewinding twist on the tow width of components with different part gradients 202
7.3.3 Influence of rewinding twist on the layer thickness of components with different part gradients 203

7.4 Summary of the Effect of Part Gradient on Braid Architecture 206
7.5 Influence of Twist on Braid Architecture Variability for Complex Preforms for Different Part Acales 207
7.5.1 Effect of Converging and Diverging Frusto-Conical Sections on Braid Architecture for a Large Scale Preform 207
7.5.2 Comparison of the Braid Architecture for Scaled Preforms Using Small and Large Machinery 210
7.5.3 Process Simulation of Frusto-Conical Structure 212
7.5.4 Summary for large conical preforms 215
7.6 Increasingly Complex Preforms- the 'Oscar' geometry 216
7.6.1 Influence of geometrical complexity of the 'Oscar' on braid angle 216
7.6.2 Influence of geometrical complexity of the 'Oscar' on tow width 217
7.6.3 Summary of the braiding of increasingly complex geometries such as the 'Oscar' 219
7.7 Conclusions 220
8 Conclusions 223
8.1 Final Remarks 223
8.2 Contributions to wider research community 224
8.2.1 Conclusions of the Influence of twist of mechanical properties of braided composites 225
8.2.2 Conclusions on the manufacture of cylindrical braided preforms. 227
8.2.3 Conclusions on the manufacture of axisymmetric non-prismatic geometries 228
8.3 Further Work 230
Appendix A: 232
Bibliography 239

Equation List:

Equation 3.1 Braid Angle 32
Equation 3.2 ISO10122 Braid Angle Calculation Method 33
Equation 3.3 Cover Factor 33
Equation 3.4 Fibre Volume Fraction Equation 34
Equation 3.5 Kyosev approximation for triaxial cover factor assuming central alignment of the axial yarn 35
Equation 3.6 Calculation of Tow Cross Sectional Area for Lenticular Assumption 75
Equation 4.1 Relationship between rpm and PPM 85
Equation 4.2 Volume Fraction 116
Equation 4.3 A-basis allowable [94] 126

Table of Figures:

Figure 2.1 Schematic of the Braiding Process with an Axial Braiding Machine based on [1] 5
Figure 2.2 Serpentine Carrier Path 6
Figure 2.3 Horn Gear 7
Figure 2.4 Schematic of carrier transfer between adjacent horn gears with four slots 7
Figure 2.5 (a) Horn Gear and Yarn Carrier Arrangement, (b) track plate for circular braiding 8
Figure 2.6 Yarn Path through a braid carrier 9
Figure 2.7 Guide Ring in Manufacture at NCC 10
Figure 2.8 Formation of braided preforms using the 48-carrier Steeger braider 10
Figure 2.9 Undulation pattern of different braid patterns 11
Figure 2.10 Biaxial and Triaxial Schematic 12
Figure 2.11 Steeger Axial Braider at the University of Nottingham 13
Figure 2.12 Radial Braider with a robot-arm take-up mechanism 13
Figure 2.13 Distance between braid point and carrier for radial and axial braiders 14
Figure 2.14 NCC Braider Schematic 15
Figure 2.15 Basic Zones of the winding process for braiding [2] 16
Figure 2.16 Start of a bobbin being wound demonstrating tow pitch 18
Figure 2.17 A bobbin wound with a too great an amplitude 19
Figure 2.18 Bobbin wound with correct amplitude 19
Figure 2.19 Check for Knots during Rewinding 20
Figure 2.20 Braid with Inconsistent Tension 21
Figure 2.21 CEZOMA CE-1187 Rewinding Machine 22
Figure 2.22 Yarn Twist Types [15] 22
Figure 2.23 Effect of twisting on the diameter of Glass Fibre/Polypropylene commingled yarn [17] 24
Figure 2.24 Twist Cabinet supplied by Eurocarbon [26] 26
Figure 2.25 Method of adding twist to fibres during rewinding 27
Figure 2.26 Airbus Prototype Production Line 29
Figure 2.27 Large rocket nozzle preform produced by A&P's line of Megabraiders [30] .. 29
Figure 2.28 Porsche Carbon Fibre Wheel 30
Figure 3.1 Image of Braid Angle Measurement [3] 32
Figure 3.2 Unit Cell and Tow Geometry [3] 34
Figure 3.3 Triaxial unit cell with a centrally aligned yarn (left) and shifted axial yarn (middle and right) [34] 35
Figure 3.4 Effect of preform surface on laser line signal intensity 1) Direct reflection and maximum intensity, 2) no reflect- no interaction with preform, 3) reduced intensity due to scattering [36] 37
Figure 3.5 Test Mandrel (1) 39
Figure 3.6 Test Mandrel (2) [6] 39
Figure 3.7 Detailed Dimensioned complex mandrel. [43] 41
Figure 3.8 Take-up speed profile as output and coarsened for machine input. [43] 42

Figure 3.9 Experimental and Modelled Braid Angle Values: X for warp & O for weft for Modelled (mod) and Experimental (exp) 43
Figure 3.10 Realistic Yarn Path on a Rectangular Mandrel with Circular Guide Ring 44
Figure 3.11 Braiding angle for rectangular mandrel in parallel orientation 45
Figure 3.12 Braiding angle for rectangular mandrel in normal orientation 46
Figure 3.13 Mandrel Progression in the Capability Development Program 47
Figure 3.14 Manufacturing Set-Up for Eccentric Braiding 47
Figure 3.15 Measured Braid Angle for Eccentric Braiding 48
Figure 3.16 Braid Production using different spring stiffness (a) braid appearance, (b) carbon tows in braid cone [24]. 50
Figure 3.17 Gravimetric Test Results [47] 52
Figure 3.18 Permeability as a function of the braid angle for different volume fractions [51] 54
Figure 3.19 Mandrel geometries used (a) Constant square cross-section (b) Varying square cross-section. 55
Figure 3.20 Micrograph of the Cross-Section of Triaxial Composite 56
Figure 3.21 Full field strain data showing edge initiation. 57
Figure 3.22 Examples of problems testing straight sided coupons 58
Figure 3.23 Final failure images for axial, fibre and transverse directions using a high speed camera 59
Figure 3.24 A&P Test Modification for Longitudinal Tensile Testing [61] 62
Figure 3.25 A&P Coupon modification for compression testing [61] 63
Figure 3.26 A&P Coupon modification for longitudinal and transverse in-plane shear [61] 64
Figure 3.27 Diagonal Brick Model Representation 67
Figure 3.28 Comparison between experimental, Diagonal Brick (Analytical) and FE Model for Longitudinal and Transverse Moduli 68
Figure 3.29 Computational time of various modelling approaches 69
Figure 3.30 Comparison between two methods of using an analytical model to predict mechanical properties for tubular structures 70
Figure 3.31 Experimental validation of inverse kinematic model [73] 71
Figure 3.32 Details and dimension of the braiding mandrel used in work by Pickett 72
Figure 3.33 Comparison between analytical and FE models for predicting yarn path 73
Figure 3.34 Example tow geometry shape 74
Figure 3.35 Biaxial braided fabric modelled in TexGen using repeats defined by the unit cell 76
Figure 3.36 Mandrel Shapes (a and b) the conical mandrel 77
Figure 4.1 48-carrier Steeger 140/48 HS axial braider and Kuka KR30-60 robotic arm at the UoN 82
Figure 4.2 192/288-carrier Eurocarbon braider Set-Up at NCC [84] 83
Figure 4.3 Loading of axial yarns 84
Figure 4.4 Reverse guide ring overbraided due to too little vibration 85
Figure 4.5 Direction of the braid carriers (a) blue clockwise carriers (b) yellow anti-clockwise carriers 87
Figure 4.6 Machine chucks to secure the mandrel 88
Figure 4.7 Schematic of 5.4° gradient frusto-conical mandrel 89
Figure 4.8 Schematic of 10.6° gradient frusto-conical mandrel 90
Figure 4.9 Conical Mandrel for Braiding Trials at NCC 92

Figure 4.10 MDF mandrel loaded at NCC 93
Figure 4.11 Oscar Mandrel Geometry 94
Figure 4.12 Tow Path through a CE-1187 winding machine 96
Figure 4.13 Large Bobbin Mounted in the Twist Cabinet 97
Figure 4.14 Direction of orientation of bobbin loaded in the twist cabinet and resulting twist 98
Figure 4.15 Tow path through fibre tensioner 99
Figure 4.16 Tow Path over measuring roller through final guiding elements 100
Figure 4.17 Mechanism for altering pitch and amplitude 101
Figure 4.18 'S' and 'Z' Twist 102
Figure 4.19 Braid angle measurement and frequency domain 104
Figure 4.20 Steps of the Image Processing of the In-Process Monitoring System at the NCC 107
Figure 4.21 Mean Pixel Intensity 108
Figure 4.22 Difference in ImageJ and IPM measurements 109
Figure 4.23 Typical Image Output from the AVS 111
Figure 4.24 Braid angle on and off mandrel for (a) 0 Tpm preforms (b) 7 Tpm preforms 114
Figure 4.25 Preform bagged for infusion set-up 115
Figure 4.26 Multiple preform infusion set-up 115
Figure 4.27 Progression of infusion of untwisted and twisted preforms 118
Figure 4.28 %Fill of each preform throughout infusion 119
Figure 4.29 Braid angle comparison off mandrel and post-infusion 120
Figure 4.30 Measured Tow Width at Each Stage of the Manufacturing Process for 0 Tpm and 7 Tpm Panels 121
Figure 4.31 Shimadzu AG-X+ Tensile Test Machine 123
Figure 4.32 Test Set-Up 123
Figure 5.1 Visible difference in fibre damage when winding with twist 129
Figure 5.2 In-process fibre damage during manufacturing with untwisted fibres 129
Figure 5.3 Gravimetric fibre damage test results 132
Figure 5.4 Damage progression through manufacturing process 133
Figure 5.5 Untwisted coupon failure images sorted by failure type. 136
Figure 5.6 Twisted coupon failure images sorted by failure type 137
Figure 5.7 Pre and Post Test for Untwisted Coupons 137
Figure 5.8 Pre and Post Test for Twisted Coupons 138
Figure 5.9 Lateral Failure Type Stress-Strain Graphs 139
Figure 5.10 Angled Failure Mode Stress-Strain Graphs 139
Figure 5.11 Mean Stress-Strain Trend 141
Figure 5.12 Goodness of Fit Test (a) Untwisted, (b) Twisted 143
Figure 5.13 Range of UTS Data for Untwisted and Twisted Coupons 144
Figure 5.14 Average Tensile Modulus 146
Figure 5.15 Tensile Modulus Range data for Untwisted and Twisted Coupons 147
Figure 5.16 Tensile Strain at Failure 148
Figure 6.1 Braid Angle Deviation CS1-CS3 153
Figure 6.2 Braid Angle Deviation TS1-TS3 153
Figure 6.3 Average Tow Width CS1-CS3 154
Figure 6.4 Average Tow Width TS1-TS3 155
Figure 6.5 Stabilisation Length for Different Sized Guide Rings 157
Figure 6.6 Measured braid angles for different sizes of guide ring 158

Figure 6.7 Measured tow width for different guide ring size 159
Figure 6.8 Measured cover factor for preforms manufactured with different guide ring sizes 160
Figure 6.9 Measured Tow Width for Different Levels of Twist 162
Figure 6.10 Microscopy images of preforms with different levels of twist 163
Figure 6.11 Individual Tow Intersections for Different Levels of Twist 163
Figure 6.12 Maximum layer thickness of braided preforms with different levels of rewinding twist 164
Figure 6.13 Tukey Pairwise Comparison for Maximum Layer Thickness 165
Figure 6.14 Tukey Pairwise Comparison for Tow Widths 166
Figure 6.15 Relationship between tow width and corresponding tow thickness 167
Figure 6.16 Tow Width for different levels of rewinding twist 169
Figure 6.17 Tukey Pairwise Comparisons for Different levels of Twist 170
Figure 6.18 Interval plot for deviation from predicted braid angle 171
Figure 6.19 Relationship between cover factor and number of twists 173
Figure 6.20 Braid Angle Variability for 0 Tpm Multilayer Preform 176
Figure 6.21 Braid Angle Variability for 5 Tpm Multilayer Preform 177
Figure 6.22 Stabilisation Length for Small and Large Mandrels for 0 Tpm Preforms 178
Figure 6.23 Stabilisation Length for Small and Large Mandrels for 5 Tpm Preforms 179
Figure 6.24 Bias Tow Width for Biaxial and Triaxial Braid for 7 Tpm Fibres 181
Figure 6.25 Measured tow width between axial tows and biaxial tows with untwisted fibres 182
Figure 6.26 Statistical Test Analysis for Axial and Untwisted Fibres 182
Figure 6.27 Measured Axial Tow Width Along the Part Length 183
Figure 6.28 Images of Triaxial Braided Preforms and Calculated Cover Factor Using ImageJ 184
Figure 6.29 Triaxial Braided Preform 185
Figure 7.1 Deviation in predicted braid angle for different part gradients in both converging and diverging section orientations for 0 Tpm preforms in comparison to a cylindrical geometry. 191
Figure 7.2 Description of Proportion of Axial Length for Converging and Diverging Conical Sections 192
Figure 7.3 Deviation in predicted braid angle along the axial length of preforms of different part gradients manufactured in a diverging and converging orientation for 0 Tpm fibres. 193
Figure 7.4 Comparison of measured tow width for cylindrical, diverging and converging mandrels 195
Figure 7.5 Preform thickness along the preform length for diverging preforms of different part gradients manufactured with 0 Tpm Fibres 196
Figure 7.6 Preform thickness along preform length for converging preforms of different part gradients manufactured with 0 Tpm Fibres 198
Figure 7.7 Deviation from predicted braid angle due to different part gradients for components in both converging and diverging orientations with twisted fibres 200
Figure 7.8 Deviation from predicted braid angle along the preform length for both diverging and converging mandrel orientations, of different part gradients braided with twisted fibres. 201
Figure 7.9 Measured tow width for converging and diverging preforms of different part gradientst when braided with twisted fibres 202
Figure 7.10 Preform thickness along the length for diverging cross-sections of different part gradients with twisted fibres 204

Figure 7.11 Preform thickness along the length for converging cross-sections of different part gradients with twisted fibres 205
Figure 7.12 Recorded braid angle deviation along the axial length of preform for cylindrical, diverging and converging 208
Figure 7.13 Measured tow width for cylindrical, converging and diverging preforms with different levels of twist 209
Figure 7.14 Comparison of braid angle deviation for conical sections on 48-carrier and 192-carrier braiders 210
Figure 7.15 Comparison of tow width measurements for 48-carrier and 192-carrier braiders, with both conical and straight sections 211
Figure 7.16 CBX Braid Angle Simulation in Diverging Orientation 213
Figure 7.17 CBX Braid Angle Simulation in Converging Orientation 214
Figure 7.18 Comparison of the braid angle deviation for simulation and manufacturing. 214
Figure 7.19 Magnitude of Braid Angle Deviation for Different Sections of the Oscar..... 217
Figure 7.20 Measured tow width comparison to stabilised 7 Tpm braid 219
Figure 0.1 Twisted Sample Data..... 232
Figure 0.2 Untwisted samples 234
Figure 0.3 Method of Modulus Calculation 236

Summary of Tables:

Table 2.1 List of Commercially Available Rewinding Machines 25
Table 2.2 Recommended Twists per Metre [26] 26
Table 3.1 Visual Damage Inspection Scale 51
Table 3.2 Summary of test methods for braided coupons 60
Table 3.3 Longitudinal Elastic Modulus Data for Tubular Specimens 65
Table 3.4 Shear Modulus Data for Tubular Specimens 66
Table 3.5 Material architectures 67
Table 4.1 Braider speeds calculated from the voltage defined by the Kuka control unit. ... 86
Table 4.2 Test ID for Small Conical Preform Manufacture 91
Table 4.3 Test on conical section on 192-carrier braider 92
Table 4.4 Section Gradient of the 'Oscar' Mandrel 95
Table 4.5 Braid angle deviation comparison for AVS and ImageJ 112
Table 4.6 Thickness Measurement Method Summary 113
Table 4.7 Preform parameters 113
Table 4.8 Ply Thickness 116
Table 4.9 Ply GSM 116
Table 4.10 Volume fraction for composite panels 117
Table 4.11 Machine Parameters for Preform Manufacture 122
Table 4.12 Average coupon dimensions 124
Table 5.1 Fibre damage material test categories 130
Table 5.2 Average visible fibre damage ranking 131
Table 5.3 Tukey pairwise comparison for gravimetric tests 133
Table 5.4 Mechanical Property Summary for Untwisted and Twisted Coupons 134
Table 5.5 Failure Type Key 135
Table 5.6 Failure Type Summary for Untwisted and Twisted Coupons 135
Table 5.7 Calculated Strain Energy 142
Table 5.8 UTS Summary 142
Table 5.9 UTS Summary including A-basis allowable 145
Table 5.10 Failure Strength, A-basis allowable summary 145
Table 5.11 Poisson's Ratio Panel Summary 148
Table 6.1 Effect of braid carrier speed test parameters 152
Table 6.2 Effect of take-up speed test parameters 152
Table 6.3 Rewinding Parameters 161
Table 6.4 Braiding Process Parameters 161
Table 6.5 Maximum layer thickness for different rewinding twist levels 165
Table 6.6 Average Tow Geometry Measurements for different levels of twist 166
Table 6.7 Calculated tow cross-section area based from different approximations 168
Table 6.8 Corresponding Process Parameters for UoN and NCC Braiders 168
Table 6.9 Measured tow width for different 12K fibres 169
Table 6.10 Calculated cover factor for different tow widths 172
Table 6.11 Average Tow Width for Multilayer Preforms 174
Table 6.12 Average Layer Thickness Summary for Multilayer Preforms 175
Table 6.13 Measured Tow Width for both mandrel diameters. 180
Table 7.1 Summary of the Tests Conducted on the Small Cone at UoN 190
Table 7.2 Summary of tests on large conical mandrel 207

Table 7.3 Measured Braid Angle on the Oscar Mandrel 216
Table 7.4 Measured Tow Width on the Oscar Mandrel 218
Table 0.1 Data Summary for Twisted Coupons 233
Table 0.2 Summary of the data for the untwisted coupons 235
Table 0.3 Summary of tensile modulus from test standard and graphical analysis 236

Nomenclature

IDC	Industrial Doctorate Centre
UoN	University of Nottingham
NCC	National Composites Centre
AVS	Apodius Vision System
IPM	In-Process Monitoring
TPM	Twists per metre
RTM	Resin transfer moudling
R	Mandrel radius
D	Mandrel diameter
v	Take-up speed
ω	Carrier rotational speed
θ	Braid angle
W_y	Biaxial Tow Width
W_{inlay}	Axial tow width
N_c	Number of braid carriers
θ_{jammed}	Braid jam angle
γ	Half cone angle
L_t	Length of the braid preform on the mandrel
L_v	Length of the braided tow once it has been removed from mandrel
a	Tow thickness
L_s	Length of braid yarn in unit cell
Vf	Volume fraction

1 Introduction

1.1 History of Braiding

Braiding is one of the most versatile manufacturing technologies for producing fibre reinforced composite geometries with structural applications including I-beams, vehicle chassis components and box spars in aerospace [1]. Braided composites are distinguishable by their interwoven structure and characterised by the interlacement of their component yarns. Braided preforms consist of three or more yarns interlaced diagonally about an axis. This can be used to over-braid a 3D core or mandrel; or produce a self-supporting tube which can be subsequently formed into a shape. Modern braiding is a versatile automated process that is applicable to the production of net-shaped continuous fibre composite components. The high material deposition rate of the process accompanied by the low material wastage make this technique particularly attractive for a variety of industrial sectors due to its lay-up speed and cost efficiency [2].

Braiding is potentially the earliest form of textile manufacturing process, with examples of braided ropes dating back 28,000 years [3]. The first mechanical braider was patented in 1748 in Manchester in the UK and 1767 saw the development of the first iron-built machine [4]. Traditionally braiders were used to produce textile cords, electrical cables, and ropes. McDonnell Douglas in the 1960's first explored using braids for aerospace engine fan casing.

Braided composites possess high specific stiffness and strength and can be manufactured into complex geometries. As a result, applications of braided composites have expanded across multiple sectors including aerospace, automotive, construction, energy, subsea and other industries. The increase in size of applications have led to the development of larger machines such as the Megabraiders at A&P Technologies [5].

1.2 Research Environment

The content of this work was written under the Engineering Doctorate Programme (Industrial Doctorate Centre (IDC) in Composites Manufacture) at the University of Nottingham (UoN) sponsored by the Engineering and Physical Sciences Research Council through the EPSRC Centre for Doctoral Training in Composites Manufacture [EP/L015102/1].

The project as part of the EngD programme funded by the National Composites Centre (NCC) in Bristol and the UoN is uniquely placed to combine the novel aspects of academic research with pull from industry and technology application. The UoN has a world-renowned composites manufacturing laboratory with a wide range of composites manufacturing technologies and experience in overbraiding. The NCC is part of the High Value Manufacturing Catapult network which is focused on fostering national research and development. It acts as an intermediary between academia and industry to develop manufacturing processes tailored to the pull of industry. The combination of research facilities enables conceptual ideas to be developed and applied at an industrial scale.

1.3 Thesis Outline and Project Aims

In the current manufacturing environment, there is a variation in whether an additional rewinding twist is added to the braiding tow during rewinding. This has been shown to result in changes in tow geometry and resultant braid architecture. This work investigates the influence of rewinding process parameters such as the number of additional twists added to the tows during rewinding prior to the braiding process on braid architecture.

The following objectives are addressed to achieve this aim:

- Characterisation of the influence of rewinding twist on the tow geometry of a braided preform.
- Understanding the influence of additional rewinding twist on the mechanical properties of a braided composite
- Characterisation of braid architecture behaviour on a geometry of non-prismatic cross-section
- Understanding of the differences in braiding on small and large machinery.

Chapter 2 introduces the braiding process and relevant terminology. Chapter 3 reviews the literature published on the braiding manufacturing process to date. Prior research primarily on the braiding and rewinding processes is reviewed. This outlines the current knowledge gaps to be addressed in the thesis.

Chapter 4 provides a detailed description of the methodologies used in conjunction with this work. A detailed description of the rewinding and braiding process is presented, and their corresponding influence on producing high quality braided preforms. Rewinding twist is highlighted as a critical parameter and discussed at a greater depth. Measurement methods used to quantify key process variables are also summarised. The manufacture of braided composite test coupons and subsequent mechanical testing of braided preforms with different levels of rewinding twist is described.

Chapters 5, 6 and 7 summarise the impact of rewinding twist on the properties of braided composites. Chapter 5 studies impact of rewinding twist on fibre processability using fibre damage test methods outlined in the literature. The work continues presenting data for the tensile testing of braided coupons manufactured with different levels of rewinding twist. Chapter 6 analyses the influence of rewinding twist on the braid architecture of geometries of constant cross-section. Different levels of rewinding twist are analysed on mandrels of different cylindrical cross-sections. The key process variables of braid angle, tow width, cover factor and braid thickness are studied. Chapter 7 develops the work in Chapter 6 to study the influence of rewinding twist on the braid architecture of parts manufactured with geometry of changing cross-section. Conical sections of different gradients are used for the initial section of this work. These are braided in both diverging and converging orientation with twisted and untwisted fibres. The braid architectures in the manufactured preforms are compared to those predicted by kinematic simulation tools.

2 Introduction to the Braiding Process

2.1 The Braiding Process

In the braiding process, bobbins are loaded onto carriers which move around the braiding machine allowing the interlacement of the braiding tows. Using a guide ring, the braiding tows are deposited onto a mandrel producing a net-shape component. These process steps are explained in the following sections. The rewinding process precedes the braiding process, rewinding material from large bobbins supplied by the manufacturer onto smaller bobbins suitable for the braiding machine.

A preform is the term used for an assembly of dry fibre layers. Braiding enables the manufacture of net-shaped preforms in a wide range of shapes and structures. The braid itself can also be used as an independent structure, which requires the preforms to be manufactured without a core and then used as an over-wrap. The versatility of near-net shape component development is something that is particularly attractive from an industrial perspective reducing multi-stage component manufacture [3]. The following section details the various elements of the braiding machine along with the various machine types.

2.1.1 Mechanical Braiding Process

2.1.1.1 Braiding Machine Configuration

A minimum of three yarns are required for braiding, however industrial braiders typically have a minimum of eight to produce tubular structures. The size of the braiding machine must be considered in relation to the intended application with the number of carriers currently ranging from 8 to 800. Figure 2.1 shows a schematic of an axial braiding machine along with relevant terminology. This depicts the overall set-up of the braiding process for a braider forming a triaxial braid. The axial fibre creel is at the rear of the braiding machine consisting of axial fibre bobbins. These axial fibres then move through nozzles of the back of the braiding machine to feed the fibres in the braid cone. The braid cone consists of axial tows and tows from the biaxial bobbins which are mounted on carriers which move around the machine. The point at which the fibres in the braid cone are deposited on the mandrel is termed the braid point. The distance between the braid point and the bobbin plane is called the convergence length.

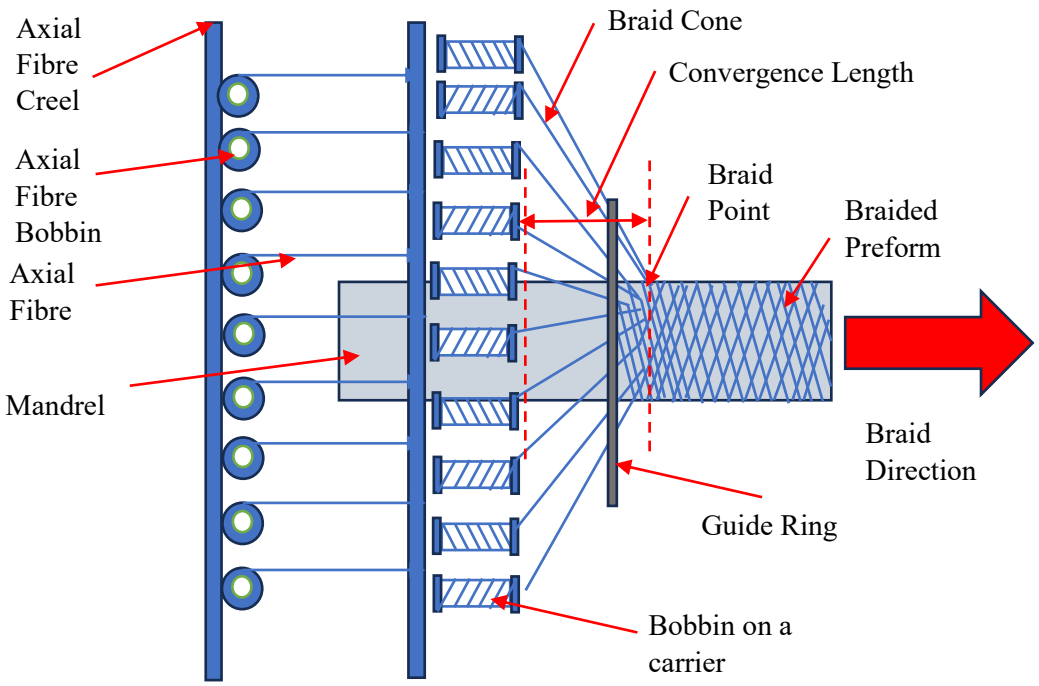


Figure 2.1 Schematic of the Braiding Process with an Axial Braiding Machine based on [1]

The braider frame consists of many braiding carriers. Each of these carriers support a braiding bobbin. As shown in Figure 2.2, one-half of these carriers move in a clockwise direction and the others an anticlockwise direction. The carriers move at an angular velocity ω and mandrel is pull at velocity v. The mandrel refers the geometry that is being overbraided, this forms the shape of the preform. The motion of the carriers around the braider track is shown in Figure 2.2 [6]. The dark arrows demonstrate the motion of an individual carrier, an arrow is used to highlight both an anticlockwise bobbin set and a clockwise bobbin set. This forms the serpentine path that is characteristic of a braiding machine [3].

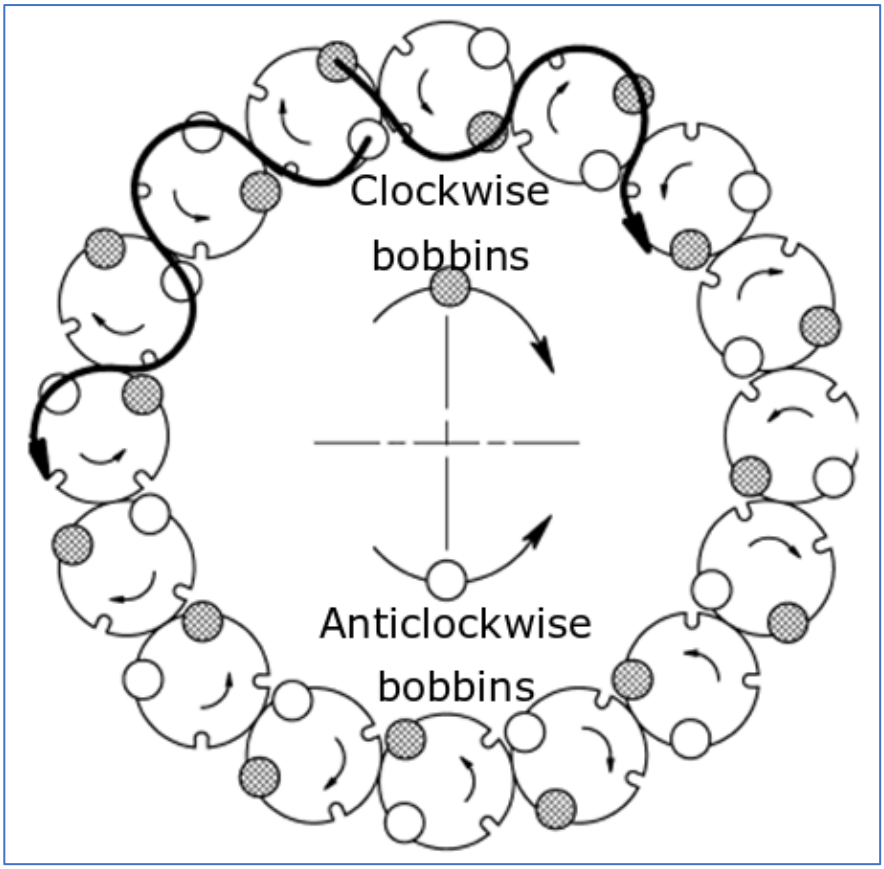


Figure 2.2 Serpentine Carrier Path

The fell point or braid point is the point at which the braiding strands deposit onto the mandrel. The distance of the fell point from the guide braiding plane is known as the convergence length. It is common practice to use a guide ring to shorten the convergence length as shown in Figure 2.1. Mandrel and machine size influence of the convergence length.

2.1.1.2 Carriers and the Carrier Track

Tow supplied by material manufacturers is rewound onto smaller bobbins with the desired rewinding parameters. These bobbins are loaded onto carriers. Carriers transport the braid bobbins along the carrier track with the aid of horn gears. A horn gear as shown in Figure 2.3 is a slotted plate used to transfer the carriers as they move around the carrier track [7]. The foot of the carrier goes into the horn gear slot. Typically, horn gears consist of four horn gear slots as shown in Figure 2.3, the number of horn gear slots dictates the size and pattern of braid that can be produced.

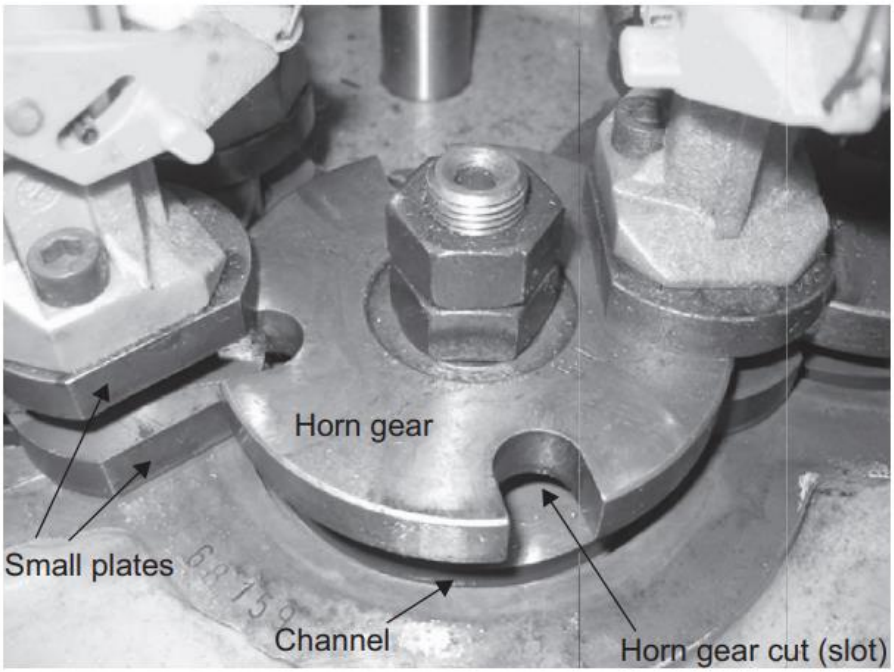


Figure 2.3 Horn Gear

The method of carrier transfer between horn gears is summarised Figure 2.4 [1]. Carriers are typically placed on alternating horn gear slots to allow for carrier transfer between horn gears without collisions. Adjacent horn gears rotate in opposite directions.

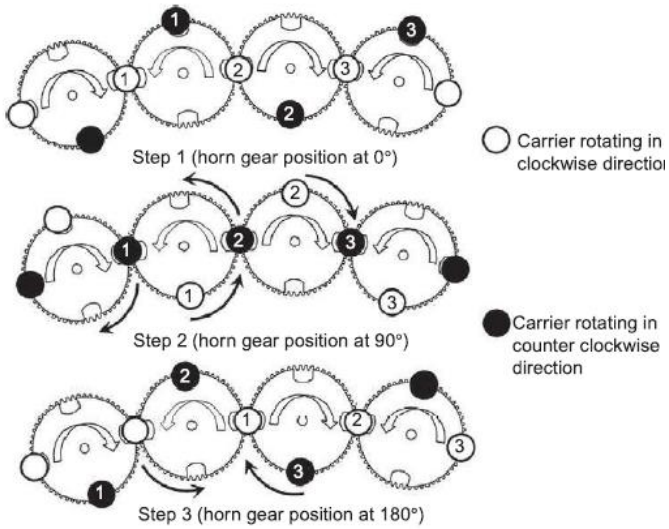


Figure 2.4 Schematic of carrier transfer between adjacent horn gears with four slots

The interaction between horn gear and yarn carrier is summarised in Figure 2.5 [8]. The carrier slots into one of the horn gear slots as shown. The arrangement of the horn gears on the base plate dictating the pattern of the braid is also shown.

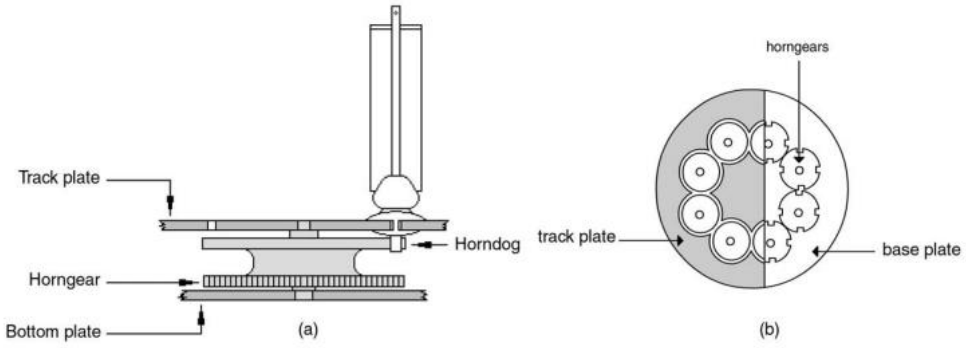


Figure 2.5 (a) Horn Gear and Yarn Carrier Arrangement, (b) track plate for circular braiding

Carriers are a critical component of a braiding machine and must meet certain requirements for the process to function effectively. Carriers must support the bobbin and rewound material. The carrier mechanism should also compensate for differences in yarn length during braiding to maintain yarn tension by controlling the release of yarn as required. This is particularly necessary with axial braiders where the length from carriers to braid point is not consistent [2].

Figure 2.6 shows the yarn path through a typical lever balanced carrier as used on the axial braider at the NCC. The lever transmits a force from the yarn tensioning spring mounted inside the carrier body. This causes the lever to rotate which tenses the connected yarn, when enough yarn is available the lever rotates back.

This compensation mechanism on carriers allows for the differences in yarn length as the distance between the carrier and braiding point vary during braiding.

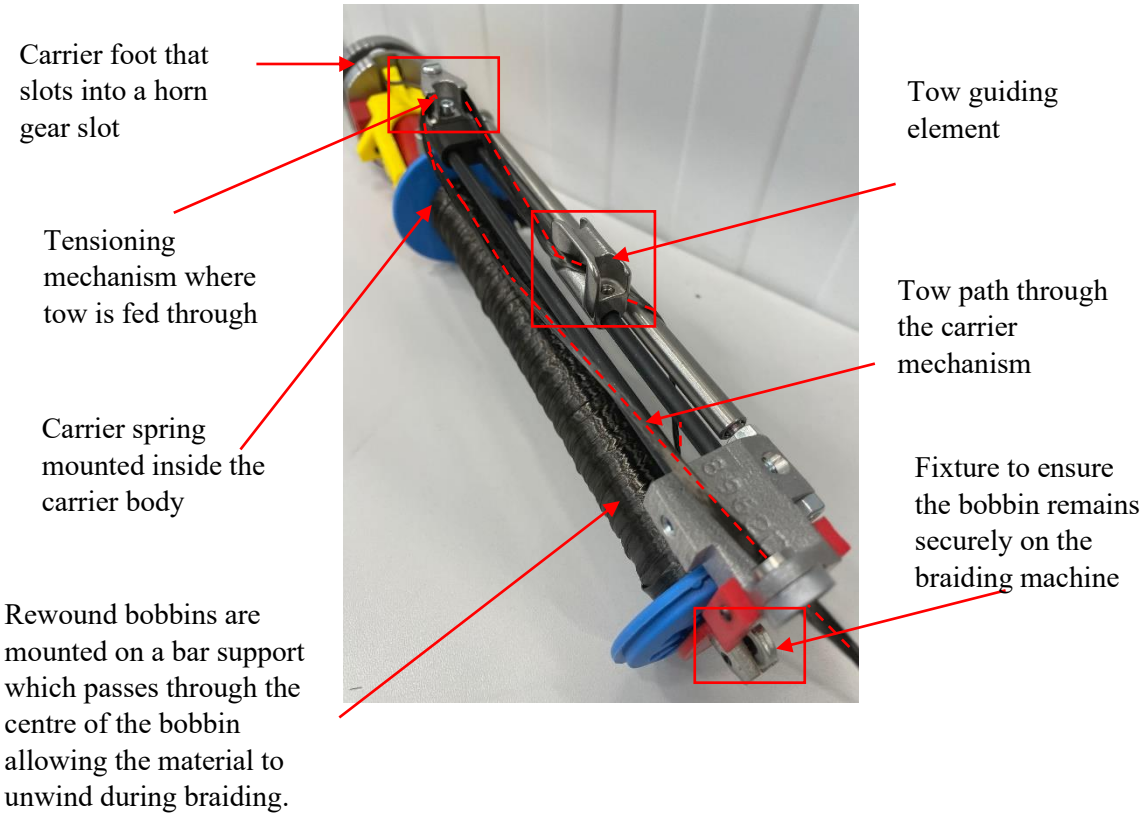


Figure 2.6 Yarn Path through a braid carrier

2.1.1.3 Guide Rings

For best braiding results a smaller guide ring should be used. Increasing the diameter of the guide ring increases the stabilisation length of the braid. Stabilisation length is defined as the distance along the preform required for the braid angle to achieve a range of ±1° from the programmed braid angle. Akkerman et al. examined the effect of the dimensions of the circular guide ring on the deposition of braiding yarns onto the mandrel and the resulting braid angle. It was determined that the guide ring dimensions and spacing significantly influence the braid architecture [9].

Guide rings shown in Figure 2.7, are used in braiding to ensure a consistent convergence point of the braiding yarns and improve the quality of the final preform [3]. As shown the braiding tows pass under the guide ring to guide the fibres to the braid point. The use of these rings allows for braiding in both the forward and reverse direction. Typically guide rings are circular with a diameter slightly larger than that of the mandrel, but there is limited data on the influence of guide ring size on the fibre architecture of a braided preform. An example of a guide ring being used to control the convergence point of the braid yarns is shown in Figure 2.7.

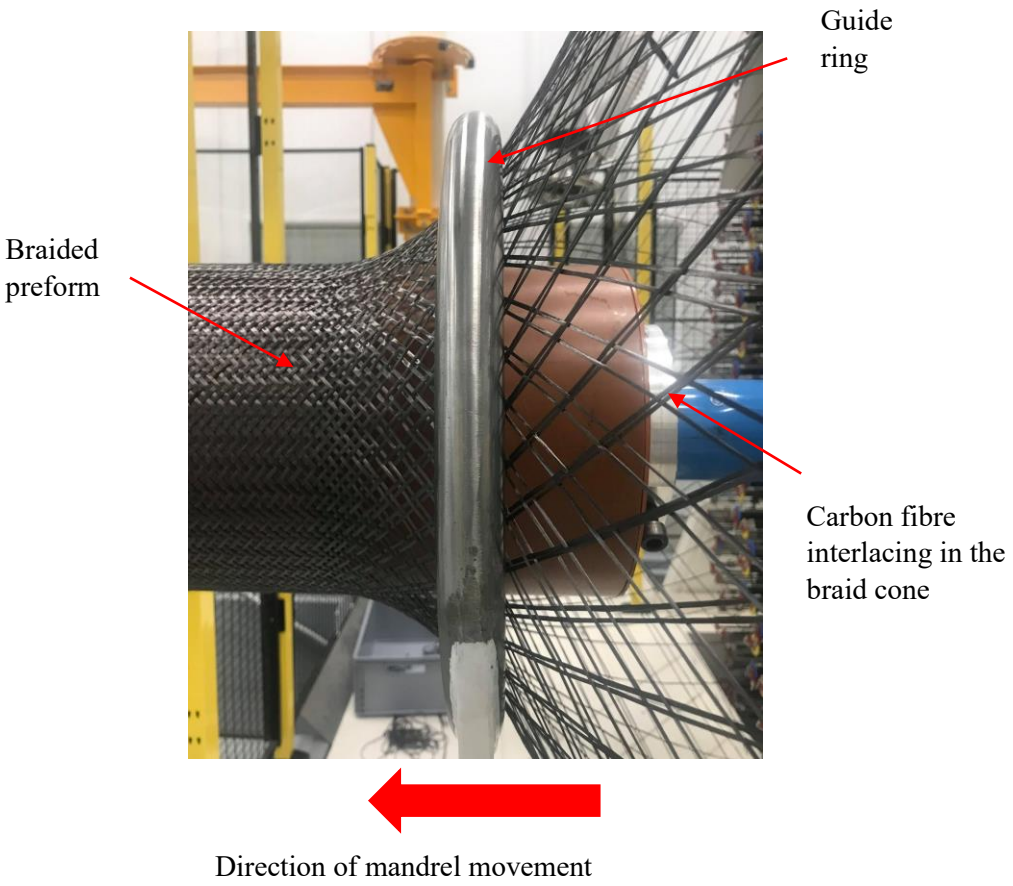


Figure 2.7 Guide Ring in Manufacture at NCC

Figure 2.8 shows the application of a guide ring in a fully loaded configuration producing a 2/2 regular braid pattern, the undulation of a braiding tow passing over two, under two yarns can be seen.

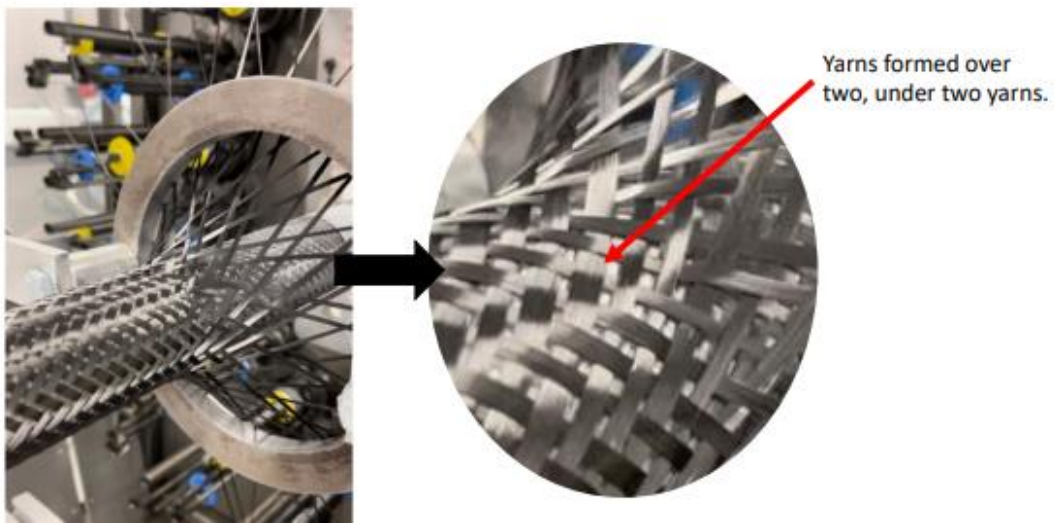


Figure 2.8 Formation of braided preforms using the 48-carrier Steeger braider

2.1.2 Braid Architecture

Braid architecture refers to factors such as the braid pattern, braid type and key process variables which are all design considerations when braiding.

2.1.2.1 Braid Pattern

The carrier track path can be designed so that the braiding machine can produce several braid patterns. Figure 2.9 shows the examples of the three main braid types. Diamond, Regular and Hercules patterns are manufactured respectively by crossing one, two or three tows over and under one, two or three tows. These are also called (1/1) for Diamond, (2/2) for Regular and (3/3) for Hercules [3]. Figure 2.9 shows the difference in undulation period for a diamond pattern compared to a regular or Hercules pattern [10]

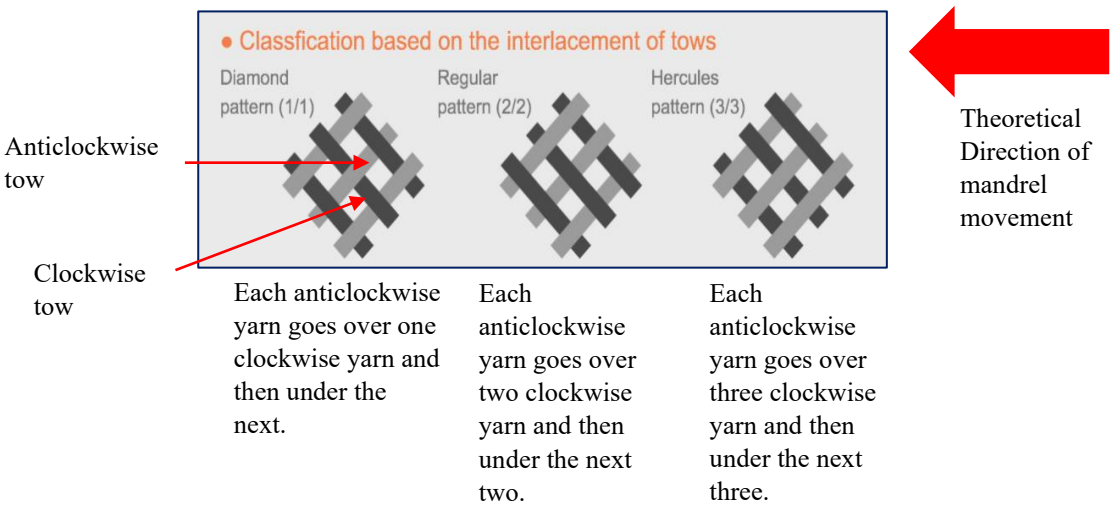


Figure 2.9 Undulation pattern of different braid patterns

Braiding machines are usually designed to produce a regular braid pattern in a fully loaded configuration. Machines can be partially loaded to configure the braid pattern.

2.1.2.2 Triaxial Braided Preforms

A typical braided preform using only braiding yarns is referred to as a biaxial braid. Some braiding machines can insert yarns along the axial direction which are interlaced with the bias yarns and form a triaxial braid. Axial yarns are often added to improve properties in the 0° direction of the component. A visual representation of a triaxial braid is shown in Figure 2.10 [10]. The axial yarn in green is seen passing through the crossing point of the intersecting biaxial yarns at a 0° angle.

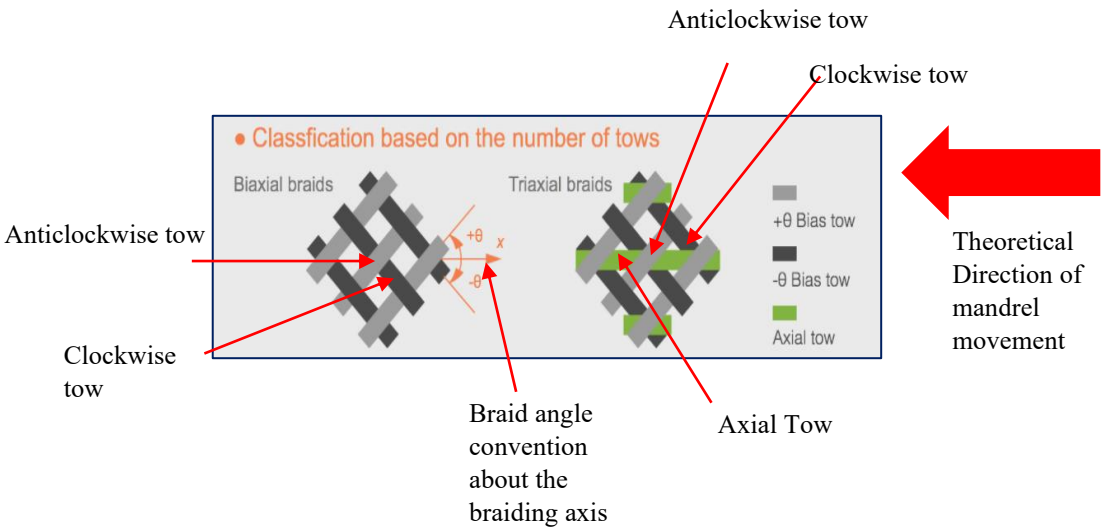


Figure 2.10 Biaxial and Triaxial Schematic

The architecture of a braided preform is highly dependent on the machine parameters.

2.1.3 Braiding Machine Type

There are two main types of braiders: radial and axial, with the difference being the carrier orientation. In an axial braider as shown in Figure 2.11, the carriers point towards the direction of fibre take-up. The distance between the carrier and the braid point is not constant. Contrastingly, the carriers on a radial braider, Figure 2.12, point towards the braid point. This minimises tension fluctuations of the braid yarn as it only passes through the carrier mechanism once instead of twice as with the axial braider. This reduces yarn damage [11]. These braiders enable the production of biaxial braid structures in several different architectures.

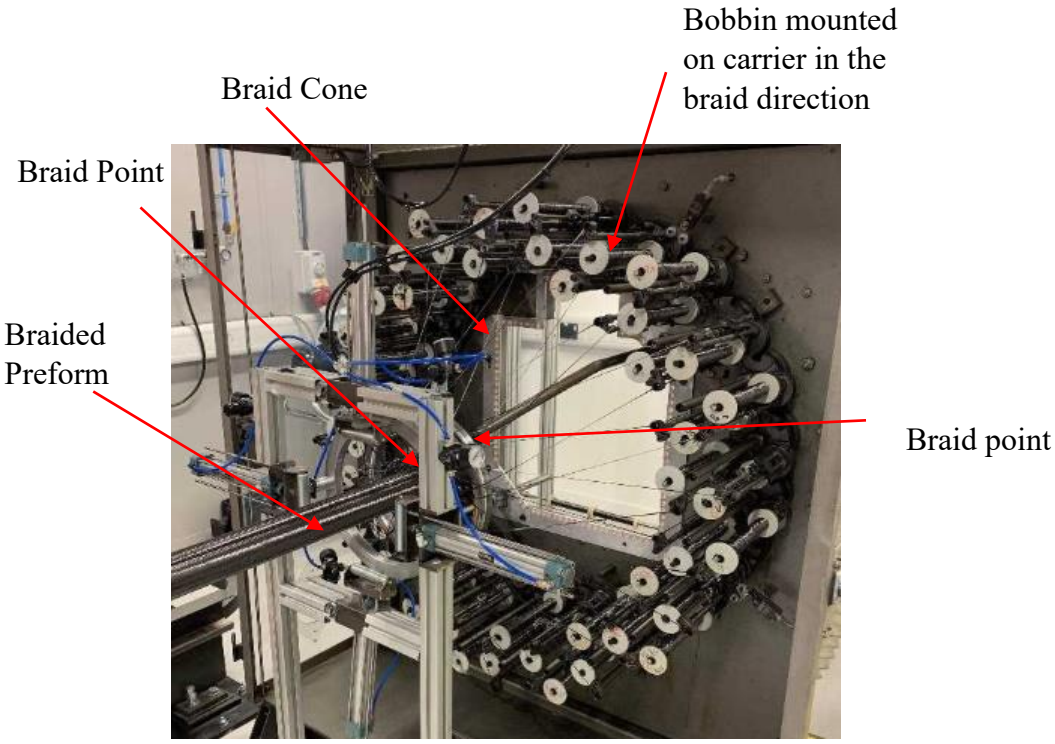


Figure 2.11 Steeger Axial Braider at the University of Nottingham

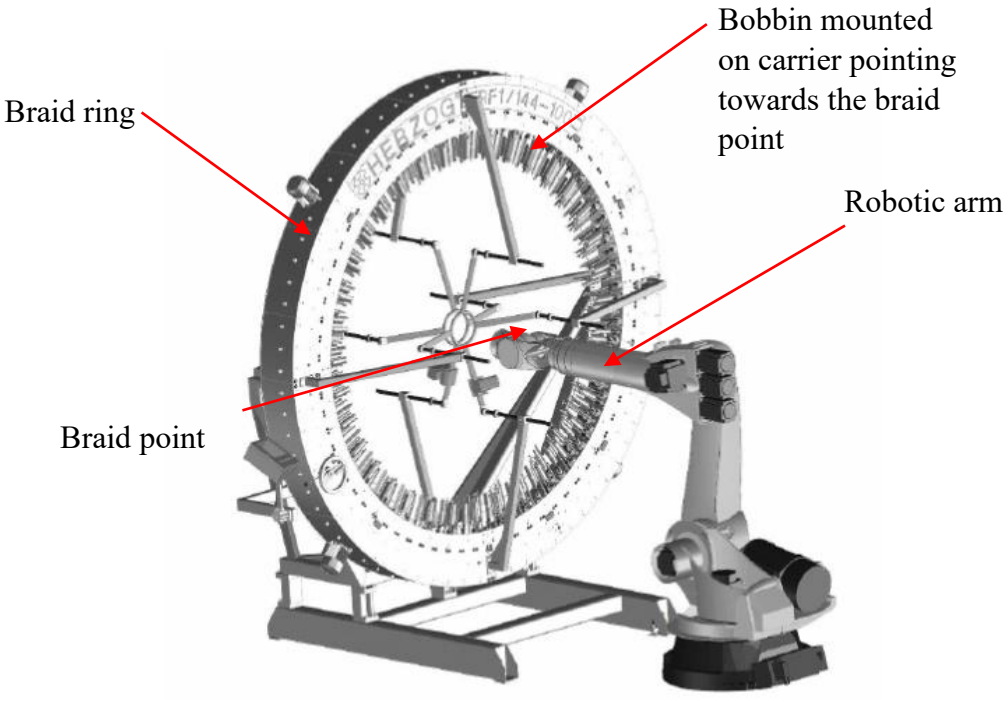


Figure 2.12 Radial Braider with a robot-arm take-up mechanism

A simplistic demonstration of the difference in distance between carrier and braid point for radial and axial braiders is shown in Figure 2.13. The orientation of the carriers are shown by one single carrier and the braid point where the yarn deposits onto the mandrel is identified.

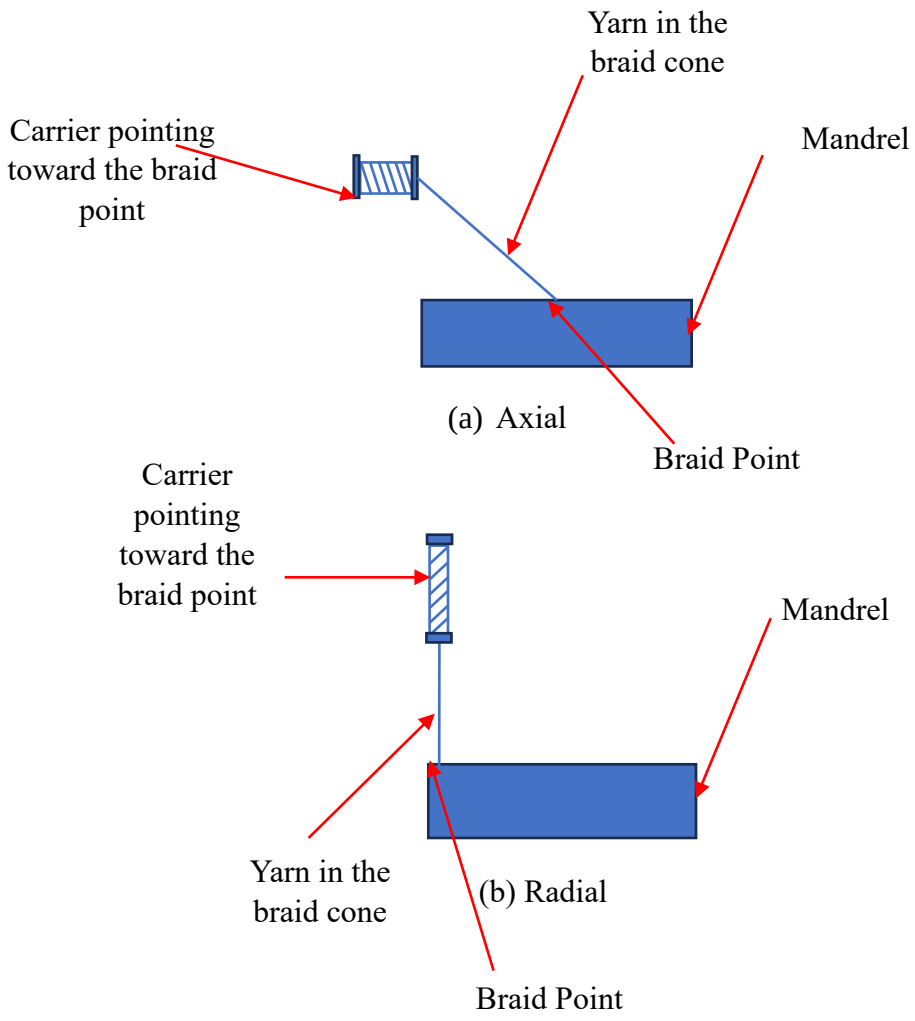


Figure 2.13 Distance between braid point and carrier for radial and axial braiders

The size of the braid cone is reduced with the radial braider along with the length of the yarn from the carrier to the braid point. This is due to the carrier orientation within the braider frame.

Braiding machine size varies depending on application. Steeger in the USA produce braiding machines manufactured with any multiple of 4 carriers with the most common sizes being between 8-144-carriers [12]. Leading radial braider manufacturers Herzog produce braiding machines with carrier numbers ranging from 72- 192 [13]. Similarly, Eurocarbon manufacture custom made braiding machines in sizes up to the double ring 192/288- carrier axial braider at the NCC [14]. A&P in the US, produce a line of Megabraiders ranging from 72-864 carriers.

A triaxial braid structure can be produced this is through the addition of another ‘axial’ fibres in the 0° direction which are fed through fixed tubes on the machine.

A take-up mechanism is required to progress the manufacture of a braid structure. Advanced braiding systems can use a robot arm as a take-up device, as shown in Figure 2.12 [2]. Another method is the installation of an axis gantry system as set-up at the NCC pictured in Figure 2.14.

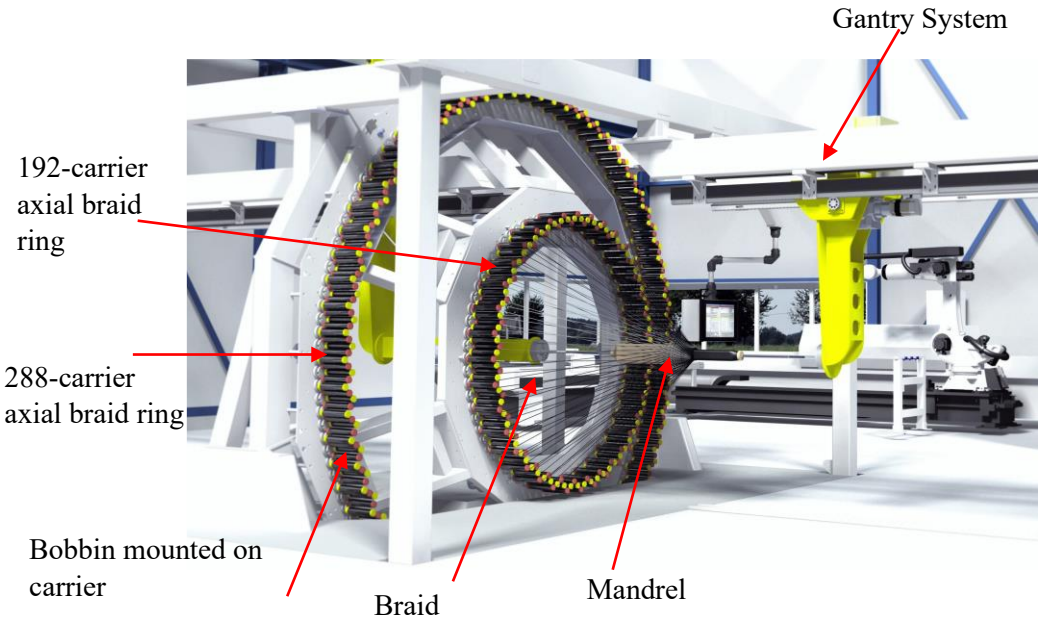


Figure 2.14 NCC Braider Schematic

The NCC-braider consists of two braid rings of 192- and 288-carriers. Its traverse can move at speeds up to 2000 mm/min. This leads to a high fibre deposition rate. The gantry is 10m long in both the forward and reverse direction which enables parts of up to 10m to be manufactured at a maximum diameter of 1m.

2.1.4 Fundamentals of the Rewinding Process

The rewinding process precedes the braiding process. Typically, the material for braiding is stored on large bobbins and must be transferred onto the yarn carriers on the braiding machine. This is done through rewinding; this is an essential process step. Applying the incorrect settings to the rewinding process at this stage can lead to preform defects, yarn breakages or breakages of yarn carriers and other machine components [2]. If instability in the rewinding process is sufficient the resulting rewinding tension on the bobbins will vary across the bobbin set. The effects of this are something that will become apparent to the operator much further down the manufacturing stream, affecting both the mechanical and visual properties of the braid.

The quality of the rewound bobbins from the material preparation stage contributes significantly to the subsequent quality of final braided preform [2]. There are a multitude of process parameters which can be controlled and manipulated to produce a high-quality bobbin package. These parameters determine the density and quality of the bobbin package used in the braiding process which influence the final quality of the braided composite.

2.1.4.1 Unwinding

The first stage of the rewinding process is the unwinding of material from bobbins supplied by manufacturers. These bobbins cannot be used on the braiding machine as their weight and size would limit processing speeds and carrier functionality. Consequently, the yarn is unwound from the large bobbins supplied by the manufacturer onto bobbins specifically designed for the braiding machine. These bobbins will vary in size and shape between different braiding machines. Figure 2.15 demonstrates this process.

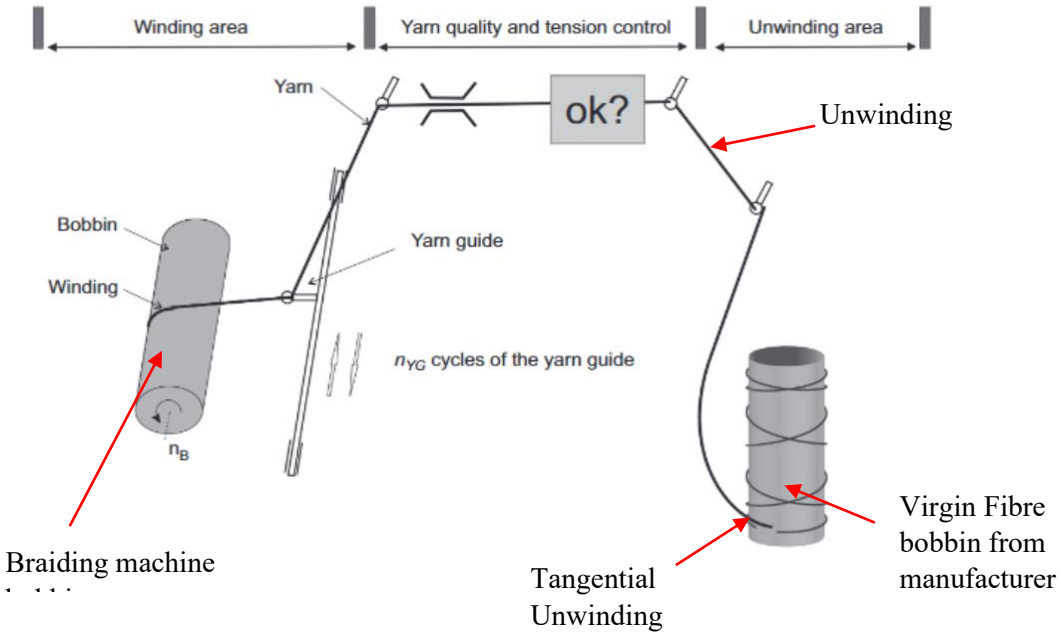


Figure 2.15 Basic Zones of the winding process for braiding [2]

Large bobbins can be unwound either axially or tangentially. Axial unwinding is used for large bobbins that are either cylindrical or conical without flanges. As it unwinds the yarn goes 'over the head' of the bobbin this creates what is called a 'balloon' around the bobbin. This 'balloon' must be unimpeded and stable during the rewinding process. Tangential winding is utilised when the yarn is wound onto a bobbin with

flanges, the bobbins is heavy or the material to be unwound is delicate. In this case the yarn is pulled out in a direction tangential to the surface of the bobbin.

The unwinding process can accommodate a wide range of materials. Care must be taken when rewinding high performance material such as carbon- and glass-fibre, as these should not bend over small radii as fibres can be damaged.

2.1.4.2 Types of Rewinding

The bobbin package for braiding must be sufficiently small to reduce the final machine size and inertial forces during braiding, whilst maximising the length of material on the bobbin. This will reduce the frequency of bobbin changes which are time costly from an industrial perspective.

Parallel winding is one of the most used winding types for braiding where the bobbins have flanges. During the parallel winding process the motion of the yarn guide is adjusted so that each winding lies directly next to each other this is shown in Figure 2.16. The movement of the guide is defined as the pitch. If the guide is moving too slowly and the pitch is low, the windings will lie very close to the previous and effectively be on top of each other. This creates an irregular layer of material.

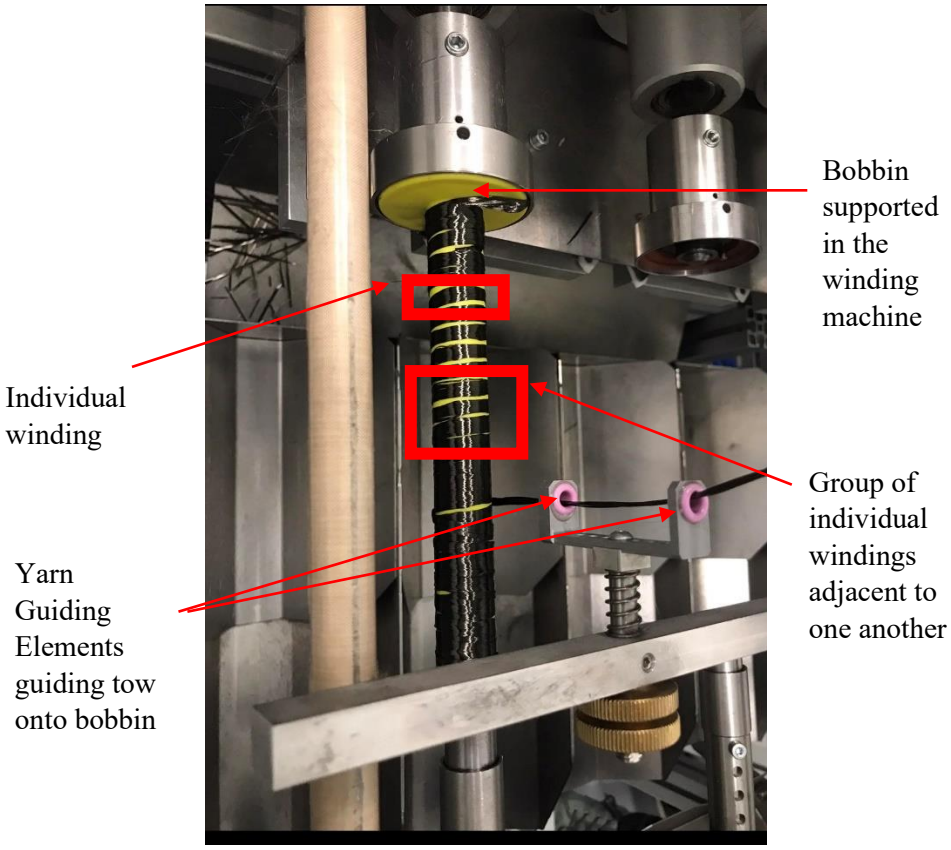


Figure 2.16 Start of a bobbin being wound demonstrating tow pitch

Similarly, the same result is attained if the yarn guide moves too fast and the pitch is high, then the windings will be too spaced out, and material layer is irregular. The amplitude of the movement of the guide element must also be monitored. If this is too small, the guide turns back too early, and the windings do not fill the entire bobbin length. If the amplitude is too great, the bobbin package ends will be excessively thick, Figure 2.17. This is shown by the sloped bobbin end as a result of material build-up. A bobbin wound with a correct amplitude will be consistent along the bobbin length, Figure 2.18. This is shown by the lack of material build-up at the bobbin edge. Practically, the amplitude of guiding element motion should be exactly the bobbin length.



Figure 2.17 A bobbin wound with a too great an amplitude

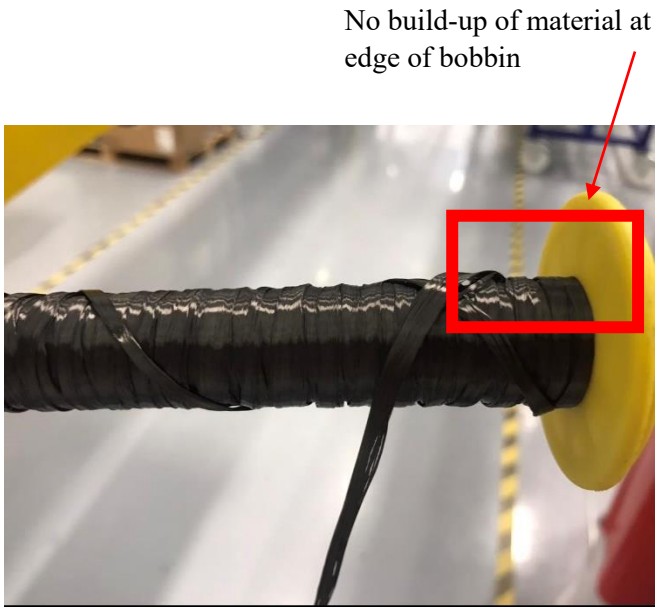


Figure 2.18 Bobbin wound with correct amplitude

2.1.4.3 Control and Regulation Devices

An assortment of devices can be employed to control and regulate the winding process. The selection of device is dependent on the requirement. Mechanical devices can be used for the detection of yarn breakages, in its most simplistic form of a yarn

guide on a swinging metal part. If the yarn tension is constant the guide remains in a vertical position, however, if a yarn breaks the guide swings under its own weight to stop rewinding. Knots can be detected using a plate as shown in Figure 2.19.

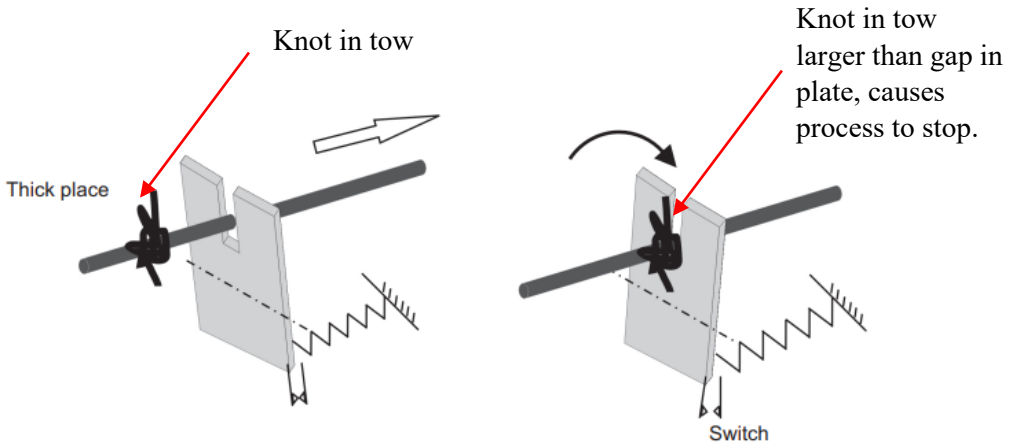


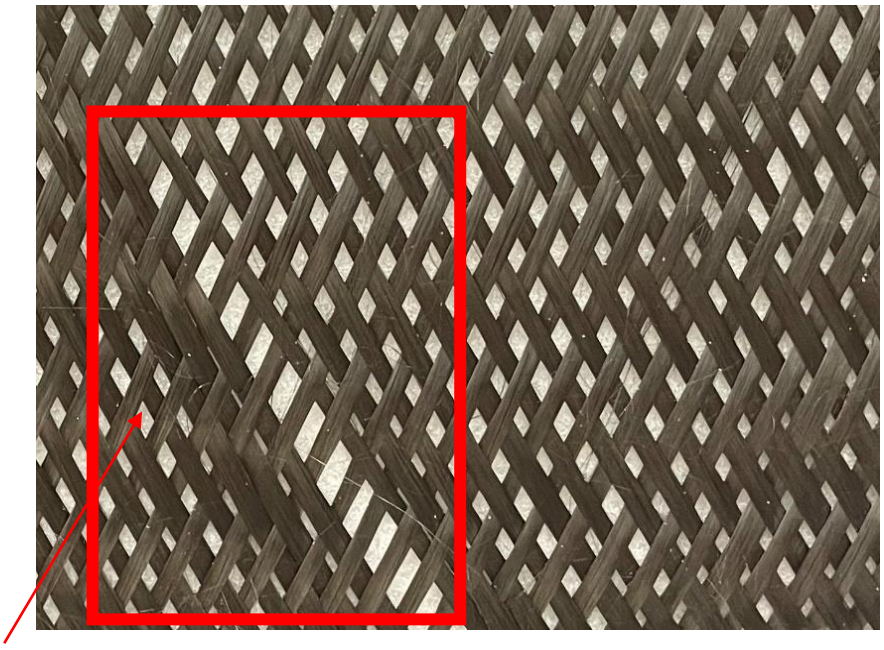
Figure 2.19 Check for Knots during Rewinding

The opening corresponds to the maximum acceptable yarn diameter. If a knot occurs, the plate rotates triggering a switch to stop rewinding. An active automatic tension regulation system prevents variations in yarn tension. Modern state-of-the-art rewinding machines utilise these devices, but this will depend on cost and required level of accuracy.

Sets of bobbins used in braided preform manufacture are required to be consistent in length. Different lengths on the bobbins are a problem for industrial manufacture as when one runs out, the remaining bobbins must be unloaded and unwound for the next machine set-up. This is a significant wastage of material resulting in an increase in process cost. This problem can be reduced by the application of simple devices used on the winding machine to measure the yarn length on the bobbin. The majority of these rely on the sticking effect of cylinder friction by using a roller rotating at the same peripheral velocity of the yarn. Modern winding machines can stop automatically after the required length is wound. This prevents any irregularities in bobbin length.

2.1.4.4 Rewinding Tension

Rewinding tension determines the density and stability of the final bobbin package. Tension variations during rewinding lead to elongations and relaxations of the yarn on the bobbin. If a yarn is rewound with inconsistent tension some regions of the yarn will be more deformed than others. The tension during winding must be equal to or higher than the braiding tension so that the bobbin package can remains stable to prevent any deformations or defects in the braided preform. Problems can arise when bobbins are rewound with inconsistent tension. Variability in the set of bobbins can result in evident defects in the braided preforms as the yarns will have relaxed to different lengths. Figure 2.20 shows the result of braided preform is wound with different tension. This disrupts the regularity of the braid and introduces defects shown by the inconsistent spacing of the braiding tows.



Inconsistent spacing of braiding tows because of variable tow tension

Figure 2.20 Braid with Inconsistent Tension

Rewinding tension is regulated through a series of control devices between the unwinding and winding areas. Figure 2.21 shows the set-up of the state-of-the-art CEZOMA CE-1187 rewinding machine at the NCC. A total of 4 guiding elements are visible from the larger bobbin in the winding cabinet to the small bobbin. Ceramic

coated guiding elements are used on the machine to reduce friction on the tow and resultant damage during the rewinding process.

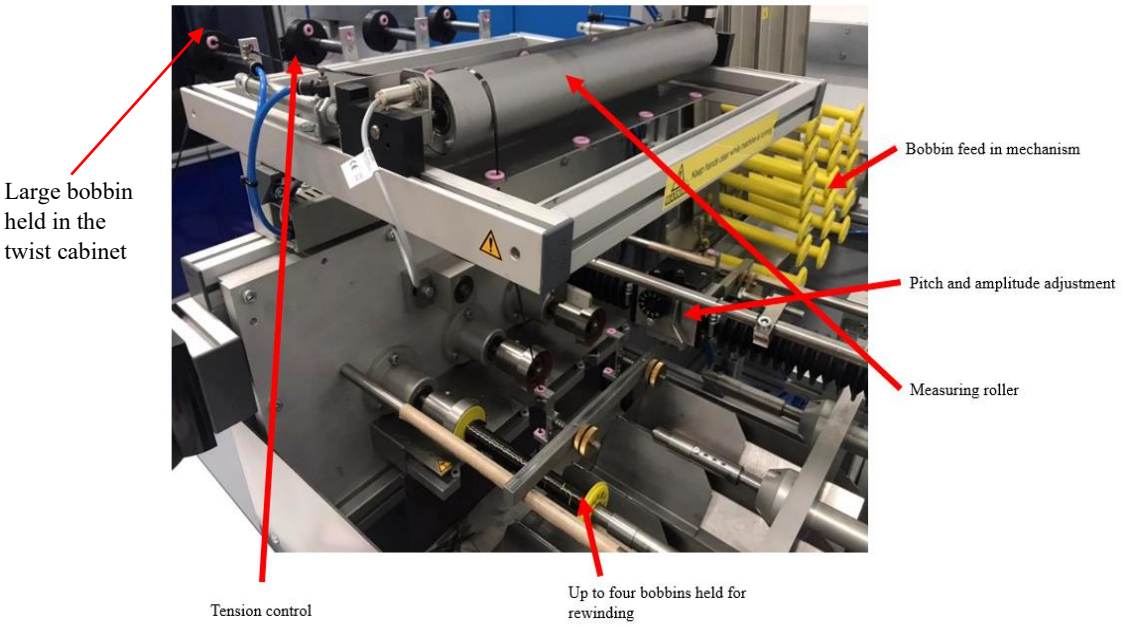


Figure 2.21 CEZOMA CE-1187 Rewinding Machine

2.1.4.5 Rewinding Twist

Yarn twist is defined as the rotation of the yarn about the axis of any line on the yarn previously drawn before twisting parallel to the yarn axis. In rewinding, the direction of the twist is indicated by two letters, S and Z, Figure 2.22 [15].

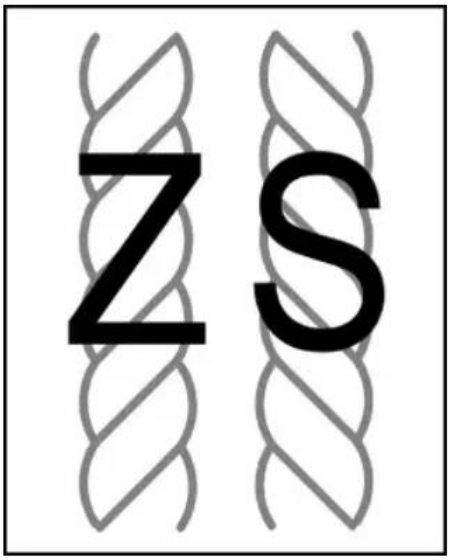


Figure 2.22 Yarn Twist Types [15]

A yarn has an ‘S’ twist has a clockwise twist on it if when held vertical the filaments of the fibre bundle incline the same way as central portion of the ‘S’. Similarly, yarns have a ‘Z’ or anticlockwise twist if the filaments align with the central portion of the ‘Z’. In braiding a balance of ‘S’ and ‘Z’ twist bobbins are required to produce a balanced braided preform.

The inclusion of an additional twist to fibres during the rewinding stage of the process is an optional step included by some braiding manufacturers such as Eurocarbon [16]. It has been suggested that twisting influences the tow diameter along with friction coefficient and longitudinal strength. However, there are limited contributions in the literature on the influence of twist on braiding.

When multiple yarns per bobbin are wound in cases such as with commingled fibres where a polymer is rewound simultaneously to the carbon, twisting can be useful to attain a good distribution of thermoplastic to reinforcement fibre. This is critical for composite quality. Torun et al studied the effect of twisting on the mechanical properties of Glass Fibre/Polypropylene commingled yarns to determine if the application of twisting to commingled yarns improved processability [17]. The influence of the number of twists per metre (TPM) on the tow diameter and mechanical properties were analysed. Figure 2.23 demonstrates that a large number of twists significantly influence the yarn diameter. Torun found that the standard deviation of the commingled yarn diameters stayed generally uniform. It is stated that twisting decreases the average yarn diameter and creates a more compact structure.

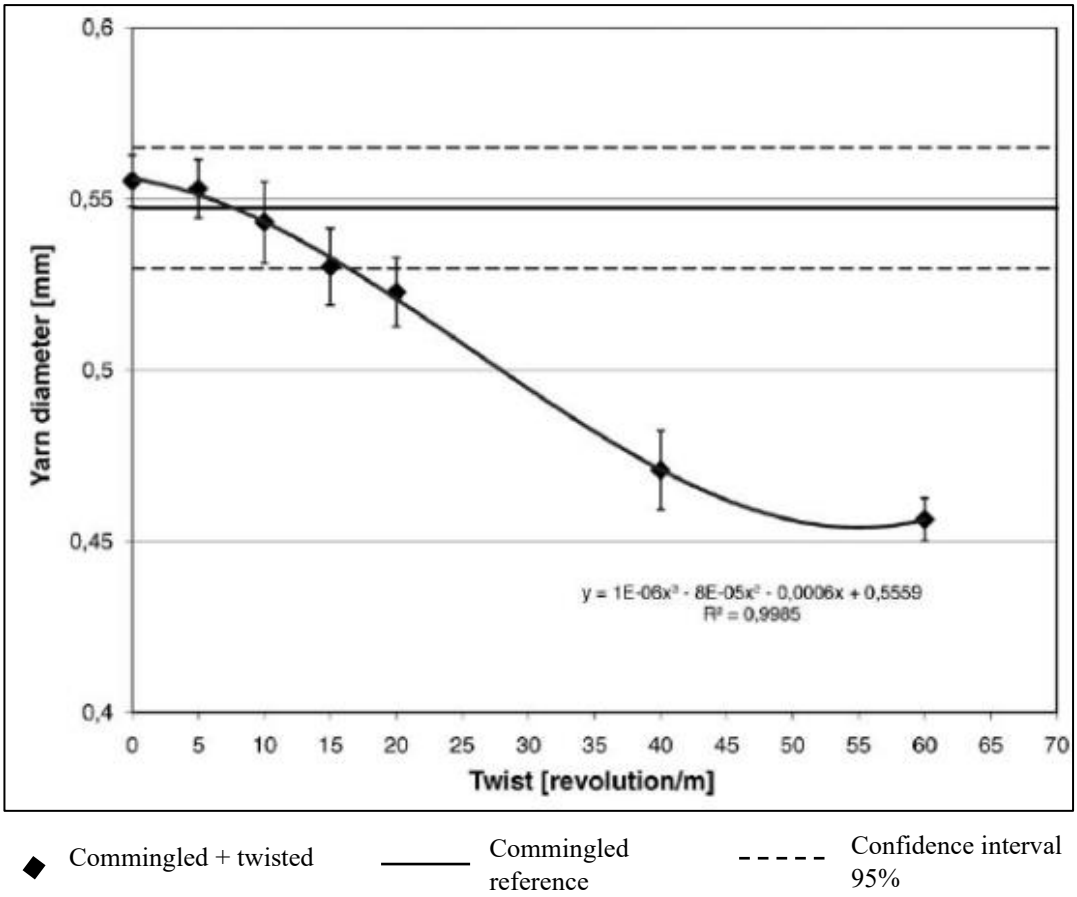


Figure 2.23 Effect of twisting on the diameter of Glass Fibre/Polypropylene commingled yarn [17]

Torun reported an increase in tensile strength of commingled yarns until 40 TPM. However, the composite tensile strength values of twisted samples were approximately 10% less than the reference value. A reduction in transverse modulus was noted from 20 TPM, this is in line with the reduction in yarn diameter. In summary, Torun recommends no more than 10 TPM to have a compromise between the diameter uniformity and friction benefits with no reduction in mechanical performance [17].

Alagirusamy also concurred that a few twists on commingled yarns are beneficial to the process [18]. A slight twist in the commingled fibres helps to preserve the location of the PEEK filaments used in their investigation. Non-twisted commingled yarns showed some piling of the polymer filaments due to different elongations of carbon and PEEK. An additional ‘two twists per inch’ was recommended. Bunzel et al [19], Lefebvre et al [20] and Jeguirim et al. [21] also discuss the potential for yarn twist to increase yarn strength and provide greater resistance to friction. Eurocarbon extend

this recommendation to all fibre types as well as commingled yarns to improve the processability of the yarns and reduce in-process fibre damage [16].

2.1.4.6 State-of-the-art of Rewinding

2.1.4.6.1 Rewinding Machines

State-of-the-art rewinding machines offer the control of multiple process parameters such as rewinding tension, rewinding speed, and rewinding twist, whilst measuring wound material length and detected thread breakages. Multiple bobbins can be rewound simultaneously with variable speed settings. Yarn length is measured using an electronic counter with thread breakage detection. Tow pitch is determined manually [22] [23] [24] [25]. Table 2.1 provides some examples of currently available rewinding machines.

Table 2.1 List of Commercially Available Rewinding Machines

Manufacturer	Machine Model Name
Herzog	SP280 Eco
CEZOMA	CE-1187
Ratera	2PVLU/220

An optional parameter used by many braid operators is to braid with fibres rewound with an additional twist. This parameter is not controllable on a standard rewinding machine however, Eurocarbon have manufactured a twist cabinet that is cable of adding specified numbers of twists per metre, Figure 2.24.

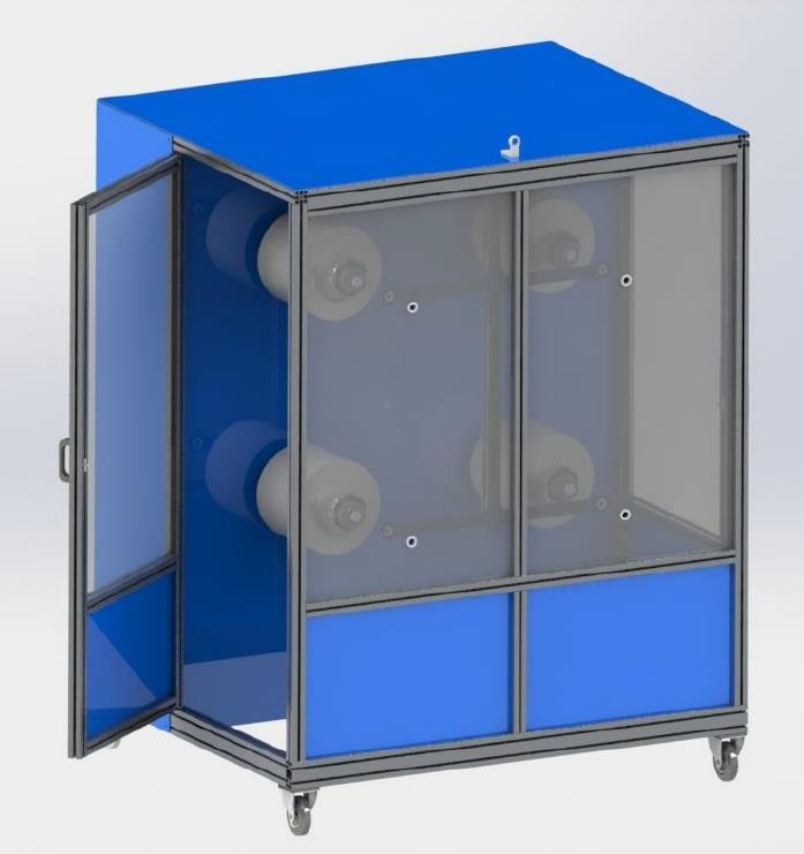


Figure 2.24 Twist Cabinet supplied by Eurocarbon [26]

The recommended number of twists per metre by Eurocarbon is summarised in Table 2.2 for carbon fibres.

Table 2.2 Recommended Twists per Metre [26]

Tow Size	Number of Twists per metre
3K	15
6K	12
12K	9
24K	5
50K	5

The twister applies twist to a yarn before it is wound onto a bobbin. Therefore, the twist cabinet is designed to be used in conjunction with a bobbin winding machine. Figure 2.25 demonstrates how twist is added to fibres during the rewinding process.

The set-up consists of two separate components, the twister and the rewinding machine.

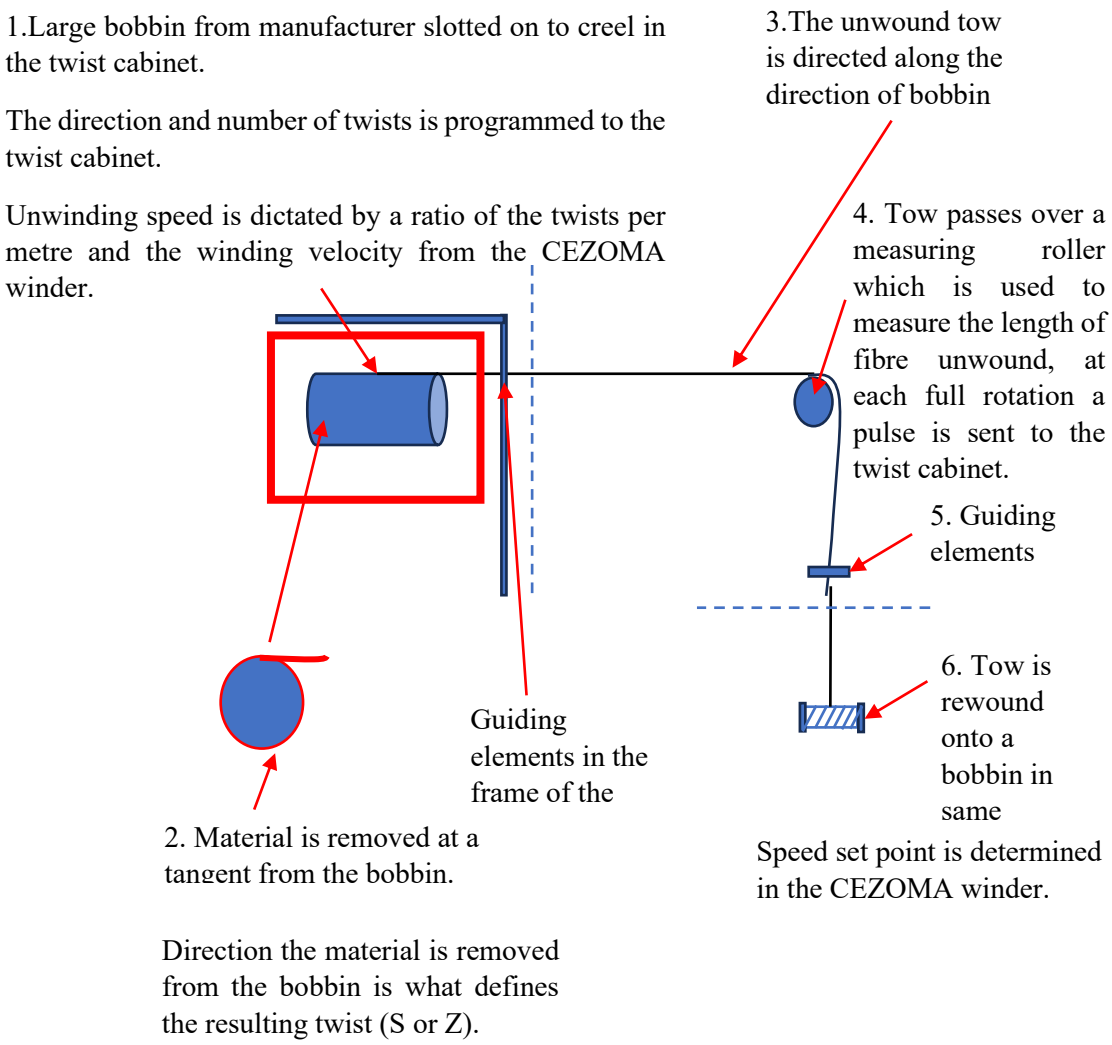


Figure 2.25 Method of adding twist to fibres during rewinding

The twist direction is selected as a Z or an S-twist and entered by the user into the twist machine. A user entered setpoint of twists per metre from the twister and winding velocity inputted to the winder are combined to calculate the rotation speed of the bobbins on the twist machines. It is the difference in rotational speed for the larger bobbins in the twist and the small bobbins on the winder that impart the twist into the fibres.

Continuous pulses are received by the twister from the bobbin winding machine. These pulses are dictated by the measuring roller on the winding machine. Every time

the roller rotates, a pulse is received. One rotation is equivalent with 20.01cm, therefore 1 pulse is equal to 20.01cm.

2.1.4.6.2 Knowledge Limitations of Rewinding

There is a correlation between quality of the rewinding process and the resultant quality of the braided composite product. This has been discussed in relation to rewinding tension [2] [3] and rewinding speed [24]. However, there is limited understanding on the influence of rewinding twist on the quality of the braided product and its effects on the braid architecture itself, previous work has been focussing on twisting with regards to other textile processes [17].

2.2 Commercial Braided Components

A wide range of geometries have been braided. The versatility of the process and high potential for automation whilst minimising waste have resulted in a range of attempts at braided components across a range of industrial sectors including automotive, aerospace and sport. BMC a Swiss bike manufacturer used a Herzog radial braider to produce a 100% carbon fibre bike frame. The technology uses a glass fibre mandrel which is manipulated by a robotic arm through the braiding machine to produce a component with varying cross section [27].

Within the aerospace industry, Airbus have developed a prototype production line for producing braided fuselage parts for the A350, Figure 2.26. This was designed to move away from prepreg layup. The development process has been ongoing since 2007 with an outlook to the components being implemented on the A350-100 aircraft [28]. Fokker industries have also developed a braided landing gear used on the NH90 helicopter; the component offers a reported 20% weight saving. The European Aeronautic Defence and Space Company NV have also developed a production method for aircraft frames due to the increasing demand for automation in the industry [29].



Figure 2.26 Airbus Prototype Production Line

A&P in the US, produce a line of Megabraiders ranging from 72-864 carriers. Such large braiders enable the production of structures such as the rocket nozzle preform pictured in Figure 2.27 [30]



Figure 2.27 Large rocket nozzle preform produced by A&P's line of Megabraiders [30]

These machines are bespoke built for specific applications and developed because of General Electric Aircraft Engines needing a braided tape in excess of 22” wide for a Jet Engine containment belt in 1985. Subsequently, A&P were asked to design a biaxial sleeve for side impact airbag for automobiles. As this design required very small yarns for a very high coverage, which required a large machine, A&P built a 600-carrier braiding machine. This airbag material has been used by BMW, Land Rover, MINI Cooper and Cadillac Escalade [5].

Several examples of braided components are present in the automotive industry. Porsche became the first vehicle manufacturer to offer braided carbon fibre wheels, Figure 2.28. The wheels on the Porsche 911 Turbo S offer a weight saving of 8.5kg, approximately 20%. The rim base is manufactured on a 9m diameter Herzog braider. Prior to infusion, the wheel centre is then braided into the rim base.



Figure 2.28 Porsche Carbon Fibre Wheel

According to Porsche [31], braiding increases the structural rigidity of the wheels as the components are denser. Eurocarbon have also collaborated with Mercedes-Benz to produce a braided crash cone on their Mclaren SLR [32]. This is designed to facilitate energy absorption during a crash. Aston Martin and Lamborghini have also ventured into braiding by equipping some vehicle models with braided A-pillars. The BMW-i8 has a braided A-pillar in development with braided parts announced for the new BMW-7 series, this includes a braided roof beam [29]. The roof frame is manufactured via overbraiding a thermoplastic core and followed by Resin Transfer Moulding. It is predicted that braided components will further spread into the mass automotive market.

2.3 Challenges in Braiding

As a manufacturing process, braiding is highly advantageous, however there are some challenges preventing large scale industrial application. The application of braiding as a manufacturing process is dictated by the component geometry. Prediction of final-part properties requires development. Currently, predictive capabilities are built from generalised yarn assumptions. Developing predictive

capabilities will increase confidence in braiding as a manufacturing process and improve its uptake in the automotive and aerospace industrial sectors. The development of standardised test methods for braiding is required. Due to the nature of the braided material, standard test methods are often modified to be applicable for braided components.

Quality of braided components is still determined at an individual part level through inspection. Recently, developments have been made to increase in-line inspection of the key process variables for braided components. The wider application of in-process monitoring systems can identify the key process variables of components. The efficiency of the process particularly the set-up, can also be developed to increase production rate and reduce machine downtime. There is a demand for greater automation in composite manufacturing processes to increase production capacity, identify defects and capture part data. Literature also highlights a limitation in the understanding of the rewinding process, particularly its impact on the mechanical properties and geometrical properties of the braid architecture. The multitude of process parameters that can be controlled offer the potential for further process optimisation and improvement however the impact of the rewinding process of the mechanical properties on the braided composite is unknown.

The focus should be part complexity and quality. Improving the consistency between simulation and manufacturing can aid in increasing the uptake of braiding as an industrial composites manufacturing process. This work aims to resolve some of these outlined challenges such as providing a greater understanding of the rewinding process particularly the inclusion of a rewinding twist. This is something that is used widely in industry but to date limited publications exist. This work provides an improved understanding of the key process variables of braid architecture for both simple and complex geometries. Better understanding of the tow geometry of braided composites particularly because of rewinding twist will enable future work to develop the predictive capabilities to improve consistency between manufacturing and simulation.

3 Review of Literature related to Manufacturing Braided Composites

3.1 Key Process Variables for Braiding

Braid angle, cover factor and braid thickness are typically seen as critical design parameters or key process variables for the braiding process.

3.1.1 Braid Angle

This is the angle that the braiding tows make with the structural axis [3], Figure 3.1. The braid angle directly impacts the mechanical properties of the composite. It is also influential for other parameters such as braid cover factor and layer thickness. Practically, the range of braid angles for biaxial braiding is ±15° to ±80° depending on the part diameter [1].

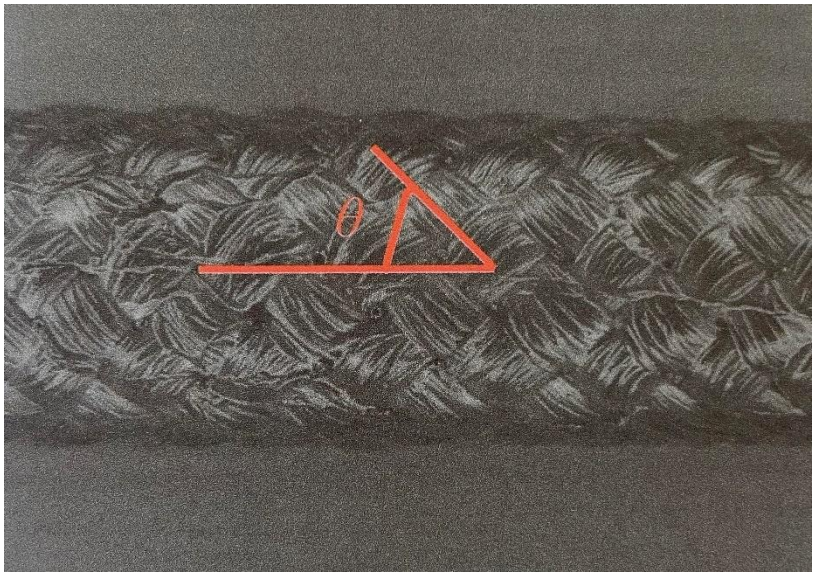


Figure 3.1 Image of Braid Angle Measurement [3]

This metric is a function of mandrel radius *(R)* and production variables of take-up speed (v) and carrier rotational speed (ω). Equation 3.1 shows the relationship between these production variables for the calculation of braid angle on a tubular mandrel [3].

$$\theta = \arctan\left(\frac{\omega R}{v}\right)$$

Equation 3.1 Braid Angle

The quality of a braided component is verified through accurate measurement of the braid angle parameter. Conventionally, tubular braided preforms are cut off the mandrel along the longitudinal axis then flattened before measuring the angle. This is a destructive process so would be used during the trial stages of production to determine the appropriate processing parameters. Alternatively, braid angle can be measured non-destructively from an image of the braided preform.

At the time of writing, ISO10122 is the only standard that offers an approach for calculating the braid angle of a manufactured tubular preform [33]. The standard assumes that the tows follow a perfect helical path along the mandrel and then uses trigonometric relationships to relate the length of the braid preform as it sits on the mandrel (L_t) to the length of the braided tow once it has been removed from the mandrel (L_v), Equation 3.2. The main limitation of this standard is that local variations in braid angle are not accounted for.

$$\cos(\theta) = \left(\frac{L_t}{L_v}\right)$$

Equation 3.2 ISO10122 Braid Angle Calculation Method

3.1.2 Cover Factor

The cover factor is a measure of surface area covered by braiding tows [3]. This metric is often used as a design parameter for braided preforms. For a cylindrical preform, Equation 3.3 can be used to calculate cover factor [3]. This equation is applicable for biaxial preforms and uses tow width (W_y), number of carriers (N_c), mandrel radius (R) and braid angle (θ) as input parameters.

$$Cover\ Factor = 1 - \left(1 - \frac{W_y N_c}{4\pi R cos(\theta)}\right)^2$$

Equation 3.3 Cover Factor

Fibre volume fraction is the ratio of braided yarns relative to the total composite volume. Equations to calculate fibre volume fraction will depend on the assumed geometry of the braided unit cell. Carey proposes a method where the tow shape is assumed to be elliptical and the unit cell a parallelogram. The representative area of the unit cell and tow cross section are shown in Figure 3.2 where *Wy* is the tow width,

a tow thickness, L_s length of the braid yarns, r_o nominal radius of the braiding mandrel, *n* number of carriers and *h* the height of the unit cell.

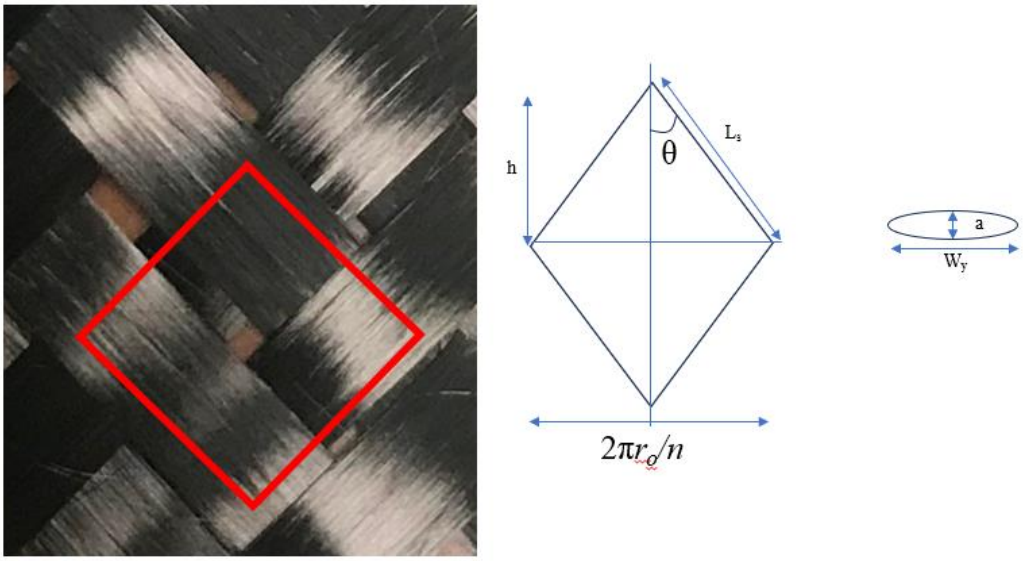


Figure 3.2 Unit Cell and Tow Geometry [3]

The fibre volume fraction is calculated using Equation 3.4. N_c is used to refer to number of carriers in this equation. Tow geometry parameter of tow width (W_y) as shown in Figure 3.2 is used in calculation of the volume fraction, along with θ, which dictates the shape of the unit cell as shown in Figure 3.2.

$$V_f = \frac{W_y N_c}{8R\cos\theta}$$

Equation 3.4 Fibre Volume Fraction Equation

Axial tows added to the braid for increased structural performance result in an increase the cover factor of a braided preform. Analytical calculation of cover factor is more difficult with triaxial braids as they are often distributed unevenly in the braided unit cell. Kyosev presents an equation for the cover factor of a triaxial braid using different widths for biaxial and axial yarns, Equation 3.5, but this provides an overestimate as a central alignment of the axial tow within a unit cell is assumed [29]. Where N_c is the number of bobbin carriers, D is the diameter of the mandrel, W_y is the width of the biaxial yarns, θ is the braid angle and w_{inlay} is the width of the axial yarns.

$$CF = \left\{1 - \left(1 - \frac{N_c W_y}{2\pi D \cos\theta} - \frac{N_c w_{inlay}}{2\pi D}\right)^2 ; if \ \frac{N_c W_y}{2\pi D \cos\theta} + \frac{N_c w_{inlay}}{2\pi D} < 2\right\}$$

Equation 3.5 Kyosev approximation for triaxial cover factor assuming central alignment of the axial yarn

However, axial yarn placement within a unit cell is not always uniform due to manufacturing forces applied on the yarn during processing. Figure 3.3 shows a schematic of the different locations of the axial tow within a unit cell.

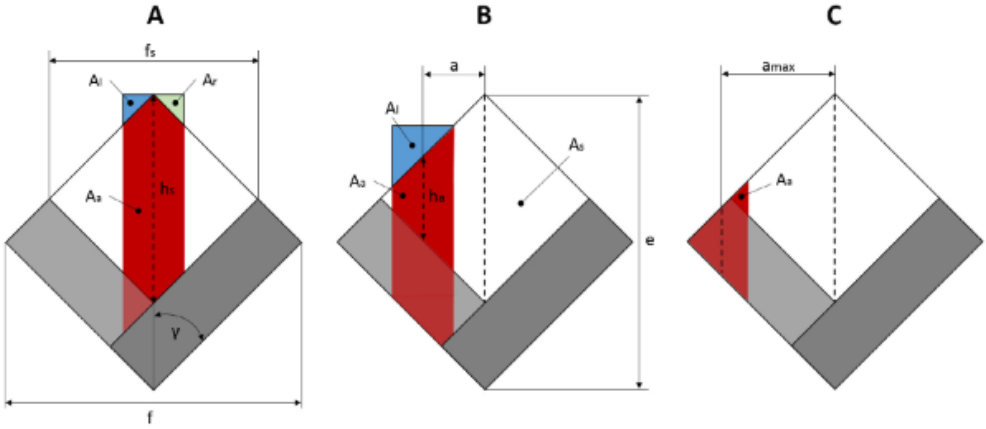


Figure 3.3 Triaxial unit cell with a centrally aligned yarn (left) and shifted axial yarn (middle and right) [34]

Heieck used the assumptions shown in the schematic to develop a new approach accounting for the fact axial tows are typically shifted towards the side of the unit cell within a regular braid. The area covered by the axial yarn depends on their position occupied within the unit cell, parameter 'a' account for this with $0 \leq a \leq a_{max}$, where $a=a_{maz}$ when the yarn is in its most extreme shift position. A system of equations has been derived for each case A, B and C, by calculating the area of the unit cell, the area of the braiding yarns (A_s) and area of the axial yarns (A_a) [34]. Manufacturing experience has demonstrated that this provides a good approximation as axial tow distribution is not always uniform.

3.1.3 Braid Thickness

Braid thickness refers to the perpendicular distance between the preform substrate and the mandrel. Whilst in theory this is a point measurement, due to the undulating nature of the preform surface the preform thickness is an average value over a preform length. Typically, this done on a dry preform prior to impregnation.

Monitoring the preform thickness layer-by-layer is important for preform manufacture. Manually, this can be done with a depth gauge or a vernier calliper which enables point measurements. However, this method requires contact with the preform surface which results in deformation of the braided preform introducing errors into the results. Thickness measurements using depth gauges require the braiding process to be interrupted to take measurements [35].

For a non-contact assessment of preform thickness, a laser line scanner can be used. These instruments create a 3D point cloud of the surface being inspected. For in-situ measurements of preform thickness a scan of the mandrel surface prior to braiding is required. The measurements are then compared between the point cloud data and a fitted feature (baseline mandrel surface scan) to produce an approximation of preform thickness. The thickness is determined by the laser line signal intensity.

This work uses a laser line scanner as tools for measuring preform thickness, this has been demonstrated in the literature. However, the structure of a dry fibre preform as bundles of individual fibres can present issues causing scattering of the incident laser light, this reduces the intensity reflected as shown in Figure 3.4. Therefore, a long exposure time is used to obtain a strong signal of at least 5ms per profile *[36]*.

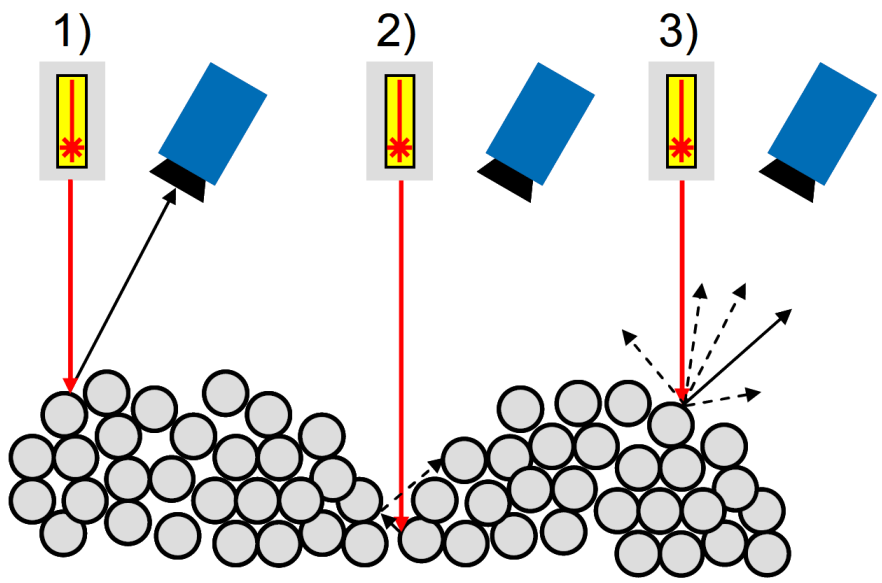


Figure 3.4 Effect of preform surface on laser line signal intensity 1) Direct reflection and maximum intensity, 2) no reflect- no interaction with preform, 3) reduced intensity due to scattering [36]

Thompson trialled some methods of determining the braided preform thickness [37]. One of these was a white light scanning system, HP 3D Structured Light Scanner Pro S3. The scanner can create a digitised 3D model of 0.05mm resolution. The scan takes 2.3 million vertices per scan. The 3D images can then be used to take braid architecture measurements post-process. The surface of the braid is sprayed with a white surface colouring to improve the image resolution and prevent the white light being reflected off the carbon fibre.

The Apodius Vision System (AVS) 3D by Hexagon was also used. The AVS is used for advanced carbon-fibre part inspection and can be used to attain parameters of braided preforms through point measurement of the resulting preforms using locations specified by the operator. The datasheet states that the system is accurate to 0.026mm and measure 1.2 million points per second. The scanner is certified to standard ISO 10360 8. The high-quality camera image can be used for part inspection. A texture segmentation algorithm detects the edges of the yarns, reinforcement direction is manually assigned by the user. The AVS uses the known global location and image orientation, the braid angle can also be determined [38].

3.2 Manufacturing of Braided Composites

Braided composites require a high level of design and often significant amount of trial-and-error. Simulation tools are improving to reduce the number of design iterations; however, development is required to accurately predict braid architecture and mechanical properties as many simulation tools are built from generalised yarn assumptions. This section of the literature review discusses the braiding of complex geometry, the infusion of braided preforms and development of fibre damage. A summary of the mechanical testing methods for braided composites is also included.

3.2.1 Braiding of Complex Geometries

Mandrel geometry is often a limiting factor with braiding. Under certain process conditions, the braiding tows cannot deposit onto the surface of the mandrel when the geometrical gradient exceeds a certain level. This restricts the range of geometries that can be braided to achieve a constant braid angle or cover factor. Du and Popper investigated this by braiding and modelling a conical mandrel on a 72-carrier braiding machine [39]. A half cone equation was formulated and implemented to develop this limitation which accounts for the rate of change of mandrel diameter in a defined time increment. The study concluded that braiding is more uniform when a component with cross-sectional diameter change is braided in a converging orientation. Converging refers to the cross-sectional area of the part reducing in the direction of braiding, whereas diverging refers to an increase cross-sectional area along the braid direction. The kinematic model assumes that no yarn-mandrel slippage after yarn deposition occurs and that the braid angle is equivalent to the cone angle, so interyarn friction is not accounted for. The equation highlights that convergence length is not a steady state value when braiding a complex geometry. When a change in cross-sectional shape causes severe transients in key process variables the uniformity of the braid can be improved by profiling the axial velocity. A computer model was developed based on the experimental data which outputs a complete description of the braid microstructure and key process variables. The program is capable of operating in the inverse solution to provide the machine speeds required for a given braid angle or cover factor distribution [39]. The exact range of geometries that can be braided successfully is machine dependant so would vary on a larger braiding machine.

Kessels and Akkerman used a purpose-built mandrel with drastically varying square cross-section and eccentricities to analyse the fibre architecture when braiding complex preforms [6]. These are shown in Figure 3.5 and Figure 3.6. The two mandrels were braided on a 72-carrier braider with a constant guide ring diameter of 170mm. The braid angles were measured on each of the four surfaces at 25mm intervals.

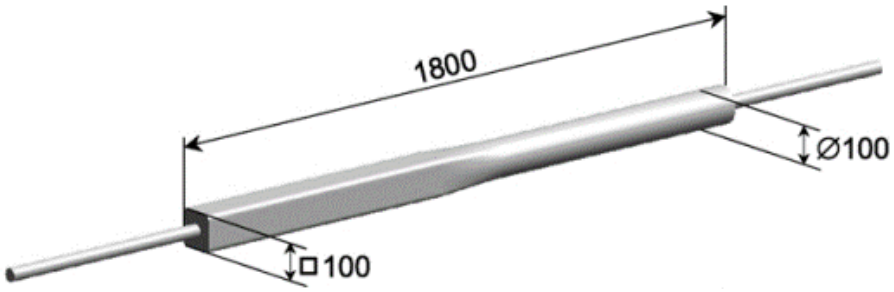


Figure 3.5 Test Mandrel (1)

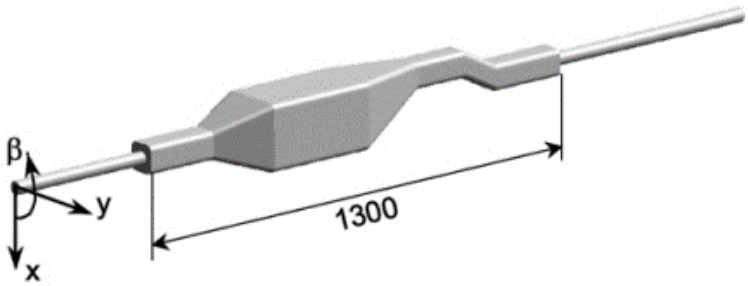


Figure 3.6 Test Mandrel (2) [6]

A cluster of yarns at section changes was observed, but this evolved to reach an even yarn distribution. At the beginning of section changes fluctuations were noted in braid angle, a change in convergence length due to changing mandrel diameter was used to explain this. At maximum eccentricity in the Y-direction, 20% difference between warp and weft yarns were measured. Experimentation identified that yarn slip was more apparent when the braid structure had a low degree of a coverage. At a high braid velocity slip was not observed. The mathematical model developed by Kessels and Akkerman provided good prediction of the fibre direction in a braided preform of complex geometry with sharp curvatures [6]. The model assumes the yarns are continuous, yarn trajectories lie on the mandrel surface, yarn motion stops at the fell point where the yarn touches the mandrel and that yarns are straight in the convergence zone.

Guyader, Gabor and Hamelin develop the modelling for complex geometries to establish the adapted relationship between the architecture of complex braids and the process parameters. The importance of differentiating between the deposition speed and carrier speed in both angular and axial direction is emphasised. A 3D kinematic model is proposed, this excludes yarn interaction. It is stated that angular speed of the fell point varies as friction increases which results in a reduction in braid angle, this does not hold for steady state conditions. Good agreement with other kinematic models was noted for stead-state processes and symmetric revolution shapes, with good accuracy noted for circularly eccentric geometries. Validation for a transitionary state was completed through suddenly increasing or decreasing the mandrel speed. This mimics the change in geometry. The change in location of the braiding point for multiple speed changes was modelled to good accuracy. However, this does not mean that the model is accurate for complex shapes as factors such as yarn relaxation due to friction in the convergence zone or changing geometry is not accounted for. Experimental validation of the model is required for this [40].

An optimised speed profile can be used to improve architecture on more complex geometries. However, for components with an extreme aspect ratio such as rectangular geometry with constant cross-section braid angle will vary around the perimeter of the braid if a circular guide ring is used due to the changing length of yarn in the convergence zone. Fouladi and Nedoushan proposed some formulae for predicting braid angle on flat mandrels accounting for the distance of the fell point from the guide ring [41]. It was demonstrated that the braid angle on each face of the mandrel could be optimised towards a more desired angle. This was further developed by Fouladi who proposed the concept of controlling the braid pattern on every side of a flat mandrel with an elliptical guide ring which alters the distance of the fell point from the guide ring on every surface [42]. The applicability of an elliptical guide ring was verified by using a guide ring with dimension a= 150mm and b=80mm. It was used for braiding a concentric square mandrel, concentric rectangular mandrel, and eccentric rectangular mandrel. The experimental results showed that changing the form of the guide ring significantly impacted the braid angle on the different sides of the flat mandrel.

Van Ravenhorst used a complex mandrel, Figure 3.6 to validate the proposed inverse kinematic model, the geometry is shown in more detail in Figure 3.7. Numbers 1→4

refer to the side number, this notation is continued in Figure 3.9 where the braid angles on each side are discussed. It is considered a more difficult shape to most practical manufacturing cases due to the constant changes in cross-section and eccentricities.

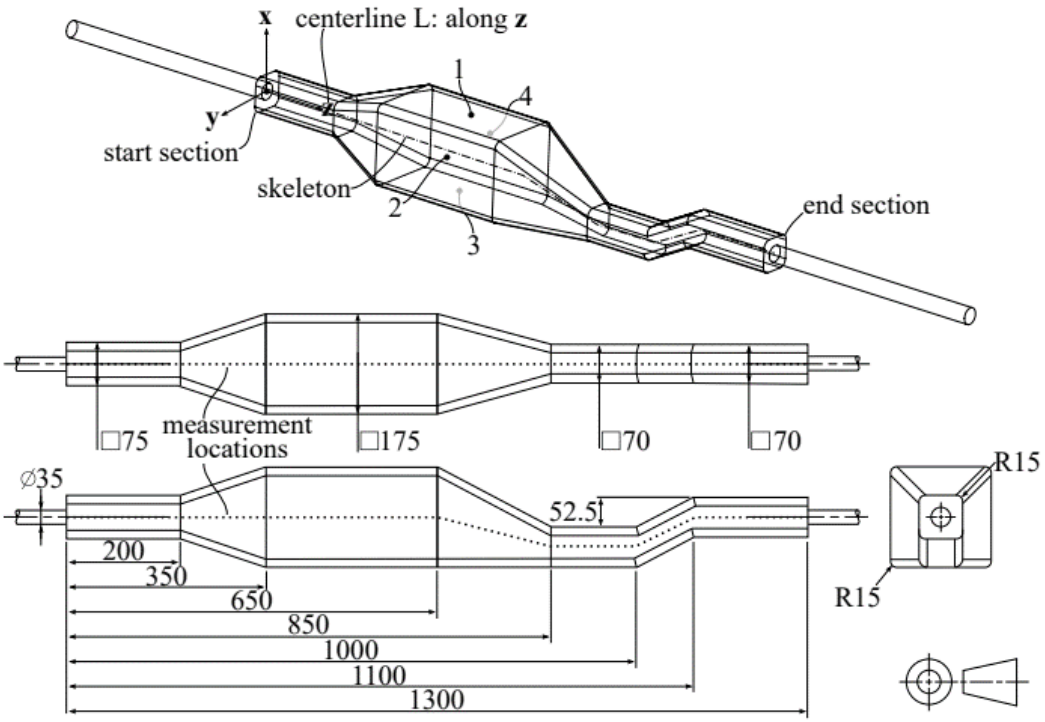


Figure 3.7 Detailed Dimensioned complex mandrel. [43]

The braiding of a triaxial preform was completed at Eurocarbon using the 48-carrier braiding machine. The program was designed so that a 60° braid angle was achieved on all surfaces with the generation of the process take-up speed assuming that all mandrel sides and bias yarns contributed equally to the calculation. The inverse solution was used to calculate the speed profile which is summarised in Figure 3.8. The output profile is coarsened to reduce the complexity of the machine input.

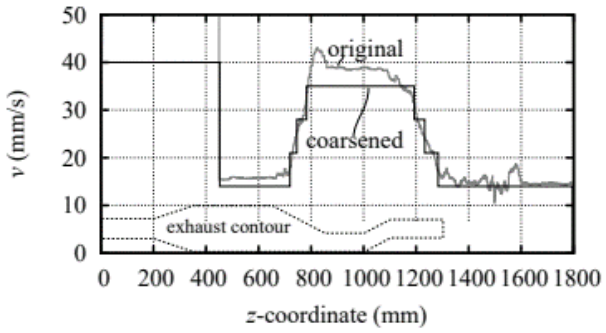


Figure 3.8 Take-up speed profile as output and coarsened for machine input. [43]

Simulation outputs indicated that the coarsening steps resulting in an increase in braid angle at 5°. This emphasises the importance of refining a program with a sufficiently small coarsening step to increase the accuracy of results. During the physical braiding of the geometry, minimal slip was observed for the triaxial braid. This contrasts with a biaxial preform manufactured on the same mandrel where slip was observed. The only observed slip occurred at the sharp corner edges of the mandrel. Figure 3.9 shows the braid angle along the length of the mandrel for each side of the preform as shown with numbers 1→4, this corresponds to the sides shown in Figure 3.7.

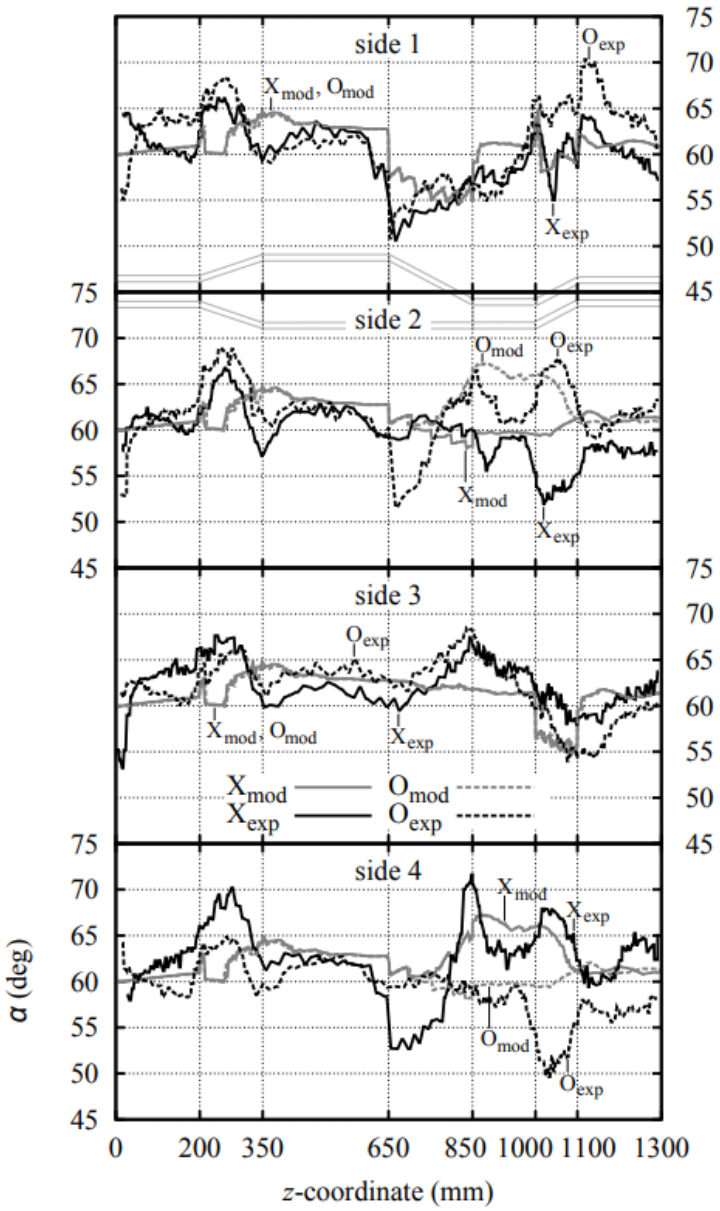


Figure 3.9 Experimental and Modelled Braid Angle Values: X for warp & O for weft for Modelled (mod) and Experimental (exp)

Braiding on a diverging cross-section, between a Z-coordinate of 200-400mm, saw a rapid increase in braid angle that exceeded the modelled value. The main reasoning for this is presumed to a reduced convergence length in comparison to the model. Similarly, braiding on a converging cross-section resulted in a deviation from modelled braid angle however the lagging effect is smaller as the convergence zone length does not decrease at the same magnitude. Braid angle agreement was good on the longest constant section of the mandrel. The braid was also found to be affected by eccentricity in the 850-1000mm section. For non-tapered regions the model

showed good agreement to the experimental values, around 3°. The tapered regions showed a variation of approximately 7°.

3.2.2 Guide Ring Studies

Ebel demonstrated the deviations in braid angle on a rectangular mandrel with the use of a circular guide ring. Figure 3.10a shows the rectangular mandrel with high aspect ratio orientated in the centre of a circular guide ring. The braiding machine was programmed at a constant speed to achieve a constant braid angle as shown by the blue line in Figure 3.10b. The change in yarn path as a result of the high aspect ratio is shown with the red and black lines. It was proposed that deviations in braid angle on a non-cylindrical mandrel can be controlled by using an elliptical guide ring [44].

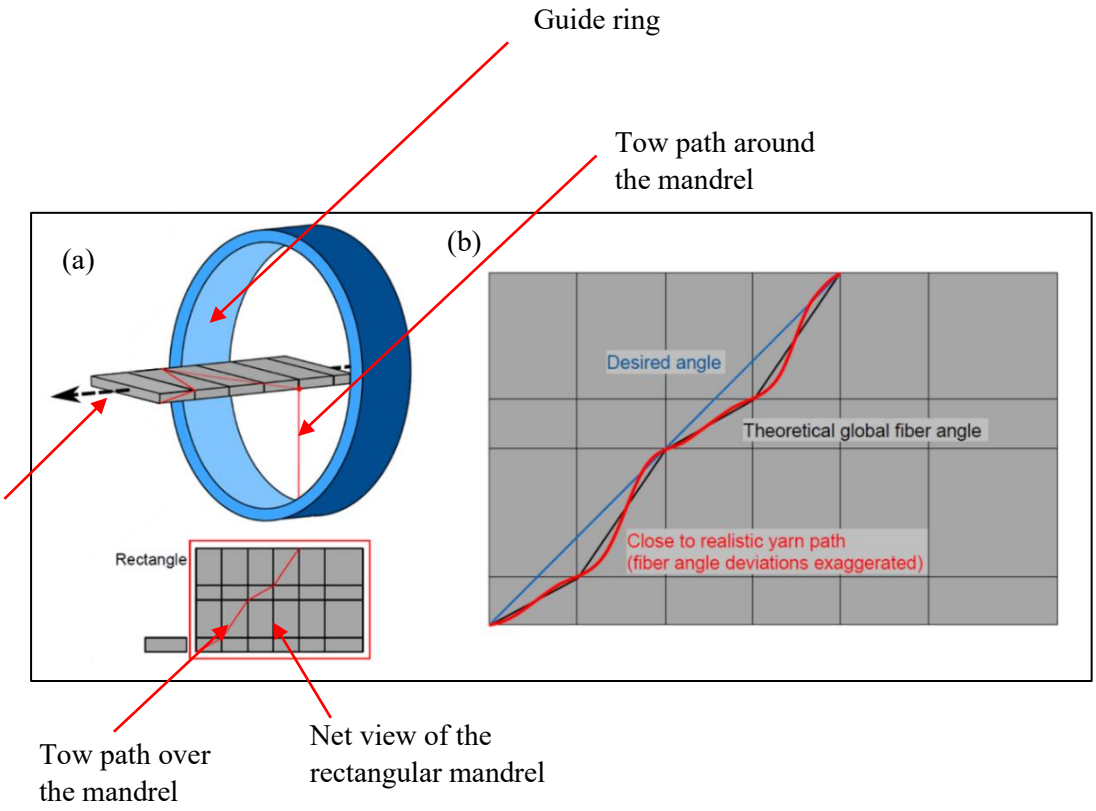


Figure 3.10 Realistic Yarn Path on a Rectangular Mandrel with Circular Guide Ring

Figure 3.11 and Figure 3.12 present the results from experimental trials where a rectangular mandrel was processed through three different elliptical guide rings and a circular guide ring acting as a reference, in both a parallel and normal orientation respectively. The results clearly identify the normal orientation as the optimum

processing method with a maximum deviation of 6° in contrast to a 11° deviation for the circular guide ring.

In parallel orientation in Figure 3.11 five measurements are taken along the top, one on the right, five on the bottom and one on the left moving around the circumference of the mandrel in a clockwise direction.

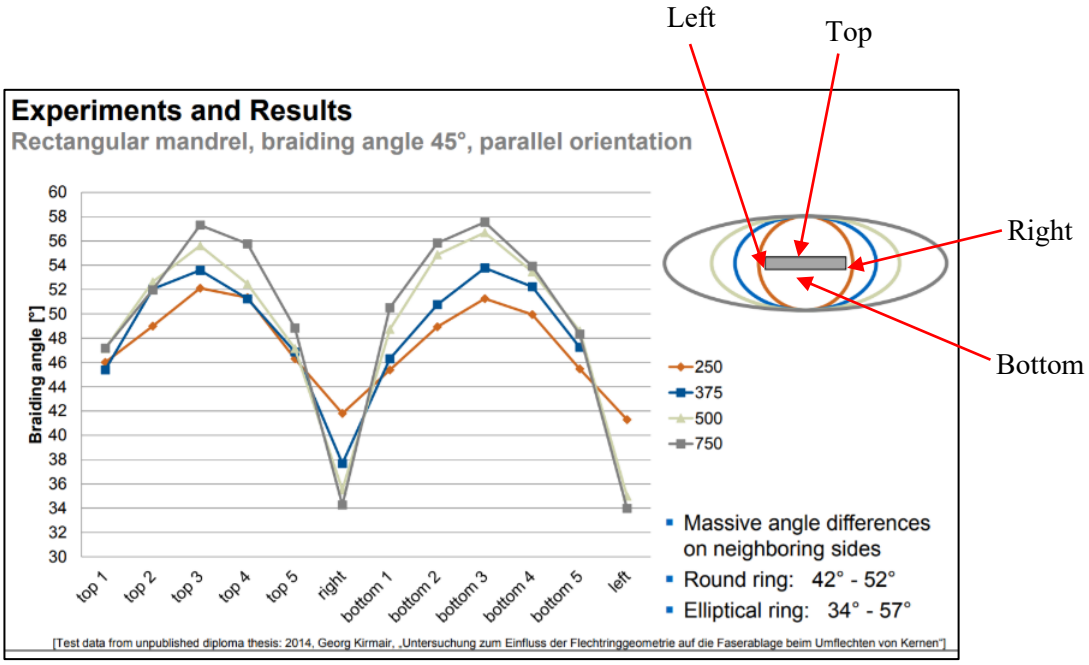


Figure 3.11 Braiding angle for rectangular mandrel in parallel orientation

In normal orientation one measurement is taken on the top, five down the right-hand side, one at the bottom and then five on the left. Like the data in parallel orientation measurements are taken clockwise around the circumference of the mandrel.

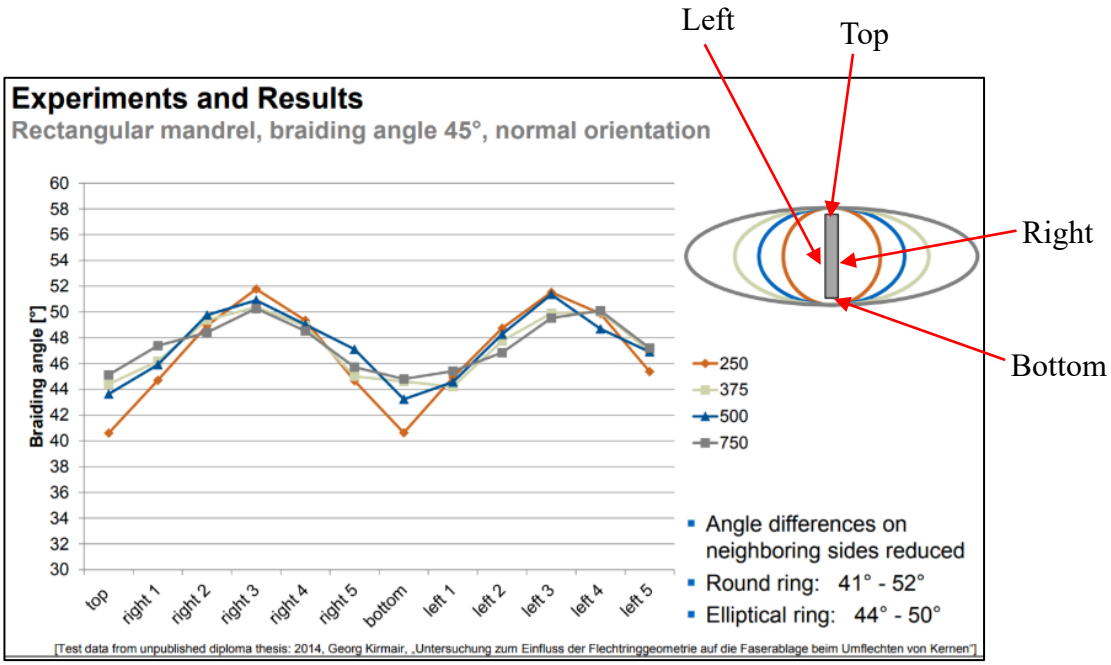


Figure 3.12 Braiding angle for rectangular mandrel in normal orientation

The application of an elliptical guide was also studied by Nishimoto. This was designed to provide more fibres towards the longitudinal direction of the component [45], a method was presented to predict the braid angle in these circumstances. Guide ring geometries can be manipulated to influence the braid architecture. Fouladi used elliptical guide rings to control the braid angle to control the braid angle on every side of a complex mandrel with flat faces [42]. This investigation demonstrates that altering the shape of the guide ring significantly alters the braid architecture. A suggested application of this is for non-uniform loading conditions where the braiding angle of each side of the mandrel can be adjusted to allow the required load conditions. Fouladi and Nedoushan developed this by proposing formulae for the braid angle prediction for flat mandrels based on the distance of fell point from the guide ring [41]. It has also been affirmed that the 'taper angle' of the braid cone influences the braid angle. Na et al. used a concentric guide that can be moved forward or backward to control the angle of the braid cone, preventing premature touching of the fibres onto the mandrel. The importance of a guide ring was emphasised as premature contact of the fibres to mandrel reduces the control of the braid pattern and introduce defects to the preform [46].

Work at the NCC detailed an approach to braiding a large hydrofoil geometry using a series of increasingly complex mandrels to de-risk the activity [47]. Figure 3.13

shows the progression of the test geometries used during the development study. The purpose of the test geometries was to isolate the individual geometric shape qualities.

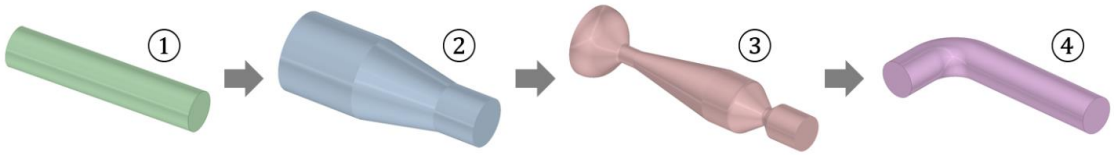


Figure 3.13 Mandrel Progression in the Capability Development Program

A 315mm diameter straight pipe, mandrel 1, was braided both centrally and eccentrically/ non-centrally with respect to the guide ring. The manufacturing set-up for the eccentric configuration is shown in Figure 3.14.

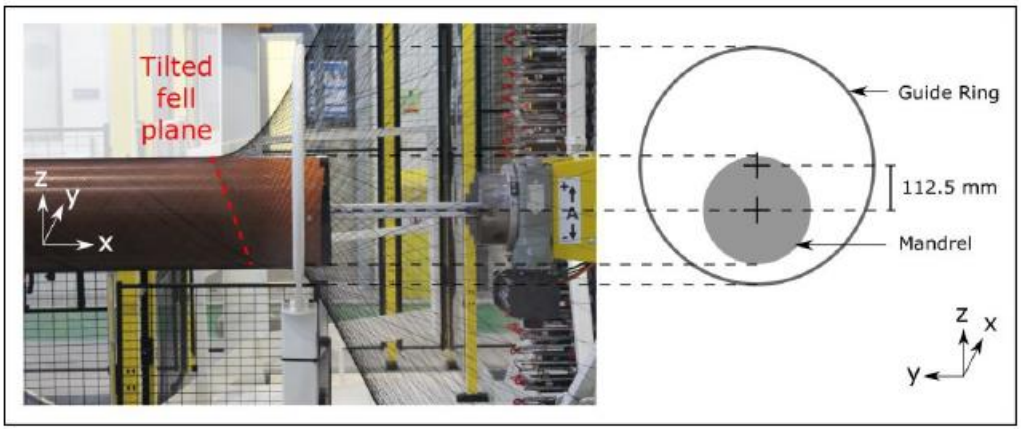


Figure 3.14 Manufacturing Set-Up for Eccentric Braiding

Machine parameters were programmed such that a constant 45° braid angle is achieved along the preform length. Braid angle measurements were taken at intervals along the mandrel on the top, bottom, and side surfaces. Both top and bottom surfaces saw significant deviation from the predicted braid angle. This is shown Figure 3.15.

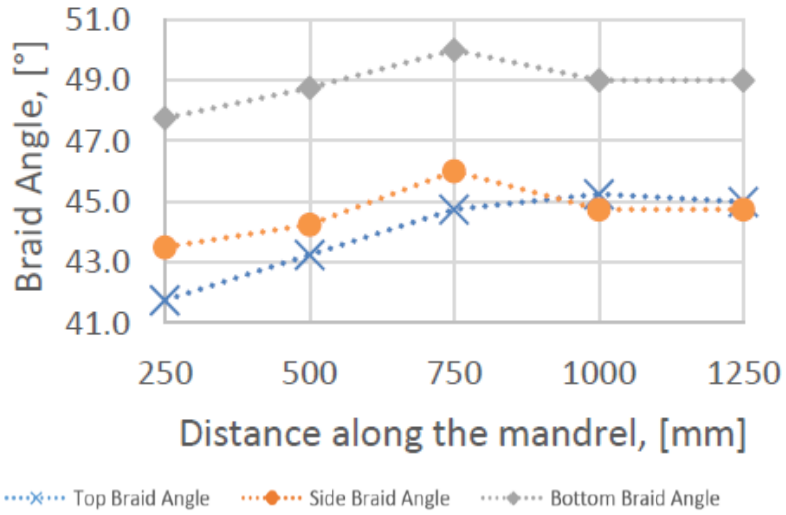


Figure 3.15 Measured Braid Angle for Eccentric Braiding

In summary, there are more considerations that are required when braiding on a complex geometry including braid direction and the step-change required to avoid coarsening the step profile too much so that the braid quality is impacted. The step profile is defined as the number of specific locations along the mandrel that the speed is defined for. Further work is required to understand the magnitude of deviation when braiding complex geometry and the variability in key process variables. The programming of complex braided parts does not currently account for the change in convergence length introduced by a cross-sectional change.

3.2.3 Process-induced fibre damage within braiding

Various methods of quantifying fibre damage have been proposed in literature. During the braiding and winding manufacturing processes. The carbon fibre tows are subjected to many sources of damage, fibre damage evolves throughout the process. This must be managed to avoid a detrimental impact to the final product. Ebel states that the quality of the braiding process is highly dependent on the quality of the rewinding stage. With lower damage levels during rewinding resulting in a lower rate of braiding errors during manufacturing. The influence of yarn tension and number of contact points during rewinding on the degradation of the braiding yarn were both studied and increases in both were found to increase filamentisation [48].

Calba presented an experimental approach to quantify the influence of the rewinding and braiding processes on the degradation of 12K carbon fibres tows [24]. Damage was found to initiate during the rewinding step and then increase during the braiding stage of the process. One of the process parameters analysed was the rewinding speed. Tensile tests and visual inspection were used to measure damage for both a low speed and a high speed. For the visual analysis, a scan of a specific length of fibre was imported into ImageJ, the damage free area was then selected and a ratio of damage area to total area was calculated. High speed rewinding was found to cause greater degradation than low speed rewinding, higher speed rewinding results in greater friction between the tows because of inter-yarn contact.

The influence of braiding tension was analysed by comparing two carrier springs of different stiffness, Braid 1 1.15N and Braid 2 2N. Both braids were biaxial with a 45° braid angle on a 144-carrier braiding machine. Carbon fibre tows were extracted before the braiding point. Interyarn friction significantly contributed to tow degradation at this stage. Figure 3.16 shows that there was a visible increase in fibre damage both in the braid cone and final preform of Braid 2 which used the higher stiffness spring. Image analysis methods using ImageJ were used to quantify the levels of tow degradation on carbon fibre tows extracted both post-rewinding and post-braiding. The results demonstrated that damage evolution starts after the rewinding stage, but this has low impact on the tenacity, which is defined as tensile strength per unit linear density. The rewinding tension was determined to significantly influence damage incurred during rewinding.

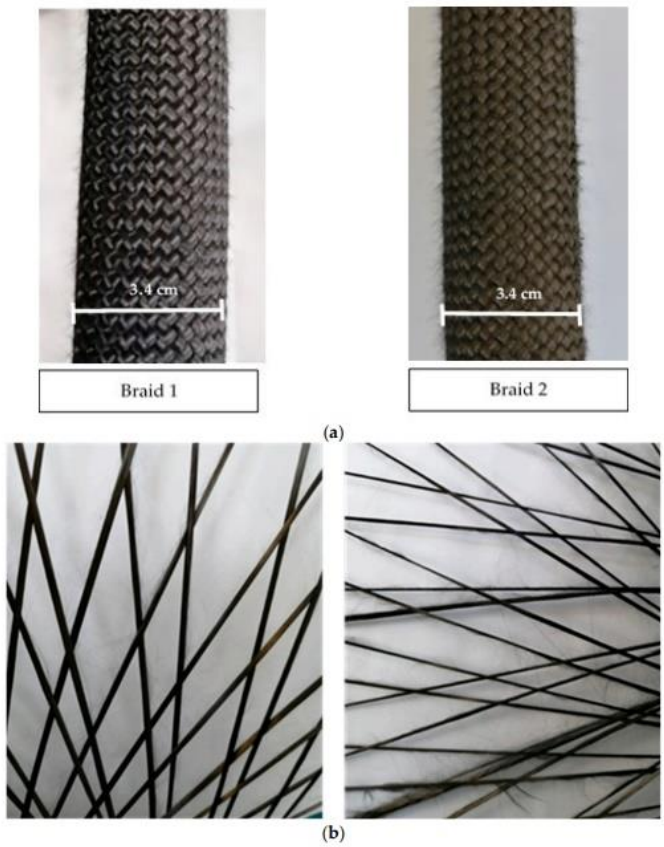


Figure 3.16 Braid Production using different spring stiffness (a) braid appearance, (b) carbon tows in braid cone [24].

A 15% degradation was measured in the braid manufactured with the stiffer spring compared to 8% degradation for Braid 1. Tensile testing of fibres demonstrated a 27% reduction in tenacity for the braided preform manufactured with the stiffer spring in comparison to virgin fibres.

According to Falzon and Herszberg fibre damage incurred during the braiding process can lead to a 20% reduction in tensile strength [49]. Fibre tow tension properties were studied for both pristine and braided tows. The SACMA SRM 16R-94 standard test method for tow tensile testing of carbon fibres was used, the specimens were 200mm in length and assumed to have an elliptical cross-section. Five specimens of both the braided tow and virgin tow were tested. A knockdown in average tow tensile strength from 3580MPa for the virgin tow to 2888MPa for the braided tows were recorded. This is a percentage knockdown from the manufacturers data of 14.8% for the virgin tow and 31.3% for the braided tows.

3.2.4 Testing of Fibre Damage

Ebel presents a numerical system for quantifying yarn damage which are summarised in Table 3.1 [48]. This is based on visual inspection and as a result is subjective depending on the reviewer as distinguishing between levels is difficult. The damage levels range from undamaged to broken yarns.

Table 3.1 Visual Damage Inspection Scale

Damage Level:	Description:	
0	Virgin Fibre: - Directly from the bobbin - Coherent sizing and no broken filaments - Glossy and reflective	
1	Sizing Degradation: - Sizing mostly lost - Matt surface finish - Irregular yarn width but no broken filaments	
2	Single broken filaments	
3	Bundles of broken filaments	
4	Severe Yarn Damage: - Yarn disintegrated into separate bundles - No well-defined surface	

5	Broken Yarn	

Ebel also suggests a gravimetric test [48]. A test segment of a yarn is weighed in its dry state. It is then immersed in water for 30 seconds. The yarn is then removed from the water and allow to drip-dry for 10 seconds and then reweighed. The percentage difference in weight is then calculated. A higher uptake in water is indicative of greater fibre damage. An increase in damage levels was seen resulting from increased tension. There is a high standard deviation in measurements. This test method is comparative between test conditions and does not provide a qualitative level of damage. This gravimetric test was utilised to demonstrate the evolution of damage during the braiding process in a capability development study at the NCC [47], Figure 3.17. At both rewinding and the subsequent braiding stages of the process an increase in % weight increase was recorded for carbon fibre. This was irrespective of the braid angle or whether the preform was braided in a non-central/eccentric position in the guide ring.

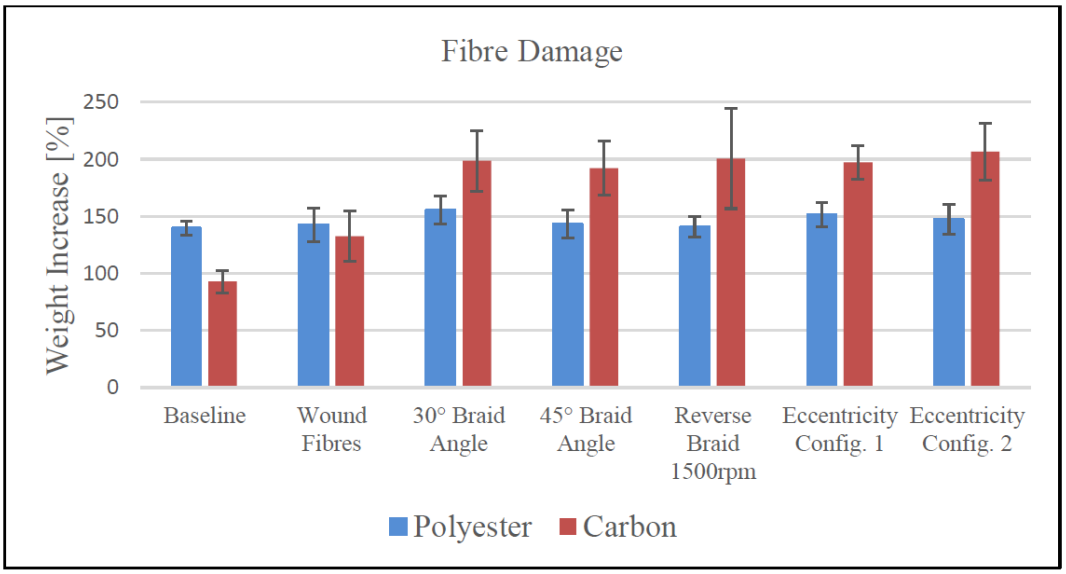


Figure 3.17 Gravimetric Test Results [47]

Dandy proposed a concept for counting the filaments within a carbon fibre bundle using an electrical impedance measurement. The electrical impedance was measured

for tow bundles between 1-20 filaments at lengths of between 80-300mm. The diameter of the tow bundle was measured to within 3% of the approximated diameter using a scanning electron microscope. When filament breakage occurs, the filament is no longer continuous between the connection points and tow cross-sectional area is reduced. A larger increase in measured impedance from predicted value based on known filament count indicates greater fibre damage. However, the accuracy of this method has not been quantified for tow bundles of high filament count such as carbon fibre bundles which consist of thousands of filaments [50]. Mechanical methods can be used to quantify yarn damage. The tensile strength of a dry fibre with damaged filaments will be lower than that of a virgin fibre. Testing the tensile strength of a fibre can also indicate fibre damage. However, mechanical methods do not offer a non-destructive testing method and fibre extraction from the preform can cause greater levels of damage.

3.2.5 Infusion of Braided Preforms

Variations in the permeability of braided preforms can lead to a non-uniform resin flow pattern during the infusion process [51]. Permeability measurements were recorded on 2D biaxially braided glass fabrics at three different braid angles, 35°, 45° and 50°, each preform contained four layers of braid. For each braid angle, three different volume fractions were measured: for 35°, 67%, 75% and 85%. At 45° and 50°, 55%,67% and 75% were used, this was due to geometry limitations. As braid angle increased from 35° to 45° the permeability increased, between 45° and 50° a reduction in permeability was recorded, this is summarised for two different fibre volume fractions in Figure 3.18 as both 67% and 75% volume fraction had date points between 35-50°.

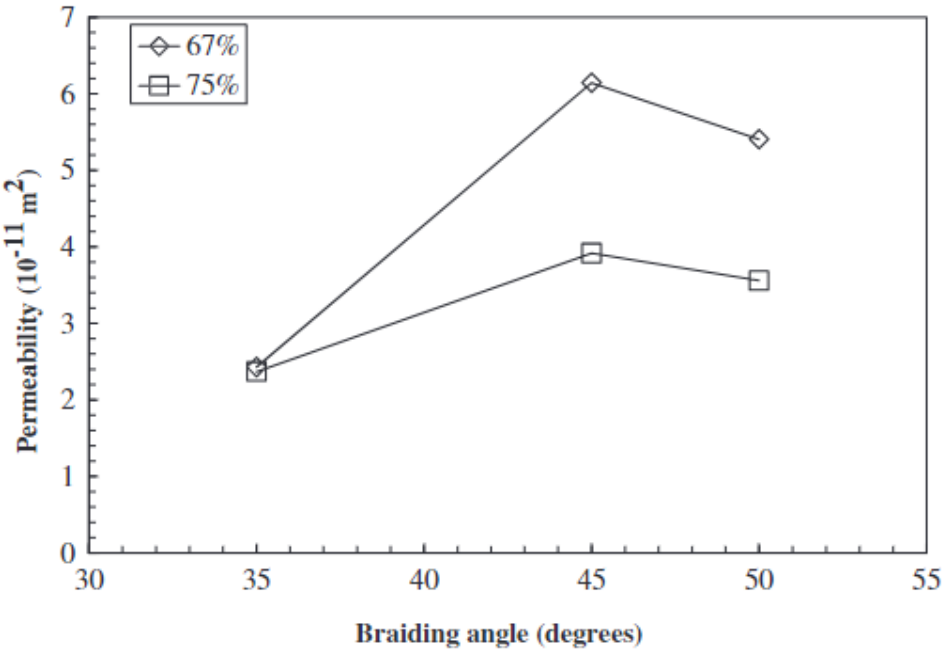


Figure 3.18 Permeability as a function of the braid angle for different volume fractions [51]

Swery analysed the effect of mandrel geometries and braid configurations on the filling time of the preform [52]. The study used a triaxially braided glass fibre structure with 3300tex Sigrafil C30 carbon yarns in the axial direction and PPG1383 300 tex E-glass yarns in the bias direction. This architecture has been used extensively in the BMW I and 7 series models [53]. The mandrel geometries used by Swery are shown in Figure 3.19.

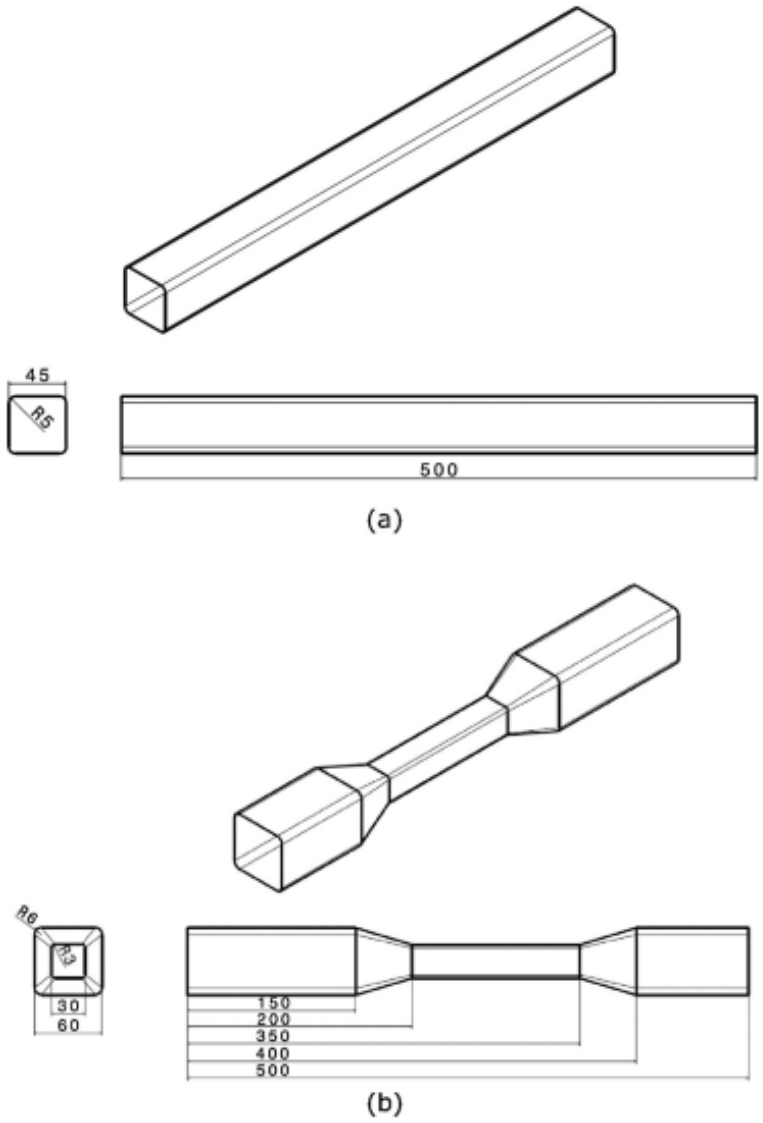


Figure 3.19 Mandrel geometries used (a) Constant square cross-section (b) Varying square cross-section.

A complete simulation tool was developed to predict the manufacturing process with permeability predictions and filling simulations to predict the resin flow front. This was completed for a range of mandrels braided with different processing parameters. The braiding simulation identified that variations in yarn spacing were more significant when braiding (b) due to the complex part geometry. This results in regions of irregular permeability. Axial permeability was found to increase with increased yarn spacing.

At a constant injection pressure, preforms with more significant nesting resulted in a higher filling time. Incomplete infusion of the preforms led to dry spots and inherent weaknesses in the structure [52]. Xiao also noted large resin pockets in braided composites with large tow sizes which leads to non-uniform properties [54]. The triaxially braided preforms were manufactured using 80K Fortafil axial tows and 12K Grafil fibres for the bias tows. The braids were manufactured by A&P, the composites were manufactured through RTM. These localised resin pockets arise due to the nesting of fibres and can be seen in Figure 3.20.



Figure 3.20 Micrograph of the Cross-Section of Triaxial Composite

Long modelled the permeability of braided preforms which was then validated experimentally using a 48-carrier braider and radial injection method [55] However, this model neglects tow path curvature. This would limit the use of the model on geometries with abrupt section changes. For tubular preforms, tow spacing increases as braid angle reduces creating flow channels which increase permeability.

3.2.6 Characterisation of Mechanical Properties

3.2.6.1 Braided Composite Testing Methods

It is argued that flattening of braid samples can introduce defects in the braid geometry such as angle deviations. Fibre continuity is lost when the samples are cut [56].

Characterisation of braided composites is complicated by the complex preform architecture as conventional testing methods do not always yield reliable results. Historically, testing straight sided coupons leads to a much lower transverse tensile strength than expected due to premature edge-initiated failure. Full-field strain measurement supports this demonstrating accumulation of edge damage prior to full failure, Figure 3.21, this can be seen by the four split points identified in the image.

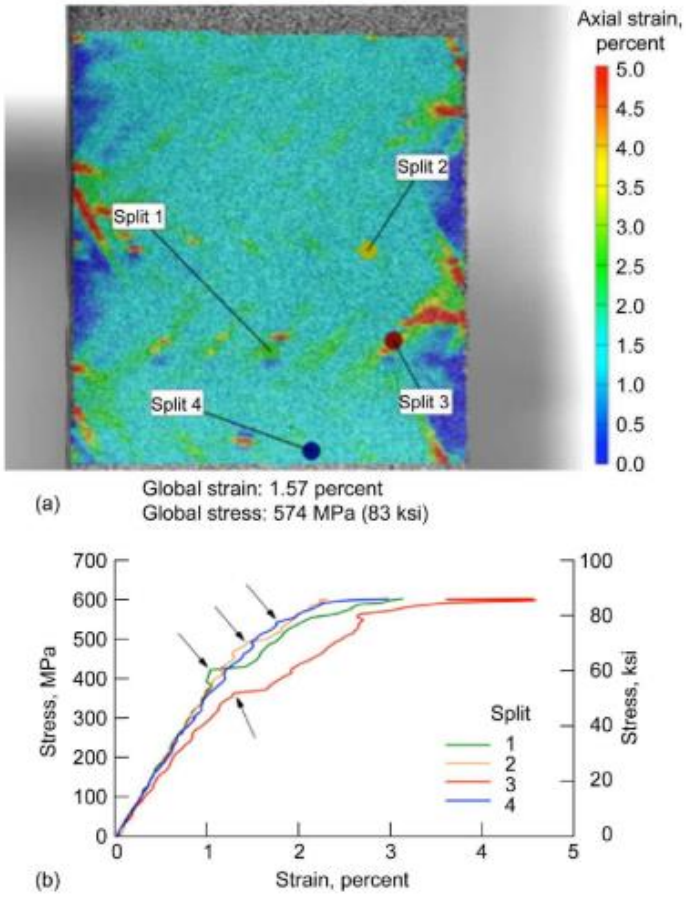


Figure 3.21 Full field strain data showing edge initiation.

Roberts and Salem used high speed video to capture the edge initiation in testing coupons [57]. Bowtie and notched specimens provide a non-uniform stress and strain field in the failure region. Testing tubes eliminates the edge failure and yields more comparable values [58]. The transverse tensile strength measurements are much higher than those of a straight sided coupon as the peak stress occurs near the mid-plane of the part. As a result, the small edge stress reduces the chance of an edge-initiated failure.

Work by Roberts and Salem used 2D triaxial braids with a 0°/60° bias architecture to develop more reliable test methods for braided composites. The preforms themselves had near equal fibre volume fraction in each of the fibre directions. Flat composite panels were manufactured using RTM with six layers of braid, measuring 3.18mm thick. Axial and transverse properties of the composite panels were tested. The failure strength of a straight sided coupon was measured as 462 MPA. Tensile testing of

straight sided coupons has some limitations for braided composites as shown in Figure 3.22.

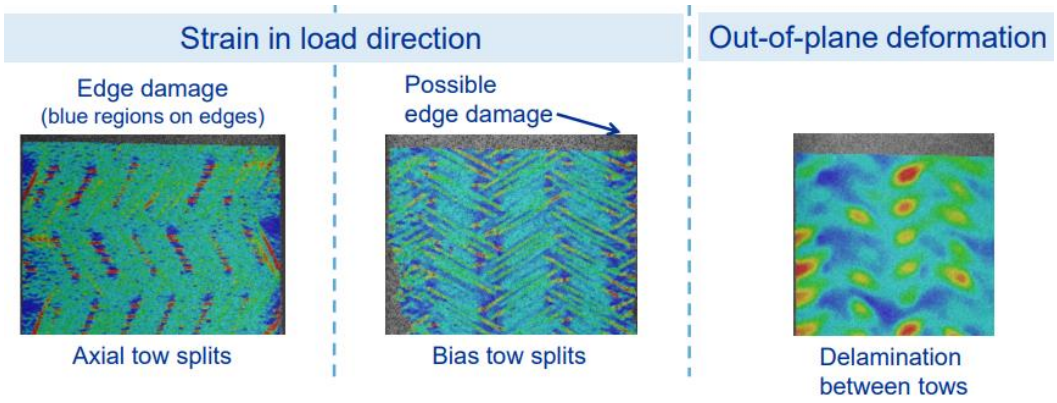


Figure 3.22 Examples of problems testing straight sided coupons

Composite tubes were also manufactured through RTM with a 9.9cm diameter and 3.2mm wall thickness. A comparative failure stress of 786 MPa was measured. Tubes were tested through internal pressurisation with a hoop stress of 449 MPa measured. This provides a measurement of transverse tensile strength in a nearly uniaxial load condition. Therefore, the failure is free of edge effects.

Wehrkamp-Richter et al. investigated the damage and failure of triaxial braided composites under multi-axial stress states for braid angles of 30°, 45° and 60° [59]. Digital image correlation measurement methods were used to identify and locate failure mechanisms, damage initiation and development. A high-speed camera was used to capture the dynamic nature of the failure. Figure 3.23 shows the high-speed camera images for tests completed in the axial, fibre, and transverse directions for each braid angle.

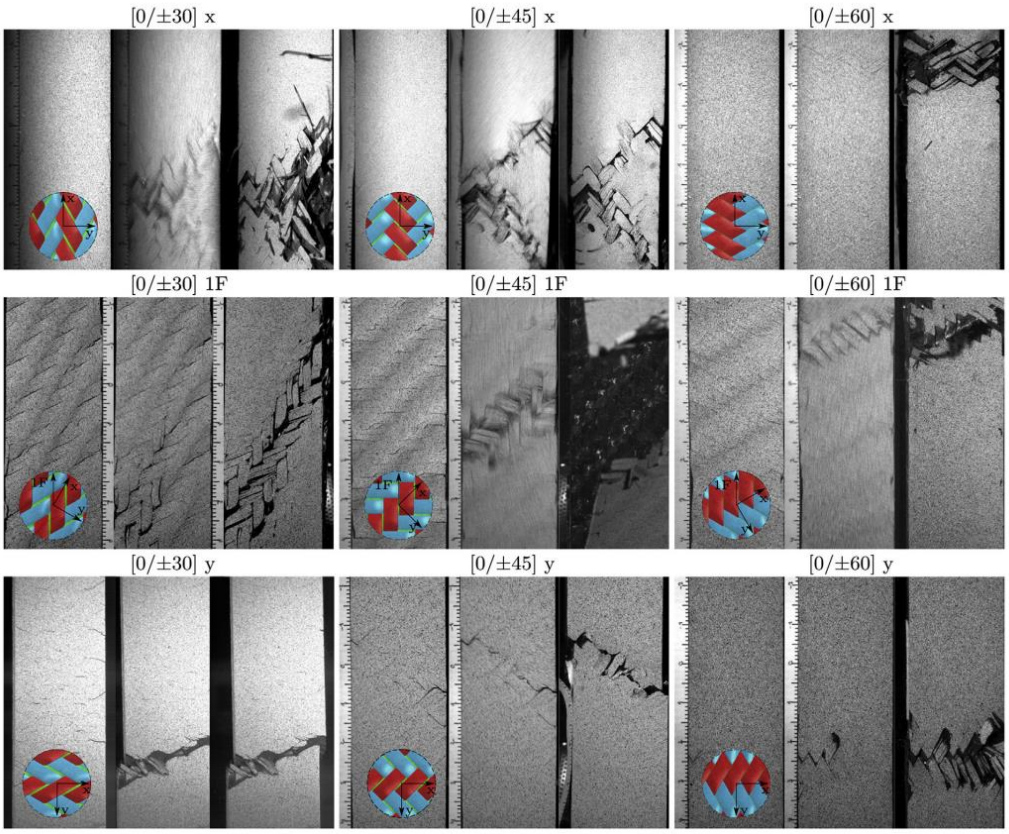


Figure 3.23 Final failure images for axial, fibre and transverse directions using a high speed camera

Untwisted HTS40 12K fibres were used for both axial and bias yarns. Composite panels of four layers were produced of each architecture and straight sided coupons in accordance with ASTM D3039 were cut. To remove the influence of edge effects a coupon width of 25mm was selected to cover a minimum of two-unit cells.

Non-linear failure behaviour was exhibited in the mechanical response prior to final failure in each test case. This behaviour is attributed to two characteristic mechanisms. The progressive development of matrix cracks in the yarns which were not aligned with the direction of the load. The natural structure of a triaxial braid structure acts as a natural crack arresting grid which limits the propagation of cracks to within yarn intersection points. As a result, loads can be redistributed without catastrophic failure. Crack deflection increases energy absorption; therefore, the braids can withstand a high strain failure even if a large proportion of the surface is saturated with matrix cracks. In the braid yarn direction, where fibres were heavily undulating, composites failed due to large scale delaminations along with the

progressive pull-out of fibre bundles. This was determined to be due to yarn straightening. Final failure of both 30° and 45° coupons was triggered by the rupture of axial yarns, the high amount of energy release resulted in several other fibre bundles failure. Whereas 60° coupons failed due to the rapid crack propagation across the specimen immediately before final failure.

Carey summarises test methods for braided composites Common testing standards for braids limit testing to mainly flat coupons [3]. These are summarised in Table 3.2.

Table 3.2 Summary of test methods for braided coupons

Property Type	Test Standard	Coupon Geometry	Mechanical Properties Acquired
In-plane Tensile	ASTM D3039	25.4mm width 127mm gauge length End Tabs preferable	- Tensile elastic modulus - Ultimate tensile strength - Ultimate tensile strain - In-plane Poissons ratio in tension.
Flexural	ASTM 6272	Depth 3.2mm Width 12.7mm Length: Depth, 40:1	- Flexural strength - Flexural modulus of elasticity
Shear	ASTM D4255/D4255M	V-notched coupon	- Shear modulus - Ultimate shear stress/ultimate strength
Compression	ASTM D3410, ASTM D6641-09	Width 25mm Gauge Length 15mm	- Compressive elastic modulus - Ultimate compressive strength

- Ultimate compressive strain
- Poisson's ratio in tension

For tensile testing, according to ASTM standard testing there should be at least two-unit cells a within the gauge section. The gauge length is recommended to be 127mm. Samples should be tested at a constant strain rate and end tabs are strongly recommended to avoid edge damage. This is particularly important when many fibres are in the direction of loading.

ASTM 6272 by three or four-point bending is recommended to evaluate the flexural properties of braided composites. The length-to-depth ratio of 40:1 should be used for most high strength fibre reinforced materials. The specimen width for a thickness of 3.2mm or less should be 12.7mm. Ohtani demonstrated that the flexural elastic modulus decreases as the braid angle increases [60]. This study was completed on tubular braids manufactured with a braid angle of 30°, 45° and 60°. Similar results were attained by Tate et al using the three-point bend configuration. Braided composites were manufactured with 25° and 30° braid angle.

Shear properties are characterised using either an Iosipescu beam V-notch test (ASTM D5379) or ASTM D4255, a standard two- or three- railed shear test.

Compressive properties of braided composites are evaluated using ASTM D3410 or D6641. The tests methods differ through their force transfer mechanism. ASTM D6641 using combined shear and end loading to produce a compressive force, whereas ASTM D3410 produces a compressive force via shear the interfaces of the wedge grips. A limitation of D6441 is that it can only be used on composites where no more than 50% of the yarn content is in any one direction.

Braiding industry leaders such as A&P have developed their own test standard modifications for testing QISO braided fabrics, these are informed by A&P's extensive manufacturing expertise [61]. For longitudinal tensile testing a modified version of ASTM D3039 is used. The specimen width is adjusted to 3.58mm to allow for a minimum of four-unit cells of the braid to fit across the width. It is also

recommended that specimens are tabbed to prevent damage due to the test grips. Figure 3.24 shows the coupon geometry.

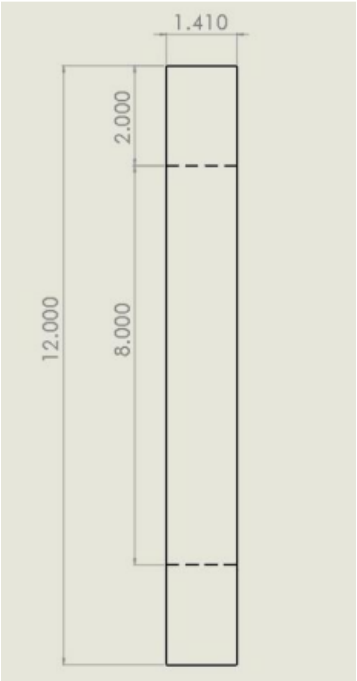


Figure 3.24 A&P Test Modification for Longitudinal Tensile Testing [61]

The same size coupon is used for transverse tensile test. A modified notched coupon is used to acquire tensile strength however due to the complex strain field of this coupon transverse modulus should not be calculated using this coupon. This is because edge effects result in artificially low strength data particularly in the transverse direction as none of the reinforcement spans from grip to grip, instead terminating at the edge. The notched coupons have been developed for this.

For compression testing ASTM D6641 is used, it is recommended to tab these with a gauge width of 1.27mm exposed. This is shown in Figure 3.25.

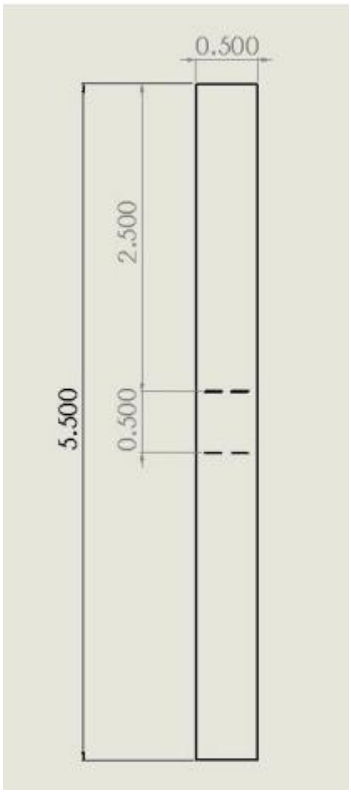


Figure 3.25 A&P Coupon modification for compression testing [61]

ASTM D7078 is used to calculate the longitudinal and transverse in-plane shear. Tabbing is not required if excessive crushing does not occur. The geometry is shown in Figure 3.26.

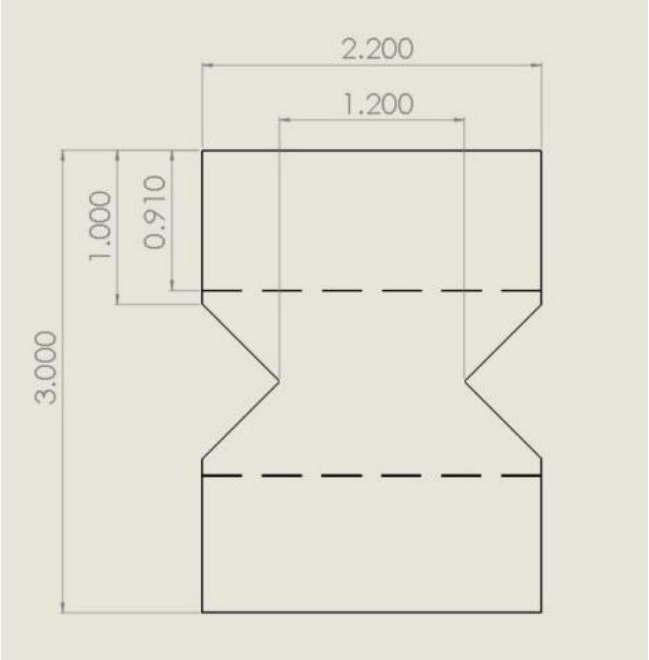


Figure 3.26 A&P Coupon modification for longitudinal and transverse in-plane shear [61]

3.2.6.2 Test methods for tubular braided composites

The test methods summarised in Section 3.2.5.2 refer to flattened specimens. Cutting samples can cause fibre distortion. Therefore, several researchers have performed tests on tubular geometry [3]. It is found that the unit cell of a braided preform becomes sensitive to curvature at a radius of curvature smaller than 500mm. As a result, a radius of curvature of 500mm is considered a flat unit cell. A mathematical predictive model was developed by Ayranci and Carey to account for this effect of curvature along with the development of mechanical testing methods for tubular braids. Ayranci and Carey performed tensile tests on tubular braided composite samples. Tests were performed on samples of inner diameters ranging from 7.13mm-10.21mm and a 152.4mm length. High strength epoxy was used to attach end tabs to the samples. This test method is suitable for small diameter braids. Tubular braids have also been studied using compression testing. Tubular braids of three different diameters were used in this investigation to validate a curved-unit cell predictive model. The tubular specimens were manufactured using Kevlar 49 fibre and Epon 825/Ancamine 1482 curing agent. The longitudinal testing results are summarised in Table 3.3 [62] [63].

Table 3.3 Longitudinal Elastic Modulus Data for Tubular Specimens

Outer Diameter, mm	Braid Angle, °	Thickness, mm	Experimental Longitudinal Elastic Modulus, GPa	Predicted Longitudinal Modulus, GPa
10.21 ± 0.04	54.06 ± 0.51	0.28 ± 0.00	3.95 ± 0.42	4.12
8.61 ± 0.05	51.44 ± 0.72	0.30 ± 0.13	3.87 ± 0.24	3.98
7.13 ± 0.01	48.06 ± 0.88	0.29 ± 0.00	4.83 ± 0.15	4.48

Compression testing showed two contributing failure mechanisms, diamond shaped buckling of the tube and fibre micro-buckling. Carey and Ayranci studied the behaviour of braided tubes in torsion using braids of varying inner diameter [64]. Samples were manufactured using Kevlar 49 fibres with Epon 825/Ancamine curing 1482 curing agent. Specimens were tested under torsional loading using an MTS-Torsion Master testing machine equipped with a 2Nm load cell. There is no is specific ASTM standard for torsional testing of braided composite, however a 0.03°/s loading rate as suggested by ASTM D5448 was followed designed to achieve specimen failure within 1-10 minutes. The results along with the comparison to the predictive model for curved until cell geometries are summarised in Table 3.4.

Table 3.4 Shear Modulus Data for Tubular Specimens

Outer Diameter, mm	Braid Angle, °	Thickness, mm	Experimental Shear Elastic Modulus, GPa	Predicted Shear Modulus, GPa
10.19 ± 0.05	53.46 ± 0.38	0.28 ± 0.01	11.19 ± 0.57	12.01
8.59 ± 0.04	51.56 ± 0.51	0.30 ± 0.01	11.59 ± 0.46	11.90
7.07 ± 0.04	47.64 ± 0.53	0.30 ± 0.01	12.32 ± 0.40	12.50

3.2.7 Using Simulation to Determine Mechanical Properties

Early braiding studies show a correlation between braid angle and the strength and stiffness of the braid [65]. Dauda supported this idea, their investigation into the effect of fibre orientation on the mechanical properties of braided components identified that controlling the braid angle and pick density of braided composites allows the properties of the component to be optimised to suit the application. Pick density refers to the number of fibre intersections in a specified length of preform. This was shown experimentally via the characterisation of tensile and flexural moduli with standard test specimens. An important conclusion from this research was that braided fabrics exhibit non-linear stress-strain behaviour. Increasing the pick density was found to increase both flexural and tensile modulus and strength [66].

A study on triaxial braids was completed by Masters which compared experimental results with an analytical model [67]. A 144-carrier braider with an additional 72 axial tows were used to produce samples with a regular 2/2 braid pattern on a cylindrical mandrel. Three different braid geometries were studied in this investigation this is summarised in Table 3.5. Once cut from the mandrel, these samples were then infused with a Shell 1895 epoxy resin for a flat fabric in RTM moulds.

Table 3.5 Material architectures

Material	Braid Pattern	Bias Yarn Size	Axial Yarn Size	Number of Layers	Mandrel Diameter/inch
A1	0/±63°	12K	24K	4	5.5
B1	0/±66.5°	6K	18K	5	4.8
B2	0/±70°	6K	18K	5	5.25

Three methods were compared to experimental data. A laminate model was the most simplistic modelling approach and ignored the undulation of braid yarns. Another model applied a correction factor to the laminate analysis that accounts for braid undulation. Another mechanical model used is the diagonal brick model, the unit cell is represented as shown in Figure 3.27. The stiffness of the bars is selected such that they reflect the amount of fibre in the unit cell. Lower young's moduli estimates were provided by the diagonal brick model in comparison to laminate analysis, resulting in slightly better correlation.

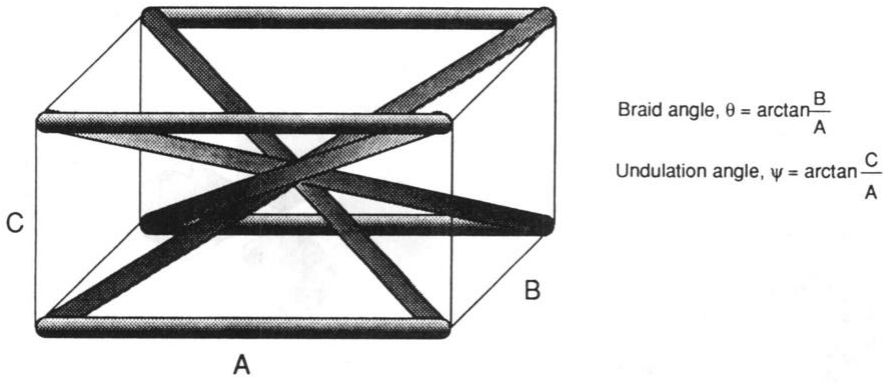


Figure 3.27 Diagonal Brick Model Representation

A finite element model was proposed. Unit cells were defined using the geometrical modelling approach which comprises of three steps; construction of mean centreline points, smoothing the centrelines with a B-spline interpolation to create a minimum strain energy and constructing a 3D object. This unit cell is subdivided into 9 sub-cells. A stiffness matrix was then proposed using appropriate boundary conditions.

The mechanical properties were determined experimentally using unnotched tensile tested. Longitudinal strengths and strains were greater than the strengths and strains

in the transverse direction. A 41% increase in longitudinal tensile strength was noted in B1 compared to B2, 80.7ksi and 57.1ksi respectively this was surprising due to the small difference in angle being the only major difference. A 431 MPa longitudinal strength for A1 was recorded, and this was 50% greater than the transverse strength (243.4 MPa). Other observations from the work include a larger scatter in the transverse data in comparison to the longitudinal.

Overall, there were inconsistencies in the measured data which suggests that tests methods for braided composites need careful selection and modification due to the unique aspect of these materials. The models gave consistent predictions for the Young's moduli of the three architectures tested however, the agreement of transverse modulus values was not as good. This is summarised in Figure 3.28 [67].

PROPERTY	MODEL	MATERIAL A1	MATERIAL B1	MATERIAL B2	RMS ERROR
Ex	EXPERIMENT	6.62	6.55	6.31	-
(MSI)	LAMINATE	6.98	7.22	6.68	7.5%
	LAM. CORR.	6.98	7.22	6.68	7.5%
	DIAG. BRICK	6.61	6.95	6.40	3.6%
	FINITE ELEM.	6.81	6.89	6.32	2.9%
E_y	EXPERIMENT	6.59	6.45	7.03	-
(MSI)	LAMINATE	7.93	9.49	7.97	30.1%
	LAM. CORR.	7.55	9.27	7.75	27.4%
	DIAG. BRICK	7.24	9.07	7.61	24.9%
	FINITE ELEM.	7.71	9.01	7.41	25.1%

Figure 3.28 Comparison between experimental, Diagonal Brick (Analytical) and FE Model for Longitudinal and Transverse Moduli

3.3 Process Simulation of the Overbraiding Process

Process simulation has become increasingly more important in composites manufacturing to optimise composite properties, reduce manufacturing time and limit material wastage. There are multiple tools under development for braiding.

3.3.1 Types of Computational Model

Braiding simulation comprises of three different model types, analytical, kinematic, and finite element (FE) models [43]. Analytical models are typically a set of formulas on a spreadsheet formulated in such a way that key variables about the braiding process can be determined. The computational time is a matter of milliseconds; the results are not often refined enough for practical use as they neglect interyarn and yarn-mandrel interaction. FE approaches include the modelling yarn tension and interactions; however, they still involve several modelling assumptions. Yarn cross section is generally assumed as circular and broken fibres are not accounted for; this can lead to systematic errors from an FE simulation. The computational time is greater than an analytical model. An alternative approach is a kinematic model. Kinematic models neglect interyarn friction and yarn slip after deposition. The yarn path is also represented as a straight line. However, the process is advantageous in early design stages as it can be completed in a matter of seconds. Figure 3.29 summarises the computational time of each modelling approach [3].

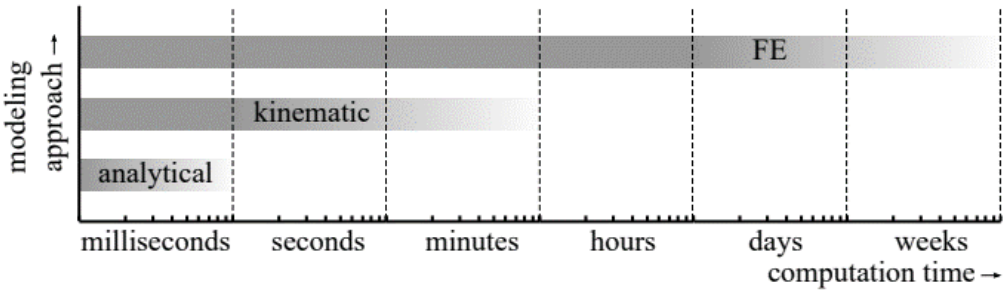


Figure 3.29 Computational time of various modelling approaches

Melenka developed a generalised analytical model of tubular braided composites which applicable for diamond, regular and Hercules braid patterns. It is designed to be easily implemented within Matlab or Python. The model was based on the geometrical and mechanical properties of tubular braided composite structures [68]. A volume average method was then applied to account for the clockwise and anti-clockwise tows within the unit cell [69]. The model used an equation for the undulation length of braid yarns in a unit cell in combination with an equation defined by Potluri et al [8]. for the volume fraction of fibres within a unit cell. For the same use case, Ayranci and Carey developed a curved unit cell model based on Classical Laminate Plate Theory [65], however this is exclusively for diamond braid

architectures. Figure 3.30 demonstrates a comparison between the two models. The model demonstrated good agreement to experimental data for both longitudinal and shear moduli.

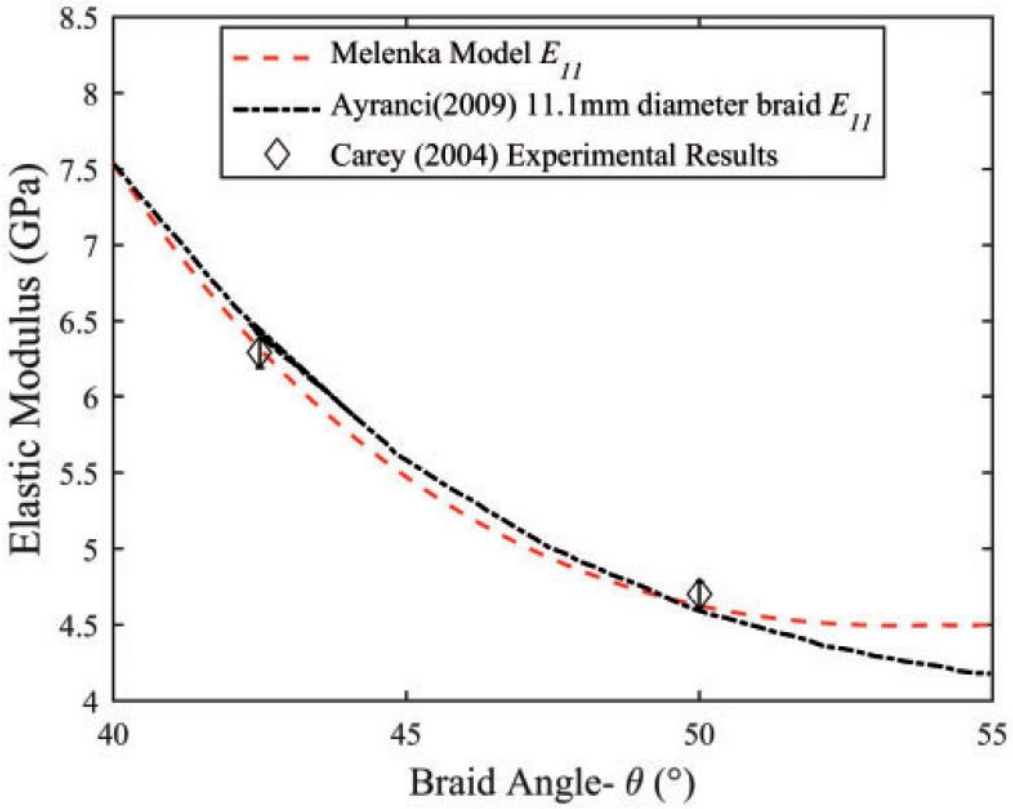


Figure 3.30 Comparison between two methods of using an analytical model to predict mechanical properties for tubular structures

This was then developed in *Braid CAM,* which is software tool designed for easy implementation. The input panels allow for entry of yarn and matrix data, including tow width and thickness which can then be used to predict mechanical properties. However, the model does not calculate the yarn geometry data. [70].

One of the earliest kinematic models for braiding is described by Du and Ko [71]. A set of equations are formulated relating convergence length and the consequent braid angle to machine speeds. Another early contribution from Du and Popper uses a kinematic model to adjust the take-up speed profile for braiding over conical mandrel, this neglected yarn friction [39]. The discrepancy between kinematic models and experimental values increases with the increasing friction levels and number of braid carriers. Zhang assumed an elliptical cross-section of the tow and did not account for any tow cross-sectional changes due to process induced yarn

deformation. According to Van Ravenhorst these assumptions are not accurate as significant yarn curvature is present in the convergence zone. Lateral compression from adjacent yarns also results in a decrease in yarn width. Van Ravenhorst et al. [72] uses process kinematics to model the change in cross sectional shape and represent the double curvature of the convergence zone. Yarn interaction including friction is modelled. A steady state process is modelled with a constant friction coefficient of 0.3. This results in a reduction in simulated convergence zone length of 25% in comparison to a model without yarn interaction. Further work by van Ravenhorst and Akkerman developed an inverse solution to calculate a take-up speed from an input of fibre distribution on the mandrel for a given braid angle [73]. This was designed to reduce the iterative trial-and-error process of obtaining manufacturing parameters. The inverse kinematic solution was tested on a complex 3D non-axisymmetric, optionally eccentric geometry. The mandrel varied size, shape, and curvature across its length. The complexity of the braided mandrel is shown in Figure 3.31. This geometry has been used in other work [6].

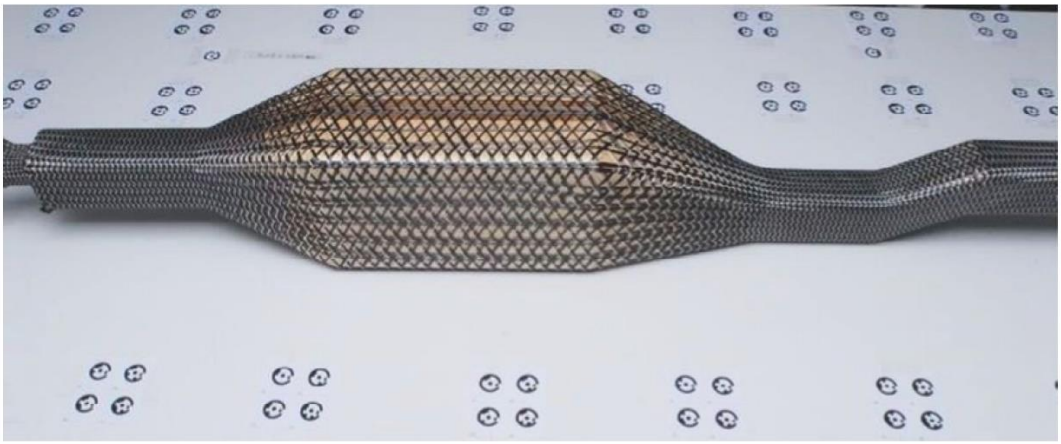


Figure 3.31 Experimental validation of inverse kinematic model [73]

Experimental validation showed the maximum angle deviation from the model was 7° due to difficulties achieving the angle on all mandrel surfaces. A typical braid angle deviation from the model of 3° was found in the centred, non-tapered sections of the mandrel. The neglect of yarn interaction between the bias tows in the convergence zone are determined as attributable for the angle deviation. Yarn interaction between the bias tows results in an increase in friction in the braid cone, consequently the angle deviates from the modelled braid angle. An FE approach is

recommended by the authors to improve accuracy; however, this is at the cost of computational time.

Software tools are being developed for kinematic braid simulation. Composites Braiding Designer is a dedicated workbench in CATIA [74] used to simulate the braiding process using process kinematics, therefore neglecting the presence of yarn friction. This tool uses a rectangular tow width approximation.

The development of Finite Element (FE) models for braiding has allowed for simple friction assumptions. Pickett et al. conducted simulations of the braiding process numerically using explicit FEM [75]. Hans et al, presents an approach for using commercial software for finite element simulation to model the braiding process for arbitrary mandrel shapes to determine the yarn alignment.

Pickett completed an investigation designed to compare an analytical and FE model on a purpose build mandrel, Figure 3.32, that was designed to have a changing cross-section with eccentric, non-eccentric, small and large sections [75].

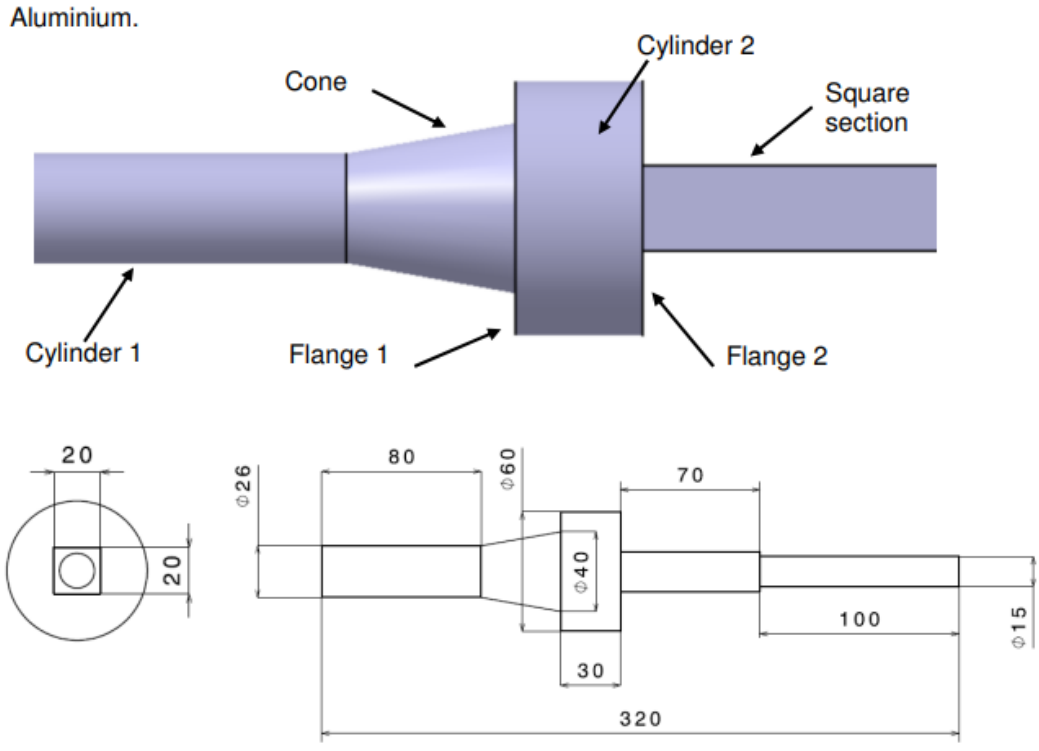


Figure 3.32 Details and dimension of the braiding mandrel used in work by Pickett

The analytical model is only valid for fully compact yarns which fit directly to the mandrel, and it does not incorporate friction or mechanical stiffness. Whereas the FE

model can implement a friction assumption and predict yarn paths and defects. However, the computational cost is considerably higher. Figure 3.33 visualises the difference in predictive yarn path for both FE simulation and analytical analysis. It indicates that the methods show good agreement for a small cylinder, but the analytical method underestimates the off-axis yarn angles. This is because the FE model and the manufacturing test capture the angle change between the braiding ring and the mandrel surface whereas the analytical method assumes this to be normal. The FE simulation accurately captures yarn slippage which occurs on the conical section.

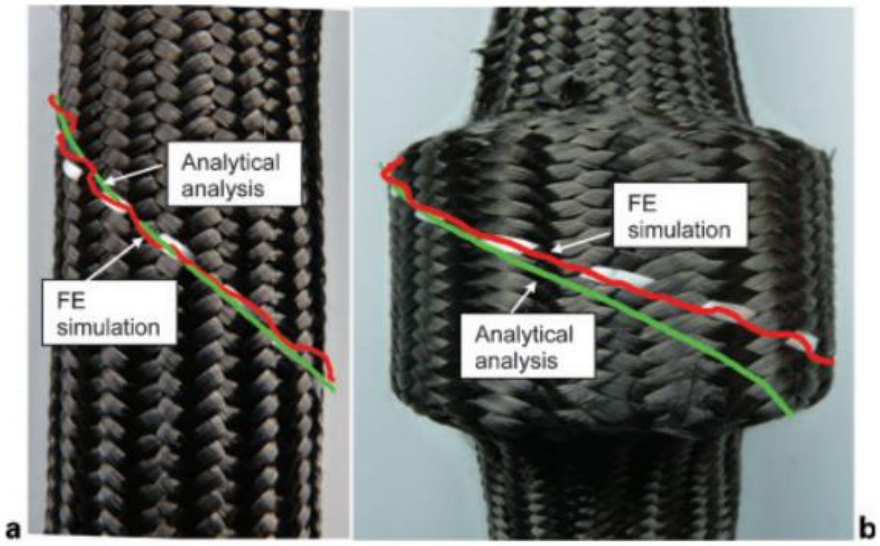


Figure 3.33 Comparison between analytical and FE models for predicting yarn path

Treviso compares kinematic simulation with an FE model for its applicability for optimising the braiding process for large axisymmetric mandrels with varying cross-section [76]. The kinematic tool utilised in this paper is Composites Braiding Designer in CATIA. It uses the imported mandrel geometry to provide a rapid solution for key process variables of braid angle, cover factor and thickness but does not account for friction or tension. The FE model proposed is a parametrised Abaqus model that is customisable by the user. A combined Kinematic-FE modelling concept is suggested which consists of two stages; the first using the kinematic tool to verify the machine set-up which enables the extraction of a mandrel path and velocity profile. The FE simulation is then run to identify the impact of interaction effects on the braid architecture including tow slip, bridging and jamming. The paper concludes

that using an optimised speed profile from a kinematic tool such as CBX reduces computational cost compared to FE models.

3.3.2 Tow Geometry Modelling

Process simulation tools have varying approaches for modelling the geometry of a braided tow. Tow geometry is a dynamic property it is constantly changing along the yarn length, this is accounted for in one of the earliest examples of kinematic models for braiding [71]. The cross-section of both braiding and axial tows in the unit cell have been assumed have a geometry described as a rectangular cross-section sandwiched by two semi-circles, this is shown in Figure 3.34.



Figure 3.34 Example tow geometry shape

Du and Ko highlight that the aspect ratio of the tow is influenced by twist to fibre [71]. With untwisted tows having an aspect ratio significantly greater than 1, slightly twisted tows having an aspect ratio greater than one and extremely twisted tows having an aspect ratio approximately equal to 1. Understanding the relationship between level of rewinding twist and aspect ratio is necessary to predict the tow geometry of a braided tow. The tow thickness, tow width and cross-sectional area are calculated because of yarn linear density, aspect ratio fibre density and fibre packing fraction. It is assumed that the packing fraction is the same for both axial and braiding yarns. The filament diameter of the E-glass is 9μm. The crimp induced by an aspect ratio of between 4 to 12 for roving bundles was found to have negligible impact on inclination and yarn length in the radial direction.

Potluri assumes yarn cross-section to be lenticular. The gap between adjacent tows is assumed to be zero, this means that tow width is equal to tow spacing. The cross-sectional area of a tow can be calculated using Equation 3.6 where A is tow cross-sectional area, T is yarn linear density in Tex, p_d is the fibre packing density in the tow and ρ is the fibre density. The fibre packing density is assumed to be 0.7.

$$A = \frac{T \times 10^{-6}}{\rho \times p_d}$$

Equation 3.6 Calculation of Tow Cross Sectional Area for Lenticular Assumption

It was determined that although a fixed fibre packing ratio is used in the work Potluri for computational purposes, fibre packing ratio does not remain constant due to inter-tow forces and tow tensions [77].

Alpyildiz [69] assumes yarns to be non-compressible and have an elliptical cross-section. This elliptical assumption is something that is common in many models, this is not realistic due to yarn interactions. The major and minor diameters of the yarn are assumed to be constant across the yarn length, with the crimp of the yarn assumed to be sinusoidal. Yarn slippage is not accounted for. The geometrical model proposes the three-dimensional yarn paths of braided structures for biaxial diamond and regular, and triaxial diamond braid architectures. The model allows for modification of parameters so that the braid structures can be produced with the desired performance criteria.

Van Ravenhorst and Akkerman assume a constant rectangular cross-sectional area of the tow [72]. The model accounts for yarn deformation through a change in aspect ratio, a decrease in tow width resulting in a simultaneous increase in tow thickness. The modelled rectangular cross-section provides a simplistic relationship between the width and thickness for constant cross-sectional area.

The University of Nottingham have developed a textile modelling software, TexGen, which is able to provide a realistic geometrical representation of textiles to determine mechanical and physical properties [78]. Yarn cross sections are still treated as a solid volume, however there are five options for describing the geometry: ellipse, power ellipse, lenticular, hybrid and polyform. The last two options can be used to account for deformation at yarn intersections. The yarn path is modelled by specifying its centreline. The smallest repeatable section of the yarn is then defined by a series of master nodes. The software also enables properties to be assigned to individual yarns. The development of a software such as this reduces the number of design iterations required of a textile. An addition of a braided model for TexGen was developed by Thompson in recent PhD work [37].

Thompson has developed a new function within the TexGen program that is capable of modelling a 2D- biaxial braided fabric as both curved and flat unit cells, Figure 3.35 [79].

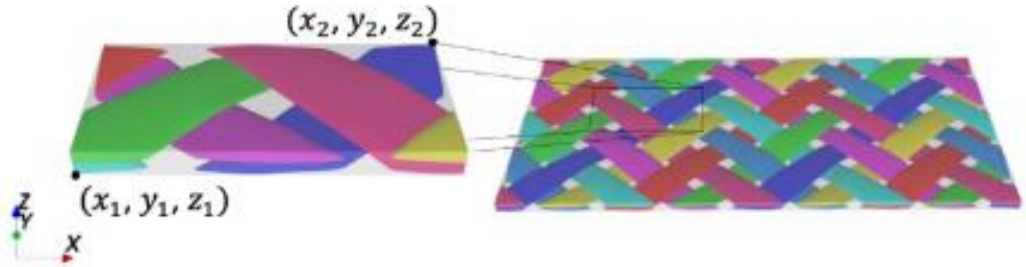


Figure 3.35 Biaxial braided fabric modelled in TexGen using repeats defined by the unit cell

Established models are used to predict the key process variables and yarn paths. The work establishes refinement functions to model the change in tow cross-section along the length of the tow, thus accounting for tow undulation. Good agreement was shown between tow geometry measurements from TexGen and the corresponding measurements from optical microscopy.

3.3.3 Yarn Modelling Assumptions

The braiding process itself is complex to simulate and as a result several yarn modelling assumptions have been incorporated into various models, these are discussed in this section of the literature review.

Zhang analysed the validity of the straight yarn assumption in calculating the braid angle via kinematic analysis [80]. The straight yarn assumption assumes that each yarn forms a straight line from bobbin to mandrel. This is not the case due to friction between the yarns in the convergence zone. As a result, Zhang introduced the concept of a particle velocity approach, which is applicable to curved yarns. The final braid structure is strongly influenced by the sliding and twisting of yarns in the convergence zone. Zhang continues by assessing the validity of the mechanics model in predicting the braid angle by comparing it to the kinematic model [80]. A 64-carrier machine with cotton yarns was used for experimentation. A deviation of 6.56°-10.39° from the experimental value was recorded for the kinematic model, with a

discrepancy of 4.26°-6° for the mechanics model. The magnitude of deviation is expected to increase for larger machines due to more significant friction effects.

Du and Popper [39] developed a detailed model relating braid outputs such as cover factor, volume fraction and yarn jamming limits to a variety of machine settings. Common assumptions for modelling yarns were applied; interactions between yarns are neglected as the yarn is considered straight in the convergence zone, each yarn is modelled as straight from the spool to a tangential interaction with the mandrel, yarn slip relative to the mandrel is not considered. Du and Popper quantify the effect of neglecting inter yarn friction to account for the 5° discrepancy between predicted and measured braid angle.

Na added an additional assumption referring to the braid point [46]. This assumed that the braid point formed as a point on the mandrel surface where the total length of the braiding yarn is minimised between carrier and braid point. This is known as the minimum path condition and was validated using a 32-carrier braider on a conical mandrel. These geometries are shown in Figure 3.36. The two different sections of constant cylindrical cross-section are shown as 20mm and 60mm diameters, and the conical transition region is shown.

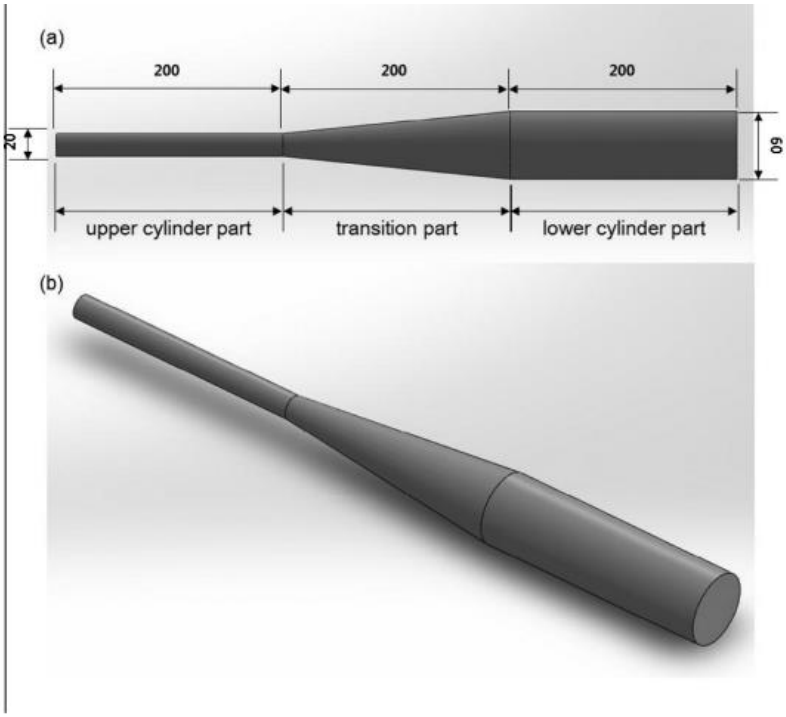


Figure 3.36 Mandrel Shapes (a and b) the conical mandrel

The braid angle over the conical mandrel was predicted using the minimum path method, comparison to simulation results indicate good agreement. The minimum path method was able to predict the braid angle to within 3° of error along the length of the mandrel, simulation showed a range of 18-28° whereas experimental angles were recorded as 19-26°. The transition section on the conical mandrel showed the greatest variation, this was explained as yarn slippage was not considered on the model.

To improve accuracy of existing models, Akkerman and Rodriguez [81] investigated yarn-mandrel interaction and produced a slip-indicator. Prior research indicated that fibre distribution was sensitive to yarn-mandrel interaction, therefore by preventing slip and utilising the slip indicator the correlation between simulation and experimental testing improved.

Studies have used mathematical models to predict the yarn path on the mandrel. Ning et al. used generalised rose curves [82], whereas Zheng used a Bezier curve [83]. Generally, models such as work by Alpyildiz describes the yarn path as helical with yarn crimp analysed as sinusoidal [69].

3.4 Conclusions and Research Needs

Previous work addressing the braiding process as well as relevant areas of research, has been reviewed and has demonstrated that current research on braiding is not yet comprehensive with many areas requiring further study.

Ebel and Kyosev have identified the rewinding process was identified as critical to the quality of the final braided component however, the qualitative understanding of this has not been identified [48], [2]. It is generally agreed that the quality of rewinding significantly influences the quality of the braiding. However, the influence of specific parameters such as rewinding tension, rewinding speed, and rewinding twist on fibre processability and mechanical behaviour have not been quantified. This work aims to define the influence of rewinding twist on braid architecture for a range of complex geometries. Quantifying the influence of rewinding twist on tow geometry is something that is not present in the literature, however it is important to understand this. Changes in tow geometry result in a change in cover factor which results in a difference between designed and manufactured braid. Rewinding twist is something that is used in industrial braid manufacture but there is limited literature

available particularly on its impact on the mechanical performance of a braided composite. This work aims to provide an initial investigation into the influence of rewinding on tensile properties of a braided composite.

Literature highlights that braid architecture variability is introduced when braiding complex geometries, this has been well documented in the literature by Van Ravenhorst, Du & Popper and Kessels and Akkerman among others, [39], [43], [6]. However, this work primarily addressed the effects on braid angle. Understanding the influence of complex geometries on other aspects of braid architecture such as tow geometry and stabilisation length are important to improve the predictability of the braiding process. This work considers the impact of complex geometry on all aspects of braid architecture along with incorporating an understanding of twist.

State-of-the-art simulation capabilities require material inputs using generalised yarn assumptions. Tow geometry is generally assumed to be elliptical, however literature acknowledges the significance of approximating the tow geometry incorrectly. This is something that varies between material type and tow size, in accordance with material preparation. An improved understanding of tow shape would enable predictive simulation capabilities to develop therefore improving the consistency between designed and manufactured preforms. This work develops the understanding of tow geometry and its relationship to rewinding twist.

Several yarn approximations are made during simulation of the braiding process across all types of computational model. Extensive research has been conducted to analyse the applicability of analytical, kinematic and FE models for braids. These models show good agreement but typically employ the same yarn assumptions. Experimental validation of the models demonstrates that this result in angle deviations of 3-5°. It has been suggested that this could be more significant on a larger mandrel. At present, a lot of work in the literature has been completed on small braiders, however there is limited work comparing small and large braiders to determine if assumptions formed from a small scale are valid for larger machinery.

In summary to increase the application of the braiding process in industrial composites manufacture the following development areas are of key importance.

- Understanding of the rewinding process to drive improvements in fibre processibility reducing preform defects and process interruptions.

- Understanding the influence of rewinding twist on the mechanical properties of braided composites
- Understanding of the influence of complex geometry on braid architecture to improve the predictability of the braiding process
- Improved understanding of tow geometry
- Validation of assumptions on small machinery to large machinery to ensure the same approach can be used at all scales.

Overcoming the outlined challenges above would increase the potential of the braiding process for an increased application across a variety of industrial sectors. This work will aim to provide useful input for each of the main challenges described.

4 Methodology

This work comprises of several studies, addressing different aspects of the braiding process. Aspects of these studies are completed on braiding machines at both the UoN and NCC.

- The effect of twist on braid architecture for both biaxial and triaxial braids
- The effect of scale using two different sized axial braiders with a different number of carriers
- The braiding of different mandrels of prismatic, prismatic-tapered, and prismatic axisymmetric geometries.
- The effect of converging and diverging tapers on braid architecture.

This section summarises the methodology behind the manufacture and testing of the braided composites used in this investigation. The following sections discuss the generalised braiding and rewinding methods used in this work. Both cylindrical and frusto-conical mandrels are braided on two different braiding machines, at the UoN and NCC with varying material parameters. The manufacturing parameters are repeated in the results section of the thesis for ease of reading. The rewinding process is explored in significant detail particularly the inclusion of rewinding twist. The methods of measurement for the key process variables are detailed along with a Gage Repeatability and Reproducibility study regarding using ImageJ as a measurement method.

4.1 Experimental Methodologies

4.1.1 Braiding

4.1.1.1 Braiding Machine Capabilities

Braiding capabilities at both UoN and NCC were used for the braiding work in this study. This allows the effect of rewinding parameters on the resultant braid architecture for small- and large-scale to be characterised.

4.1.1.1.1 48-carrier Braider

Figure 4.1 shows the Steeger 140/48 HS 48-carrier axial braider at the UoN. At a full load, the braider holds 48-carriers each with its own tensioning system. The arrangement of carriers within the horn gears in a fully loaded configuration produces a regular braid pattern.



Figure 4.1 48-carrier Steeger 140/48 HS axial braider and Kuka KR30-60 robotic arm at the UoN

A Kuka KR C2 controller is used as the control system for the braider speed and direction. An analogue output signal from the controller is processed using a Hitachi Inverter to send synchronised signals to 3 DC motors within the braider. A KR30-60 robotic arm mounted on a linear rail track controls the mandrel positions. This enables 6-axes of movement of the robot during braiding. The robot control system provides precise manoeuvrability with a repeatability of 0.07mm. A guide ring of 180mm diameter is mounted to the braiding machine.

4.1.1.1.2 192/288-carrier braider

Figure 4.2 shows the Eurocarbon 192/288-carrier axial braider at the NCC. Carrier arrangement in horn gears is such that in a fully loaded configuration a regular braid pattern is produced.

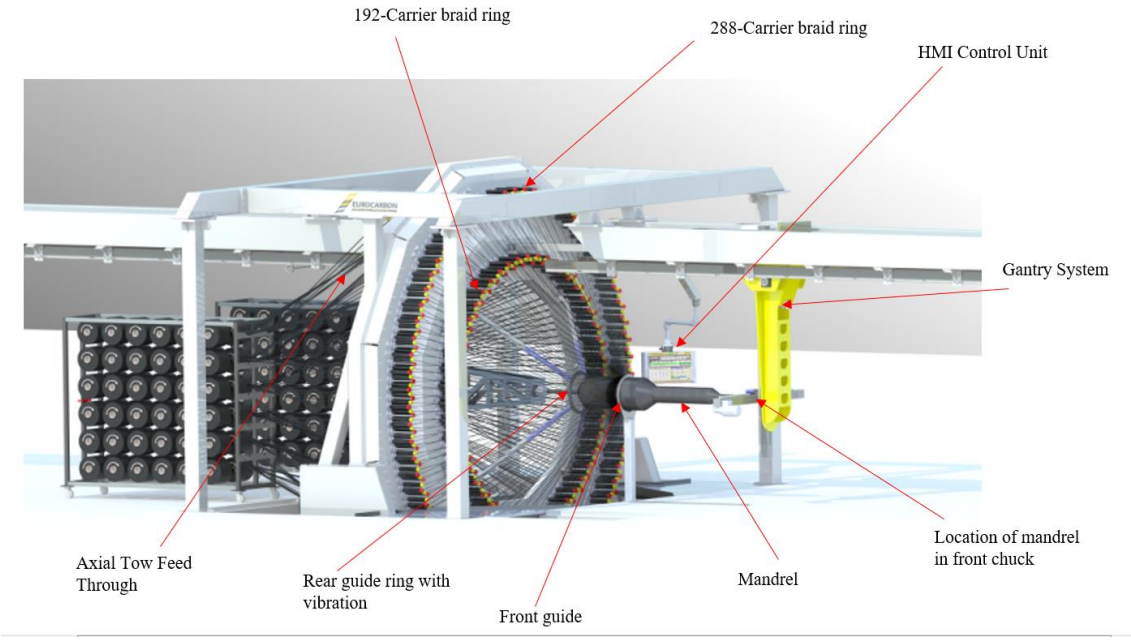


Figure 4.2 192/288-carrier Eurocarbon braider Set-Up at NCC [84]

The diameter of components that can be manufactured is dependent on the loading configuration of the braid ring. Parts of up to 1m diameter can be manufactured. The mandrel positioning is controlled through a fully referenced gantry system with precise CNC control. The location of the limit switches at either end of the gantry mean that the machine is capable of manufacturing parts up to 10m in length. The gantry system supports mandrels at chuck fixtures at both ends.

Bias braid angles in the range of 15-80° can be achieved. Reinforcement in the axial direction can be added through the axial fibres. The axial fibres are loaded onto the axial creel at the rear of the braiding machine and fed through specified locations and a metal feed in between braid carriers as shown in Figure 4.3.

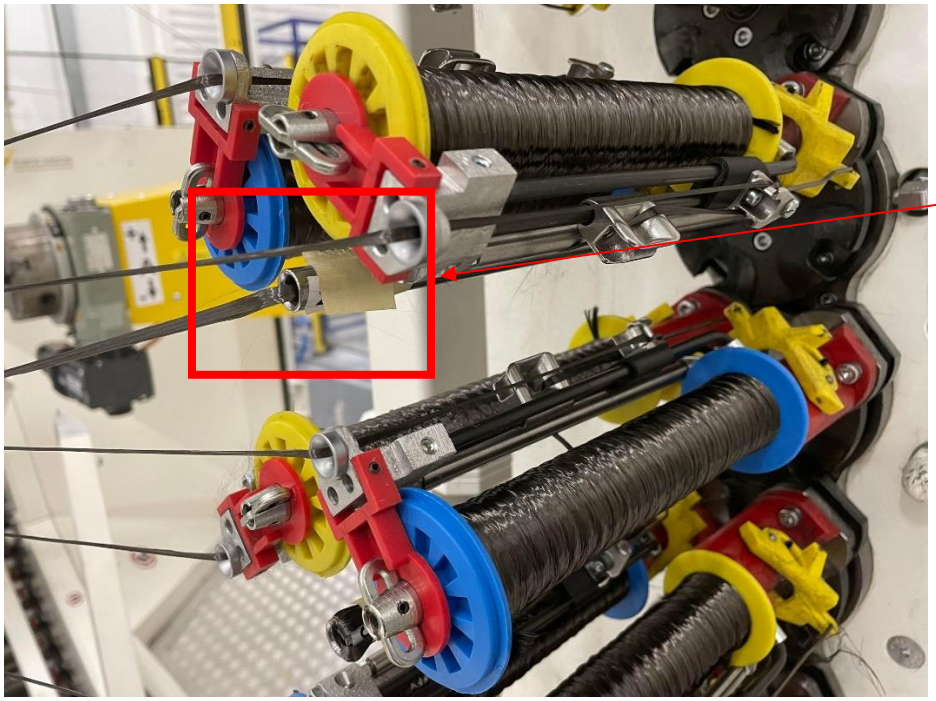


Figure 4.3 Loading of axial yarns

For simple geometries of constant cross-section where a constant angle is required, the braider can be programmed using carrier speed and traverse speed. The carrier speed is measured in picks per minute, PPM. A single thread of a warp yarn crossing a weft yarn is defined as a pick. The traverse speed is programmed in mm/min. The positional location is defined in terms of location of the master gantry at the front of the braider.

For more complex mandrels, the creation of a program is required. The position of the mandrel is defined through the position of the gantry in the x, y and z axes. The calculation of the machine speeds is completed based on required braid angle and effective mandrel diameter. These values are the inputted to the program. On completion of the program, the program is uploaded to the braiding machine. This is then completed in an automatic mode requiring limited operator intervention.

The diameter of the guide ring should be as close as possible to the diameter of the component. Guide rings ranging in size from 100-800mm diameter are available, these are mounted as shown in Figure 4.2 to reduce the convergence length of the braid. The Eurocarbon braider has the capability of braiding in the reverse direction. The application of a rear guide ring is used for this shown in Figure 4.2. The use of vibrating motors connected to the frame of the guide encourage fibre slippage when

braiding in the reverse direction. 1500 RPM of vibration is applied to prevent the guide ring from overbraiding itself as shown in Figure 4.4. Fibre locking is visible around the guide ring as the vibration is insufficient to allow the fibres to slip over the guide ring, this results in material build-up and halts preform production.

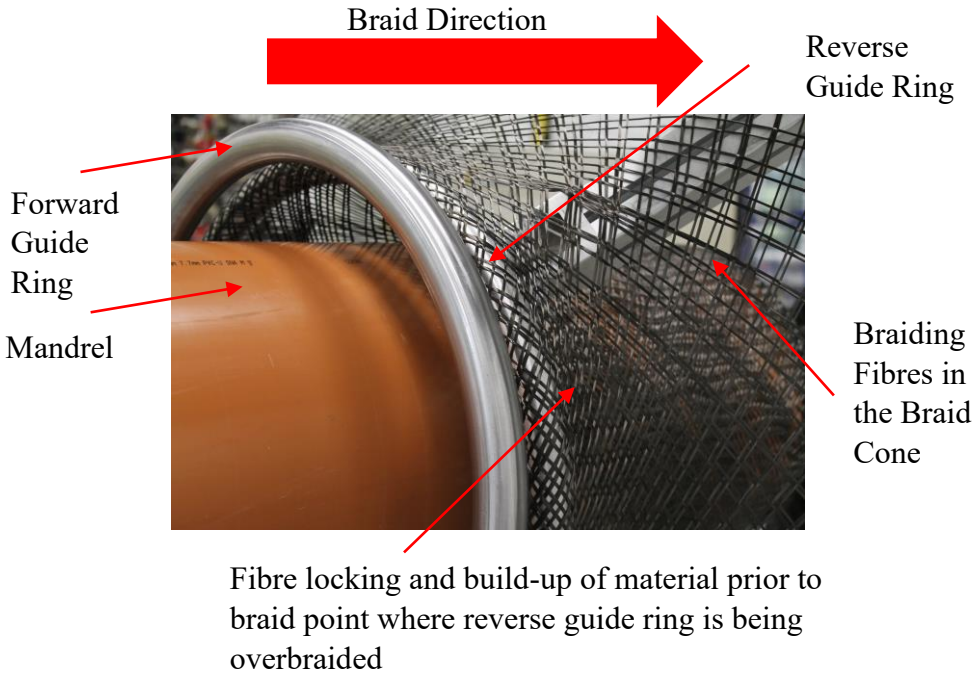


Figure 4.4 Reverse guide ring overbraided due to too little vibration

4.1.1.1.3 Calibration between braiders

The Steeger braider uses an input voltage which is translated to a carrier velocity whereas the Eurocarbon braider uses PPM. For this work, the two systems carrier speeds were calibrated to convert the input voltages on the Steeger braider to comparable PPM values. A rotational encoder was attached to an output shaft on a horn gear. This measured the rpm at various voltages, as shown in Table 4.1. Equation 4.1 demonstrates the relationship between rpm and PPM as a function of the number of picks in one revolution of the braider.

Equation 4.1 Relationship between rpm and PPM

$$rpm = \frac{picks\ per\ minute}{picks\ per\ revolution}$$

As the number of carriers influences the PPM, to scale a value for the 192-carrier braider the PPM value must be multiplied by 4 for programming the NCC braider due to the 192/48 carrier ratio.

Table 4.1 Braider speeds calculated from the voltage defined by the Kuka control unit.

Voltage, V	Horn Gear Speed, RPM	Horn Gear Speed, (rad/s)	Carrier Speed, RPM	Picks per Minute, PPM
0.8	40	4.19	3.33	80
0.75	38	3.98	3.17	76
0.7	35	3.67	2.92	70
0.65	32	3.35	2.67	64
0.6	28	2.93	2.33	56
0.55	25	2.62	2.08	50
0.5	22	2.30	1.83	44

4.1.1.2 Braiding of Cylindrical Mandrel

The current work uses a series of cylindrical geometries to develop tow geometry approximations. The individual test parameters are repeated in the results section of the work, however, a generalised methodology to produce a braided cylindrical preform is detailed here.

1. Based on the component geometry, analytical calculations are used to determine the length of material required. This quantity is then rewound onto the braider bobbins. Rewinding parameters are defined in terms of number of rewinding twists. With the operator setting up the rewinding machine so that tow pitch and rewinding amplitude provide a high-quality bobbin package. A mixture of S- and Z- twist bobbins are rewound.
2. Using the key process variables to define the component requirements, analytical calculations are used to determine the machine set-up parameters. Number of carriers, braid carrier speed and traverse speed are defined.
3. Braiding bobbins are loaded onto the braiding machine such that the anticlockwise and clockwise bobbins would with opposite twist directions either an S- or Z-. This is shown in Figure 4.5. A balance of bobbins with an S- and Z- twist are required to ensure a balanced preform.

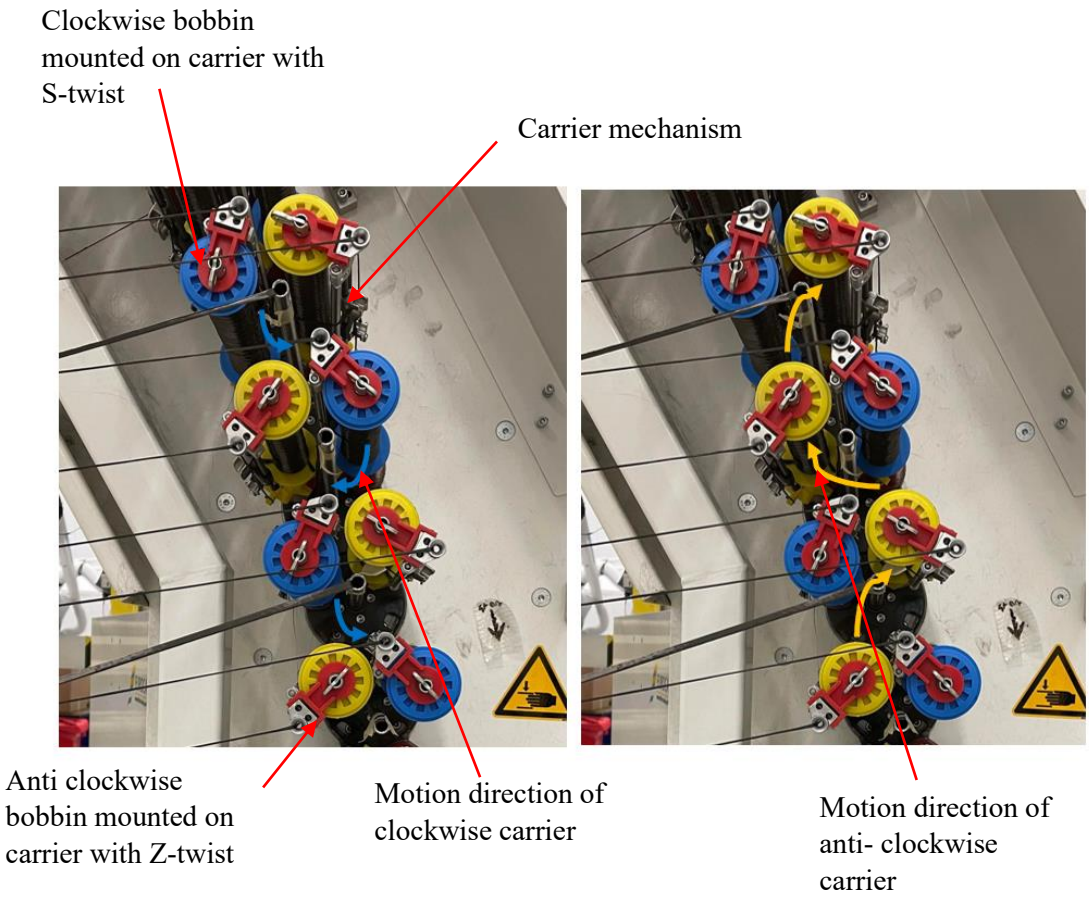


Figure 4.5 Direction of the braid carriers (a) blue clockwise carriers (b) yellow anti-clockwise carriers

4. An appropriate guide ring is selected such that it is close to the maximum diameter of the mandrel.
5. The mandrel is then loaded fixed in both the front and rear chucks, Figure 4.6. The mandrel position is then adjusted such that it is central to the guide ring. This ensures that the braid angle on each surface of the preform is consistent.

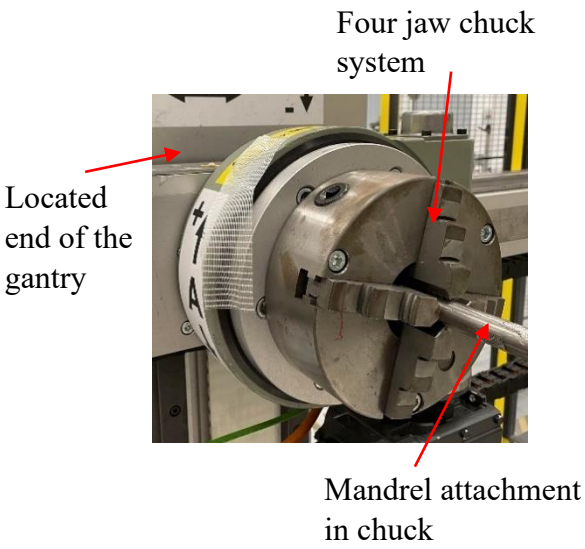


Figure 4.6 Machine chucks to secure the mandrel

6. If a program is required, this is uploaded to the braiding machine. The program is then run without the addition of the braid ring to ensure that there are no collisions with the guide ring and that the mandrel remains central to the guide ring. This is particularly important with complex geometries of changing cross-section. A lead-in tooling section is required to ensure that the braid has fully stabilised prior to the component.
7. Fibres are attached to the start of the mandrel. The braid cone is then formed.
8. Deposition braiding commences in accordance with the calculated machine parameters.
9. Once the braided layer has been deposited, the braid tows are then cut and secured.
10. The mandrel is then unloaded, and the consolidation steps can take place.

Throughout this work, for each manufacturing trial the machine parameters including number of braid carriers, carrier speed and traverse speed are specified. The material type and rewinding parameters are also outlined in relevant sections for ease of reading, along with the mandrel diameters.

4.1.1.3 Braiding of Frusto-Conical Mandrel

For the braiding of complex geometries, such as the frusto-conical mandrel the braiding process is like the generalised braiding process for cylindrical geometries. However, there are some additional considerations required.

- The guide ring selection must be suitable for the entire preform length, therefore a guide ring diameter suitable for the largest cross-section is selected to avoid collisions between the mandrel and guide ring.
- The geometrical feasibility must be considered. Braiding of drastic cross-sectional changes, including sharp edges or curved sections can pose difficulties during manufacturing.
- An appropriate step size for programming is required when calculating the inverse solution. The more complex the cross-sectional change the more steps are required to ensure good consistency between the designed and manufactured preform.

4.1.1.3.1 3D Printed Mandrel Manufacture for Small Scale Braiding

Mandrels with taper angles of 5.4° and 10.6° were 3D printed. The mandrels were specified to transition from a nominal diameter of 50mm to a maximum diameter of 87.5mm through a tapered slope. Mandrels were 3D printed using the Ultimaker 2 Extended Plus 3D printer at the UoN using RS Pro Black PLA 3D printer filament. Dimensioned images of the manufactured mandrels are shown in Figure 4.7 and Figure 4.8.

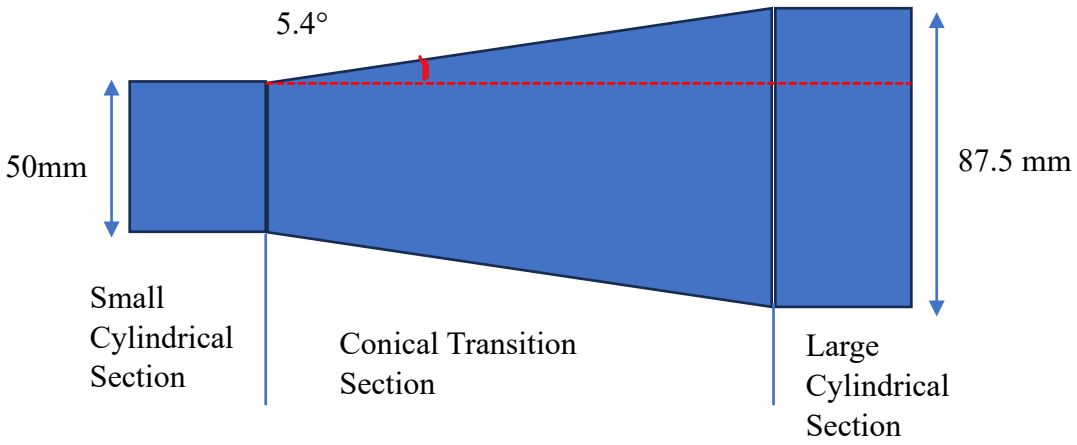


Figure 4.7 Schematic of 5.4° gradient frusto-conical mandrel

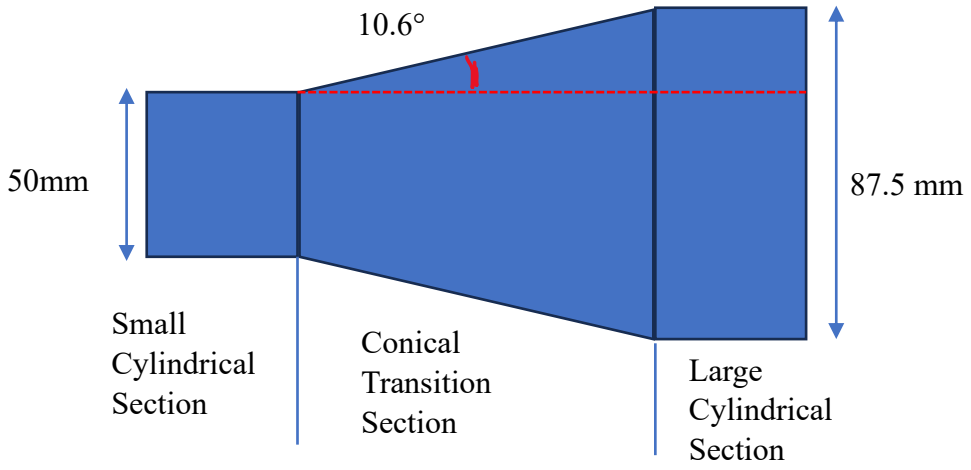


Figure 4.8 Schematic of 10.6° gradient frusto-conical mandrel

The mandrels are designed so that they can be located in the braiding machine in such a way that cross-sectional change can become either diverging or converging. They were designed in such a way that the two regions of constant cross-section were sufficient in length so that the braid had stabilised prior to the introduction of the conical cross-section change.

4.1.1.3.2 Method of Preform Manufacture for Small Scale Braiding

Two sets of bobbins were wound with the CEZOMA VLS87 winding machine and accompanying Eurocarbon twist cabinet using T700s standard modulus carbon fibre supplied by Toray. The rewinding parameters were identical except for the rewinding twist where material A was rewound with 0 Tpm and material B with 5 Tpm. The rewinding speed of 10,000 RPM was programmed to the twist cabinet and the rewinding tension of 1.5 rotations was added to the CE-1187 machine.

Preforms were manufactured. The braiding machine was operated in a fully loaded configuration to produce a biaxial braid with a regular braid pattern. The process parameters, carrier speed and take-up speed, were manipulated to produce a single layer preform with a constant braid angle of 45°.

4.1.1.3.3 Braider Control

A specialised program was derived for both mandrels in both converging and diverging orientations by translating a program created with software supplied by Eurocarbon [16] to process speeds which can be inputted to the KUKA robot at the UoN. The operator defines intervals along the axial length at which the diameter of the part is measured, typically for a mandrel of this size an interval of 10mm along

the axial length is used. For larger mandrels the interval between diameter measurements can be greater. Using the standard analytic relationships defined by the likes of Carey [3] the machine process parameters of traverse speed and braid carrier speed are calculated using the measured diameter and desired braid angle. This program development also defines the location of mandrel in relation to the braider so that the speed changes correspond to the changing geometry. The more frequent the speed changes the more representative the speeds calculated by the program will be to produce a braid with the desired braid angle.

Twist levels of 0 Tpm and 5 Tpm were selected as a representation of tows which were both untwisted and had a level of twist suitable for manufacture. Typically, 12K fibres are manufactured with a level of twist between 5-9 Tpm.

Table 4.2 Test ID for Small Conical Preform Manufacture

Test ID	Transition Section Angle, °	Transition Section Orientation	Rewinding Twist, Tpm
1	5.4°	Diverging	0
2	5.4°	Diverging	5
3	5.4°	Converging	0
4	5.4°	Converging	5
5	10.6°	Diverging	0
6	10.6°	Diverging	5
7	10.6°	Converging	0
8	10.6°	Converging	5

4.1.1.4 Large Scale Braiding of Frusto-Conical Mandrel

Large scale preforms were manufactured using the 192-carrier axial Eurocarbon braider at the NCC. The fibres were braided onto an MDF mandrel of nominal diameter 200mm, larger diameter 350mm with a transition angle of 10.6°, Figure 4.9.

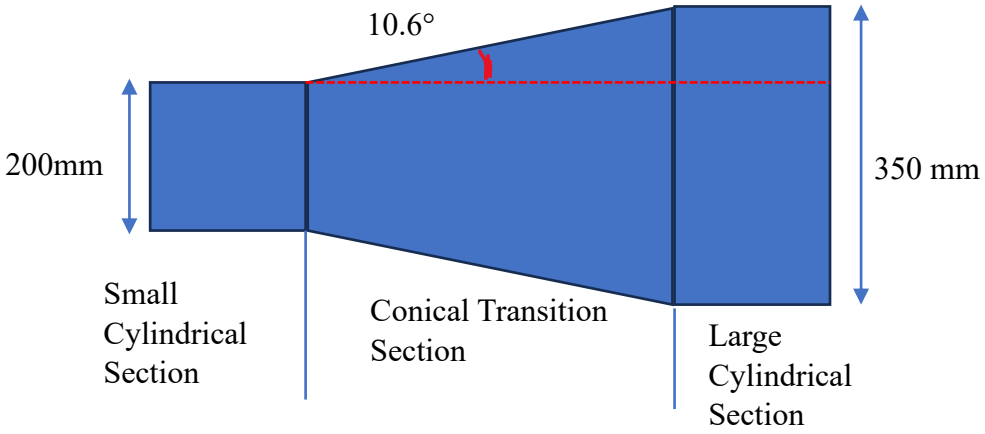


Figure 4.9 Conical Mandrel for Braiding Trials at NCC

Table 4.3 summarises the trials completed on a the MDF mandrel with conical cross-section change. The orientation of the cross-section and level of rewinding twist are specified. A twist level of 0 Tpm and 7 Tpm were selected to reflect the tow geometry of fibres both untwisted and with a suitable level of twist for manufacture. This mandrel was manufactured as part of the capability development project at the NCC where 7 Tpm was used as standard, this conclusion has been reached through trial-and-error for manufacturing with optimum twist level.

Table 4.3 Test on conical section on 192-carrier braider

Test ID	Mandrel Size	Transition Section Orientation	Rewinding Twist, Tpm
2.1	Large	Converging	0
2.2	Large	Converging	7
2.3	Large	Diverging	0
2.4	Large	Diverging	7

The machine was operated in a fully loaded configuration to create a biaxial braid with a regular braid pattern. The process parameters, carrier speed and take-up speed were manipulated to produce single layer preforms with a constant braid angle of 45° to investigate the effect of the additional twist on the stability and variability of the

braid architecture on a conical cross-section change. As in the tests detailed in Table 4.2, preforms were manufactured with T700s carbon fibre supplied by Toray rewound with 0 Tpm to allow for direct comparison to the small mandrel. Trials were also completed with material rewound with 7 Tpm to determine if the assumptions made on the influence of rewinding twist when braiding complex geometries are valid for larger machinery.

As a key conclusion of this Section will be the effect of the part gradient on tow spread the mandrel material is a key consideration. Both the 3D printed mandrels and the MDF cone have a degree of surface roughness. The machining of the MDF mandrel resulted in surface ridges of 0.085mm. Figure 4.10 shows the MDF mandrel loaded on the NCC braider.



Figure 4.10 MDF mandrel loaded at NCC

Individual programs were defined for the mandrel in both diverging and converging cross-sections as a function of the mandrel diameter and desired braid angle of 45° at discrete locations along the axial length of the mandrel. The operator defined these discrete locations so that the change in mandrel cross-section is minimal between step sizes. For this mandrel the step sizes were every 100mm in the straight section, with a step-size of every 50mm in the conical cross-section.

4.1.1.5 Braiding of the 'Oscar' Mandrel

To test the limits of the braiding process, the 'Oscar' geometry was designed through the capability development project at the NCC. The mandrel is axisymmetric with

multiple cross-section changes. These are both converging and diverging with different magnitudes of gradients and curvatures. The mandrel is split into sections for each cross-section change. The mandrel is shown in Figure 4.11 with each section labelled for reference. The braiding of the part was completed with the sections in numerical order.

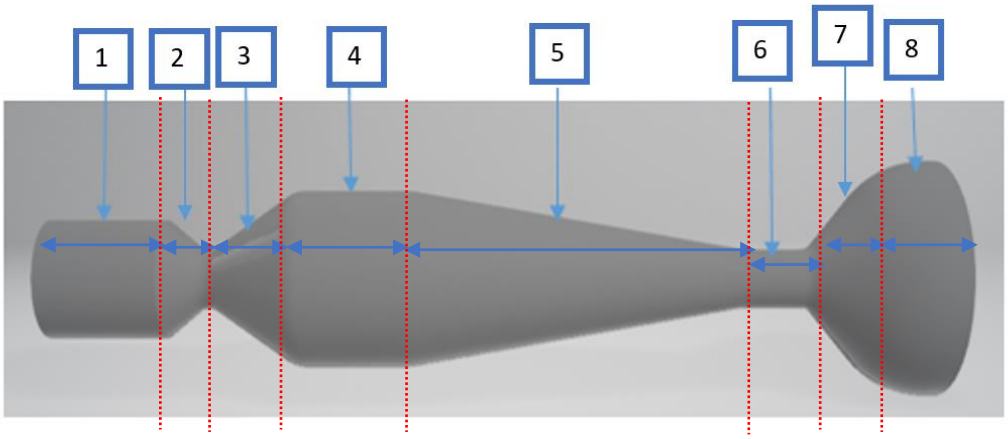


Figure 4.11 Oscar Mandrel Geometry

Mandrels of sequential cross-section changes have been braided in literature. Van Ravenhorst produced a mandrel with multiple changes in cross-section and centricity [43]. Variations in braid angle were noted on the more extreme regions of the mandrel where the cross-section changed more rapidly. Similarly, the 'Oscar' geometry locates a series of geometrical cross-section changes rapidly one after the other. Table 4.4 lists the gradients of each respective section.

Table 4.4 Section Gradient of the 'Oscar' Mandrel

Section Number	Type of Cross Section Change	Section gradient in the direction of braiding
1	Constant	0
2	Decreasing	-1.67
3	Increasing	1.40
4	Constant	0
5	Decreasing	-0.3
6	Constant	0
7	Increasing (Curved)	0.67
8	Constant	0

The ‘Oscar’ was braided at the NCC with HTS45 12K carbon fibre supplied by Teijin rewound with both 0 Tpm and 7 Tpm. A fully loaded 192-carrier braid ring was used to produce a regular braid pattern. No axial tows were used for the braiding of this geometry. A constant braid carrier speed of 220 PPM was maintained. A specific braid program was derived using the software supplied by Eurocarbon [16]. The operator specified the diameter of the mandrel at specific intervals along the axial direction. For a mandrel of this level of complexity a step size of 50mm was used. These diameters, along with the predicted braid angle were used to calculate the machine process parameters of braid carrier speed and traverse speed. The braid carrier speed was maintained at a constant 220PPM throughout the program with the traverse speed changing in response to changing mandrel diameter. Due to the extreme geometrical changes in the mandrel geometry a constant angle of 45° was not attainable for such as large number of carriers. As a result, the braid angle in section 6 was reduced to avoid tow jamming. The other sections were braided at a 45° braid angle.

4.1.2 Mechanics of the Rewinding Process

4.1.2.1 Tow Path

The tow path continues from the large material bobbin supplied by the manufacturer through several ceramic coated guiding elements on the rewinding machine until it reaches the bobbin. This can be seen in Figure 4.12 along with the capability of the machine to wind four bobbin simultaneously. The guiding elements are also visible throughout the tow path.

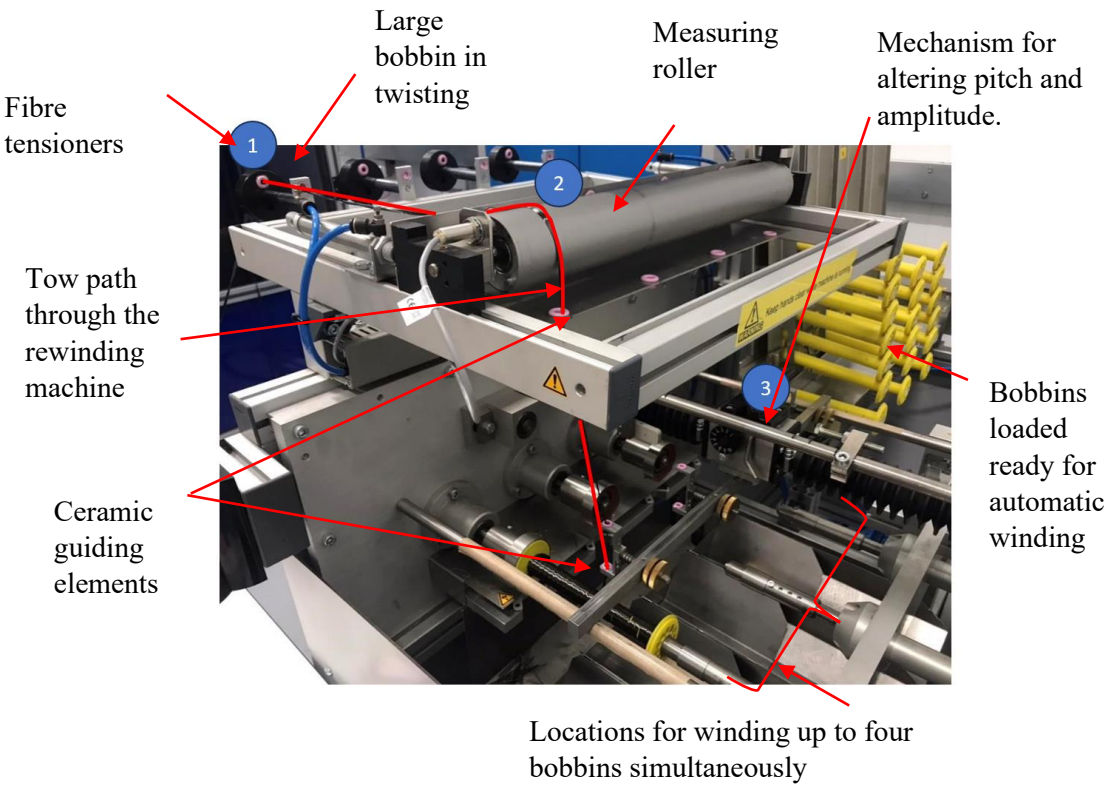


Figure 4.12 Tow Path through a CE-1187 winding machine

The unwinding of the tow originates from the large bobbins supplied by the manufacturer loaded in the twist cabinet, as shown in Figure 4.13. The twist cabinet rotates the bobbin at a speed programmed by the operator as the yarn is removed at a tangent to the bobbin.

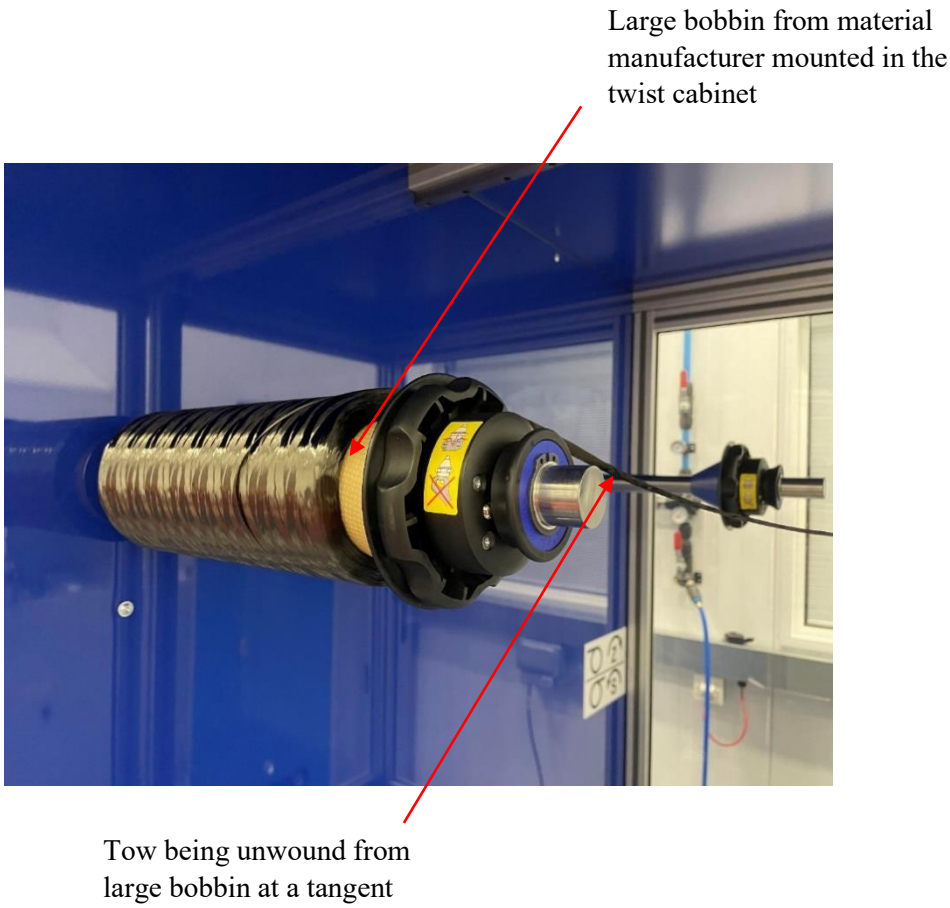


Figure 4.13 Large Bobbin Mounted in the Twist Cabinet

The direction which the large bobbin is mounted in the twist cabinet indicates the direction of twist. This is summarised in Figure 4.14.

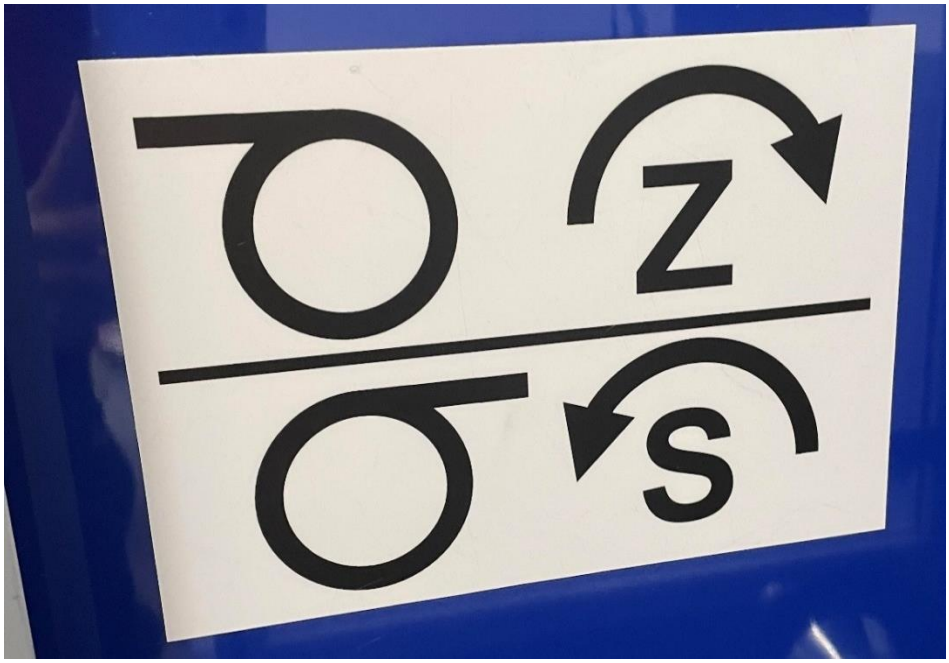


Figure 4.14 Direction of orientation of bobbin loaded in the twist cabinet and resulting twist

As the tow is pulled off the large bobbin it passes through fibre tensioners, Location 1 in Figure 4.12. These are mounted at the rear of the rewinding machine. The discs are rotated to wrap the tow around the ceramic cylinder which creates more friction. The higher the number of rotations the greater the friction These are shown in Figure 4.15.

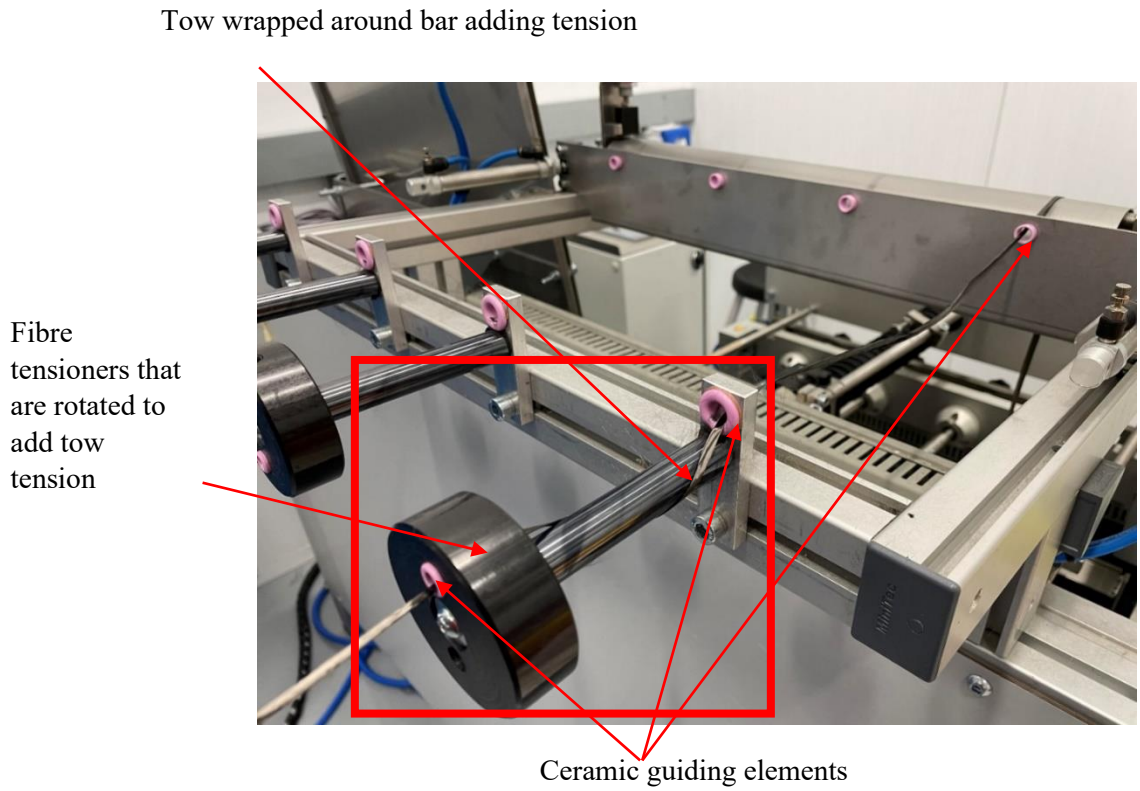


Figure 4.15 Tow path through fibre tensioner

Location 2 in Figure 4.12 is the measuring roller which calculates the exact length of material rewound onto the bobbin. Further guiding help to deposit the tow onto the bobbin. This is shown in Figure 4.16 where the tow can be seen passing over the measuring roller before moving through the final guiding elements.

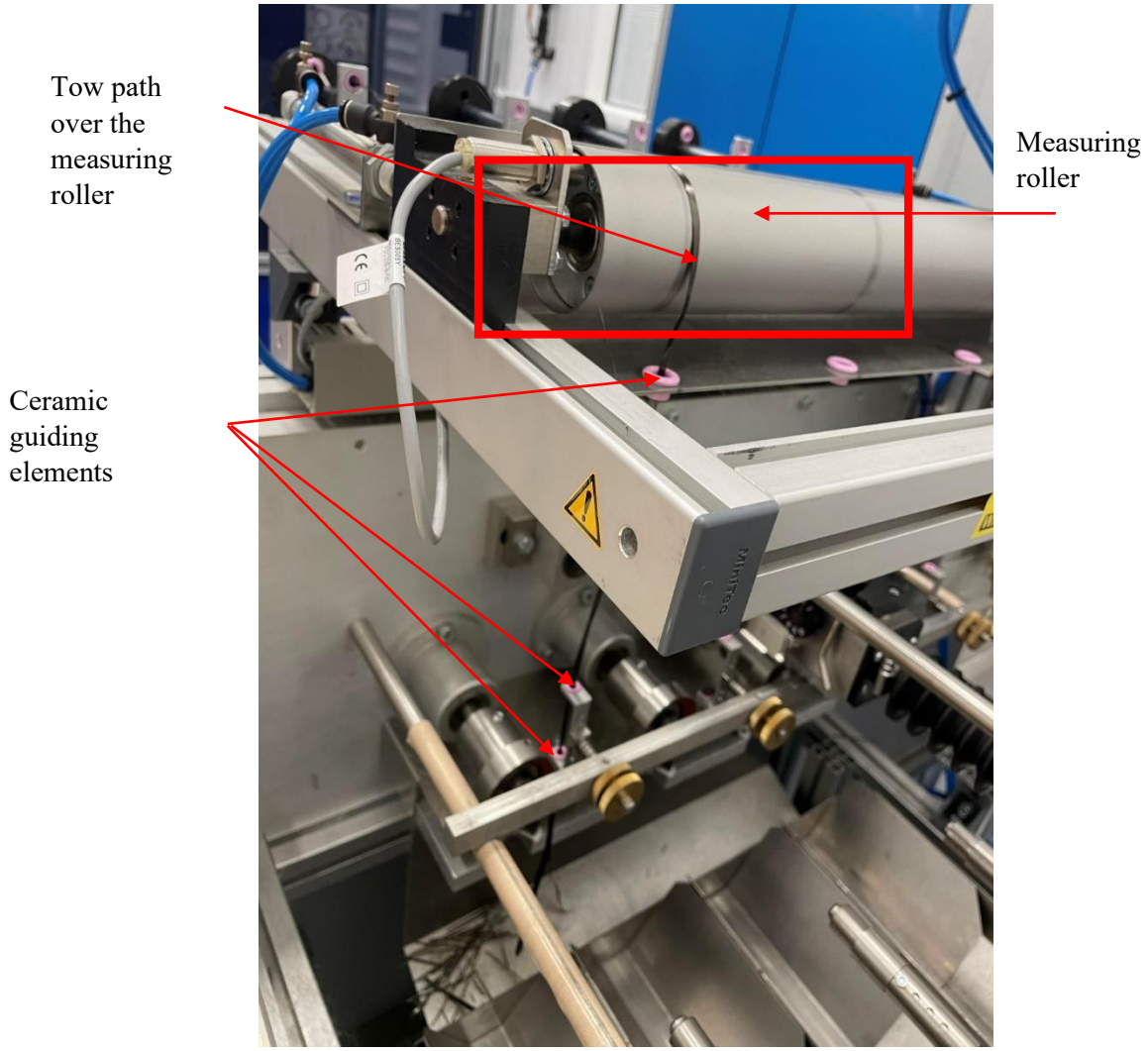


Figure 4.16 Tow Path over measuring roller through final guiding elements

The pitch of the tow, or the distance between two adjacent windings of the bobbin, is determined manually using screw fixtures at either end of the machine, location 3 in Figure 4.12. This helps to distribute the material evenly across the bobbin. The windings are required to be adjacent to each other with no overlaps or gaps to create a smooth bobbin package. Figure 4.17 shows these in greater detail.

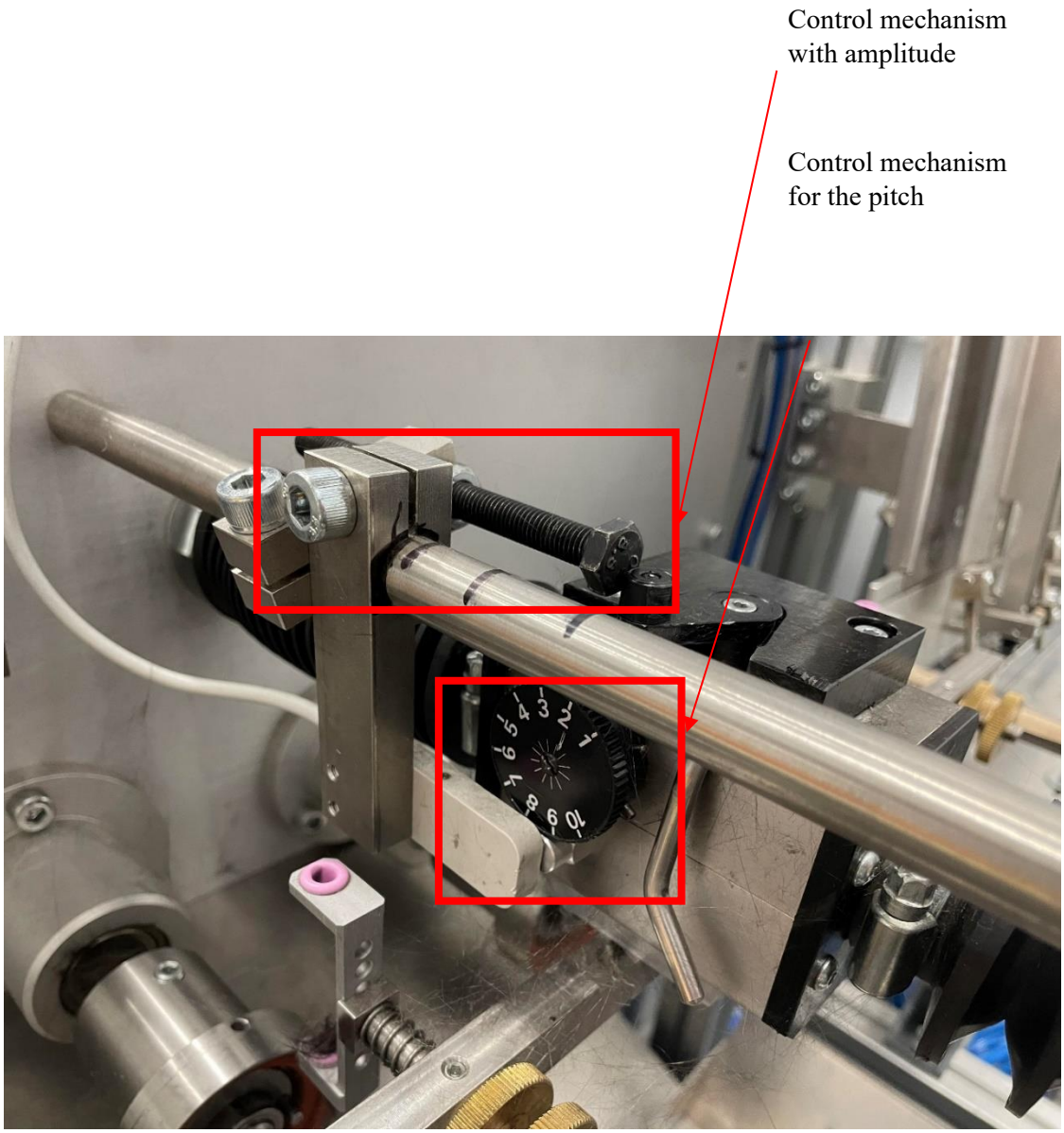


Figure 4.17 Mechanism for altering pitch and amplitude

4.1.2.2 Rewinding Process Parameters

The rewinding machine allows control of multiple parameters including rewinding speed, tension, and twist.

The CEZOMA winding machine utilises a frequency converter to achieve a constant speed. This also enables a ramp-up/ramp-down function to avoid tension shocks to the yarn.

Tow tension is controlled by the discs in location 2, rotation of these can wrap more yarn around the ceramic pipe which increases friction and consequently yarn tension. It is important to rewind with constant tension across all bobbins in a machine set-

up. Inconsistency in rewinding tension can lead to preform defects and tow breakages when braiding.

The Eurocarbon twist cabinet is an ancillary equipment using in conjunction with the CE-1187 rewinding machine. The cabinet adds twist to fibres during the unwinding of large bobbins from the material supplier which is then rewound onto smaller bobbins for braiding with the CE-1187 rewinding machine. Twisting fibres during the rewinding process is an optional choice from braid manufacturers with some choosing to braid with untwisted fibres exclusively.

4.1.2.3 Twisting

4.1.2.3.1 Rewinding with a Twist

The twisting of the fibres occurs due the relationship between the rpm of the large bobbins in the twist cabinet and the rpm of the small bobbins. The material bobbin is orientated parallel to the bobbins in the rewinding machine. There are two types of twist an S-twist and Z-twist, these are shown in Figure 4.18.

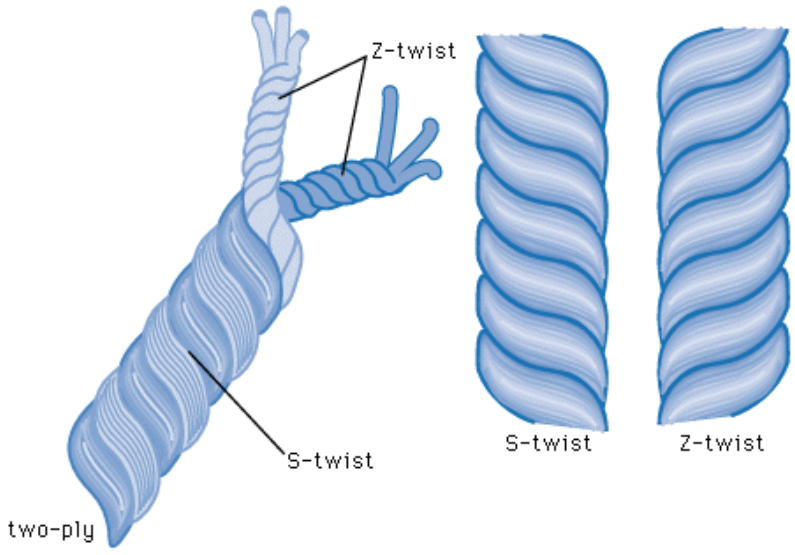


Figure 4.18 'S' and 'Z' Twist

The number of twists per metre (Tpm) recommended depends on the filament count of the tow, with the number of twists per metre increasing as the filament count decreases. The recommendations are detailed in Table 2.2.

4.1.3 Metrology

4.1.3.1 Braid Angle

A conventional method for measuring braid angle is to use a protractor, however this is often subject to significant error levels and is subjective depending on the person measuring. Image processing software such as ImageJ is a viable option for this as shown by Leung to measure the angle between braiding yarns from a photograph taken parallel to the braided preform. Other software contains custom braid angle measurements such as the processing toolbox in MATLAB.

The in-process monitoring set-up used in this work utilises image processing techniques and cameras to make real-time measurements of braid angle. The frequency components of an image are visualised using frequency domain analysis. Rotation invariance and angular preservation of image features in the Fourier domain enable the features of a braid to be measured [85]. No spatial data is contained in the frequency domain once the image has been transformed. As shown in Figure 4.19, the frequency response shows two primary directions which correspond to the braid angles. For a triaxial braid, a third fibre direction is visible [35].

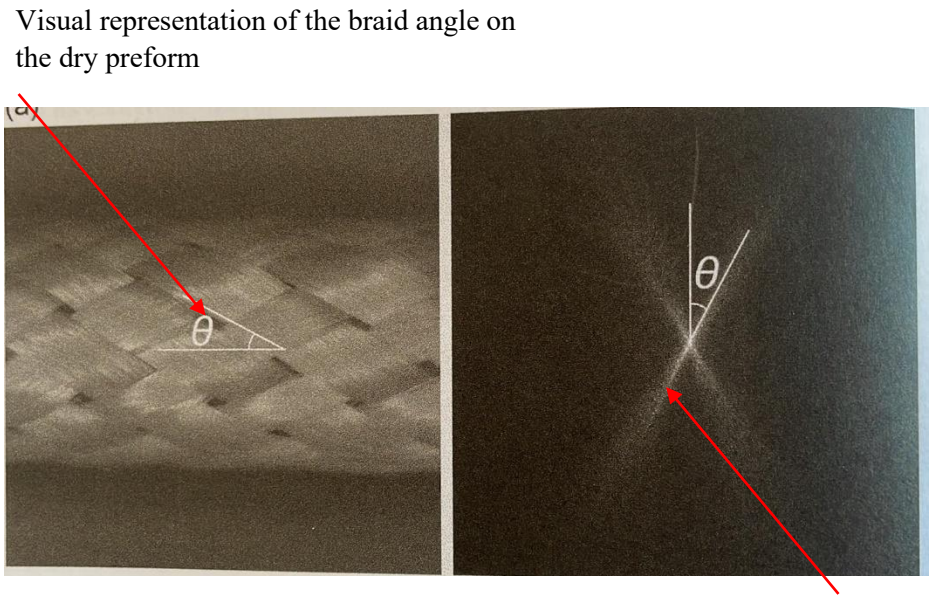


Figure 4.19 Braid angle measurement and frequency domain

4.1.3.2 Image Processing

4.1.3.2.1 Application of ImageJ as Measurement Method

Image processing software, ImageJ was used to record the braid architecture measurements of tow width, braid angle and cover factor throughout this project. Three measurement functions of ImageJ will be used for data acquisition: the protractor for braid angle, the line length for tow width and a bespoke method for determining cover factor.

A gage repeatability and reproducibility study (gage R & R) was conducted to determine the suitability of using this measurement process with regards to the reliability and repeatability of the braid architecture measurements. For each variable three appraisers were used, these were employees at the NCC in the 3D Textiles team with knowledge of braiding, each operator had a different level of experience with the ImageJ software. The same set of instructions was provided to each appraiser prior to the completion of the gage R&R to ensure that any variation was due to the measurement process rather than operator error.

Ten ‘parts’ were identified for both braid angle and tow width. Each part was identified numerically in the instruction sheet to ensure that variation in measurements was due to the application of measurement system rather than

variation of the braided preform. Each part was measured five times by each operator. As three different measurement functions of ImageJ are used in this work, three separate gage R&R studies have been conducted, each for measuring tow width, braid angle and cover factor, to determine the suitability of using ImageJ as a measurement method.

4.1.3.2.2 Gage R&R study for ImageJ as a measurement method for tow width

Statistical analysis software Minitab has been used to conduct a cross gage R&R study, where each operator measures each part. The Total Gage R&R for tow width is 25.63%. Typically, for a measurement system to be accepted without improvement the Total Gage R&R must be under 10%, however a range of 10-30% is acceptable depending on the time and monetary cost to improve the system [86]. Variation in measurement is due to part variability.

4.1.3.2.3 Gage R&R study for ImageJ as a measurement method for braid angle

The gage evaluation demonstrated a Total Gage R&R of 26.95%. Similarly, to the analysis of the measurement for tow width measurement under 30% in this case is considered satisfactory.

4.1.3.2.4 Gage R&R study for ImageJ as a measurement method for cover factor

The method for determining the cover factor of a braided preform was more bespoke than that of braid angle and tow width. The cover factor was determined by manually selecting the areas of the mandrel where there is no fibre covering the mandrel and calculating the percentage of pixels covered by the carbon fibre. Similarly, to the method analysis for braid angle and tow width, a crossed gage R&R study was conducted to determine the suitability of the measurement method. The Total Gage R&R shown from the %StudyVar is 23.20%.

In summary, after completion of a Gage R&R study for each measuring braid angle, tow width and cover factor using ImageJ it can be concluded that the method provides an acceptable level of measurement. Across all three measurement strategies most of the variation was found to be attributed to part variation rather variation in the measurement system or variation due to operator.

4.1.3.3 In-Process Monitoring at the NCC

The IPM system provides an automated acquisition of braid angle and preform thickness to provide a live readout of measurement data to the operator. It utilises a

2D Fourier transfer analysis method for data acquisition. The software-based angle measurements are made from digital images of the braided preform where the image acquisition system identifies and traces yarn edges, using this to calculate braid angle. The high resolution 12.3 MP monochromatic machine vision camera system acquires greyscale images of the preform. The set-up configuration captures an area of 47mm x 34mm. Exposure time is limited to 5ms to minimise image blur. A dark field LED ring light has also been installed to accentuate the edges features in the captured image such as the edges of the braided tows. A polarising filter is applied to reduce reflections from the dry fibre, which is a particular problem for the carbon fibre. Figure 4.20 demonstrates the output of each stage of the image processing steps. The following routine is completed for braid angle measurement, the image taken by the camera is cropped Figure 4.20a, this image is then blurred using a median filter Figure 4.20b, the edges are then detected using Scharr operator, kernal size = 3 Figure 4.20c and a logarithm of Fourier power spectral density Figure 4.20d [35].

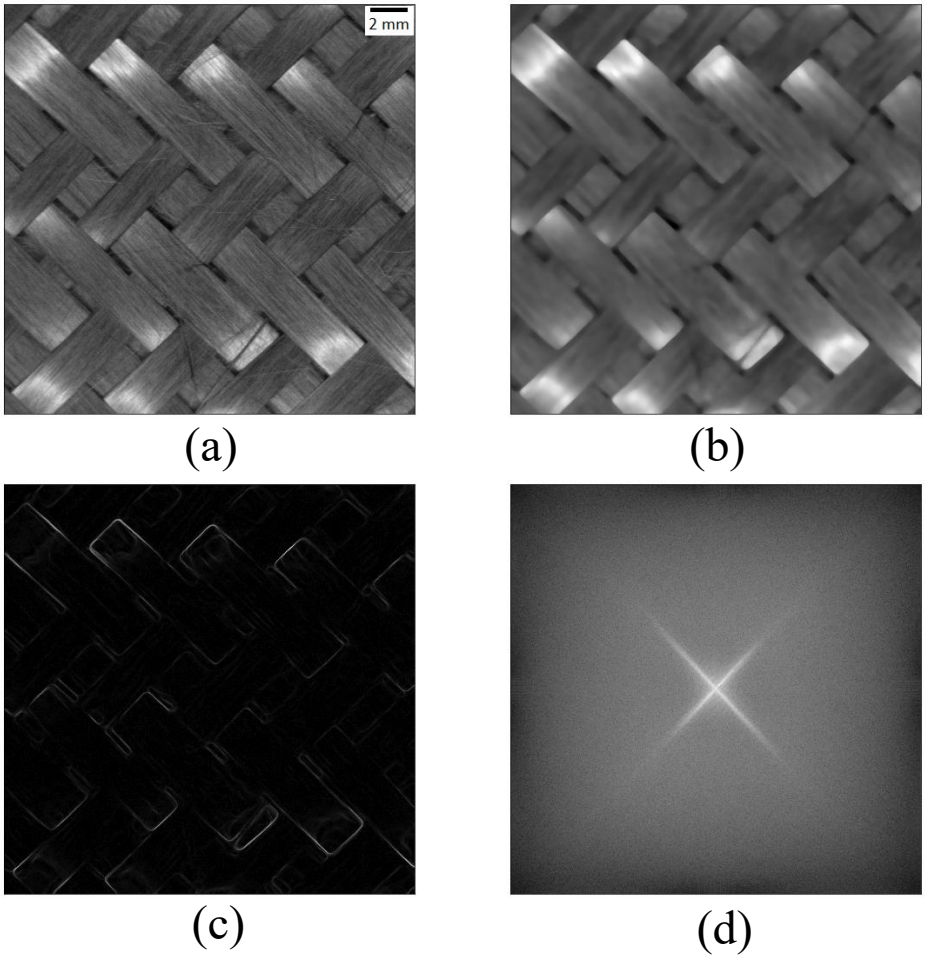


Figure 4.20 Steps of the Image Processing of the In-Process Monitoring System at the NCC

The following routine is completed for braid angle measurement, the image taken by the camera is cropped (top left), this image is then blurred using a median filter (top right), the edges are then detected using Scharr operator, kernal size = 3 (bottom left) and a logarithm of Fourier power spectral density (bottom right) [35].

The mean pixel intensity is the plotted against braid angle. The peaks are then fitted, and the position peak maxima is used to determine the measured braid angle. This is shown in Figure 4.21.

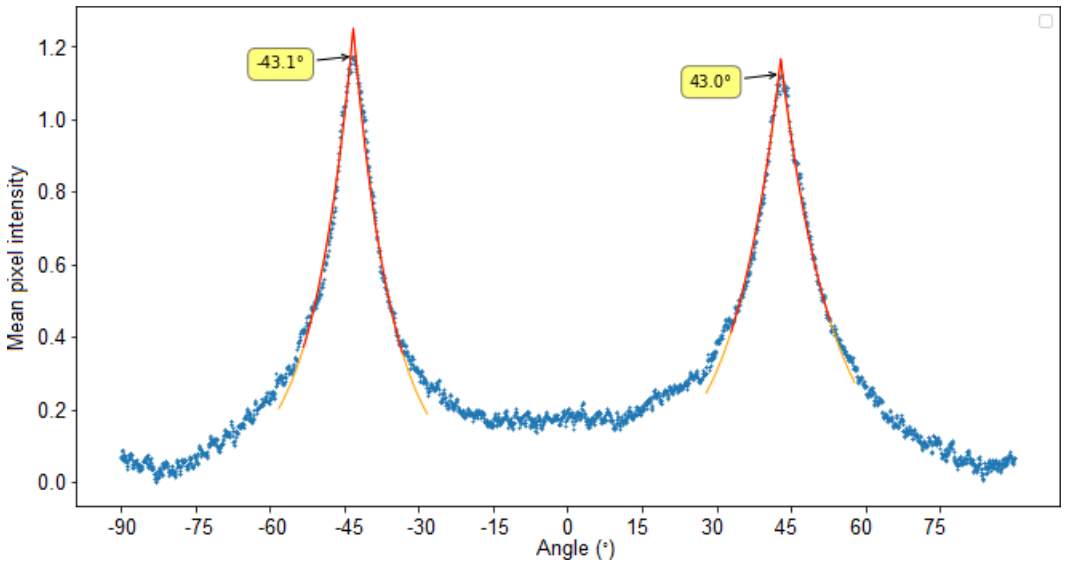


Figure 4.21 Mean Pixel Intensity

For this project, a comparison between the ImageJ measurement method and the IPM is required. Braided preforms manufactured on a 200mm diameter mandrel programmed to produce a braid angle of 45° were manufactured at the NCC. 12K HTS45 carbon fibre from Teijin was used rewound with 0 Tpm. Multilayer preforms were manufactured with four braided layers. Braid angle measurements were taken using both the ImageJ methodology and the IPM system. Figure 4.22 shows the interval differences between the two measured values. Both measurement systems showed good agreement with most measurements within ±0.5° of one another.

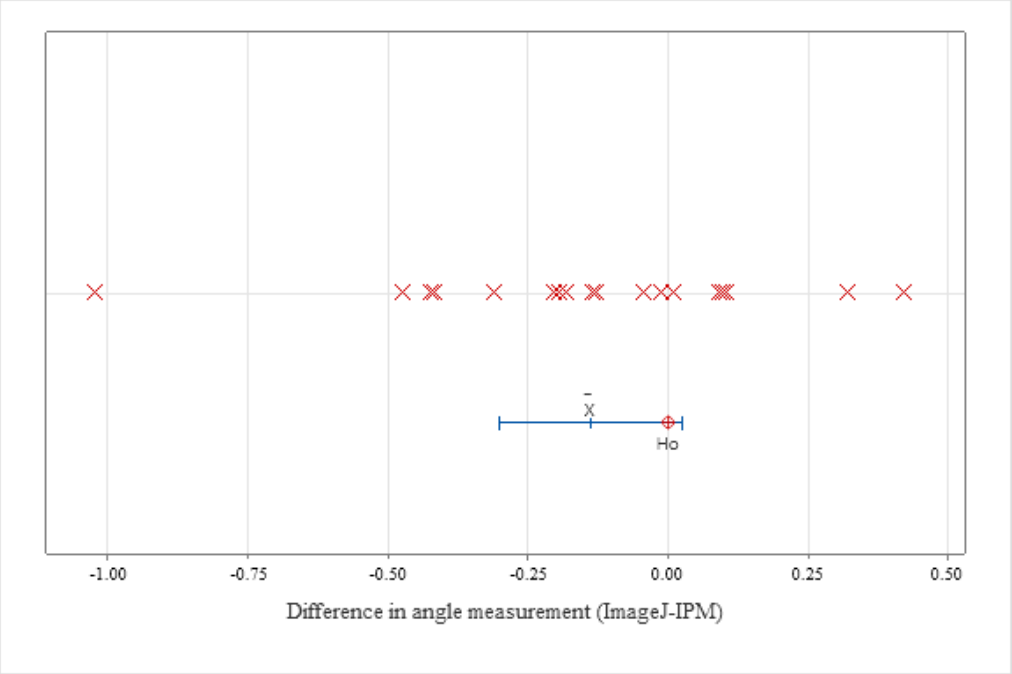


Figure 4.22 Difference in ImageJ and IPM measurements

An average difference in magnitude of 0.265° was recorded between the measurements taken using ImageJ and those using the IPM measurement system. Twenty different measurements were taken at corresponding points along the mandrel in the region where the braid was considered to have stabilised at 45°. The measurements were made on the same item under different conditions, as a result a paired T-test is used. A P-value of 0.089 is returned, there is no statistically significant difference between the measurement systems.

For braided preform thickness the IPM system has the capacity to conduct a non-contact measurement. A laser line scanner, Micro-epsilon scanCONTOL 2900-100 with red 658nm laser diode, mounted perpendicular to braiding axis in a fixed known position is used to acquire discrete profile scans of the preform surface. A baseline scan of the mandrel is required prior to the braiding operation. The surface profiles of subsequent braided layers acquired by the profilometer are then used to calculate changes in the mandrel surface height and therefore braided layer thickness.

The IPM measurement system provides a good indicator of preform thickness, however the variability of the thickness measurements is high with an approximate standard deviation of ± 0.2mm, This discrepancy is likely a result of machine noise due to process interruptions.

4.1.3.4 Apodius Scanner

The Apodius Vision System (AVS) 3D by Hexagon is used for advanced carbon-fibre part inspection, is another method of ascertaining braided preform parameters. The AVS is mounted on a 7-axis arm which allows the laser to be easily manipulated around the preform to capture the part. The datasheet states that the system is accurate to 0.026mm and can measure up to 1.2 million points per second. The RS6 laser scanner is certified to standard ISO 10360 8. Measurements were taken using the AVS post-process on the final preform. The data output for the system also enables comparison between the target and actual values of fibre orientation. Figure 4.23 shows a typical image output for the measurement system. The high-quality camera image can be used in braiding to inspect the part angle along with a qualitative detection of fibre damage by the operator. Areas of similar fibre orientation are grouped together by the system which identifies images of similar optical appearance. A texture segmentation algorithm is then used to detect the edges of the yarns. The user then manually assigns a reinforcement direction, as the AVS knows the global location and orientation of the images the local fibre orientation can be mapped to determine the braid angle of the preform.

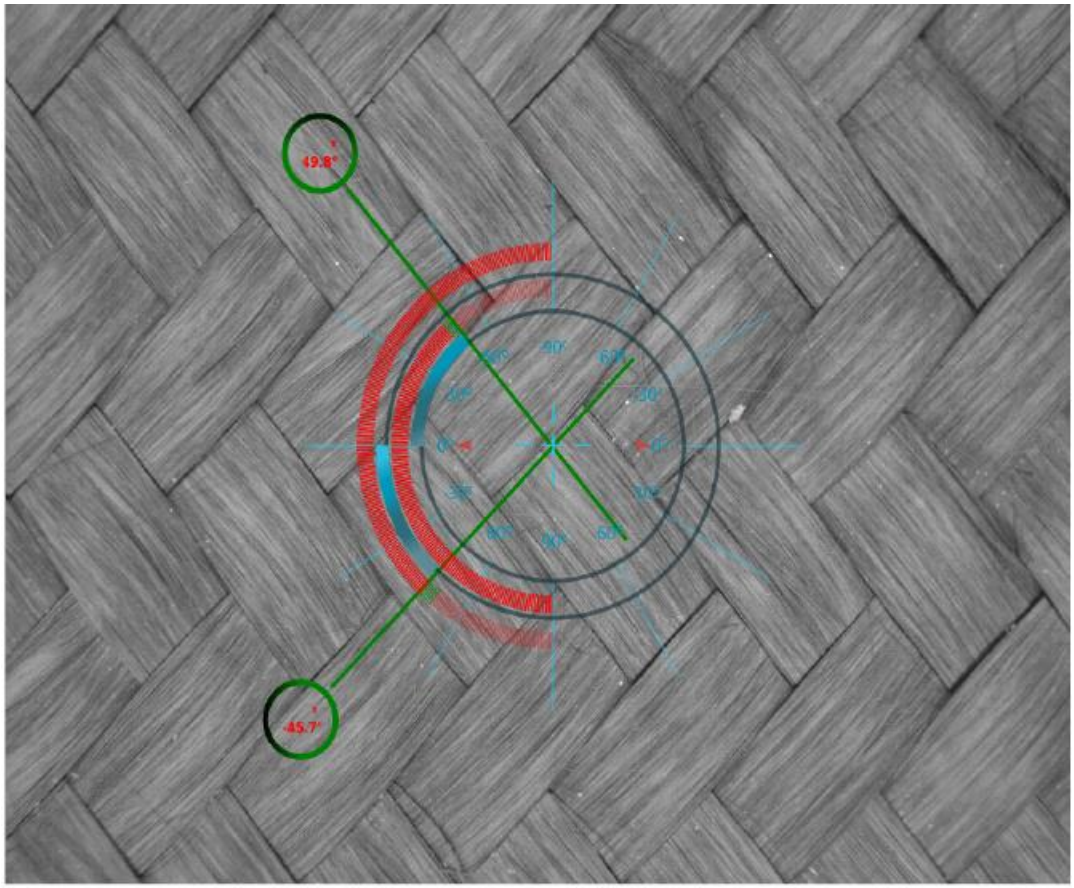


Figure 4.23 Typical Image Output from the AVS

An algorithm determines the orientation of the fibres. Typically for a braided preform, two peaks are expected one for the weft and the other for the warp yarns. Table 4.5 compares a set of measurements taken using the Apodius scanner with a range of manual measurements taken using ImageJ to assess the validity of the Apodius scanner as a measurement method for braid angle.

Table 4.5 Braid angle deviation comparison for AVS and ImageJ

Image ID	Apodius Deviation from Predicted Angle, °	ImageJ Deviation from Predicted Angle, °
1	0.3	0.005
2	-0.8	0.365
3	-0.95	-0.135
4	0.35	0.915
5	-0.7	0.735
6	-0.09	-0.385
7	-0.1	0.99
8	-0.45	0.655
9	0.35	0.44
10	0.05	-0.08

Both measurement methods provide a good approximation of braid angle in comparison to the programmed braid angle, within the acceptable range of ±1°. There is no indication that either measurement system consistently over or underestimates the braid angle of a preform. Similarly, the variation within ±1° is likely to be a result of the natural variation present within a braided preform. A two tailed paired T-test has been conducted to assess the difference in magnitude of deviation from the predicted braid angle between the measurement systems. A P-Value of 0.724 is returned this is greater than the significance level of 0.05 so the null hypothesis can be accepted that there is no significant difference between the magnitude of deviation from predicted braid angle when measuring the ImageJ and the AVS.

The AVS measurement system also provides a non-destructive method of measuring braided preform thickness. The preform is scanned post-process which avoids the machine noise influencing the measurement. As a result, braided layer thickness measurements are recorded similar in magnitude to the IPM system with much smaller standard deviations. Table 4.6 summarises the thickness measurements for the initial layer of a preform manufactured with 0 Tpm.

Table 4.6 Thickness Measurement Method Summary

IPM Thickness Measurement, mm	AVS Thickness Measurement, mm
0.703 ± 0.211	0.575 ± 0,043

4.1.4 Composites Manufacturing

4.1.4.1 Preform Manufacture Methodology

Braided preforms were manufactured on the 192-carrier braider at the NCC using HTS45 12K at two different levels of twist, 0 Tpm and 7 Tpm. The rewinding tension and speed were kept constant. The braid angle and cover factor were controlled at 45° and 96% respectively by manipulating the part diameter through using two different mandrels of 120mm and 200mm diameter. This was based off analytical calculations using Equation 3.3 and previous work completed [87] to provide a tow width approximation. The manufacturing process parameters can be seen in Table 4.7. The braid architecture was monitored using image process software ImageJ.

Table 4.7 Preform parameters.

Preform ID	Rewinding Twist, Tpm	Braid Angle,	Cover Factor, %	Part Diameter, mm
A	0	45	96	200
B	7	45	96	120

Each preform was three layers thick and the braid thickness was monitored using the in-process system. After each layer, the braid was secured to preserve the tension within the preform prior to cutting through taping the preform. This maintained the braid architecture by keeping tension on the fibres. The braided preforms were removed from the mandrel without cutting them, they were then flattened to produce flat preforms six layers in thickness. Figure 4.24a and Figure 4.24b shows the difference in the braid angle of the preform for both fibre types, on the measured on the mandrel and then once it had been flattened. In each case thirty measurements were recorded using image processing software. A two-tailed t-test was conducted with a significance level of $\alpha=0.1$ analysing the difference in braid angle whilst it

remained on the mandrel under tension and once the preform had been removed from the mandrel, for each preform manufactured with both the 0 Tpm and 7 Tpm fibre.

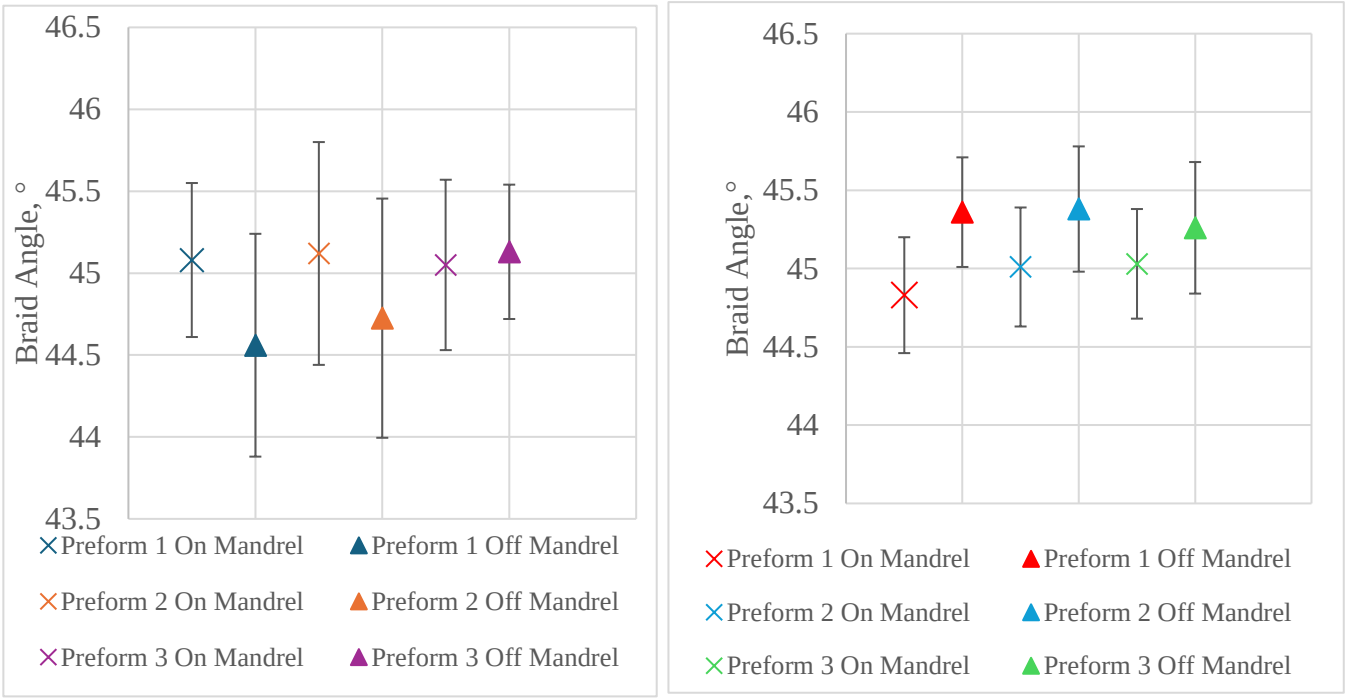


Figure 4.24 Braid angle on and off mandrel for (a) 0 Tpm preforms (b) 7 Tpm preforms

When the preforms relaxed and tension was removed off the mandrel, numerically the braid angle was noted to decrease slightly with the 0 Tpm preforms whereas a slight increase was measured with the 7 Tpm preforms. This is due to rotation of the individual filaments which relaxes once the carrier spring tension is removed. However, statistical testing found this difference to be insignificant. All braid angles remained within the ±1° tolerance which is considered acceptable for aerospace standard applications.

4.1.4.2 Liquid Moulding of Mechanical Test Samples

The 0 Tpm and 7 Tpm were infused separately with each preform bagged up for infusion as seen in Figure 4.25. Each preform is bagged separately with the vacuum outlet placed in a raised pleat to prevent resin reaching it during infusion. Tacky tape was used to dam the edge of each panel to prevent race tracking.

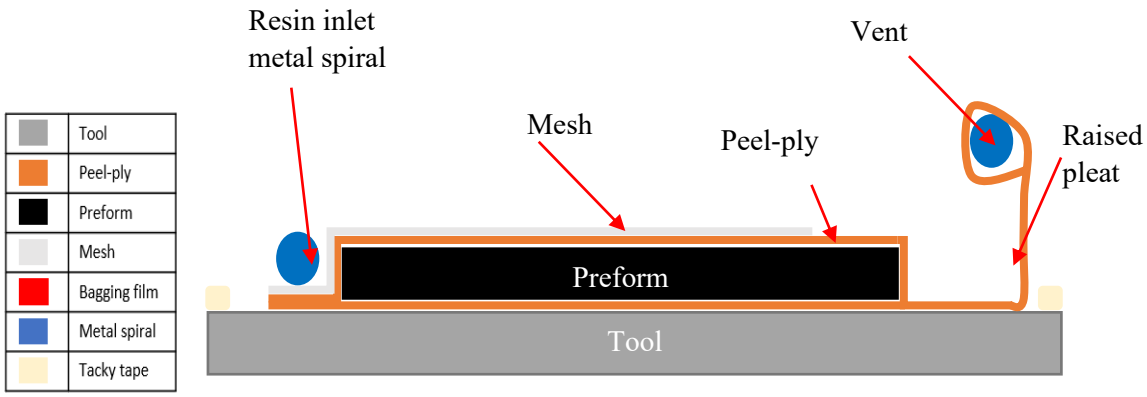


Figure 4.25 Preform bagged for infusion set-up

Once the preforms had been vacuumed down, horizontal lines were drawn on the vacuum bag 10mm apart to track resin flow. It is anticipated that the flow front will differ between the 0 Tpm and 7 Tpm preform due to the increase compaction of the tow with twisted fibres. The three preforms of each configuration were arranged on a 2480 x 1280 mm cure table in the configuration shown in Figure 4.26. Each bagging lay-up passed a drop test where the vacuum drop did not exceed 25mbar in 5 minutes.

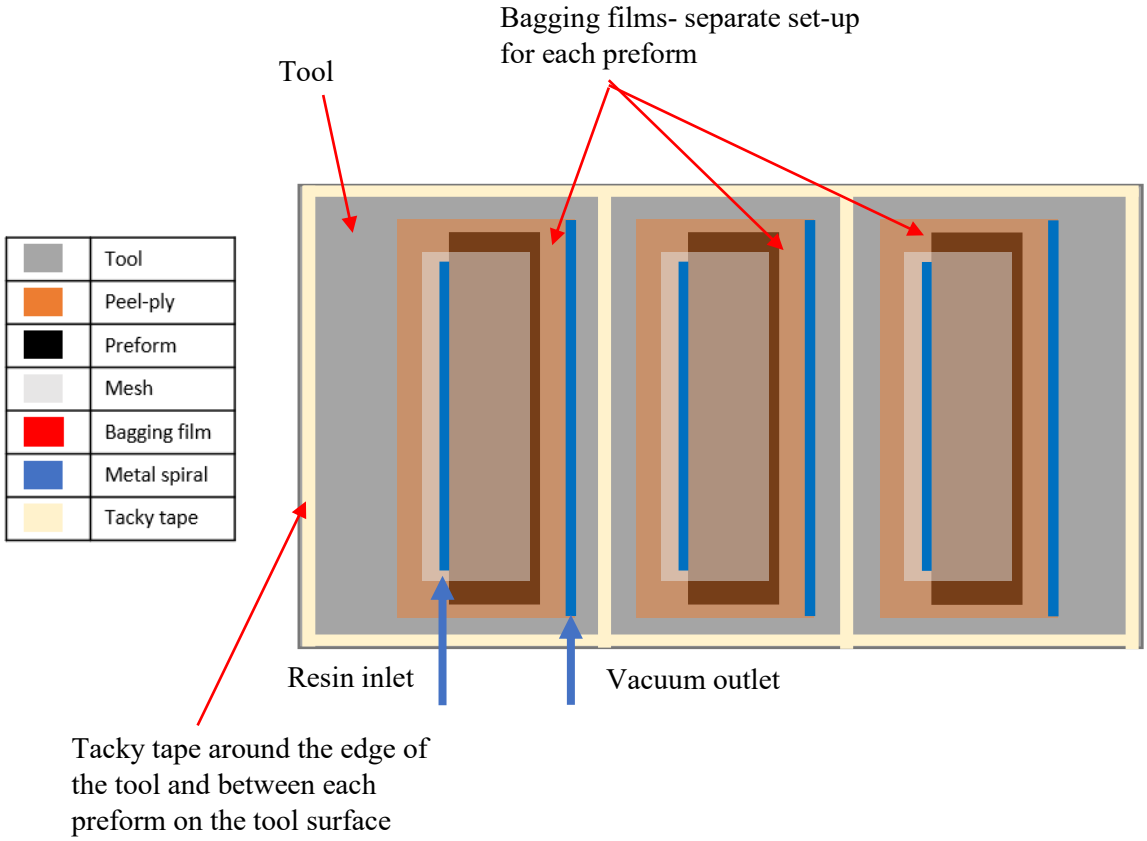


Figure 4.26 Multiple preform infusion set-up

A resin system of EPIKOTE RIMR 135 Resin (3kg) and RIMR 137 Hardener (0.9kg) was used to infuse the preforms. Infusion processing temperature for the system are generally between 15°C and 50°C, in this case the process will be conducted at room temperature.

Each preform had six plies, Table 4.8 summarises the final thickness of the preform and the final cured thickness of the panel.

Table 4.8 Ply Thickness

Sample ID	Final Panel Thickness, mm	Cured Ply Thickness, mm
0 Tpm A	2.36	0.393
0 Tpm B	2.45	0.408
0 Tpm C	2.21	0.368
7 Tpm A	3.84	0.640
7 Tpm B	4.09	0.682
7 Tpm C	3.79	0.632

Equation 4.2 is used to calculate the volume fraction of each panel for a fibre density of 1.77g/cm^3 as stated in the material datasheet [88]. The calculations for ply GSM are shown in Table 4.9.

$$Vf = \frac{Ply\ gsm}{fibre\ density \cdot CPT}$$

Equation 4.2 Volume Fraction

Table 4.9 Ply GSM

Sample ID	Ply Weight, kg	Ply GSM, g/m^2
0 Tpm A	0.154	0.367
0 Tpm B	0.151	0.361
0 Tpm C	0.149	0.355
7 Tpm A	0.194	0.602
7 Tpm B	0.225	0.698
7 Tpm C	0.208	0.646

The final volume fraction for each panel is shown in Table 4.10 calculated using Equation 4.2.

Table 4.10 Volume fraction for composite panels

Sample ID	Volume Fraction, %
0 Tpm A	53
0 Tpm B	50
0 Tpm C	54
7 Tpm A	53
7 Tpm B	58
7 Tpm C	58

A grid drawn onto the bagging film was used to monitor the resin flow front. The % fill of the preform can then be calculated for each of the three preforms infusion for both the 0 Tpm and 7 Tpm material configurations. A series of images were taken at thirty second intervals throughout the infusion process. A visible difference in the shape of the flow front can be seen in Figure 4.27. The resin propagated more linearly across the length of the 0 Tpm preforms, whereas with the 7 Tpm preform the resin

flow front propagates diagonally. This is due to more compact fibre bundles in the twisted fibres providing more resistance to the resin flow.

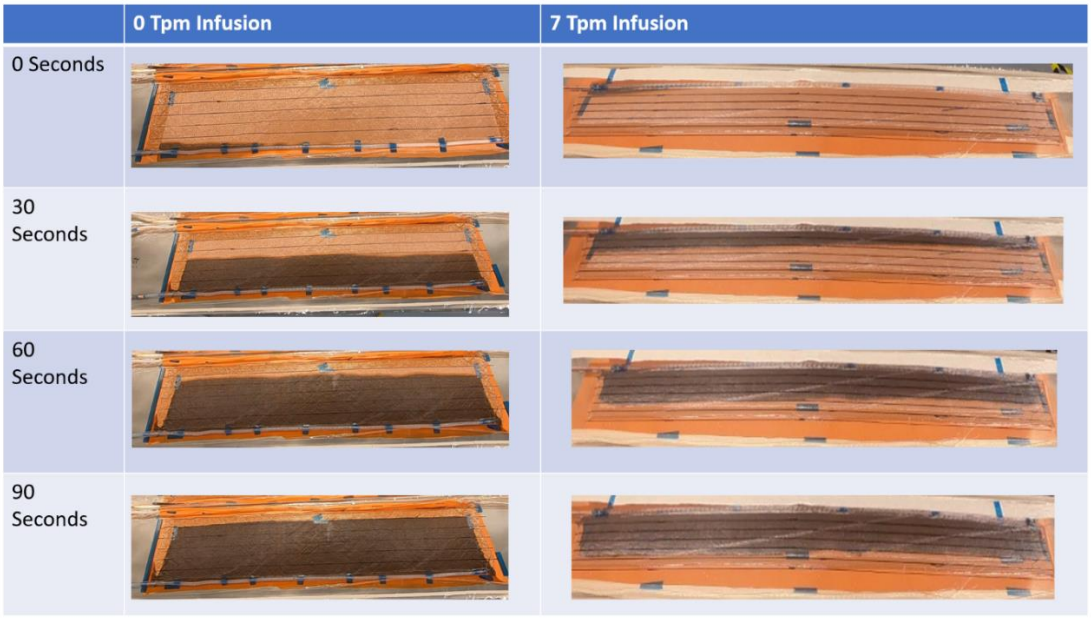


Figure 4.27 Progression of infusion of untwisted and twisted preforms

Figure 4.28 compares the % fill of the preforms at intervals during the infusion process. A slight increase in fill time was noted for the preforms manufactured with 7 Tpm, this is due to the twisted bundles increasing permeability, however the increase in time of 5-10 seconds does not suggest a significant reduction in resin flow velocity through the preform. Apart from 7 Tpm Preform 3, all braids fully wetted out under 2 minutes.

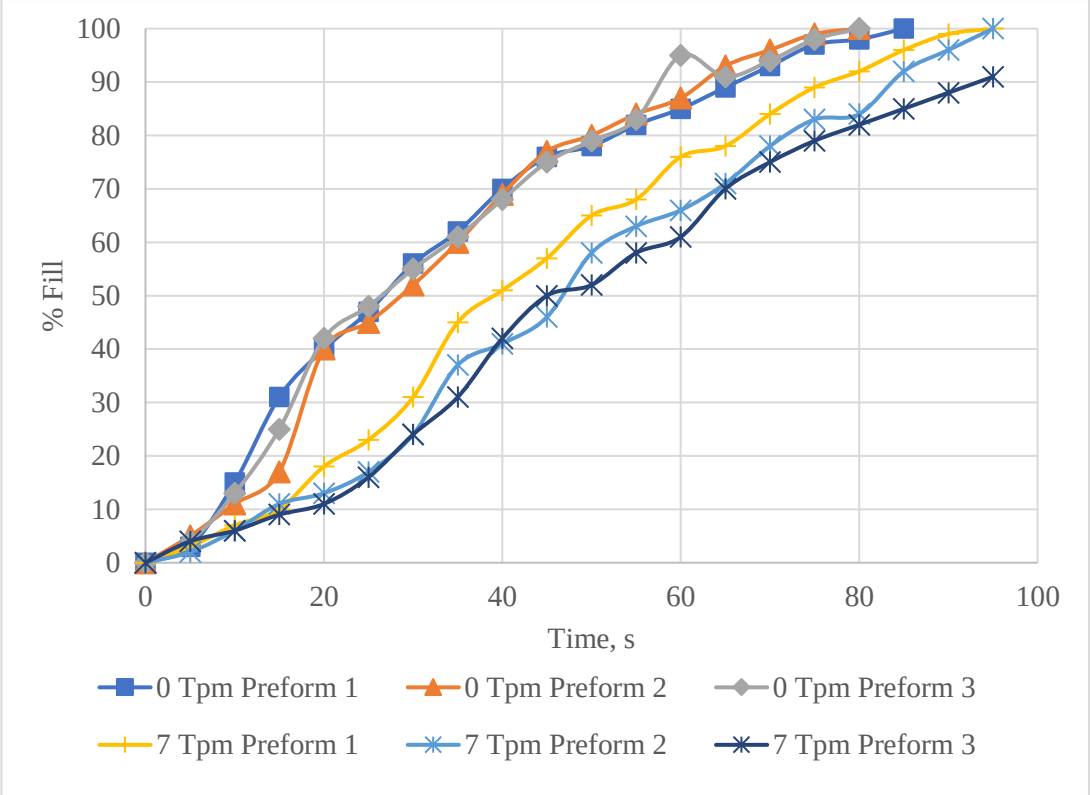


Figure 4.28 %Fill of each preform throughout infusion

Figure 4.29a and Figure 4.29b demonstrates the recorded braid angle post-infusion and compares this to the dry flattened preform for both the 0 Tpm and 7 Tpm test cases. In each preform an increase in braid angle was recorded post-infusion, this is due to the pressure the preform was under in the vacuum-bag causing the angle to increase. However, this increase was much more noticeable with the 7 Tpm preforms as shown in Figure 4.29b. Thirty measurements of braid angle were recorded in each preform both pre and post infusion, and a two-tailed t-test has been conducted at a significance level of $\alpha=0$. The difference in braid angle between the flattened dry preform and the infused preform was found to be statistically significant for the 7 Tpm only at a P-value of 0.05.

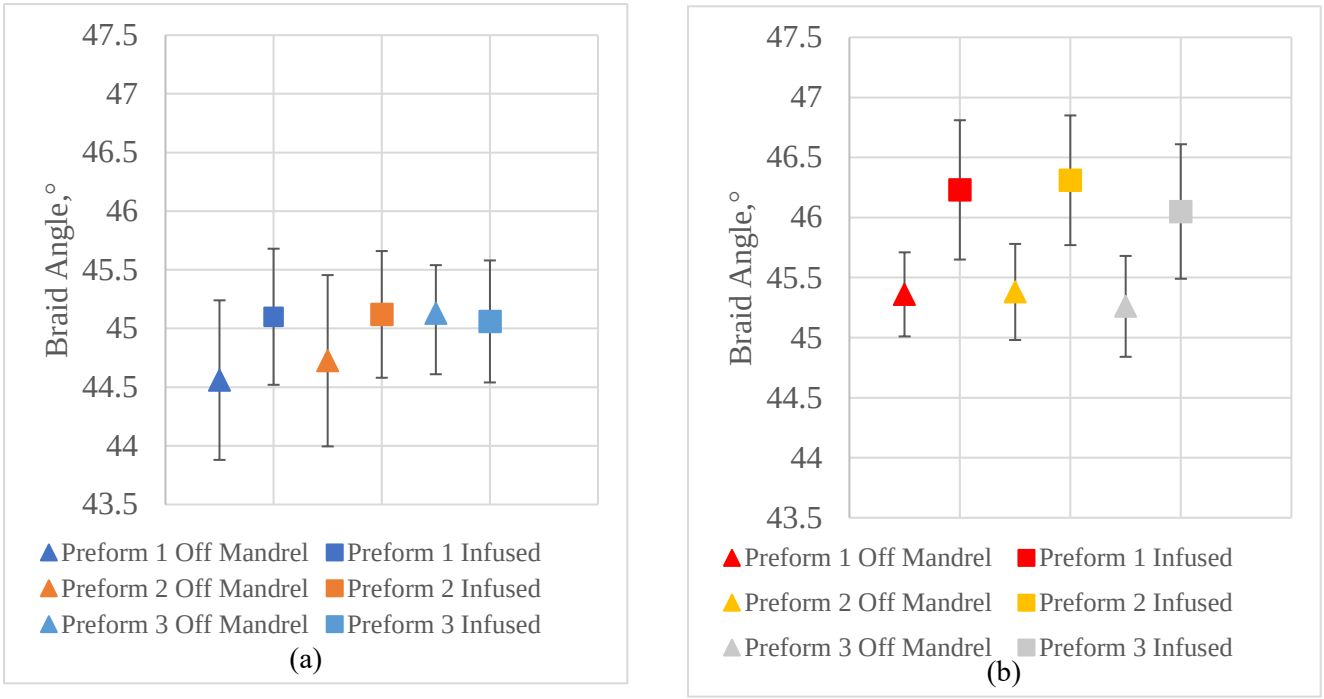


Figure 4.29 Braid angle comparison off mandrel and post-infusion

Similarly, to the braid angle, the infused tow width has been monitored using ImageJ. Thirty measurements were taken in each preform at each stage of the manufacturing process and an average tow width calculated. Figure 4.30 shows the difference in average measured tow width for the 0 Tpm preforms and 7 Tpm preforms at each stage of the manufacturing process. Once the preform had been removed from the mandrel, the tow width decreased as the fibres were untensioned which reduced the spread of the filaments in the tow. Once the preforms had been infused the average tow width increased again due to the pressure provided by the vac-bag which caused the tow to spread out.

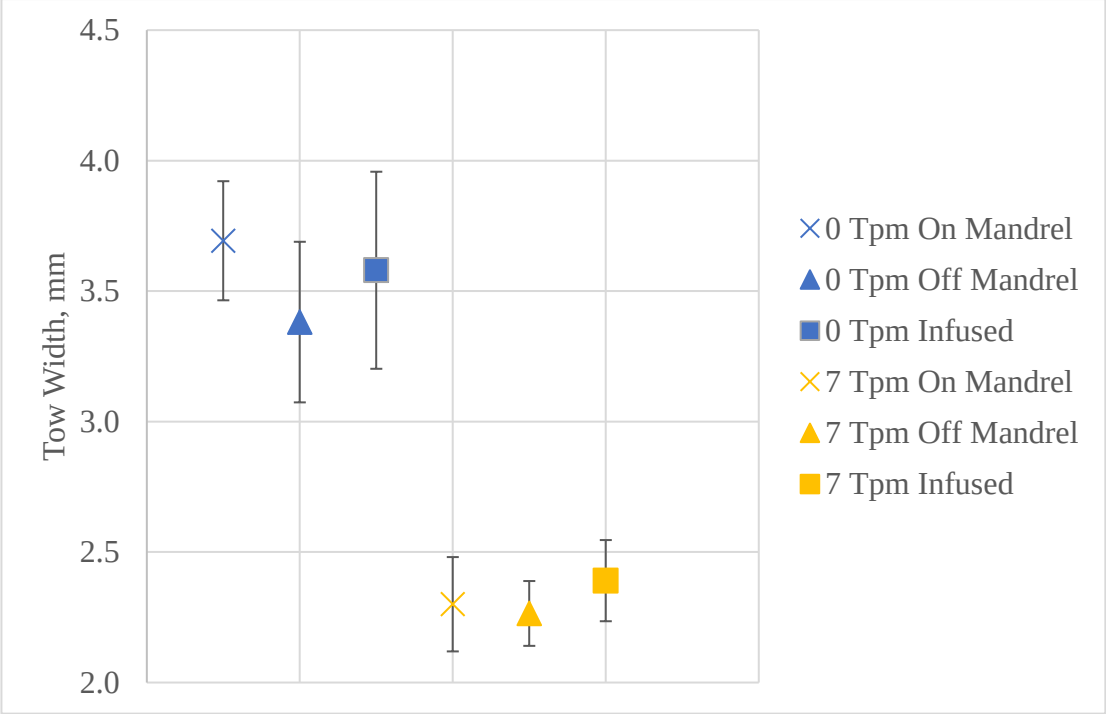


Figure 4.30 Measured Tow Width at Each Stage of the Manufacturing Process for 0 Tpm and 7 Tpm Panels

The standard deviation bars for each measurement set overlapped which indicated although the average tow width changed at each stage suggesting that the tow width approximation for 0 Tpm is valid at all stages of the process.

4.1.5 Mechanical Testing

The ISO-527-4 standard was selected to determine the ultimate tensile strength of the materials at coupon level. The diameter of the manufactured preforms was altered to maintain a braid angle of 45° and a cover factor of 96%. This investigation focussed on the effect of the additional twist on the fibres therefore a tensile test was selected to analyse the impact of the additional twist during rewinding on the strength of the fibres. Coupons were extracted from the panels with a fibre orientation of 0/90°. This ensured that some fibres were aligned with the direction of the load. Any changes in mechanical properties therefore are a result of the inclusion of the additional twist from 0 Tpm to 7 Tpm. As is common industrial practice when manufacturing braided panels, the cylindrical preforms were slid off the mandrel without cutting and flattened. The mandrel geometry and resultant required number of bobbins were selected so the preforms were wide enough to extract coupons without incurring the

edge effects caused by the flattening of the preforms, these are summarised in Table 4.11.

Table 4.11 Machine Parameters for Preform Manufacture

Level of Rewinding Twist, Tpm	Mandrel Diameter, mm	Number of Braid Carrier
0	200	192
7	120	192

The same number of braided layers were deposited for each preform, manufactured from the same fibre with the same angle and coverage. The only difference between coupons was the number of twists added to the fibres during the rewinding step. The difference in cross-sectional area of the coupons was accounted for during data processing.

4.1.5.1 Experimental Testing Set-Up

Testing was completed with the support of Composite Test and Evaluation Ltd in Honiton. A tensile test machine from Shimadzu AG-X+ with a 100 kN load cell was used. Coupons were cut from the central section of each sample to avoid the edge effects from the flattening of the braided preform. Thirty coupons were extracted from each composite panel with ±45° fibres orientated in the 0/90° direction. This kept the 50% of the fibres in the same direction as the test load. Each rectangular coupon measured 25mm in width and 210mm in length in line with the test standard. All specimens were tabbed with 2mm thick Attwater B48 Epoxy Glass End Tabs which were bonded to the specimen using 3M's AF163-2K film adhesive. The coupons were secured in the test machine as shown in Figure 4.31.

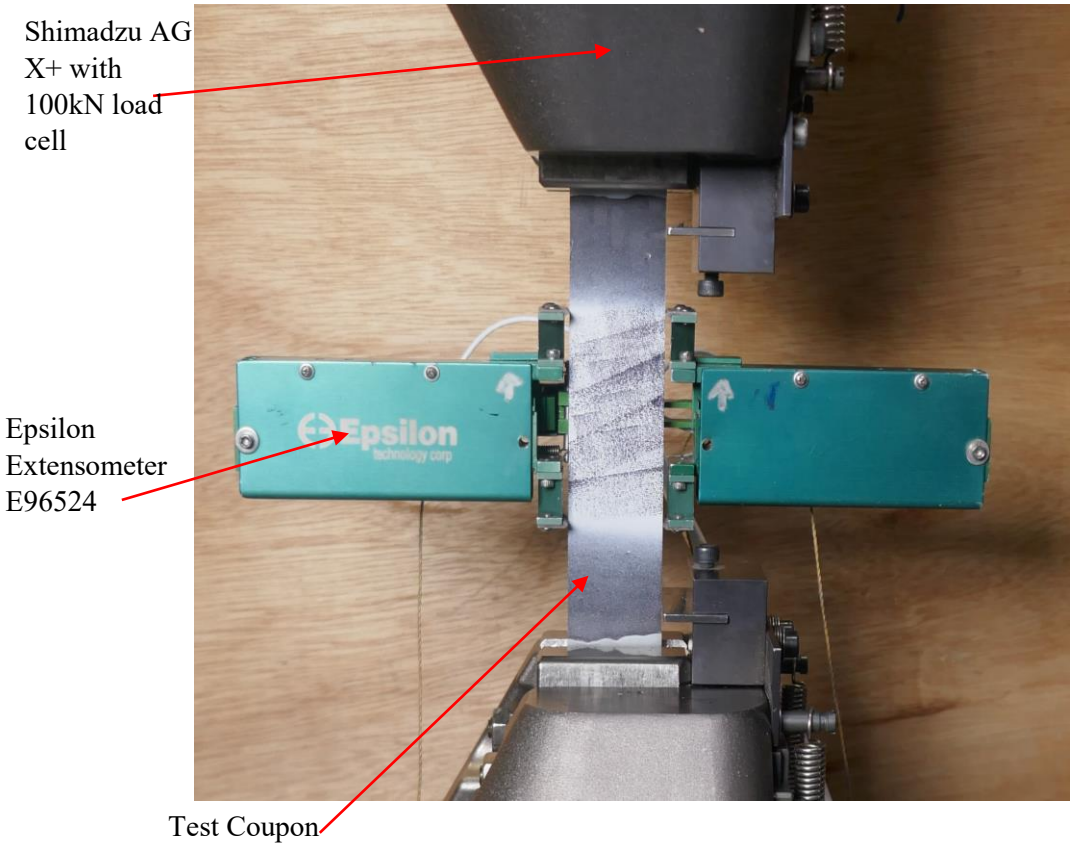


Figure 4.31 Shimadzu AG-X+ Tensile Test Machine

Strain monitoring was conducted using a Epsilon Extensometer E96524 calibrated with ISO9513 and an Imetrum Video Strain Gauge. The full set-up can be seen in Figure 4.32.

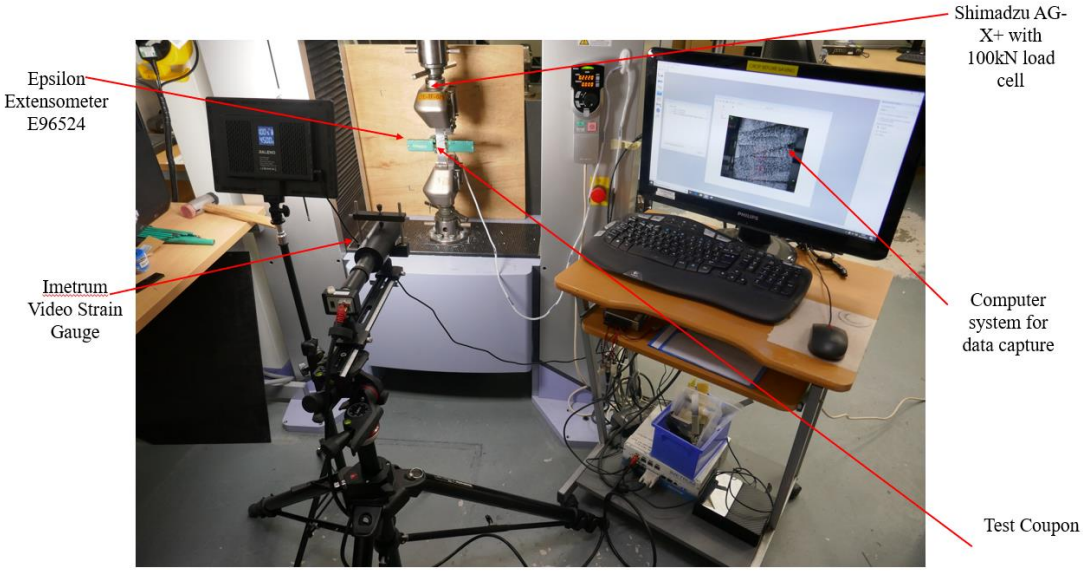


Figure 4.32 Test Set-Up

Table 4.12 demonstrates the coupon parameters for each panel. According to the test standard coupon thickness should be within 2-10mm. Due to the more rounded shape of the cross-section of the tow for the twisted fibres, there is a difference in panel thickness between the 0 Tpm and 7 Tpm preform.

Table 4.12 Average coupon dimensions

Preform ID	Coupon Width, mm	Coupon Thickness, mm
0 Tpm Preform 1	24.97 ± 0.05	2.36 ± 0.08
0 Tpm Preform 2	24.99 ± 0.12	2.45 ± 0.11
0 Tpm Preform 3	24.96 ± 0.02	2.21 ± 0.11
7 Tpm Preform 1	25.03 ± 0.04	3.84 ± 0.03
7 Tpm Preform 2	25.07 ± 0.03	4.09 ± 0.02
7 Tpm Preform 3	24.99 ± 0.05	3.79 ± 0.04

Ultimate tensile strength, extension at break, tensile modulus, and Poisson's ratio have all been captured. The comparison of this data along with conclusions regarding the influence of additional twist on the mechanical properties of braided composites are discussed in the subsequent section of this report.

4.2 Statistical Methodologies

A range of statistical methodologies have been utilised in this work to determine the significance of the data collected and trends observed.

4.2.1 Testing the Statistical Significance

4.2.1.1 Two Sample T-test

Two sample t-tests can be used to determine if there is a significant different between two means. The two samples must be independent, samples must be taken randomly, and samples should be roughly normally distributed [89]. Samples should also be assumed to have equal variance. A sample size of thirty is used because it is the point at which the central limit theorem applies. This states that if the sample size is large enough the population can be assumed to follow a normal distribution [90]. A significance level of α=0.05 is used for this work

4.2.1.2 ANOVA

The hypothesis that the means of two or more populations are equal is tested through an analysis of variance test or ANOVA [91]. The approach uses variances to

determine if the means are statistically different. The null hypothesis states that all population means are equal with the alternative hypothesis stating that at least one mean is different. A significance level of α=0.05 is used for this test. ANOVAs require data from normally distributed data sets with equal variances. If the probability or P-value is less than the significance value than at least one of he means is statistically significantly different. To determine the difference between specific means, Tukey Pairwise comparisons can be used. This method creates confidence intervals for all pairwise differences between means while controlling the error rate to a specified value.

4.2.1.3 Pearson Correlation Test

The Pearson correlation test measures the linear relationship between two variables. The correlation strength ranges from -1 to 1, the larger the numerical value the stronger the correlation. The sign of the coefficient indicates the direction of the relationship [92].

4.2.2 A-Basis Design Allowable

From a composite design perspective, the strength of the laminate must be known is this based on the 'weakest link' theory [93]. As a result, the lower strength numbers obtained from test data are used for a design purpose. The design allowable is determined through statistical analysis of the data samples. There are two types, A-Basis and B-Basis [94]. A-Basis is defined as a strength value where 1 in 100 specimens will fail with a 95% confidence level. B-Basis is defined as a strength value where 10 in 100 specimens will fail with a 95% confidence level.

4.2.2.1 Goodness of Fit Test

To calculate the A-Basis design allowable, the statistical distribution that the data set follows must be determined. The mean and standard deviation can be calculated from the sample along with the sample size. A goodness of fit test is then completed to determine if the dataset fits the chosen distribution. A goodness of fit test establishes the discrepancy between the observed value and the predicted values of a particular distribution [95]. Minitab performs a goodness of fit test for a range of distributions, the distribution that best fits the dataset is most appropriate for the analysis. For the distribution to be a good fit, the probability (P-value) must be higher than significance value (α), this is typically 0.05. If more than one distribution exceeds this value then the most appropriate distribution is the largest P-value. Minitab output

the data as a plot representing the upper and lower bounds where the P-value exceeds 0.05.

4.2.2.2 Standard Deviation

Assuming the data follows a normal distribution, the standard deviation can be used as a measure of scatter. The range of data covered by ±1 SD is 68% of the observations, ±2 SD is 95% of the observations and ±3 SD is about 99.7 of the observations. These approximations can be used to estimate data ranges that would be expected to include 68%, 95% and 99.7% of observations [96].

4.2.2.3 Calculation of A-basis allowable

When the dataset is assumed to fit a normal distribution, Equation 4.3 can be used to calculate the A-Basis design allowable. Where $\bar{X}$ is the arithmetic mean k_A is a constant for tolerance factor determined from a look-up table using the number of specimens *n,* and *s* is the standard deviation.

$$A = \bar{X} - K_A(s)$$

Equation 4.3 A-basis allowable [94]

4.3 Discussion

To this point, a summary of the methodologies used in this work to address the objectives stated in Chapter 1 has been presented. Two braiding machines have been used to conduct this work, the 48-carrier axial braider at the UoN and the 192-carrier axial braider at the NCC. The mechanics of the machines have been explained and the method of calibration between the two braiders has been addressed due to their different programming methods. This has enabled trials completed on the small machine to be compared to the larger machine.

As this work aims to address the influence of rewinding twist on the braided preforms and resulting braided composites, the mechanics of the rewinding process along with specific processing parameters such as rewinding twist, speed and tension have been described. All the rewinding for this work was completed on the CE-1187 rewinding machine with accompanying Eurocarbon twist cabinet. The method in which this set-up works is explicitly described highlighting the specific guiding elements and tensioning mechanisms used in the set-up.

This work aims to address the result of rewinding twist on the mechanical properties of braided composites, consequently the manufacture and testing of a set of braided test coupons is discussed. A novel testing approach, testing the coupons in a 0/90° orientation was utilised to determine the influence of rewinding twist on the fibres. At the time of writing, there is no literature written looking at the influence of rewinding twist on the mechanical performance of braided composites in any

capacity. Much of the knowledge of rewinding is held by braider operators in industry. A visible difference in the progression of the infusion was seen in Figure 4.27 suggesting that twisted fibres did result in a reduction in permeability due to the more compact tow bundles which resisted resin flow.

Various measurement methods are used in this work to determine if rewinding twist influences the braid architecture of a preform. A gage repeatability and reliability study were conducted for using ImageJ as a measurement method for braid angle, cover factor and tow width. The method was found to provide an acceptable level of measurement with most of the variation coming from part variation. This is known to exist in textile composites. A variety of statistical methodologies are also used in the work to support conclusions.

4.4 Conclusion

In summary, the methodology presented covers all aspects of the experimental work used in conjunction with this thesis to determine the influence of rewinding twist on braided preforms and resulting braided composite structures. Initial trends highlighted during the manufacture of braided coupons are identified along with the validation of measurement methods used in the experimental chapters of this work.

5 Effect of Rewinding Twist on Mechanical Properties of a Braided Composite

5.1 Background and Aim

The literature review highlights the link between the parameters of the rewinding step and the subsequent quality of the braided preform [2]. The mechanism of the twist, including the subsequent fibre processability benefits are discussed in this chapter. A small-scale study to quantify the level of fibre damage caused by the rewinding and braiding processes is also included utilising multiple methods of monitoring fibre damage. A set of mechanical tests were performed, at a coupon level, on preforms manufactured with 0 twists per metre (Tpm) and 7 Tpm to determine if adding twist to fibres during rewinding has an impact of the mechanical properties of the braided composite. The facilities at NCC, the CEZOMA CE-1187 rewinding machine with accompanying Eurocarbon twist cabinet, were used to prepare the material and the 192-carrier axial Eurocarbon braider was used to manufacture the preforms for the coupon testing. The coupon testing was subcontracted to external test house Composite Testing and Evaluation ltd.

5.2 Impact of Twisting on Fibre Processability

5.2.1 In-Process Fibre Damage

During the braiding process substantially more fibre damage was observed on the 0 Tpm preforms in comparison to the equivalent preforms with twisted fibres.

Figure 5.1 shows two preforms manufactured with identical process parameters. However, Figure 5.1a is manufactured with 0 Tpm and Figure 5.1b is manufactured with 5 Tpm. Visible damage such as filamentation and fuzz were noticeable in the surface of the 0 Tpm preform and may have a negative impact on the final mechanical properties of the braid. The 0 Tpm preform is considerably more matt in appearance in contrast to the glossier appearance of the fibres in the 5 Tpm preform which indicates a greater occurrence of in-process fibre damage in the 0 Tpm preforms.

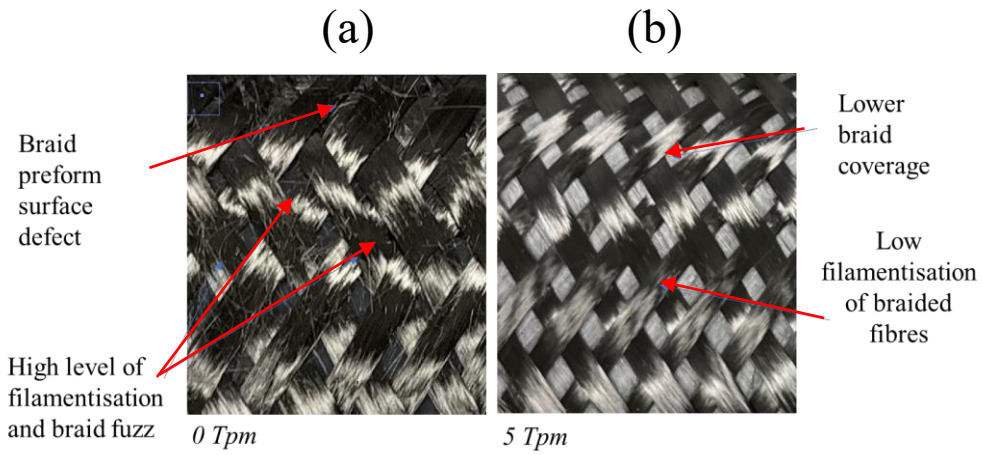


Figure 5.1 Visible difference in fibre damage when winding with twist

A greater number of tow breakages and fibre entanglements due to filamentisation in the braid cone were observed during braiding with 0 Tpm fibres. Figure 5.2 details some of the in-process fibre damage that occurred during preform manufacture. This led to an increase in process interruptions and a consequent increase in material wastage.

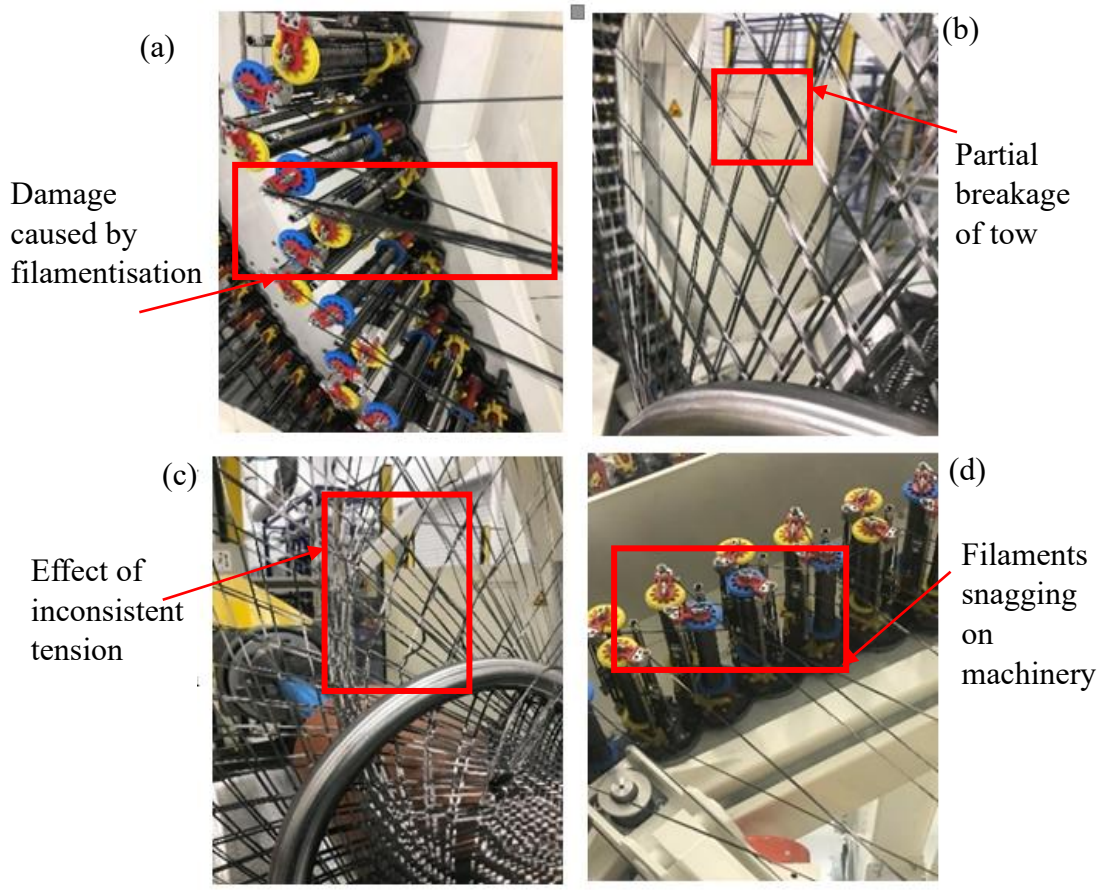


Figure 5.2 In-process fibre damage during manufacturing with untwisted fibres

Figure 5.2a demonstrates the extent of damage caused by filamentisation, damage to the tow reduces the integrity of the tow bundle causing individual filaments of the tow to become exposed. These individual filaments, once exposed snag on the machinery which results in an escalation of the damage bringing the process to a stop as shown in Figure 5.2d. This is caused when exposed carbon filaments become entangled with the carrier mechanism of the machinery.

Figure 5.2b shows the partial breakage of a tow, again the increase in exposure of filaments to the friction of the braiding process results in greater damage accumulation. The partial broken filaments create a 'spiders web' style damage. Broken filaments that remain in the braid cone result in tension deviations in the braid cone which results in further damage occurring to the braiding tows.

Figure 5.2c highlights the impact of inconsistent tensioning when braiding as a result of tow damage which produces preform inconsistencies. Tension deviations result in variations in tow length unwound from the braider bobbin as shown by the undulating fibres in the braid cone. This leads to irregular yarn spacing in the braid cone as shown in the image, which results in localised variations in cover factor.

5.2.2 Indication of Fibre Damage

Fibre damage testing has been conducted on thirty different fibres of 1 metre in length for virgin fibre, untwisted rewound fibre (non-braided), untwisted rewound fibre (braided), twisted fibre (non-braided) and twisted fibre (braided). All the fibre analysed was 12K T700s supplied by Toray. The properties of each material case are summarised in Table 5.1.

Table 5.1 Fibre damage material test categories

Material ID	Rewinding Twist, Tpm	Braided?	Rewinding Speed, RPM
A	N/A	N/A	N/A
B	0 Tpm	No	10,000
C	0 Tpm	Yes	10,000
D	7 Tpm	No	10,000
E	7 Tpm	Yes	10,000

For materials B to E the rewinding tension and speed was kept constant at 10,000 rpm with the only difference being the additional 7 Tpm added to materials D and E. The braiding process parameters were kept constant for C and E with a carrier speed of 220PPM and traverse speed of 960mm/min. Braided fibres were cut from the preform to remove them in a way which minimised additional damaged caused by inter-yarn friction. Thirty fibres of 1 metre in length were collected for each material category.

The severity of damage of each fibre was ranked according to the fibre damage scale outlined by Kyosev [2], a summary of these categories are shown in Table 3.1 as a measure of visible fibre damage in the carbon fibre tow. A ranking of 0 indicates fibre appears the same as virgin fibre supplied by the manufacturers. Fibre with a ranking of 1 suggests sizing degradation with an irregular yarn width and matte surface finish. As progressively more filaments are broken this damage ranking increases (2→3) until severe yarn damage with no defined surface (4) and ultimately a broken yarn (5). Table 5.2 shows the average ranking observed for the fibres in each of the material categories. A caveat with this method of analysis is distinguishing between the levels of fibre damage.

Table 5.2 Average visible fibre damage ranking

Material ID	0 Tpm	7 Tpm
Virgin Fibre (A)	0 ± 0	0 ± 0
Rewound	1.40 ± 0.498 (B)	0.67 ± 0.479 (C)
Braided	1.70 ± 0.651(D)	1.43 ± 0.504 €

The average fibre damage ranking increase throughout each stage of the manufacturing process due to damage accumulation. These findings correspond to the thoughts of Kyosev [2], who stated that yarns finish the rewinding process step on damage level 1 (B & D), with yarns in the finished braid reaching damage level 2 with a best case of damage level 1 (C & E). If the progression 0 Tpm fibre (Material A→B→C) is compared to the progression of the 7 Tpm fibre (Material A→D→E) the damage accumulation is visible as the magnitude of the ranking increases. It is worth noting however, that the standard deviation of both material progressions overlaps.

The water absorption methodology defined by Ebel [97] was followed. The initial weight of the individual fibres was measured, the fibres were then submerged into water for thirty seconds before being allowed to drip-dry for ten seconds. The final weight was then measured. The fibre damage was proportional to the increase in weight, with the more damaged fibres retaining more water due to filamentisation. Figure 5.3 shows the results of this initial fibre damage investigation display as the percentage increase in weight.

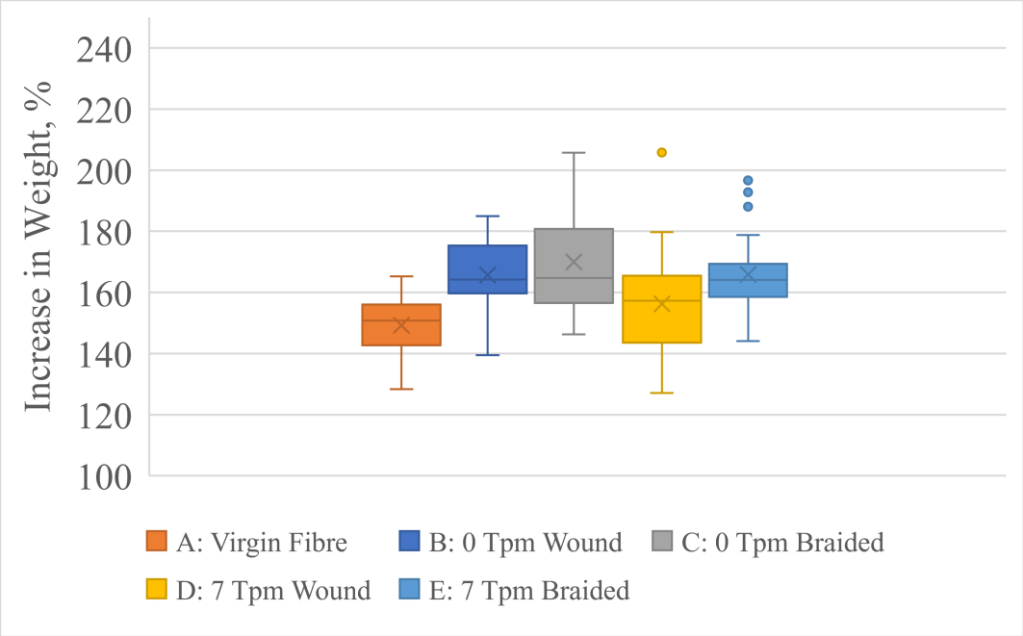


Figure 5.3 Gravimetric fibre damage test results

Material A demonstrated the lowest percentage increase. All materials that either have been wound or braided saw a percentage increase weight. This indicates the accumulation of fibre damage. A statistical ANOVA at a significance level of α=0.1 was used to compare Material ID's A→E, the thirty samples of each Material ID provide a sufficient sample size. Tukey pairwise comparisons demonstrate three separate groupings as shown in Table 5.3.

Table 5.3 Tukey pairwise comparison for gravimetric tests

Material ID	Material Details	Grouping		
A	Virgin Fibre			C
B	0 Tpm Wound	A	B	
C	0 Tpm Braided	A	B	
D	7 Tpm Wound		B	C
E	7 Tpm Braided	A		

If the progression of the 0 Tpm fibre (Material A →B→C) is compared to the progression of 7 Tpm (Material A→D →E), a steeper gradient in means can be seen in the untwisted fibres. This is demonstrated in

Figure 5.4.This suggests that damage accumulates through the manufacturing process from virgin fibre to rewinding to braiding this is something that Ebel suggests in the literature but a comparison between twisted and untwisted fibres has not been made.

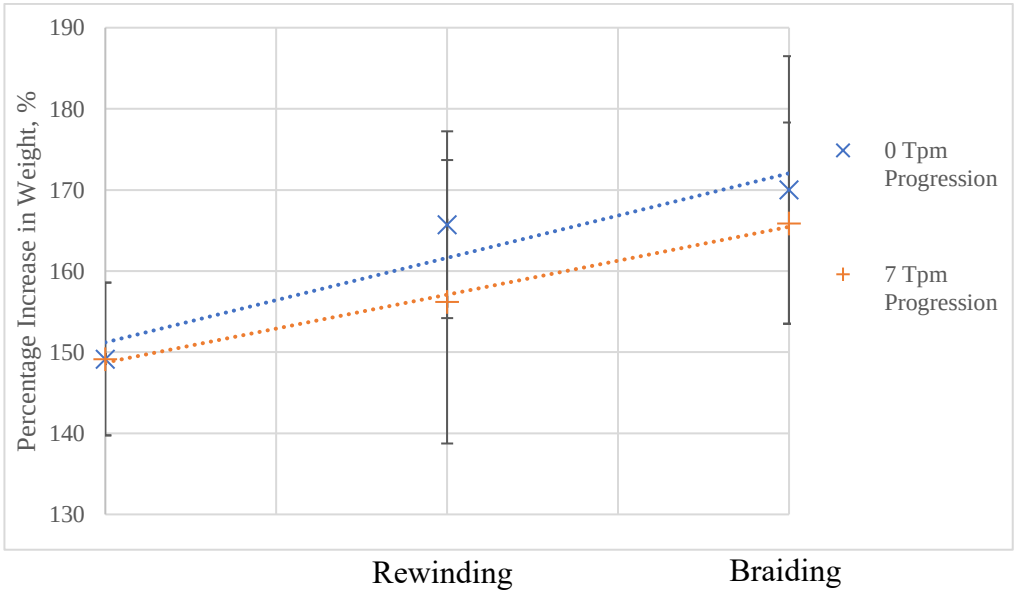


Figure 5.4 Damage progression through manufacturing process

From a manufacturing perspective, a slight increase in damage can spiral and accumulate leading to high levels of filamentisation and potential yarn breakages. These are detrimental to the efficiency of the process and final part quality.

5.3 Tensile Properties of Braided Composites

For each level of twist, three preforms are manufactured. These are then infused separately to produce three panels. The measured ultimate tensile strength, tensile modulus, elongation at break and Poisson's ratio are summarised for the average of the three panels for both in Table 5.4. A reduction in ultimate tensile strength with the twisted fibres from 672.66 MPa (0 Tpm) to 600.33 MPa (7 Tpm), however a large overlap between standard deviations is seen for the two datasets. A marked reduction in variability is seen with the twisted fibres. No significant difference in tensile modulus is noted. Tensile strain at failure is seen to increase in the twisted fibres, from 1.18% (0 Tpm) to 1.47% (7 Tpm). No significant difference in the average values for Poisson's ratio was seen. The values are discussed in more detail for each property in the subsequent sections of this work.

Table 5.4 Mechanical Property Summary for Untwisted and Twisted Coupons

Properties	0 Tpm	7 Tpm
Ultimate Tensile Strength, MPa	672.66 ± 97.61	600.33 ± 48.20
Tensile Modulus, GPa	55.30 ± 4.25	56.77 ± 2.24
Tensile Strain at Failure, %	1.18 ± 0.20	1.47 ± 0.29
Poisson's Ratio	0.10 ± 0.03	0.09 ± 0.04

5.3.1 Failure Type Analysis

The way in which each of the coupons failed for the thirty twisted and thirty untwisted coupons is summarised using the notation in Table 5.5 [98]. This identifies the type of failure, the area in which the failure took place and the location of the failure on the coupon.

Table 5.5 Failure Type Key

Failure type		Failure area		Failure location	
Angled	A	Inside grip/tab	I	Bottom	B
Edge Delamination	D	At grip/tab	A	Top	T
Grip/Tab	G	<1W from grip/tab	W	Left	L
Lateral	L	Gage	G	Right	R
Multi-mode	M (xyz)	Multiple areas	M	Middle	M
Long. Splitting	S	Various	V	Various	V
eXplosive	X	Unknown	U	Unknown	U
Other	O	-	-	-	-

The failure types for the test coupons are summarised Table 5.6 for the untwisted and twisted coupons. A range of failure types were seen for both coupon sets. All the coupons failed within the gage length.

Table 5.6 Failure Type Summary for Untwisted and Twisted Coupons

Failure Mode Type	Untwisted Coupons	Twisted Coupons
LGT	9	10
LGB	8	5
LGV	9	5
LGM	2	2
AGB	1	1
AGT	1	6
AGM	0	1

Both lateral and angled failure types were recorded for both coupon sets. Most untwisted coupons failed laterally (28 out of 30). The failure location of the untwisted coupons was spread across the gauge length. Most of the twisted coupons also failed laterally (22 out of 30) however; a greater number of angular failures were present (8 out of 30). Some edge delamination was recorded in two of the twisted coupons that failed in the LGT mode. The increase in fibre crimp due to the more rounded tow structure and resultant fibre undulation leads to more angular failures in the twisted coupon set as the tows attempt to straighten before fracture.

Delamination between layers in the failed twisted coupons was much more visible. This is due to the more progressive failure exhibited by the twisted coupons. Interlaminar failure resulted in each ply failing individually and offloading into other

plies which then subsequently failed. This failure mechanism of braids is acknowledged in the literature by Wehrkamp-Richter [59]. The structure of a braid acts as a natural crack arresting grid, this limits the propagation of the cracks to yarn intersection locations. Consequently, the loads can be redistributed without catastrophic failure through crack deflection. This increases energy absorption and the failure strain even if there is a significant amount of cracks present.

Visual representation of the failure modes for the untwisted coupons are shown in Figure 5.5. No untwisted coupon failed in mode AGM but they did fail in LGM.

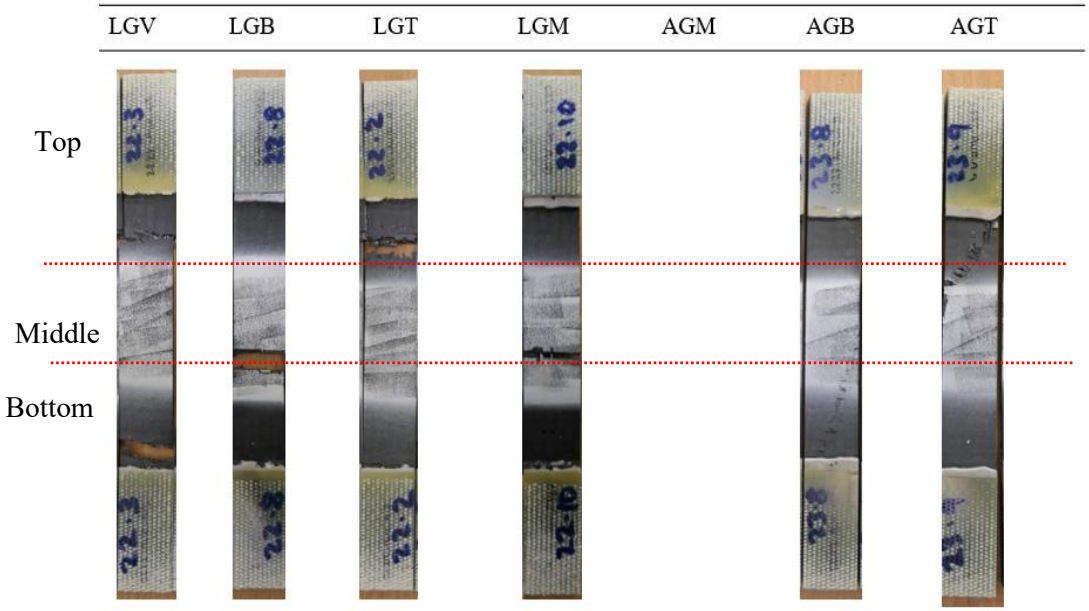


Figure 5.5 Untwisted coupon failure images sorted by failure type.

Examples of the twisted coupon failures are shown in Figure 5.6.

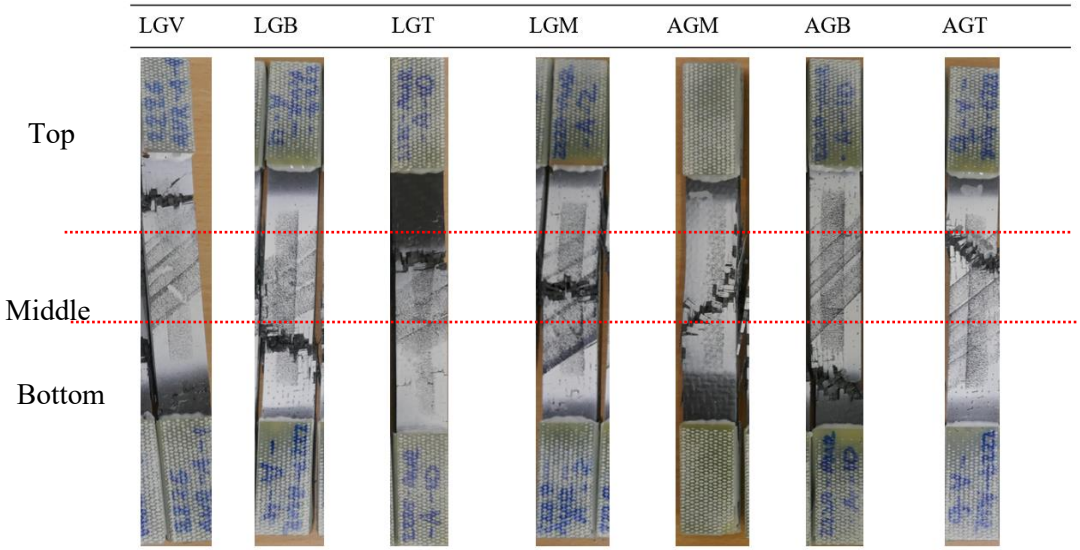


Figure 5.6 Twisted coupon failure images sorted by failure type

Figure 5.7 demonstrates the difference in pre- and post-test for the untwisted coupons in the failure region of the braid. Some delamination is noted at the failure point, but this is much less in comparison to the twisted fibres. The side view demonstrates that less tow undulation occurs in each layer.

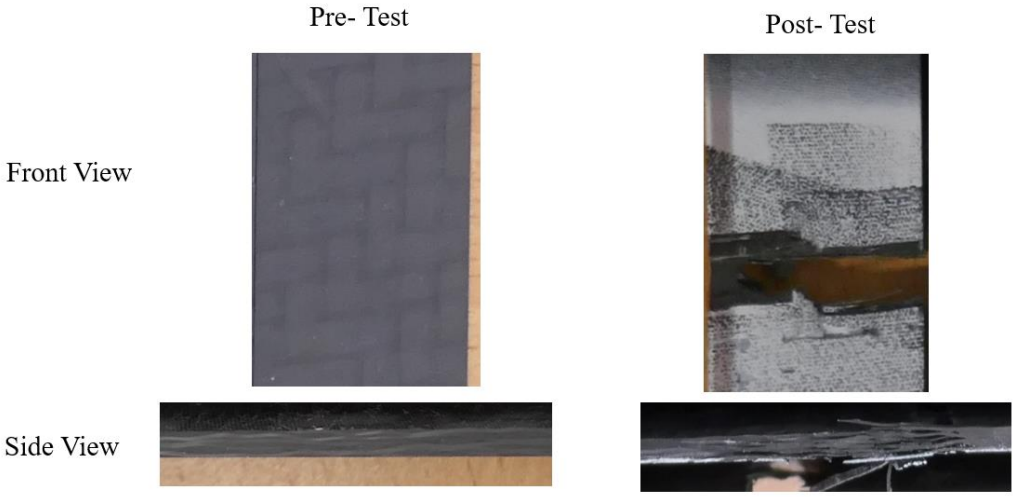


Figure 5.7 Pre and Post Test for Untwisted Coupons

Figure 5.8 demonstrates the difference in pre- and post-test for the twisted coupons in the failure region of the braid. Extensive delamination is noted in the post-test image. The side view demonstrates that tow undulation is increased in twisted panels.

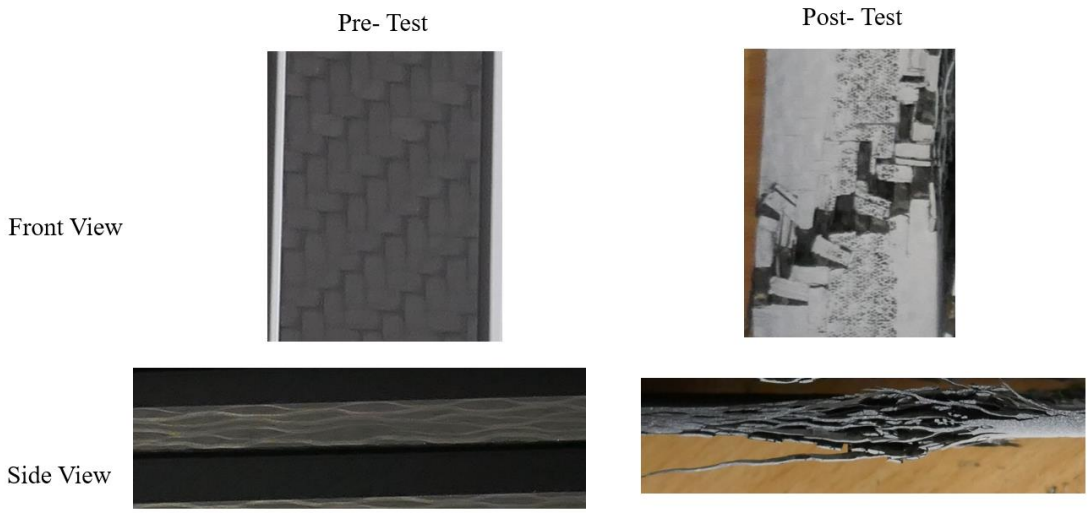


Figure 5.8 Pre and Post Test for Twisted Coupons

This delamination is clearly visible in Figure 5.8. This was irrespective of an angular or lateral failure mode. Wehrkamp-Richter [59] suggests that braided composites with greater yarn undulations fail due to large scale delaminations. The twisted fibres due to their more rounded tow cross-section result in greater undulation in compared to untwisted coupons where delamination is not seen. This is determined to be due to yarn straightening. The progressive failure occurs as high amount of energy released by initial ply failure results in the failure of several other bundles.

5.3.2 Stress-Strain Data

The stress and strain data were recorded for each of the coupon tests. A mix of failure modes occurred across the data set. As expected, a notable difference was noted in the stress-strain data with the untwisted coupons failing immediately after the yield point, whereas the twisted coupons continued to deform after the yield point until final failure. The fibres must straighten out before they can take the full load.

Figure 5.9 demonstrates examples of the stress-strain behaviour for coupons that failed in a lateral failure type. Untwisted coupons exhibited a brittle instantaneous failure irrespective of failure mode. Twisted coupons appeared to have an initial failure point at approximately 1% strain. The failure then progresses as load increases to final failure at the UTS.

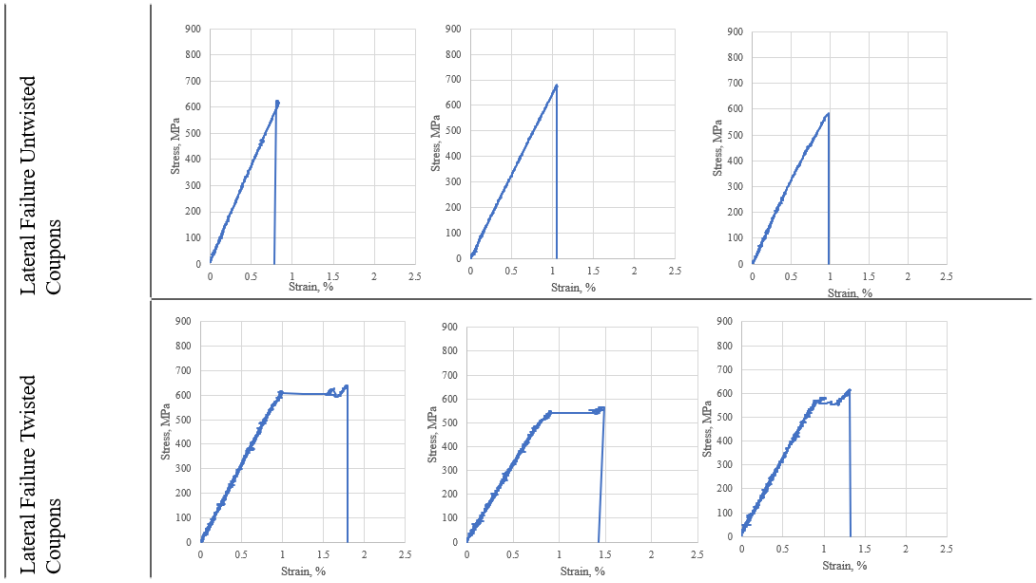


Figure 5.9 Lateral Failure Type Stress-Strain Graphs

A similar pattern was shown in the stress- strain behaviour of coupons that failed in angular failure mode, Figure 5.10. However, it is worth noting that in untwisted coupons that failed angularly a lower maximum stress was recorded.

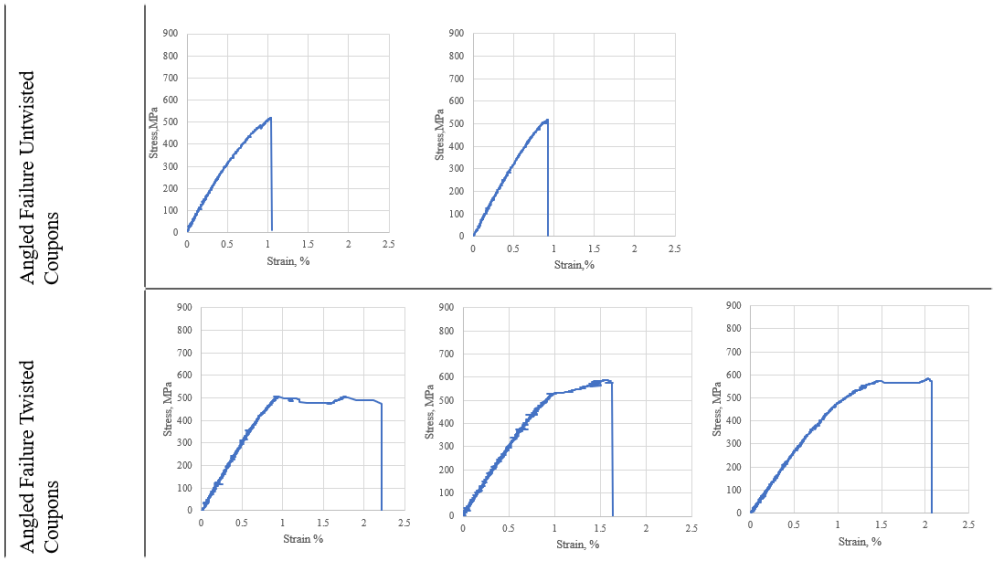


Figure 5.10 Angled Failure Mode Stress-Strain Graphs

The pattern of stress-strain behaviour is distinctly different for untwisted and twisted coupons but consistent within data sets. This indicates a potential difference in failure mechanism. Untwisted coupons demonstrated a clearly defined failure point. This brittle failure is shown by the clearly defined failure line, indicating instantaneous

failure. With twisted coupons irrespective of failure mode type an initial point of failure can be identified (this will be named as failure strength for discussion purposes). This is where the initial bundle failure occurs, as the braid structure limits crack propagation and the higher fibre undulation with twisted fibres, the twisted fibres continue to straighten out this is discussed in literature as a failure mechanism of braided coupon. The stress-strain curves indicate that deformation continues post this initial failure point. This corresponds to the apparent strain plateau as the adjacent fibre bundles straighten and fibre pull-out occurs. The ultimate tensile strength is reached, and final failure occurs. This can be explained as a progressive coupon failure. It is expected that the crimp induced into fibres because of twist leads to a change in interaction between fibres and matrix. This results in interlaminar failure. As one ply fails the load offloads into other plies which then subsequently fails. This is what causes the delamination of plies.

A clear difference in mean stress-strain behaviour is shown in Figure 5.11. Standard deviation plots for +/- 1 standard deviation have also been added to demonstrate variability. The figure demonstrates a similar tensile modulus for both twisted and untwisted coupons shown by the initial gradient. The ultimate tensile strength is higher for the untwisted coupons. The plots demonstrating the standard deviation for each data set highlight a wider range of values for coupons manufactured with untwisted fibres.

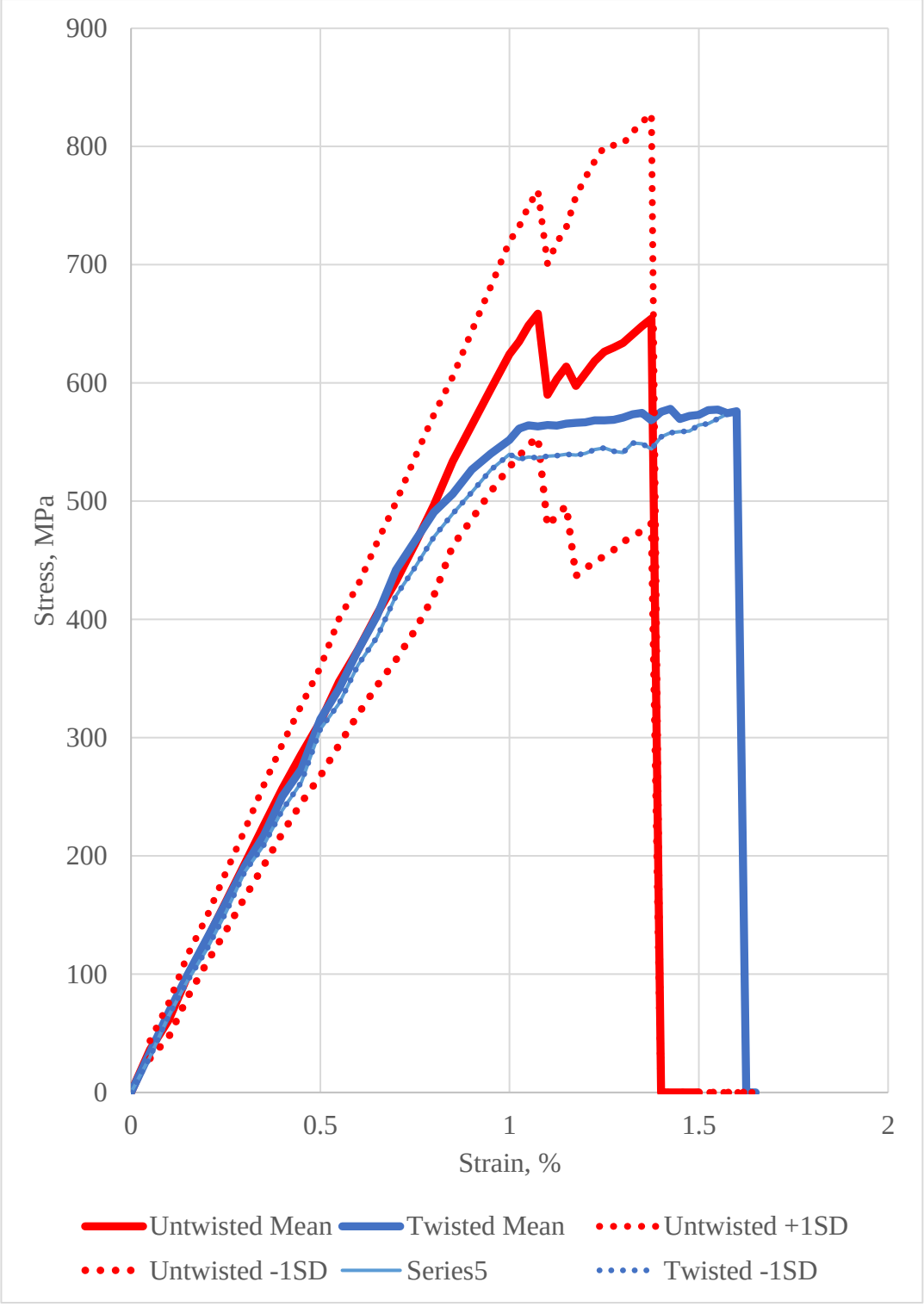


Figure 5.11 Mean Stress-Strain Trend

The area under the stress-strain curves represents the strain energy. The average strain energy was calculated using the trapezium rule for each individual coupon test. The results are summarised in Table 5.7. A larger strain energy was calculated for the

twisted coupons, this is due to the progressive failure of the fibres in coupon rather than the instantaneous failure shown by the untwisted coupons.

Table 5.7 Calculated Strain Energy

Properties	Number of Twists per Metre	
Strain Energy, MJ	0	420 ±141
	7	594 ±159

5.3.3 Ultimate Tensile Strength (UTS)

Table 5.8 details the average UTS for each panel, along with the range of data values and the standard deviation.

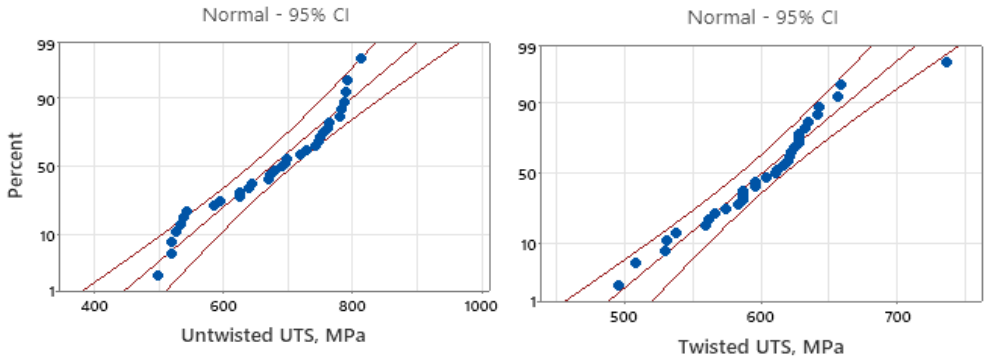
Table 5.8 UTS Summary

Panel ID	Average UTS, MPa	Standard Deviation
0 Tpm Preform 1	642.35	96.18
0 Tpm Preform 2	714.58	49.62
0 Tpm Preform 3	665.52	121.33
7 Tpm Preform 1	581.77	39.76
7 Tpm Preform 2	605.68	44.04
7 Tpm Preform 3	610.50	55.97

The average UTS is higher for the untwisted panels in comparison to the twisted panels with values ranging from 581.77- 610.50 MPa for the 7 Tpm panels to 645.35-714.58 MPa for the 0 Tpm panels. This is a result of the filaments in the twisted tow having a non-zero helix angle. However, the standard deviation of the coupon sets tested from the untwisted panels is much more variable. This indicates that although there is numerically a knockdown in ultimate tensile strength, variability is lower.

The variability of the UTS in 0 Tpm Preform 1 and 0 Tpm Preform 3 is approximately double that of each of the twisted panels. This suggests, that from a manufacturing perspective adding twist to fibres during the rewinding process can offer more reliable values for UTS.

A goodness of fit analysis using Minitab determines that both datasets can be assumed to follow a normal distribution, Figure 5.12. The twisted fibres saw a much better fit to the normal distribution with the untwisted data have a slight skew towards larger values.



(a) (b)

Figure 5.12 Goodness of Fit Test (a) Untwisted, (b) Twisted

As the data can be assumed to be normally distributed and a sample size of at least thirty was recorded for both untwisted and twisted coupons, a two-tailed T-test has been conducted at a 95% confidence level. This identified that the difference between the mean values was statistically significant returning a P-Value of 0.0004.

As the data can be assumed to be normally distributed, 95% of values would be expected to fall within ± two standard deviations of the mean. For the untwisted coupons this is a range of 477.5- 867.9 MPa and twisted coupons this is 503.9- 696.7 MPa. The lower bound value of which manufacturing values would be designed is higher for the twisted coupons, the data range for 95% of predicted twist values is also smaller. Figure 5.13 shows the ranges of the data.

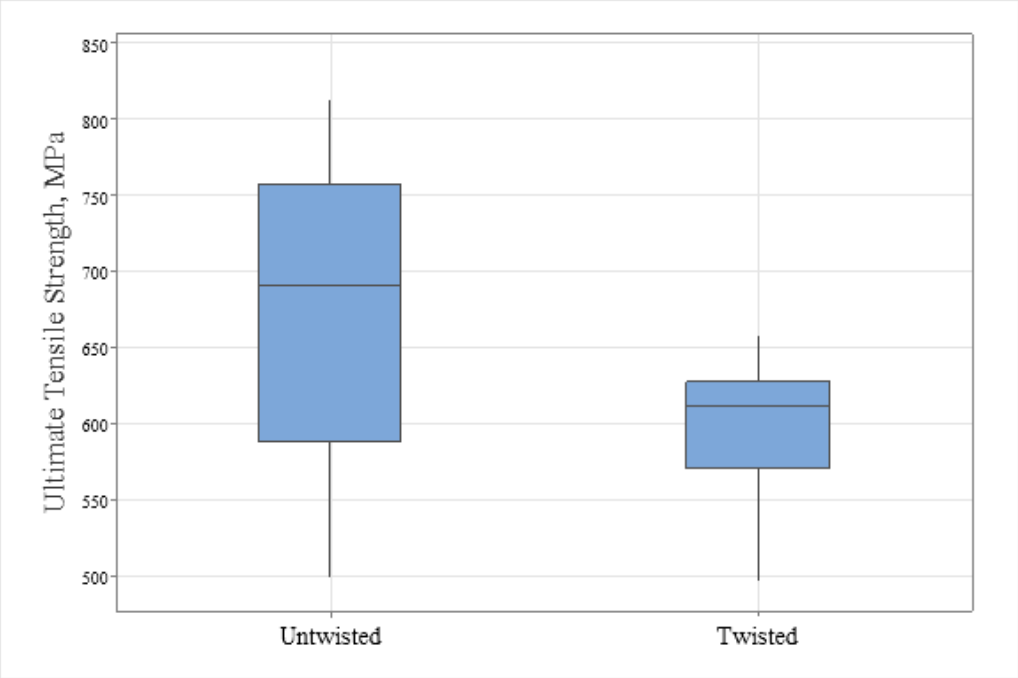


Figure 5.13 Range of UTS Data for Untwisted and Twisted Coupons

Figure 5.13 shows the larger value of mean UTS recorded in the untwisted sample, but also the smaller data range of the twisted UTS values. A potential improvement in tow bundle consistency with the twisting as the filaments pack more closely has resulted in more uniform properties of the twisted tows. Improved fibre processability resulting a reduction in preform surface defects results in more uniform coupon behaviour. Twisting alters the filament alignment which would result in a reduction in UTS. The increase in variability seen in the untwisted coupons is a result of a more inconsistent tow bundle structure with potential higher incidences of fibre damage. Whereas the twisted bundle is much more repeatable which reduces the variability of the UTS. However, the mean UTS of the twisted specimens is lower likely due to the fibre undulation.

An A-Basis allowable has been determined for the UTS data. Braiding has a high potential for application in aerospace and automotive applications therefore an extremely low failure rate is required. The A-Basis is commonly used for a catastrophic failure where there is no possible load redistribution.

Figure 5.12 demonstrates that the data fits a normal distribution. As a result, Equation 4.3 can be used to calculate the A-Basis design allowable. The constant tolerance factor for a sample number of n=30 is determined from MIL-HDBK-17-1F as 3.064.

Using this constant tolerance factor, the calculated means, and standard deviations from Table 5.4. The A-Basis allowable for the untwisted and twisted coupons based on ultimate tensile strength are shown in Table 5.9.

Table 5.9 UTS Summary including A-basis allowable

Test Statistic	0 Tpm Coupons	7 Tpm Coupons
Mean UTS, MPa	672.66	600.33
Standard Deviation	97.61	48.2
A-Basis Allowable, MPa	373	452.65

The A-basis design allowable is lower for the 0 Tpm coupons as a result of the increased variability in test data. This indicates a potential improvement in 7 Tpm coupons. However, this testing is only completed at a coupon level, further testing of braided components is required to validate this. The difference in variability was significant enough that despite the mean UTS value for 0 Tpm coupons being higher than the respective value for 7 Tpm coupons, the A-Basis design allowable was lower for the 0 Tpm coupons.

5.3.4 Failure Strength

Stress-strain behaviour of the untwisted and twisted coupons differs. This differs to twisted coupons where an initial failure point is seen at approximately 1% strain. The coupon then fails progressively until the UTS is reached. This initial failure point is defined as the failure strength. Table 5.10 records the average failure strength for both untwisted and twisted coupons. Due to the way the coupons fail, this is the same as the UTS for the untwisted coupons. However, the magnitude of the failure strength is lower in the twisted coupons than the UTS, 531 MPa compared to 673 MPa.

Table 5.10 Failure Strength, A-basis allowable summary

Properties	0 Tpm	7 Tpm
Failure Strength, MPa	673 ± 98	531 ± 42
A-Basis Allowable, MPa	374	402

The variability in failure strength in untwisted coupons is considerably greater. Therefore, with the application of an A-Basis allowable using Equation 4.3 for a sample size of n=30. The resulting A-basis allowable for untwisted coupons is lower

than that of the twisted coupons, 374 MPa in comparison to 402 MPa. This is a result of the variability in untwisted coupons despite the greater mean failure strength value.

5.3.5 Tensile Modulus

Figure 5.14 demonstrates the measured tensile moduli calculated in line with the test standard. The average tensile modulus for twisted fibres is slightly higher at 56.77 GPa in comparison to 55.30 GPa. However, a higher variability is noted for untwisted coupons.

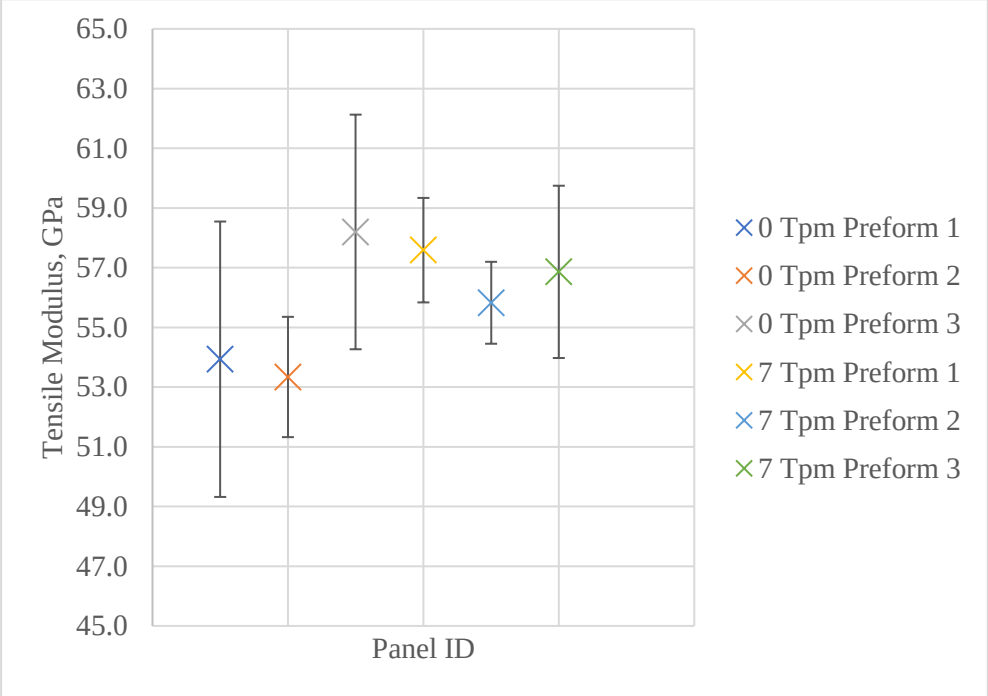


Figure 5.14 Average Tensile Modulus

This suggests that the addition of the twist to the fibres and the introduction of slight undulation because of the change in shape of the fibre bundle has no impact on the tensile modulus. As there is no obvious variation in modulus between panels, the comparison can be made between the two data sets for the untwisted and twisted fibres. A goodness of fit analysis shows that both untwisted and twisted samples fit a normal distribution. A two-tailed T-test has been conducted at a significance level of α=0.5. A total of over thirty samples from the untwisted panels and thirty from the twisted panels were taken. A P-Value of 0.086 was returned showing any difference between the tensile modulus values was not statistically significant. Figure 5.15 shows the ranges for both the untwisted and twisted datasets.

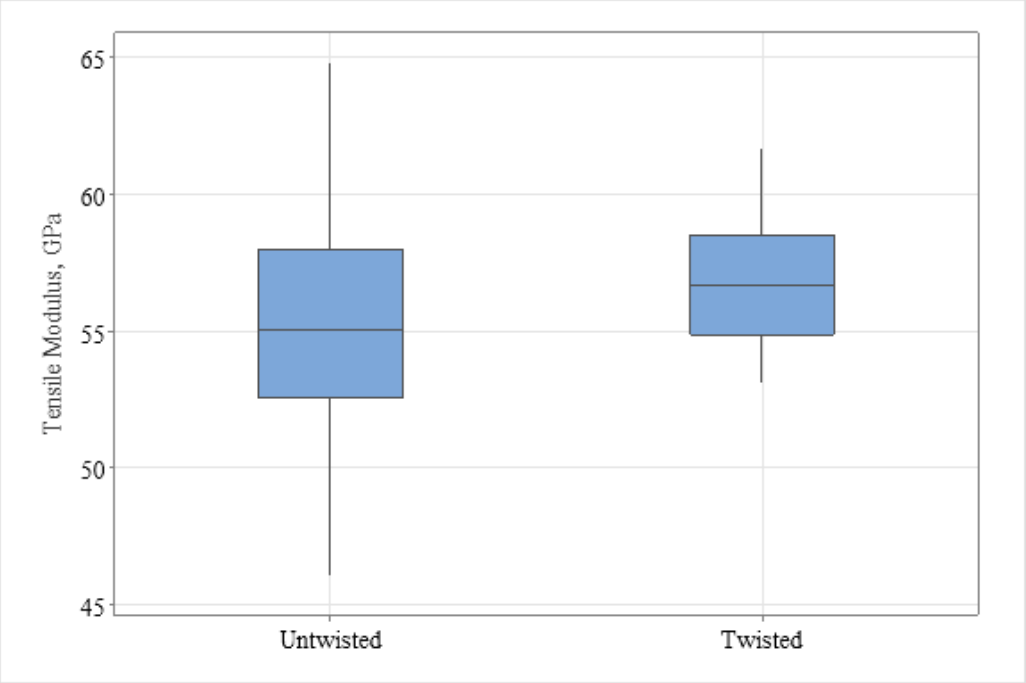


Figure 5.15 Tensile Modulus Range data for Untwisted and Twisted Coupons

Similarly, to the UTS the data, range is much lower for the twisted modulus. As the data is normally distributed 95% of the values will fall within ± two standard deviations of the mean. For the untwisted panels this provides a range of 46.8 - 64.8 GPa and the twisted panels this is 52.29- 61.25 GPa.

5.3.6 Tensile Strain at Failure

As the twisted fibres have a more rounded cross-section, it would be expected for there to be higher undulation of the fibres in the preform. Consequently, a higher tensile strain to failure as the fibres would have to straighten out before they can transfer the full load. Figure 5.16 shows the % strain at failure for each of the panels tested.

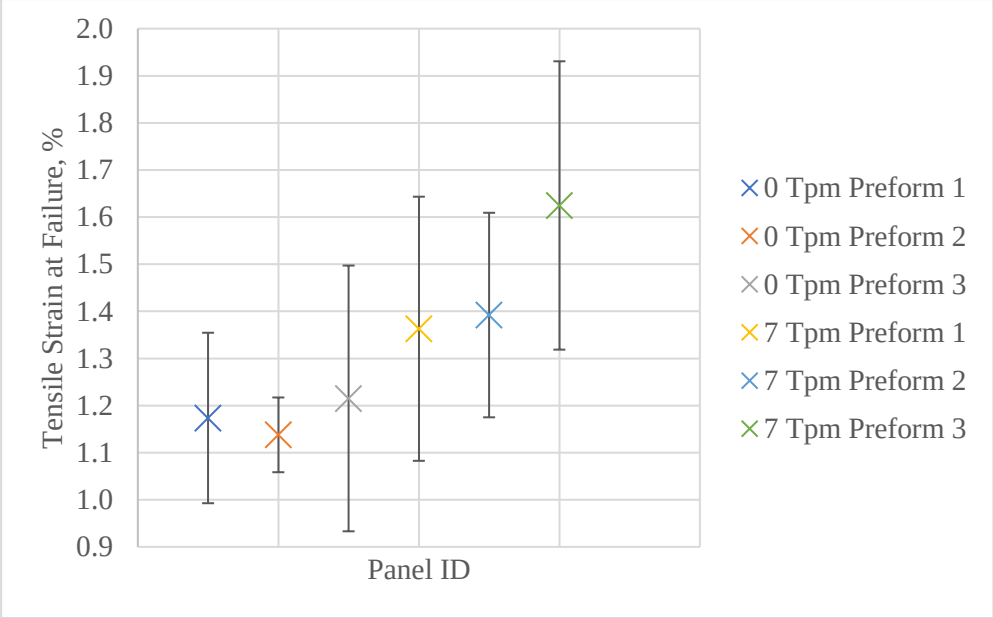


Figure 5.16 Tensile Strain at Failure

The average strain to failure increases in the 7 Tpm preforms in comparison to the 0 Tpm. However, there is overlap between the standard deviation bars and a two-tailed T-test demonstrated that although there was a numerical difference it was not statistically significant. The standard deviation is consistent across all the panels except for 0 Tpm Preform 2. There was no clear difference in the testing of 0 Tpm Preform 2 so therefore the numerical data is due to natural deviation in the 0 Tpm test specimens.

5.3.7 Poisson's Ratio

Table 5.11 lists the Poisson's ratios for each panel tested. There is overlap between the standard deviations of each panel.

Table 5.11 Poisson's Ratio Panel Summary

Panel ID	Poisson's Ratio	Standard Deviation
0 Tpm Preform 1	0.102	0.029
0 Tpm Preform 2	0.107	0.031
0 Tpm Preform 3	0.090	0.031
7 Tpm Preform 1	0.073	0.058
7 Tpm Preform 2	0.091	0.026
7 Tpm Preform 3	0.111	0.031

A goodness of fit analysis demonstrates that both the untwisted and twisted A two-tailed T-test determines that the datasets fit a normal distribution for both untwisted and twisted coupons for Poisson's ratio. A two tailed t-test at a significance level of α=0.05 was conducted and P-Value of 0.666 was returned. This shows that adding twist to fibres during the rewinding process has no noticeable impact on the Poisson's ratio.

5.4 Discussion

To this point, a range of information has been presented comparing untwisted and twisted fibres. There is a clear difference in stress-strain behaviour as shown in Figure 5.11. This suggests that untwisted fail instantaneously whereas twisted coupons fail more progressively. Figure 5.7 and Figure 5.8 supports this as failed twisted coupons show delamination corresponding to progressive failure. The braid with higher undulation acts as a crack arresting grid reducing the crack propagation. The delamination occurs due to yarn straightening and fibre pull out. As the adjacent yarn bundles failed the large amount of energy released resulted in adjacent fibres failing. However, testing at a part scale is necessary before this information can be concluded as industry have noted differences between coupon and part level testing.

There is a significant reduction in both ultimate tensile strength (maximum strength at failure) and failure strength (initial point of failure) in the twisted coupons in comparison to their untwisted counterparts. The variability for the untwisted coupons is higher. The implementation of an A-basis allowable emphasises this, as the 0 Tpm A-basis allowable is lower than that for 7 Tpm despite the initial average failure strength being greater.

A higher strain at failure was seen in the coupons manufactured from twisted fibres, this is due to the individual plies offloading as they fail onto adjacent plies which results in additional elongation of the fibres as the plies take on the load. The additional crimp in twisted filaments due to the more elliptical fibre cross-section results in the fibre straightening out before the load is offloaded. This increasing in strain at failure results in an increase in average energy.

5.5 Conclusions

The complete process of coupon manufacture and testing has been detailed so far in Chapter 5 from the initial rewinding of carbon fibre tows for braiding to the tensile testing and failure mode analysis. This determines the influence of an additional twist to fibres during the rewinding step of the braiding process in all aspects of the process. The conclusions from this are summarised: It was observed that fibre damage accumulates at each stage of the rewinding process manifesting itself as filamentisation and tow breakages. This confirms work by Ebel [97] which demonstrated the evolution of fibre damage through the braiding process but links this with a visual inspection scale proposed by Kyosev [2]. However, this work builds on this by applying the analysis to twisted and untwisted fibres. This damage was more severe with untwisted fibres, this results in greater accumulation of damage in the preform. Fibre damage testing methods determined a correlation between number of twists added during rewinding and the level of fibre damage. However, this methodology was qualitative and required destruction of the preform. The development of an in-process methodology to determine the extent of fibre damage is required.

Tensile testing of both untwisted and twisted coupons demonstrated a difference in failure behaviour with twisted coupons failing more progressively with greater delamination whereas untwisted coupons failed in a more brittle manner with instantaneous failure. This builds on work by Wehrkamp-Richter [59], which suggest that braided composites with higher undulation failed due to extensive delamination due to yarn straightening. This work builds on this by specifically linking the delamination to the inclusion of the rewinding twist to fibres which create a more rounded fibre structure. For twisted coupons, an initial failure point termed the failure strength was identified after which the test coupons continued to deform progressively offloading into adjacent plies. Higher variability was noted in the untwisted coupons resulting in a lower A-basis allowable for untwisted failure strength. There was no significant difference in tensile modulus between twisted and untwisted coupons.

6 Effect of Rewinding Twist on Braided Fibre Architecture of Cylindrical Preforms

6.1 Background and Aim

Causal links between the braiding process parameters and resulting stability and variability of the braid architecture are not known. This chapter aims to determine links between the braiding process parameters and their impact on the final quality of the braided preform. A certain level of variability is present in all braids, this is likely to be a consequence of several steps within the process. A comprehensive analysis of the influence of the additional twist added to the carbon fibre tows during the rewinding process is then utilised to build tow geometry approximations.

6.2 Braid Architecture Variability Induced by Process Parameters

Carrier speed, take-up speed and guide ring dimensions have been identified as three principal process parameters that impact the resultant braid architecture. The following sections discuss the work carried out to determine the relationship between each parameter and the consequent variation in the braided preform.

6.2.1 Machine Speeds

6.2.1.1 Experimental Methodology

Preforms were produced on a 48-carrier axial braider at the UoN on a 50mm diameter cylindrical mandrel. The braider was operated in a fully loaded braid configuration to produce a regular braid pattern. A biaxial braid architecture was produced as no axial tows were incorporated. The parameter selection is shown in Table 6.1 for the effect of braid carrier speed on braid architecture variability. The speeds tested were within the normal operating range of the machine.

Table 6.1 Effect of braid carrier speed test parameters

	Test CS1	Test CS2	Test CS3
Braid Carrier Speed, $rads^{-1}$	1.84	2.10	2.35
Take-Up Speed, mms^{-1}	5	5	5
Braid Angle,°	43.78	47.44	50.66

Table 6.2 shows the parameter selection for the influence of take-up speed on braid architecture variability.

Table 6.2 Effect of take-up speed test parameters

	Test TS1	Test TS2	Test TS3
Braid Carrier Speed, $rads^{-1}$	2.35	2.35	2.35
Take-Up Speed, mms^{-1}	5	6	7
Braid Angle,°	50.66	45.47	41.07

12K T700s carbon fibre supplied by Toray was used to manufacture the braided preforms. A balance of bobbins wound with an S and Z twist were used, and the bobbins were rewound with a controlled rewinding speed of 10,000 rpm and tension with 0 Tpm. All preforms in this investigation were a single layer.

6.2.1.2 Results and Discussion

The deviation in braid angle from the programmed braid angle of 45° is shown in Figure 6.1 for the tests with variation of carrier speed and in Figure 6.2 for the tests where traverse speed is varied. For each test case 30 measurements were taken in the stabilised region of the preform. The observable average deviation was within ±1° for each test case, with similar magnitudes of variability. No notable correlation between increasing carrier speed or traverse speed and deviation from predicted braid angle was recorded.

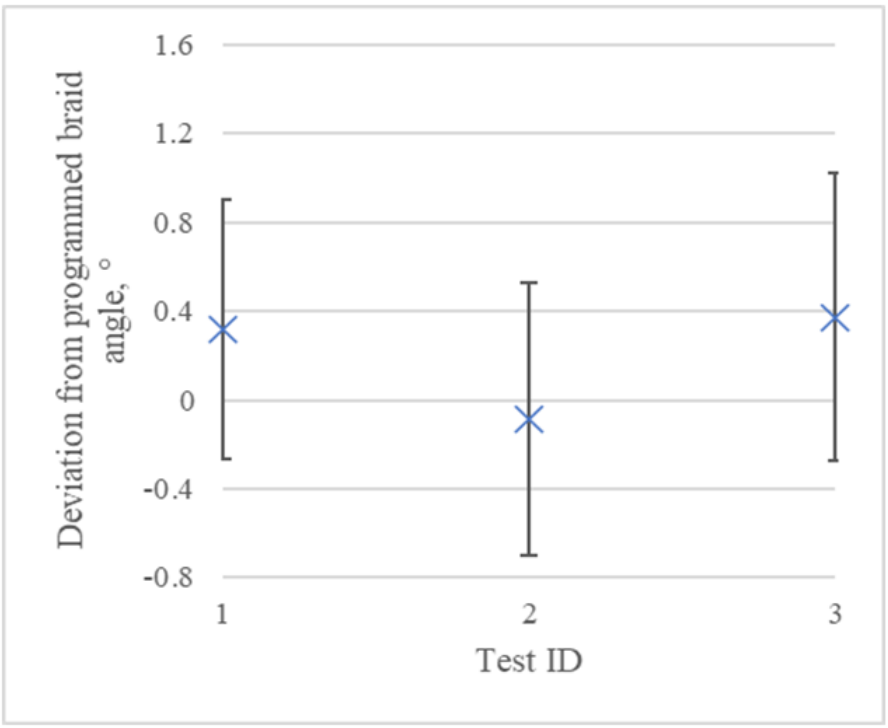


Figure 6.1 Braid Angle Deviation CS1-CS3

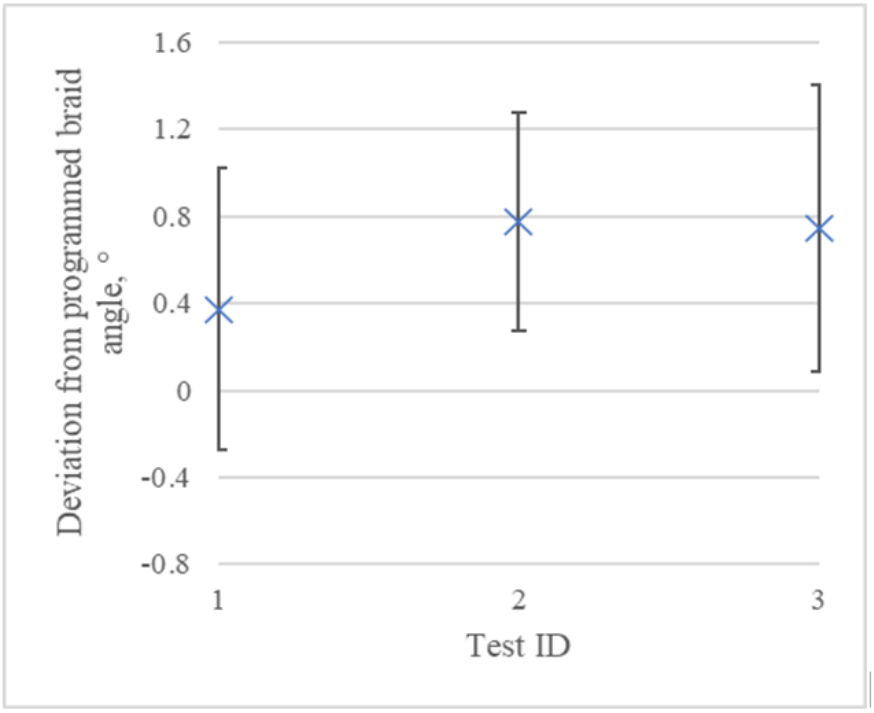


Figure 6.2 Braid Angle Deviation TS1-TS3

Thirty tow width measurements were recorded in the stabilised section of the preform for each test case and the average tow width can be seen in Figure 6.3 for the carrier speed test cases and Figure 6.4 for the traverse speed. There is no observable difference in tow width magnitude or variability as a result of varying the machine parameters of carrier speed and traverse speed.

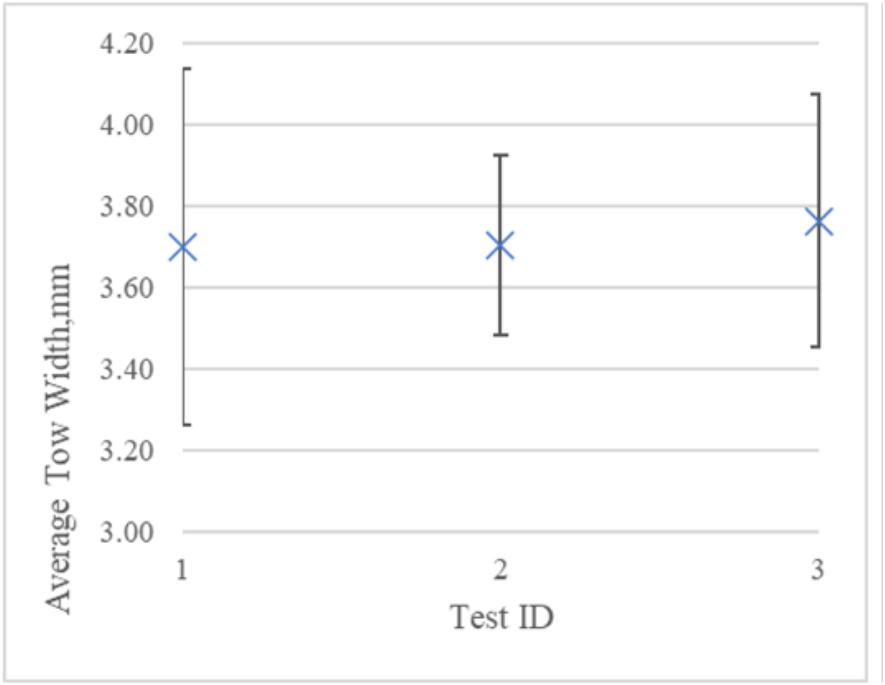


Figure 6.3 Average Tow Width CS1-CS3

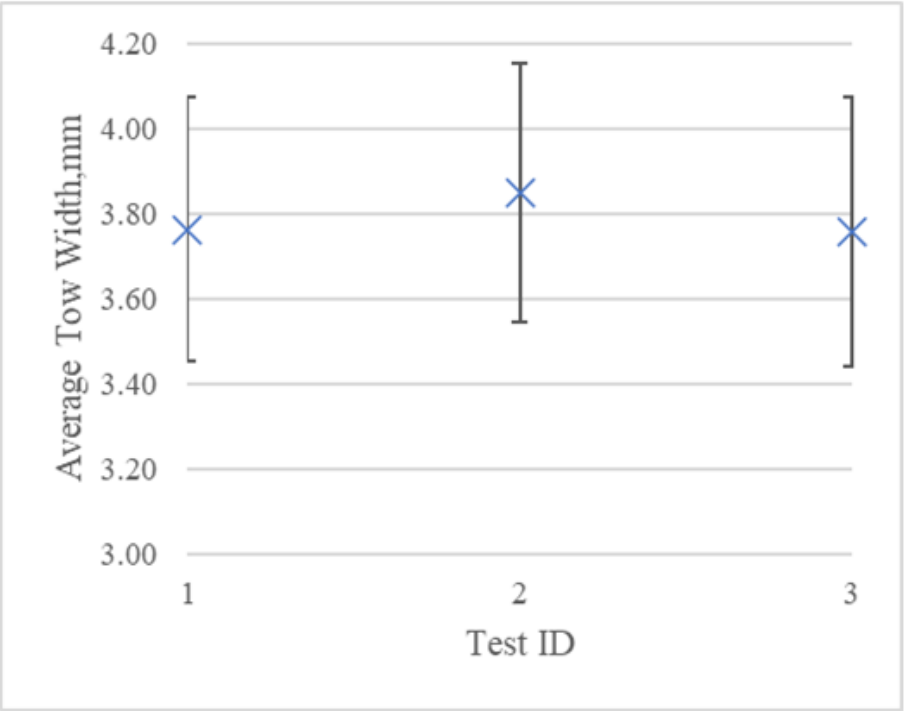


Figure 6.4 Average Tow Width TS1-TS3

In summary, this data set confirms that carrier speed and traverse speed have no notable effect on the variability of the key process metrics of braid angle and tow width.

6.2.2 Application of Guide Ring

Guide rings play a key part in the effective preforming of braided composites and are used to ensure a consistent convergence point of the braiding yarns. Typically guide rings are circular with a diameter slightly larger than that of the mandrel. At present there is limited manufacturing data on the influence of guide ring diameter on the stability of the architecture of a braided preforms. Different manufacturing facilities accept slightly different ratios between the mandrel diameter and guide ring diameter, a typical value of 1.5x mandrel diameter is used.

6.2.2.1 Experimental Methodology

Braided preforms were manufactured using the 192-carrier Eurocarbon braider at the NCC. Three different guide ring diameters of 1.5x, 2x and 3x the mandrel diameter were used to assess the impact of guide ring diameter on preform variability and stability. The guide rings were steel and coated to reduce the friction between the fibres and the guide ring. Carbon fibre tows were 12K T700s supplied by Toray, for

this investigation they were rewound with an additional 5 Tpm. The machine was operated in fully loaded configuration which produces a regular braid pattern, all the braids were biaxial. All the preforms were designed to achieve a 45° braid angle on a cylindrical mandrel of 200mm diameter.

6.2.2.2 Braid Stabilisation

Stabilisation length of a braided preform is the length of the preform where the braid is in a transient state prior to reaching the desired braid architecture. For this investigation this is defined as the point at which three consecutive braid angles are within ±1° of the programmed braid angle. Braid angles were measured every 10mm along the preform. Figure 6.5 shows the stabilisation profiles. The region of braid angles which satisfy this condition are shown by the horizontal dashed lines.



Figure 6.5 Stabilisation Length for Different Sized Guide Rings

Figure 6.5 demonstrates that the stabilisation length is strongly influenced by the diameter of the guide ring- increasing the guide ring diameter increases the stabilisation length of the preform from 340mm for the 1.5x ring to 680mm for the 3x guide ring. A greater amount of variability was seen in the braid angle as the guide ring diameter was increased.

6.2.2.3 Braid Angle Variability

Figure 6.6 shows the measured level of braid angle variability once the stabilisation point is attained for each of the braided preforms. This is irrespective of guide ring size. This was not reflected in the manufactured preforms.

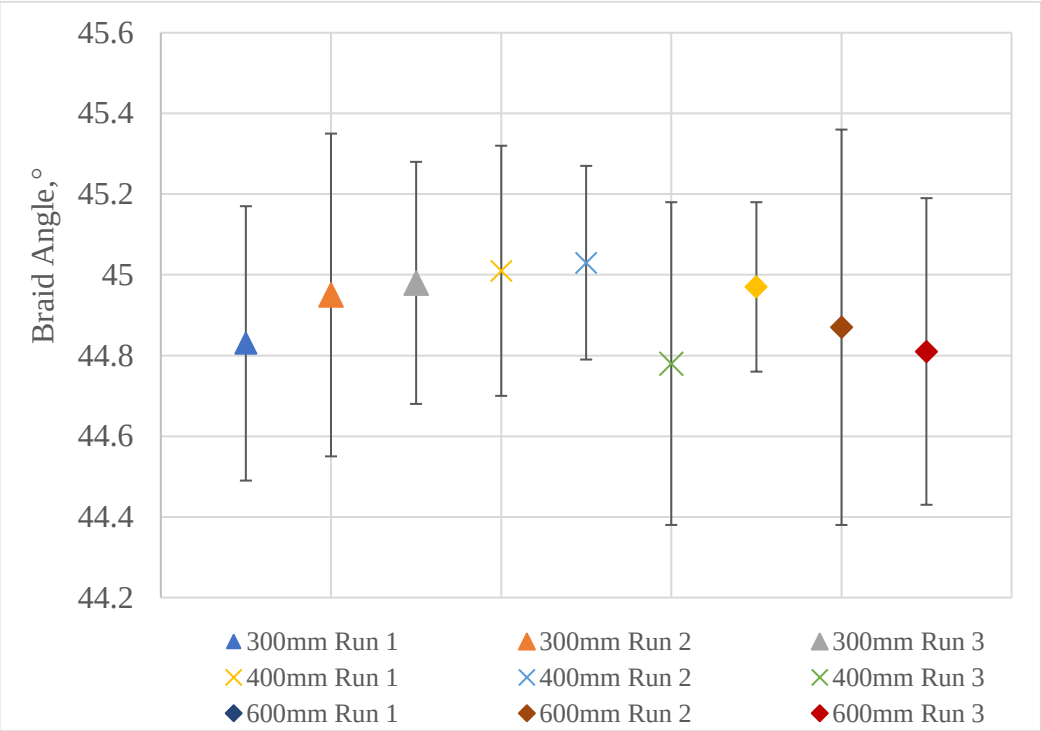


Figure 6.6 Measured braid angles for different sizes of guide ring

Tukey pairwise comparisons show no statistically significant difference in measured braid angle between any of the manufacturing trials. This suggests that the implementation of different guide ring sizes does not influence the braid angle once the preform has stabilised.

6.2.2.4 Tow Width Variability

Figure 6.7 shows that the recorded tow width values increased slightly with guide ring diameter, from 2.53mm for the 1.5x ring to 2.64mm for the 3x ring. Variability increased significantly with guide ring diameter.

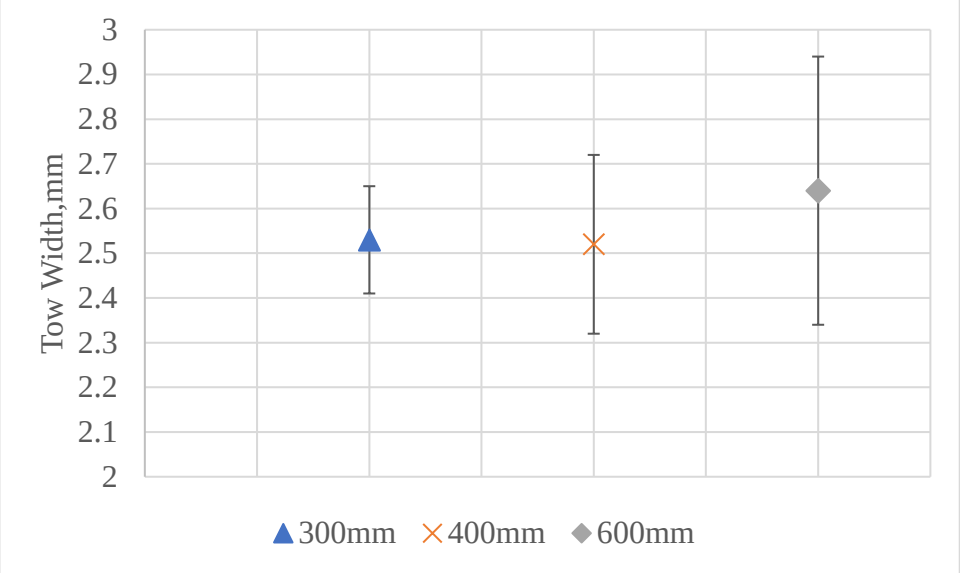


Figure 6.7 Measured tow width for different guide ring size

An ANOVA statistical analysis was used to determine that any observed difference in tow width as a result of changing guide ring diameter was not statistically significant. A minimum of 30 measurements were recorded for each set-up in the stabilised region of the braid so the data sets can be assumed to be normally distributed. At a 95% confidence level, a P-Value of 0.307 was calculated meaning that tow width is independent of guide ring diameter. Tukey pairwise comparisons also demonstrated that this was common across all three guide ring diameters. The tow width variability does increase as guide ring size increases, this is because of the preform conforming less easily to the mandrel shape resulting in variations in tow tension.

6.2.2.5 Cover Factor Variability

Figure 6.8 shows the measured cover factor of the braided preform once the stabilisation point has been attained and the braid has converged to a consistent pattern. The cover factor reduced slightly from an average of 79% for the 1.5x guide ring to 77% for the 3x guide ring. Variability was seen to be constant at 3% for all guide ring sizes.

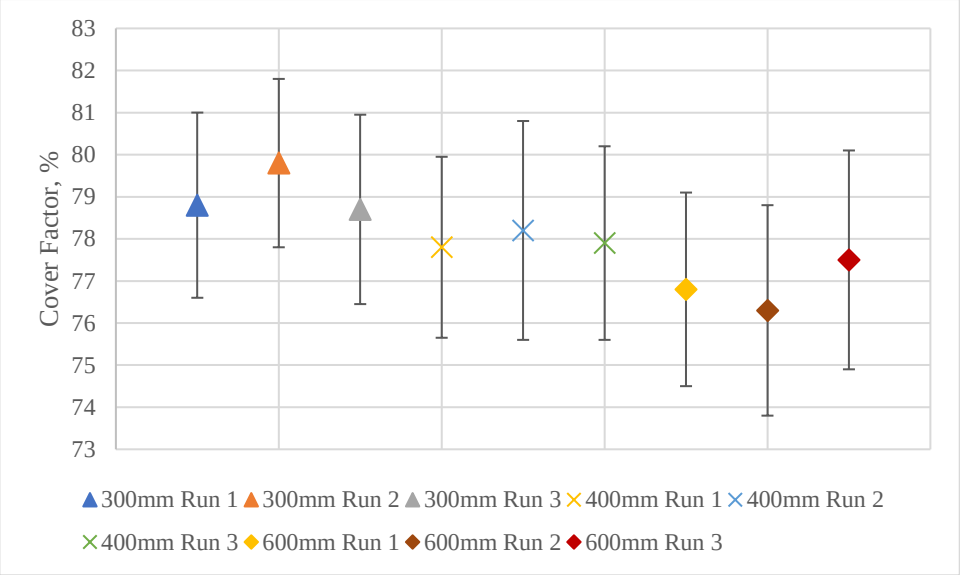


Figure 6.8 Measured cover factor for preforms manufactured with different guide ring sizes

No statistical difference in cover factor was found between the different manufacturing set-ups for the experimental data.

6.2.2.6 Discussion

The findings demonstrate that for best braiding results a smaller guide ring should be used, increasing the guide ring diameter increases the stabilisation length of the braid, increases the variability of braid angle, cover factor and increase tow width and variability in tow width across the preform length.

6.3 Braid Architecture Variability as a Result of Twisting

This section of the thesis identifies the relationship between the addition of the twist during rewinding and the resulting tow geometry, along with the variation in key process variables.

The following preforms discussed in this section were manufactured on a 50mm diameter cylinder using the 48-carrier Steeger axial braider at the UoN, operated in a fully loaded braider configuration to produce a regular braid pattern with biaxial braid architecture. 12K T700s carbon fibre supplied by Toray was rewound at the NCC with the following speed settings shown in Table 6.3.

Table 6.3 Rewinding Parameters

Material Preparation ID	Number of Twists per metre, Tpm	Rewinding Speed, rpm
A	0	10,000
B	3	10,000
C	5	10,000

The rewinding speed and rewinding tension were kept consistent for each different material preparation condition, with only difference being the number of additional twists per metre added to the carbon fibre. Braiding process parameters are shown in Table 6.4.

Table 6.4 Braiding Process Parameters

Process Parameter	Value
Braid Carrier Speed, rpm	2.33
Take-Up Speed, mms^{-1}	5
Braid Angle,°	50

6.3.1 Influence of Twisting on Tow Width

Figure 6.9 compares the recorded tow width for the three different levels of twist; 0 Tpm, 3 Tpm and 5 Tpm. Tow width measurements were taken in the stabilised part of the braid using ImageJ from photographs taken parallel to the braided preform to prevent distortion due to the cylindrical surface of the mandrel. Each test configuration was repeated five times, and twenty measurements were recorded for each preform.

The first observation is that adding twist to the carbon fibre reduces the tow width, for 5 Tpm this reduction was approximately 28%. The additional twist in the winding process results in the compaction of the carbon fibre filaments in the tow. This reduces the tow spread leading to a smaller tow width.

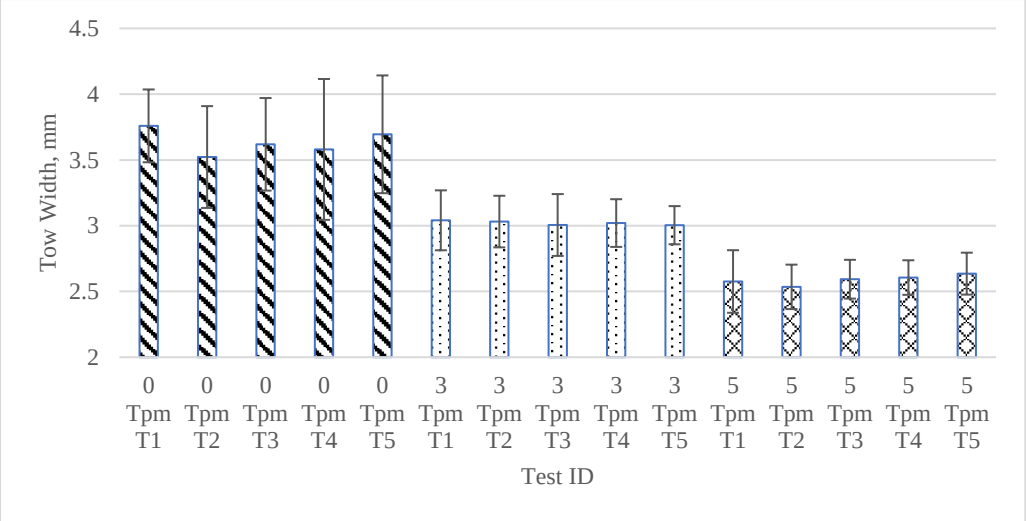


Figure 6.9 Measured Tow Width for Different Levels of Twist

Another observation is that increasing the number of twists per metre appeared to reduce the variation in tow width, the addition of the twist restricts the ability of filaments to move within the tow bundle. 0 Tpm saw the highest level of variability with both test conditions where twist was seeing a visible reduction in variation. This can be attributed to the compaction of the tow structure due to the twisting of the fibre.

6.3.2 Influence of Twisting on Tow Geometry

Measuring braid thickness is difficult without with causing distortion to the dry preform. In this study, the preform was coated in a casting resin to minimise distortion to the braid. These samples were then potted for microscopy analysis. Optical microscopy was conducted on several samples for each level of twist. Two different metrics can be used for thickness, individual tow thickness and the maximum layer thickness. Samples were cut both along the fibre direction to record individual tow thickness and circumferentially to record the maximum layer thickness.

Figure 6.10 shows the microscopy images of the three different levels of twist taken as a circumferential cut. There is a notable difference in tow shape, as the number of twists per metre increase the tow becomes significantly more compact with increase in thickness. More tow spread is observed in the 0 Tpm fibres.

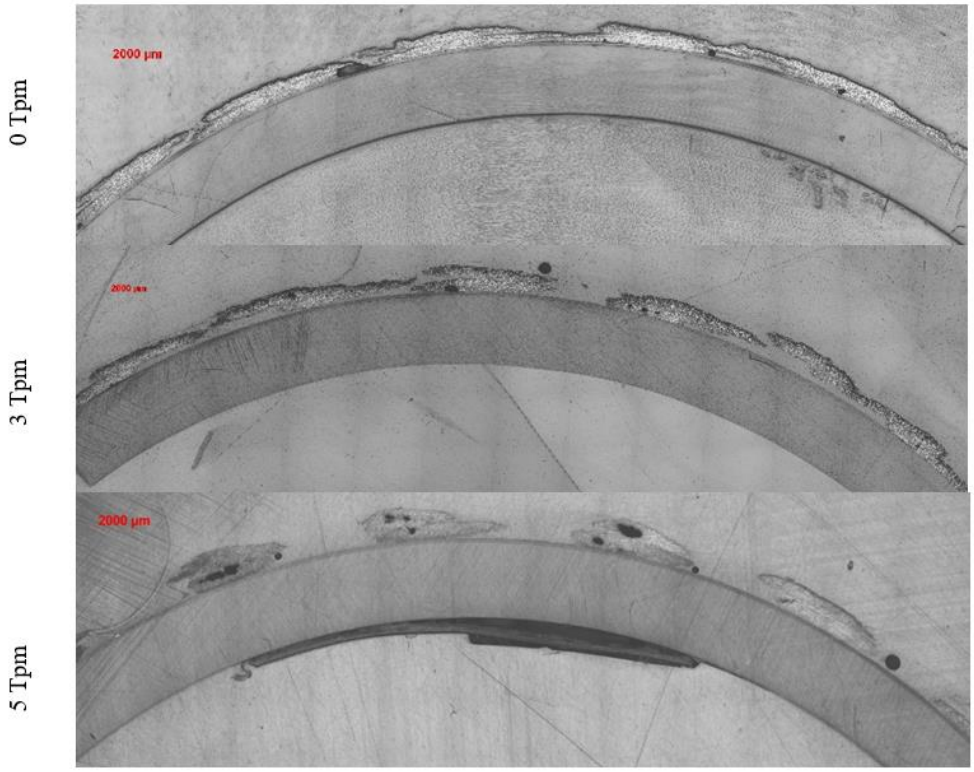


Figure 6.10 Microscopy images of preforms with different levels of twist

Figure 6.11 highlights an individual bias tow intersection for each level of twist studied. The more rounded tow cross-section is visible as the number of twists per metre increases.

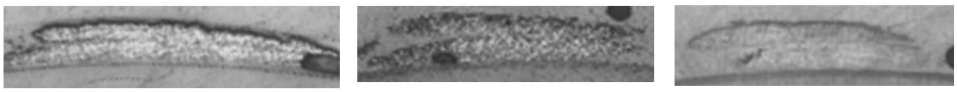


Figure 6.11 Individual Tow Intersections for Different Levels of Twist

Figure 6.12 compares the data recorded for the maximum braid layer thickness. Thirty measurements were recorded across multiple samples for each level of twist. A high level of variation is present in the thickness measurements. However, an increase in maximum layer thickness can be observed for increasing levels of twist.

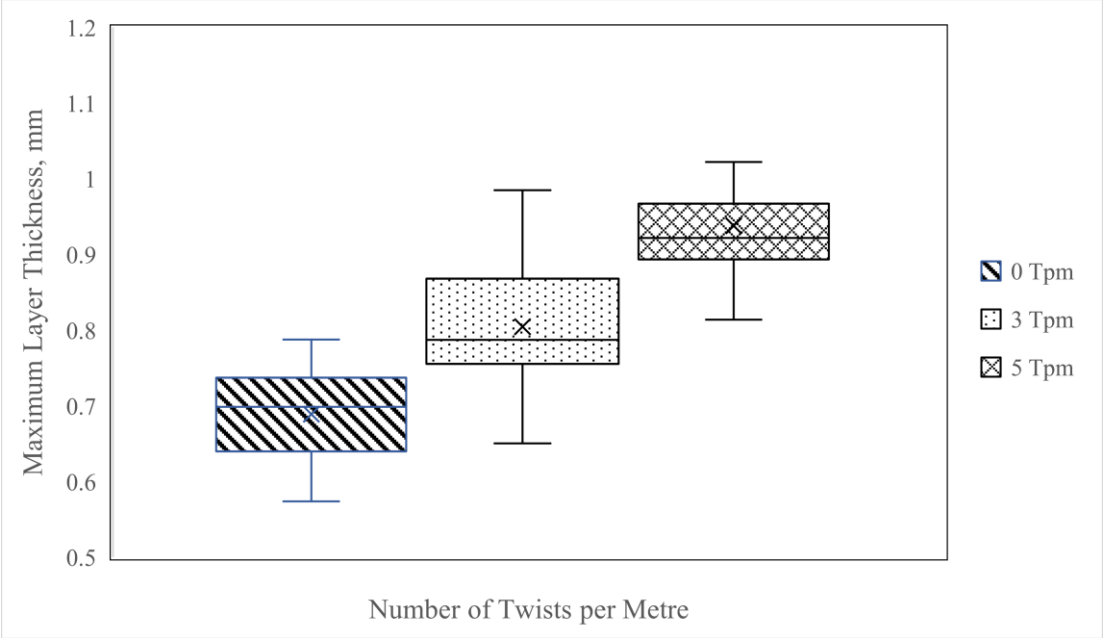


Figure 6.12 Maximum layer thickness of braided preforms with different levels of rewinding twist

Statistical analysis on this data for a 95% confidence level demonstrates that the mean maximum layer thickness for 0, 3 and 5 Tpm are statistically significantly different. Tukey pairwise comparisons at 95% confidence are shown in Figure 6.13 demonstrating that the recorded average maximum layer thickness is different for each different level of additional twist. If the interval on the chart does not contain zero that the corresponding means are significantly different. Each mean is compared directly to each of the other means, as there is no interval that contains zero it can be stated that the maximum layer thickness is statistically significantly different for each different level of rewinding twist.

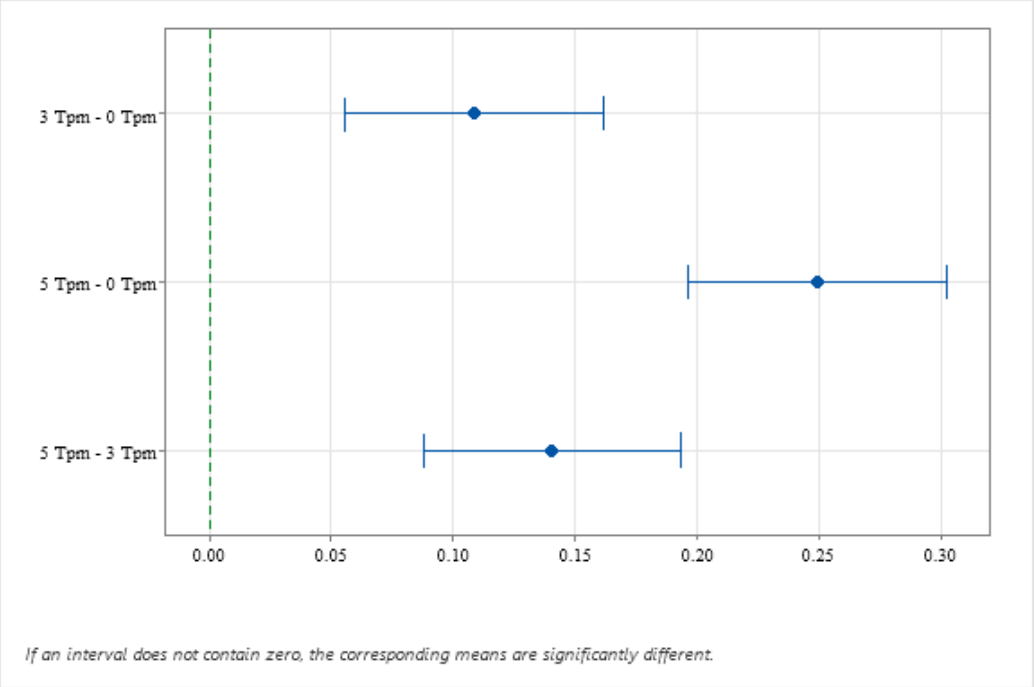


Figure 6.13 Tukey Pairwise Comparison for Maximum Layer Thickness

The average values for maximum layer thickness are summarised in Table 6.5. An increase in layer thickness can be seen concurring with the more rounded shape of the tows as seen in the microscopy images in Figure 6.10.

Table 6.5 Maximum layer thickness for different rewinding twist levels

Rewinding Twist, Tpm	Maximum Layer Thickness, mm
0	0.689 ± 0.057
3	0.797 ± 0.103
5	0.938 ± 0.091

Thirty measurements of the tow thickness were taken across multiple samples for each level of twist, therefore statistically the distribution can be assumed to be normal. A summary of the average tow geometry measurements is summarised in Table 6.6. Tow thickness is shown to increase as the number of Tpm increases.

Table 6.6 Average Tow Geometry Measurements for different levels of twist

Number of Twists per metre, Tpm	Tow Width, mm	Tow Thickness, mm	Estimated Tow Area Using Elliptical Yarn Assumption,m^2
0	3.75	0.397	1.089E-06
3	3.06	0.440	1.072E-06
5	2.58	0.521	1.071E-06

Differences in tow width data has previously been shown to be statistically significantly different in this thesis. Similarly, an ANOVA has been conducted on the data for individual tow thickness. The Tukey pairwise comparisons in Figure 6.14 demonstrate that all tow thickness measurements are statistically different from one another as zero is exempt from each interval plot. As a result, it can be concluded that in the initial layer of a braided preform the tow thicknesses are directly influenced by the inclusion of a twist during the rewinding process.

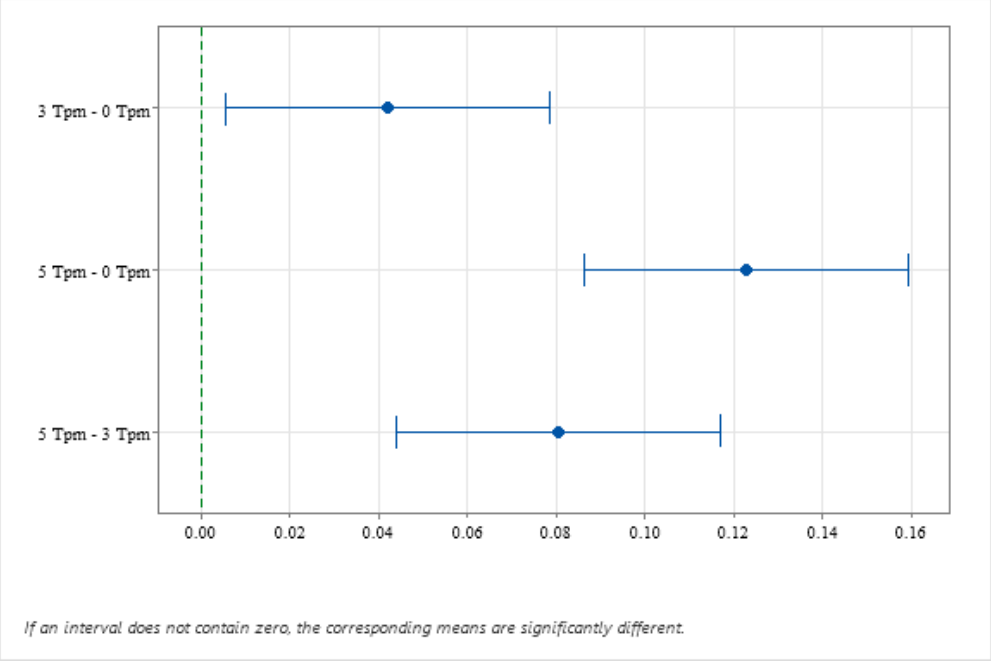


Figure 6.14 Tukey Pairwise Comparison for Tow Widths

A plot for the tow width and corresponding tow thickness for each braided tow is shown in Figure 6.15. A Pearson Correlation Coefficient was calculated based on

this data, a correlation of -0.753 was returned which suggests a strong negative correlation between tow width and thickness. The observed linearity of the data suggests the change in the overall tow shape was consistent across all twist levels.

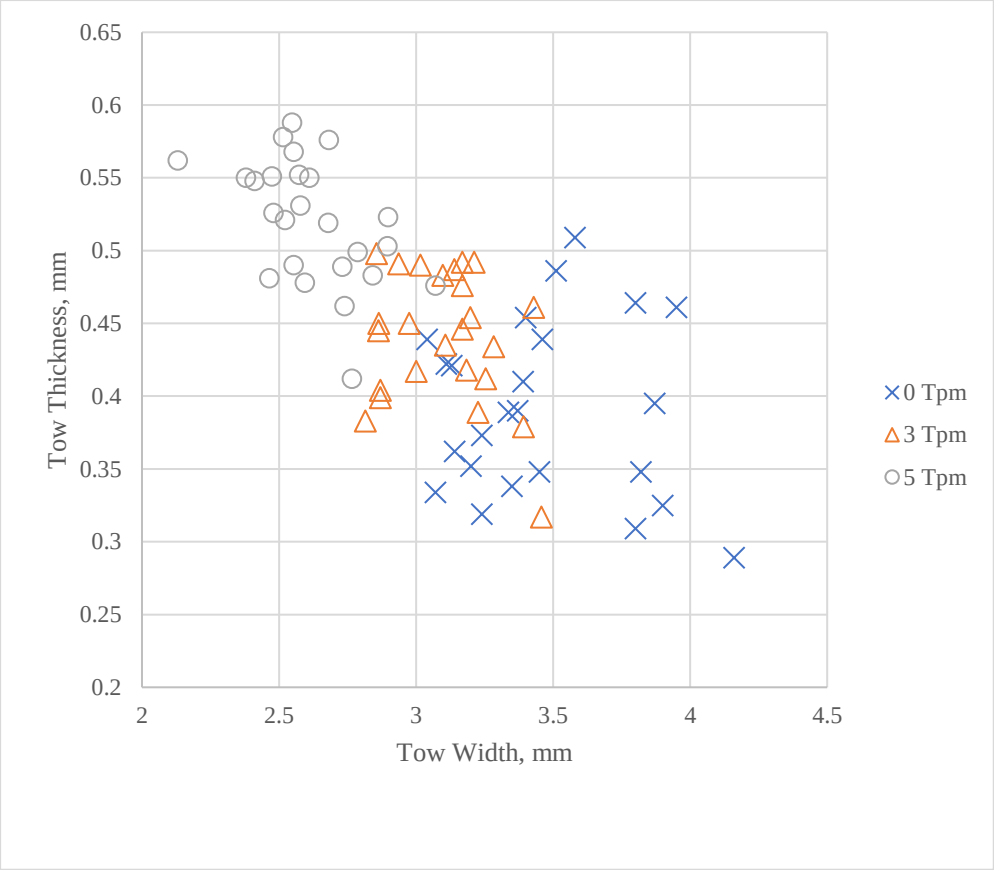


Figure 6.15 Relationship between tow width and corresponding tow thickness

Typically, braiding simulation requires approximation of the shape of the tow as this is not always constant and varies depending on if the yarn is in a transient or intersecting state. Table 6.7 uses the values measured for tow width and tow thickness to estimate tow area using both rectangular and elliptical approximations for tow geometry.

Table 6.7 Calculated tow cross-section area based from different approximations

	Approximated Tow Shape, mm^2	
	Rectangular	Elliptical
0 Tpm	1.489	1.089
3 Tpm	1.346	1.072
5 Tpm	1.344	1.071

Table 6.7 quantifies the over-approximation in tow area of using a rectangular tow approximation. The reduction in cross-sectional area of a tow shape was not statistically significant respective to number of twists for both the rectangular and elliptical approximation.

6.3.3 Validation of Assumptions with Different Material

The next data set looks at a repetition of the 0 Tpm measurements with HTS45 12K fibre from Teijin. These tests were completed on the 192-carrier axial braider at the NCC using a partially loaded braider configuration to produce a braided preform consisting of 48 biaxial tows. This allows the data to be directly compared to that collected at the UoN. Table 6.8 shows the scaled machine parameters for the NCC machine to produce a braid angle of 50°. The carriers were loaded in such a way that a braid with a regular braid pattern was produced.

Table 6.8 Corresponding Process Parameters for UoN and NCC Braiders

Process Parameter	48-Carrier Braider (UoN)	192-Carrier Braider (NCC)
Braid Carrier Speed, rpm	2.33	9.33
Take-Up Speed, mms^{-1}	5	20
Braid Angle	50	50

Tow width measurements were taken from the stabilised region of the braided preform using ImageJ. Table 6.9 shows the comparison of measured tow width for T700s and HTS45 rewound with 0 Tpm. The rewinding tension and rewinding speed were kept consistent for both sets of bobbins using the same parameters as stated in Table 6.3. A T-test was used to assess the statistical significance of the differences between the means of the two data sets, the P- value of 0.780 was calculated which

is larger than the significance level of 0.05. This means that the null hypothesis should be accepted and there is no significant difference between the two means.

Table 6.9 Measured tow width for different 12K fibres

Material	Tow Width, mm
0 Tpm T700s	3.801 ± 0.379
0 Tpm HTS45	3.754 ± 0.286

Figure 6.16 shows the complete set of data for 0 Tpm, 3 Tpm, 5 Tpm, 7 Tpm and 10 Tpm.

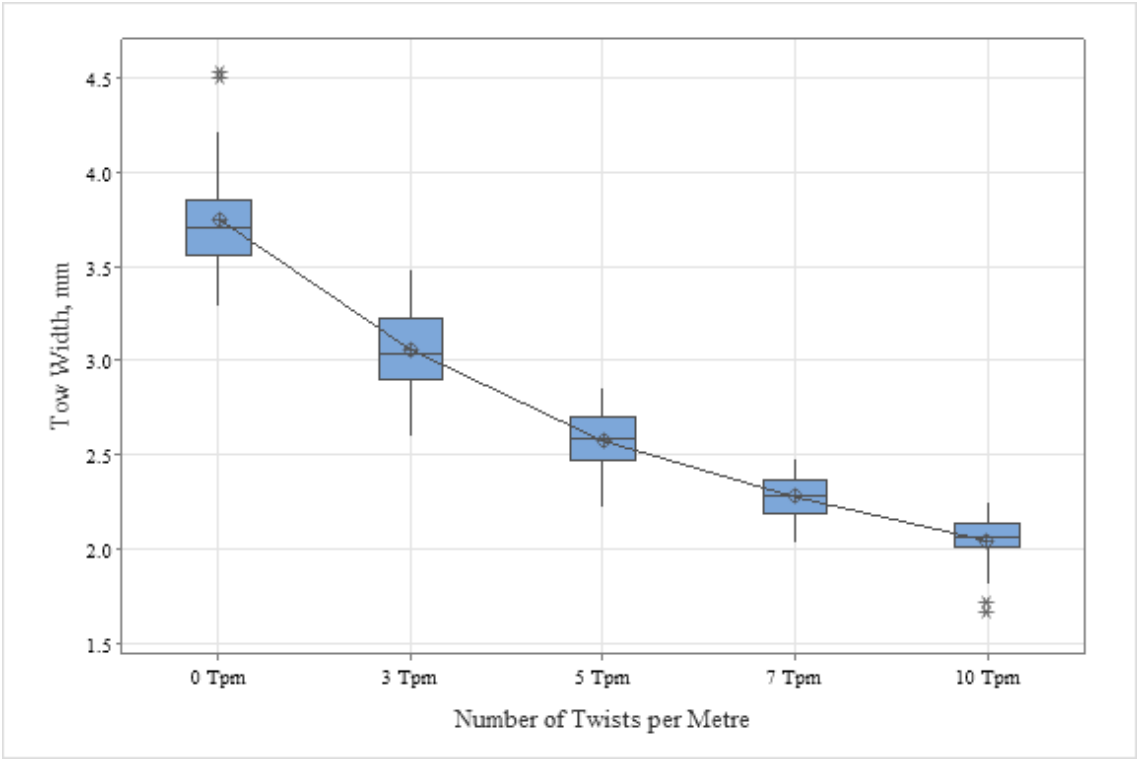


Figure 6.16 Tow Width for different levels of rewinding twist

The addition of twist to tows during rewinding is seen to reduce both tow width magnitude and variability. This is supported by Figure 6.16. This indicates a more reproducible braid architecture manufactured by braiding with twisted fibres.

Figure 6.17 demonstrates the results of Tukey comparison performed in conjunction with an ANOVA to assess the statistical significance of the differences in tow widths. None of the comparison intervals contain zero which indicates that the corresponding intervals are all statistically significantly different.

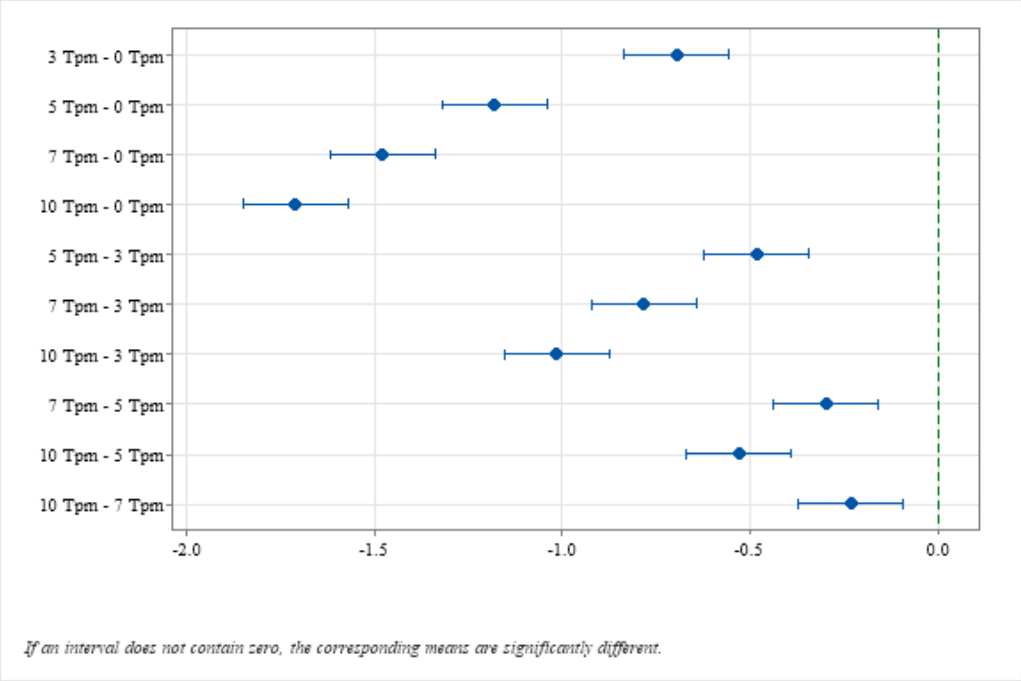


Figure 6.17 Tukey Pairwise Comparisons for Different levels of Twist

6.3.4 Influence of Twist on the Variability of Key Process Variables

The data in this section of the report is a combination of braided preforms produced on 50mm diameter mandrels. Both at the UoN on the 48-carrier braider with a fully loaded configuration (0 Tpm, 3 Tpm and 5 Tpm) and at the NCC on the 192-carrier braid ring with a partially loaded configuration (7 Tpm and 10 Tpm). The loading of bobbins at the NCC was configured to produce a regular braid pattern. The variability of the braid architecture was monitored through the measurement of the key process variables of braid angle and cover factor. These measurements were taken in the stabilised region of the braid.

6.3.4.1 Braid Angle Variability

Figure 6.18 shows the average braid angle recorded for each trial. Thirty measurements were taken in the stabilised region of each preform, each test was repeated three times. It can be observed that the number of twists per metre has no discernible effect on the braid angle as all measurements are within the ±1° which is considered a tolerable range for braid angle. The interval bars represent the 95% confidence limits of the data, there is considerable overlap between many datasets, which suggests that differences are not statistically significant however, this overlap is not inclusive to all data sets. All standard deviation bars do overlap which allows

the conclusion that any differences in braid angle variability are irrespective of the number of twists per metre.

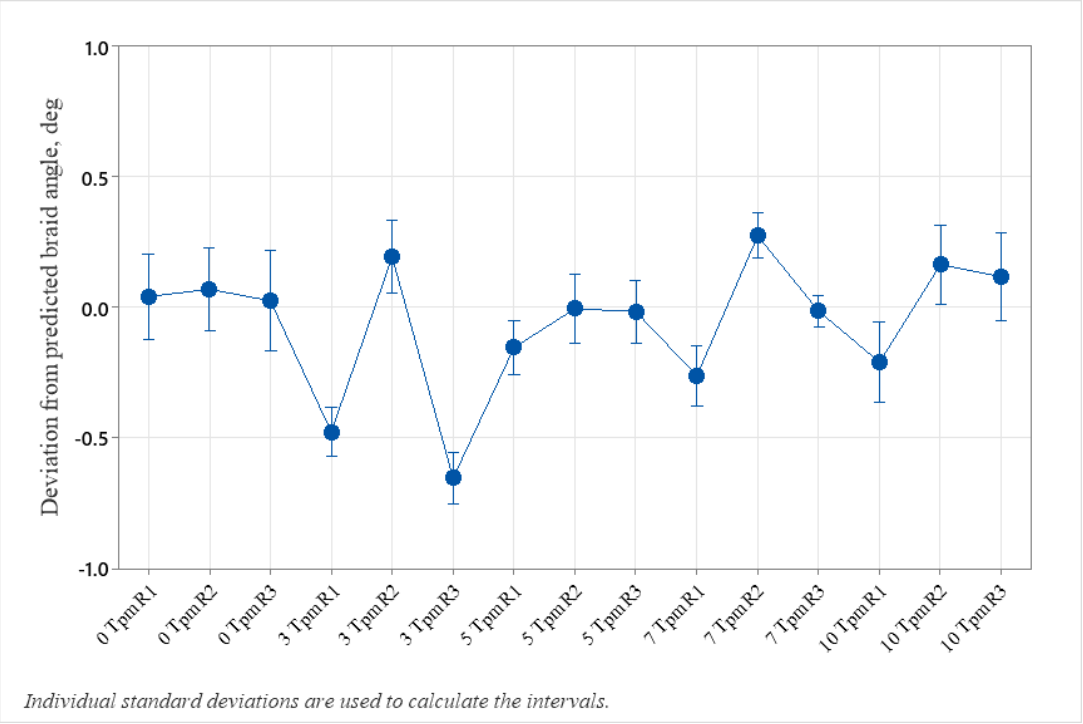


Figure 6.18 Interval plot for deviation from predicted braid angle

From a prediction perspective as all measured braid angles were within ±1˚ of the programmed braid angle.

6.3.4.2 Cover Factor Variability

Table 6.10 shows the predicted cover factor calculated using Equation 3.3 based on the average tow widths from each of the different levels of twist shown in Table 6.10 for a 50mm diameter cylindrical mandrel. The data shows that for the same sized tow, an inclusion of 10 Tpm results in a reduction of approximately 27.58% in cover factor based on analytical calculations.

Table 6.10 Calculated cover factor for different tow widths

Number of Twists per Metre, Tpm	Tow Width, mm	Predicted Cover Factor using Equation 3.3, %	Measured Cover Factor, %	Measured Cover Factor Range, %
0	3.75 ± 0.29	96.43	91.51 ± 3.76	15.90
3	3.06 ± 0.21	88.51	87.89 ± 3.19	13.90
5	2.58 ±0.16	80.32	79.50 ± 2.96	11.60
7	2.28 ± 0.14	74.19	74.73 ± 2.22	8.00
10	2.05 ± 0.13	68.85	70.50 ± 2.22	7.10

Table 6.10 shows the actual cover factor of the braided preforms was measured by photographs using ImageJ. Thirty measurements of cover factor were recorded in the stabilised region of the braided preform. As the number of twists per metre increase the range of measured cover factor values decreases. This indicates that twisted fibres reduce localised cover factor inconsistencies. Notably, the average cover factor for the 0 Tpm preform is lower than the analytical value. This is because the analytical equation does not account for localised deviations in cover factor, more of these regions of localised deviations are observed in the preforms manufacture with 0 Tpm fibres. This is because twisting helps maintain a more consistent tow bundle, without the twist the tow is more exposed to filamentisation which create localised deviations. This supported by the larger variability in tow width for 0 Tpm fibres. This is summarised in Figure 6.19.

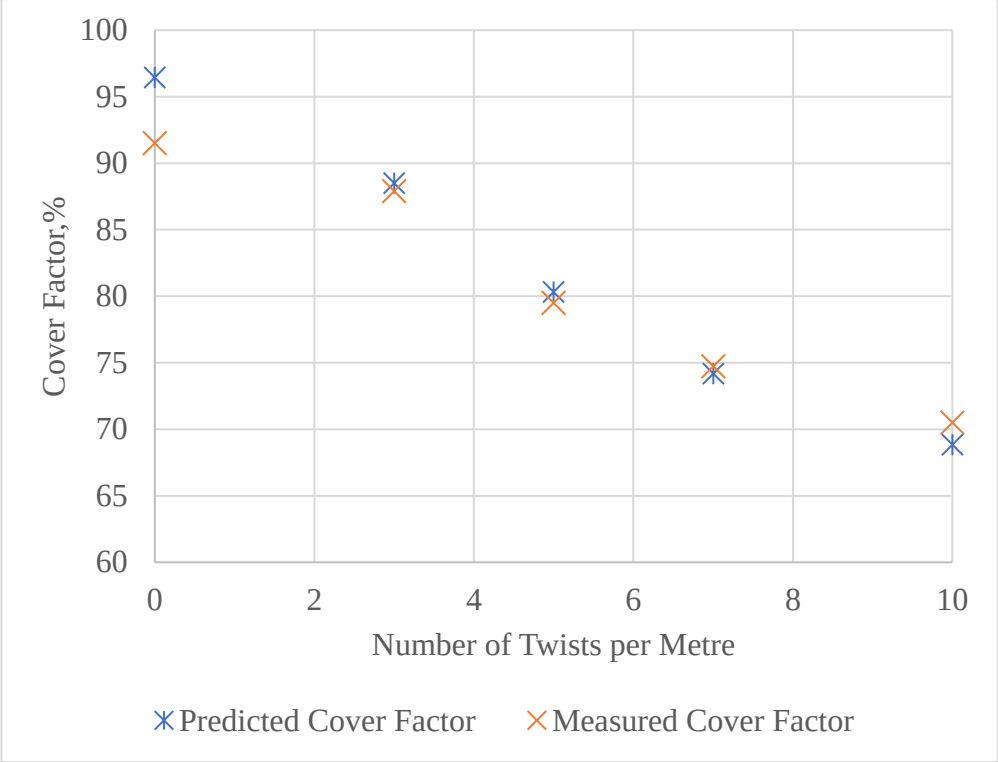


Figure 6.19 Relationship between cover factor and number of twists

6.3.5 Single Layer Preform Summary

The following section summarises the conclusions made to this point with regards to single layer preforms manufactured on a straight axisymmetric mandrel of constant cross-section. Braid angle and tow width were unaffected by machine parameters of carrier and take up speed. However, the inclusion of a twist to fibres during rewinding resulted in a change in tow geometry. For a 12K carbon fibre, the inclusion of 5 Tpm resulted in a tow width reduction of 28%. Twist was found to alter the aspect ratio of the tow. Therefore, a reduction in tow width because of twist corresponded to an increase in tow thickness. This was found to be statistically significant. An assumption for tow aspect ratio has been developed to approximate tow width and thickness for tow sizes between 3K-50K with varying level of twist. Comparisons to microscopy data showed good agreement.

6.4 Braid Architecture Variability of a Multilayer Preform

In manufacturing, typically an understanding of multilayer preforms is required. Braided preforms were manufactured on a cylinder of 50mm diameter using the process parameters in Table 6.4, each preform consisted of four layers. Similarly, to the single layer preforms, 12K T700s carbon fibre was used with the braider in a fully

loaded configuration to manufacture a regular braid pattern with 48-carriers. Three repeats of each preform were manufactured for two different levels of twist: 0 and 5 Tpm. Deviation in variability of key process variables of cover factor and braid angle are analysed using ImageJ. Tow geometry parameters are monitored using ImageJ to measure tow width and the Apodius 2D scanning system to measure the part thickness along the length of the preform.

6.4.1 Tow Width Variability of a Multilayer Preform

The layer-to-layer friction differs between the initial layer mandrel-to-fibre interaction and the fibre-to-fibre interaction of subsequent layers, this can cause changes in tow spread and tow width variability. The next dataset is used to determine if the tow width approximations developed in Section 6.3.4 are valid for the subsequent layers. Table 6.11 shows the average tow width recorded in the stabilised region of the preform for layers 1 to 4 for both 0 Tpm and 5 Tpm preforms. Thirty measurements were taken in the stabilised region of each layer. Any difference in tow width was not found to be statistically significant between layers 1 to 4 for each level of twist.

Table 6.11 Average Tow Width for Multilayer Preforms

Rewinding Twist, Tpm	Layer 1 Tow Width, mm	Layer 2 Tow Width, mm	Layer 3 Tow Width, mm	Layer 4 Tow Width, mm
0	3.75 ±0.29	3.62 ±0.20	3.71 ±0.17	3.69 ±0.17
5	2.56 ±0.16	2.68 ±0.18	2.67 ±0.18	2.62 ±0.17

For the 0 Tpm preforms no statistically significant difference in tow width between the initial and subsequent layers was recorded. For the 5 Tpm preform the overlap between 95% confidence limits about the respective means demonstrates that the slight increase in mean tow width in the subsequent layers is not statistically significant difference between the means for each layer of the braided preform.

In summary, neither the magnitude nor variability of the measured tow width is altered in the subsequent layers of a multilayer preform. As a result, the tow width assumptions outlined in Section 6.3.4 are valid for multilayer preforms.

6.4.2 Maximum Layer Thickness Variability of a Multilayer Preform

Subsequent layers of a multilayer preform nest together to produce the overall part thickness. The inclusion of twist to the fibres can alter this nesting capability by reducing the resultant tow spread.

6.4.2.1 Layer thickness variability using the Apodius RS6 on a small scale preform

The Apodius RS6 is used to measure the layer thickness of multilayer preforms manufactured on the 50mm diameter mandrel. The overall preform was thicker for the 5 Tpm preforms. An ANOVA with a 95% confidence level identifies a statistically significant difference in preform thickness between the 0 Tpm and 5 Tpm.

Table 6.12 summarises the average recorded maximum layer thickness across the length of the preforms for preforms of one to four layers for 0 Tpm and 5 Tpm preforms. This is done by comparing the respective thicknesses of the preforms at discrete locations along the mandrel for each braided layer. For both the 0 Tpm and 5 Tpm the initial layer was seen to be significantly thicker than the addition in preform thickness for the subsequent layers due to the nesting of the braided material as more braided layers are added.

Table 6.12 Average Layer Thickness Summary for Multilayer Preforms

	Total Preform Thickness, mm			
Rewinding Twist, Tpm	Single Layer	Two Layer Preform	Three Layer Preform	Four Layer Preform
0 Tpm Run 1	0.687 ±0.078	1.074 ±0.103	1.454 ±0.119	1.828 ±0.112
0 Tpm Run 2	0.707 ±0.076	1.063 ±0.126	1.489 ±0.117	1.802 ±0.139
0 Tpm Run 3	0.664 ±0.063	1.011 ±0.096	1.438 ±0.116	1.765 ±0.118
5 Tpm Run 1	0.839 ±0.087	1.269 ±0.122	1.639 ±0.156	2.051 ±0.169
5 Tpm Run 2	1.008 ±0.127	1.419 ±0.140	1.916 ±0.178	2.326 ±0.225
5 Tpm Run 3	0.962 ±0.104	1.324 ±0.145	1.813 ±0.126	2.300 ±0.212

The thickness variation shown in the measured maximum layer thickness is consistent in Layers 2→4 for both 0 Tpm and 5 Tpm preforms, suggesting that the nesting factor for the subsequent braided layers is consistent for each additional layer. The preform thickness magnitude increase was slightly greater for the 5 Tpm preforms. Thickness variability was higher in the 5 Tpm preforms in comparison to

the 0 Tpm preforms due to the more rounded tow cross-section leading to greater undulation.

Assuming that the thickness of each subsequent is the same as the initial layer, the nesting factor can be calculated. Nesting can be defined as the percentage of the deposited layer that is within the preform that had already been deposited. A greater average level of nesting was observed for the 5 Tpm preforms, 54%, in comparison to the 0 Tpm preforms 46%. However the thickness of a twisted preform is still greater despite the increase in nesting behaviour due to a thicker tow bundle.

6.4.3 Braid Angle Variability of a Multilayer Preform

The average braid angle of each layer of the 0 Tpm and 5 Tpm preforms was determined using thirty measurements taken in the stabilised section of the preform using ImageJ. This is shown in Figure 6.20 and Figure 6.21. All braid angle measurements were within ±1° of the programmed angle.

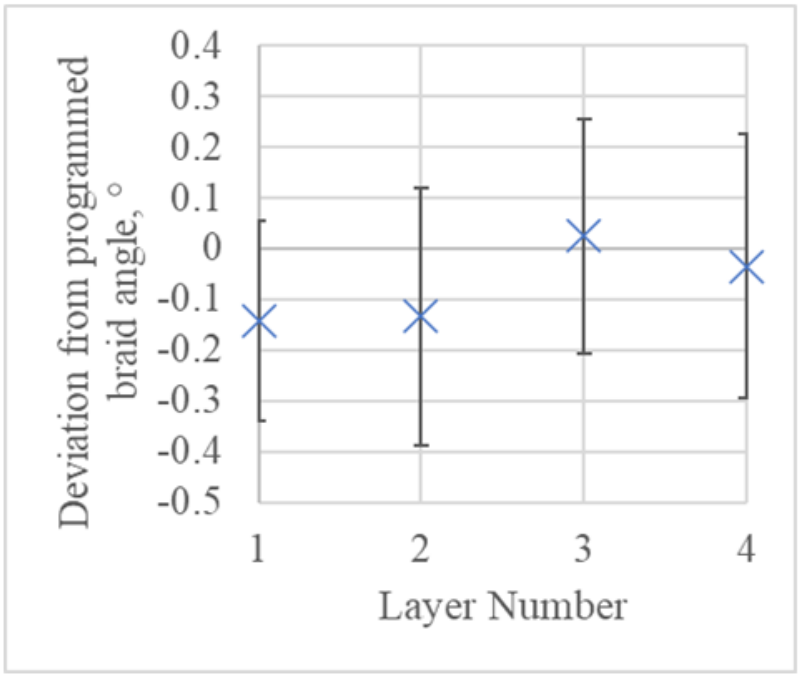


Figure 6.20 Braid Angle Variability for 0 Tpm Multilayer Preform

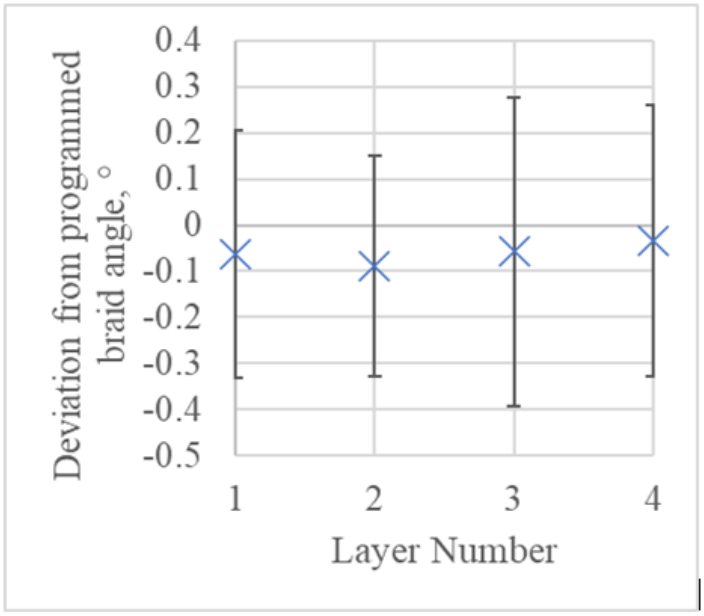


Figure 6.21 Braid Angle Variability for 5 Tpm Multilayer Preform

The magnitude of the braid angle and its variability was no different in the subsequent layers of a braided preform. This is shown through statistical testing and the overlap of the standard deviation bars. Any observed difference between preforms manufactured with twisted fibres compared to the untwisted fibres was also not statistically significant. Therefore, we can conclude that the key process variable of braid angle is not influenced by twist added to fibres during rewinding.

6.4.4 Multilayer Preforms Summary

Any differences in braid angle and tow width between the initial and subsequent layers of a braided preform is not statistically significant. Therefore, the assumptions developed for single layer preforms are valid for multilayer preforms. The subsequent layer thickness addition is less than that of the initial layer, however it is linear in each of the subsequent layers. The magnitude of the thickness addition is greater in the twisted preforms. The aspect ratio tow geometry assumption was developed using experimental data to determine the layer thickness addition for subsequent layers.

6.5 Braid Architecture Variability Induced by Machine Size

The majority of the preforms discussed to this point in the thesis have been small-scale 50mm diameter, manufactured using the 48 braid carriers. The manufacturing facilities at the NCC provide the opportunity to scale the manufacturing process by a

factor of four to 192-carriers. A caveat with using a larger machine is the potential for the influence of gravity on the variability of the part.

6.5.1 Experimental Methodology

Process parameters were scaled so that the key process variables of cover factor and braid angle were comparable for both the 48-carrier braider at the UoN and 192-carrier braider at the NCC. The variability of these process parameters were measured using ImageJ. T700s 12K standard modulus fibre supplied by Toray was used on both machines to manufacture cylinder of 50mm and 200mm diameter respectively. This investigation was completed with bobbins rewound with two different levels of twist, 0 Tpm and 5 Tpm. Both machines were fully loaded to produce a biaxial braid with a regular braid pattern.

6.5.2 Preform Stabilisation

Figure 6.22 shows the deviation from the predicted analytical braid angle along the length of the mandrel for 0 Tpm. The distance along the mandrel has been normalised as a ratio of distance along the mandrel and mandrel diameter. The dotted lines reflect an angle region of ±1˚.

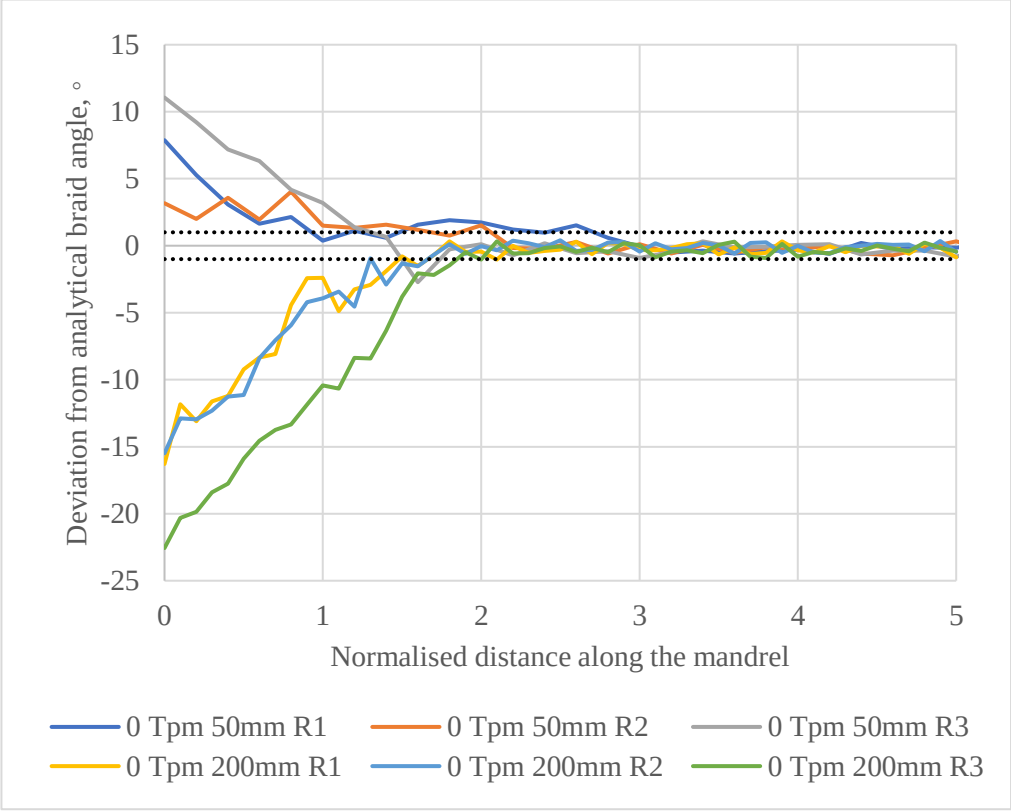


Figure 6.22 Stabilisation Length for Small and Large Mandrels for 0 Tpm Preforms

When the starting angle was not controlled, the braid stabilised at approximately 2x the mandrel diameter irrespective of mandrel or machine size. The contrast in starting angle between mandrel sizes can be explained through inspection of the manufacturing set-up. The larger machine starts the braid from fibres tied to a lead in of smaller diameter hence the smaller starting angle. The smaller machine starts the braid from a tight braid around the start of the 50mm mandrel resulting in a starting angle greater than the predicted angle. The data demonstrates that the set-up method does not impact the stabilisation length. Figure 6.23 shows data for fibres rewound with 5 Tpm.

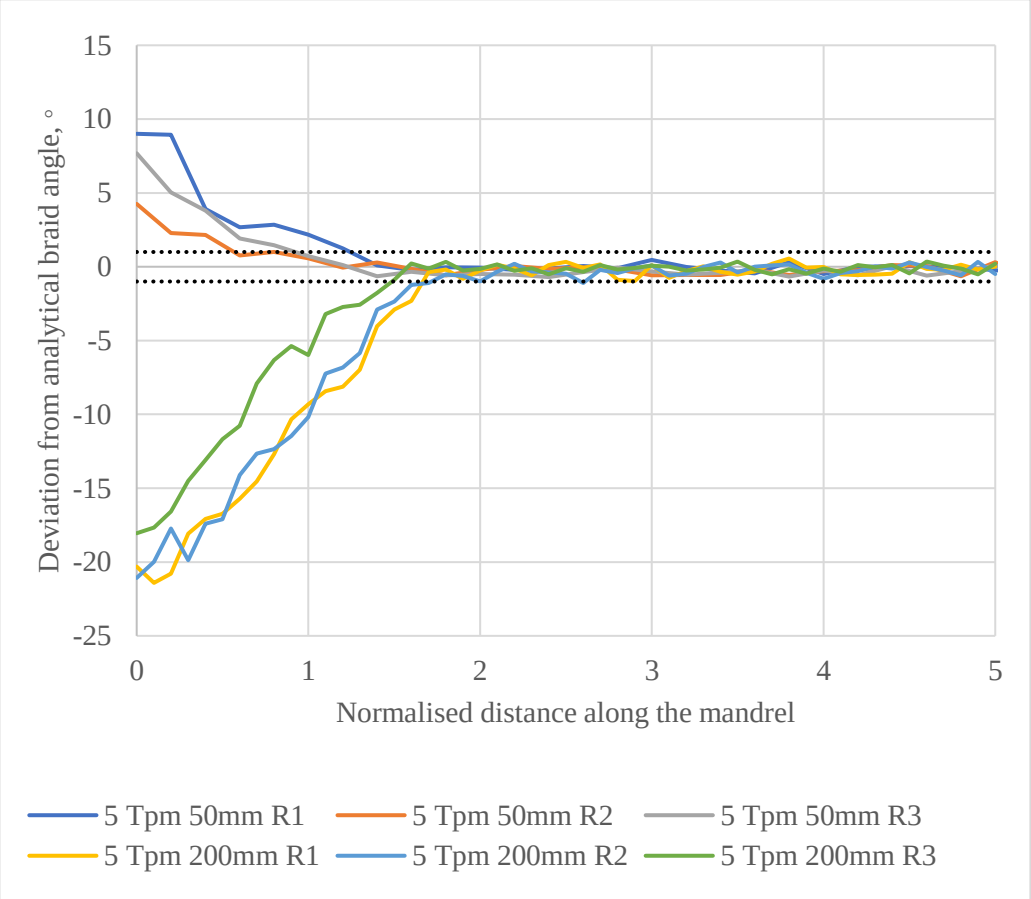


Figure 6.23 Stabilisation Length for Small and Large Mandrels for 5 Tpm Preforms

All preforms were found to stabilise slightly earlier with the twisted fibres between 1.5x and 2x the mandrel diameter. Through statistical testing, a correlation of -0.74 between twist and stabilisation length was determined. This is a strong negative correlation. This suggests that adding twist to fibres during the rewinding process reduces the stabilisation length of the preform. A similar test was completed to analyse the relationship between mandrel diameter and stabilisation length and no correlation

(0.135) was found between the variables. Therefore, any variation in stabilisation length of the preform was not a result of the mandrel or machine size.

6.5.3 Influence of machine size on tow width variability

Thirty tow width measurements were recorded in the stabilised section of each preform and the combination averages for each set of three repeats in the corresponding manufacturing configurations are shown in Table 6.13.

Table 6.13 Measured Tow Width for both mandrel diameters.

	Measured Tow Width for different mandrel diameters, mm	
Number of Twists per Metre, Tpm	50mm	200mm
0	3.50 ±0.28	3.55 ±0.20
5	2.68 ±0.20	2.56 ±0.15

The overlap in standard deviation bars between tests of the same level for twist but different mandrel diameters demonstrates that there is no statistically significant difference as a result of mandrel diameter. The findings related to tow width and twist are unaffected by the mandrel within tested range.

6.5.4 Machine Size Summary

Machine size was found to have no influence of the tow width magnitude for both twisted and untwisted fibres. The preforms were found to be scalable between the small and large machinery with preforms braided with untwisted fibres stabilising at approximately 2x mandrel diameter along the length of the mandrel. This is irrespective of the starting angle of the braid. Twisted fibres slightly reduced the stabilisation length of a braided preform. A strong negative correlation of -0.74 was determined between twist and stabilisation length.

6.6 Triaxial Braid Architecture

The next dataset studies triaxial braids to assess any deviation in braid architecture and tow geometry due to the inclusion of an axial tow. Triaxial preforms were manufactured using the 192-carrier braider at the NCC. The bias tows were 12K HTS45 carbon fibre from Teijin rewound with 7 Tpm. 12K HTS45 was also used for

the axial fibres, a fully loaded (96) axial configuration was used for the manufacture of the preforms. Axial tows were untwisted. Preforms of seven layers are manufactured on a tapered mandrel with effective diameter 213-246mm. The preform was programmed to achieve a constant cover factor across the part.

6.6.1 Braid Architecture of Single Layer Triaxial Preforms

Figure 6.24 shows a comparison between the bias fibres in a biaxial and triaxial braid. Thirty measurements were taken in the stabilised region of each braid. An average tow width of 2.22mm ± 0.12 was recorded for the bias tows in the triaxial braid and 2.28mm ± 0.14 for bias tows in the biaxial braid. A two-tailed T-test demonstrates that at a significance level of 0.05 a P-Value of 0.058 is recorded.

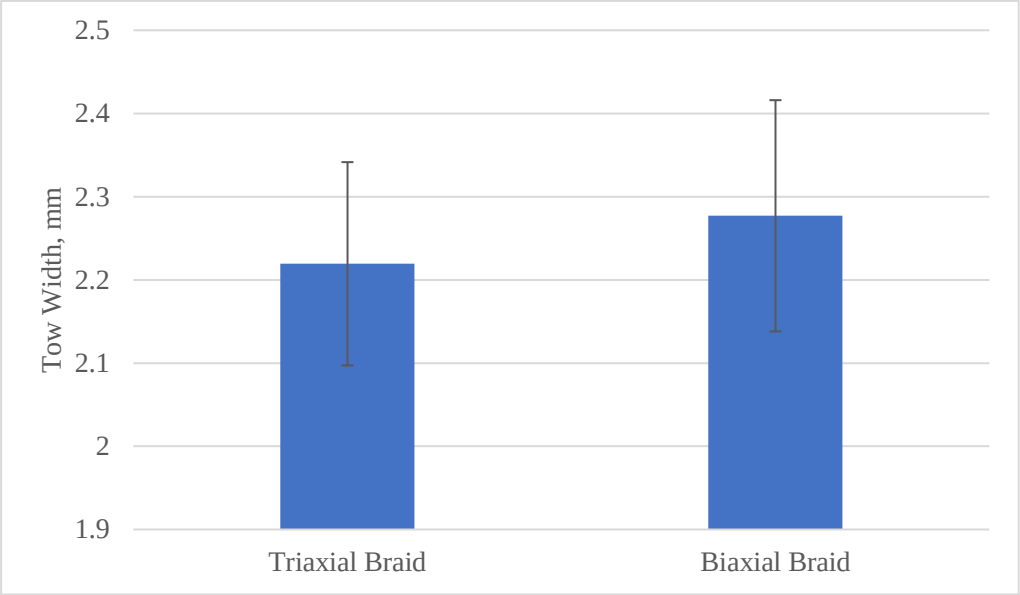


Figure 6.24 Bias Tow Width for Biaxial and Triaxial Braid for 7 Tpm Fibres

During the braiding process the tensioning of the axial fibres comes from the movement of the mandrel in the gantry system. This contrasts to the bias fibres which are tensioned using the carrier spring mechanism. Figure 6.25 compares the 0 Tpm bias fibres from previous tests with the untwisted axial fibres. Thirty measurements were taken using ImageJ in the stabilised section of the braided preforms. The average recorded tow width is considerably higher in the bias untwisted fibres, 3.75mm, than in the axial fibres, 3.31mm. This difference is likely to be as result in the difference in tension applied to the tow during the braiding process and compression of the axial tow by the bias tows.

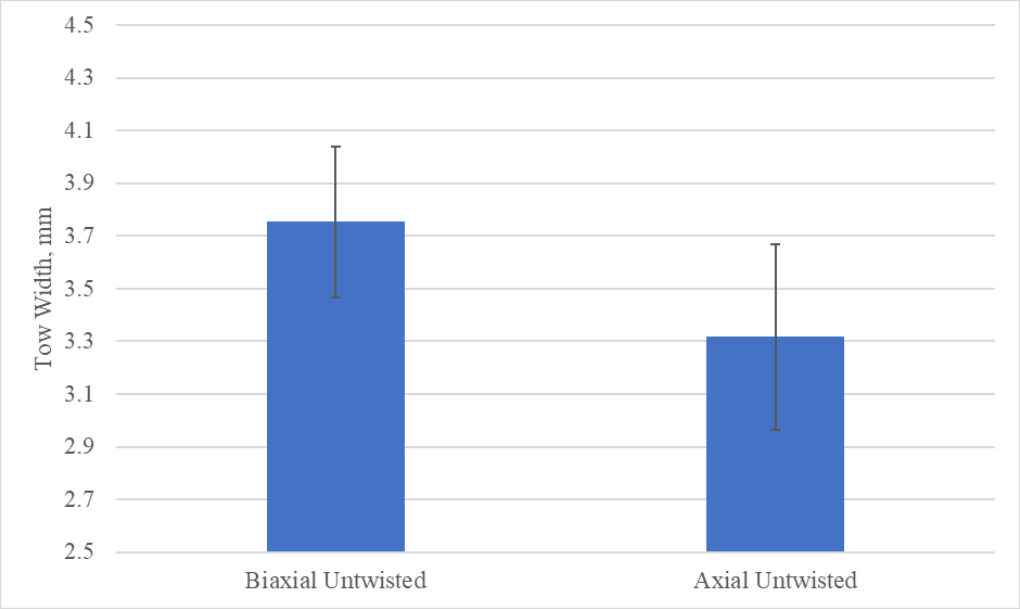


Figure 6.25 Measured tow width between axial tows and biaxial tows with untwisted fibres

Using a two-tailed T-test this difference was found to be statistically significant, recording a P-Value of 0.000002 at a significance level of 0.05. Figure 6.26 shows the results of this test, a greater data range and variability can be seen with the axial fibres.

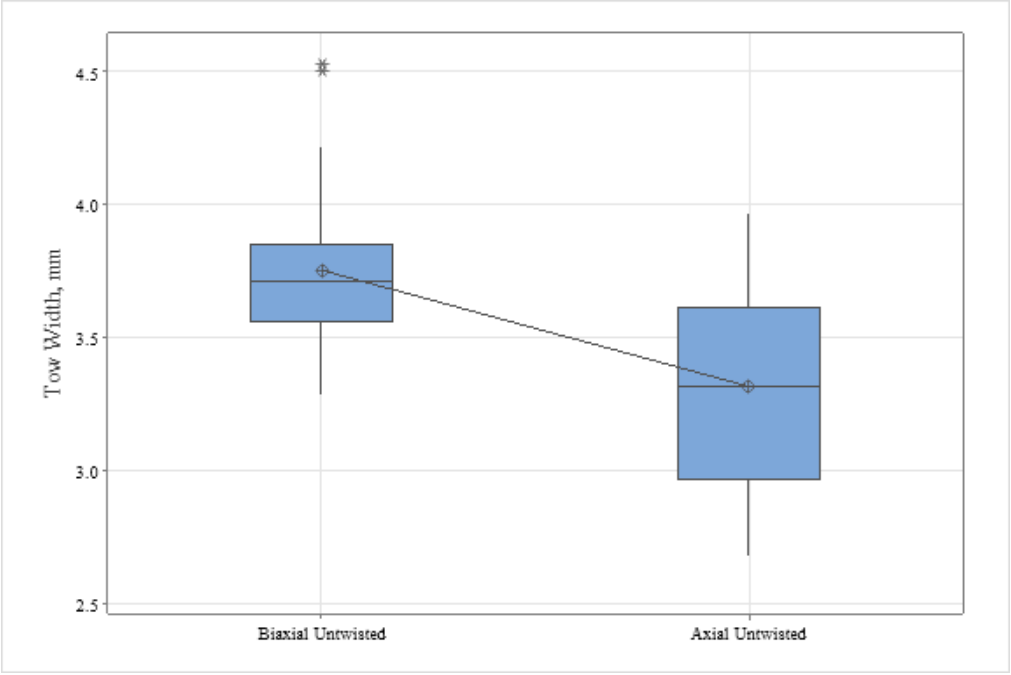


Figure 6.26 Statistical Test Analysis for Axial and Untwisted Fibres

Figure 6.26 shows a high level of variability, particularly in the axial measurements. Figure 6.27 demonstrates the variability along the length of the part in five different axial fibres. A substantial variation in each fibre along the length of the mandrel is seen, this difference is up to 2.3mm with some fibres. A large variation in tow geometry can result in localised cover factor variations. Across the five axial tows measured, the tow width varies from 2.3mm to 4.8mm. The measured tow width of axial tow 4 varies from 2.3mm to 4.6mm along its length.

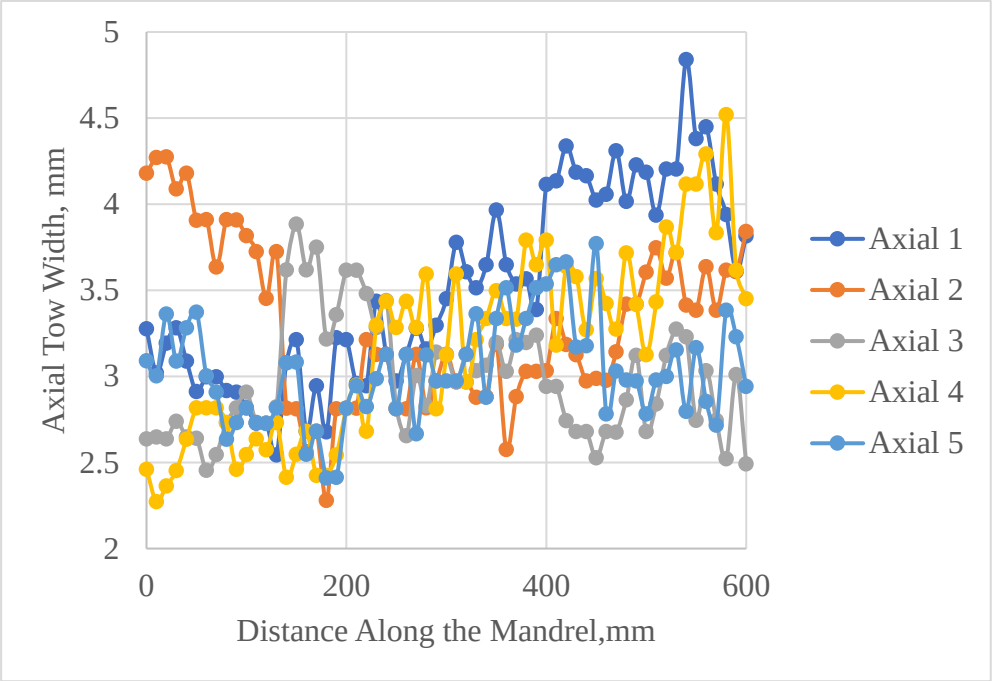


Figure 6.27 Measured Axial Tow Width Along the Part Length

The motion of the bias tows results in variation in the location of the axial tows in the unit cell. Figure 6.28 shows images taken of the triaxial braided preform. This results in localised deviations in cover factor. The measured cover factor is determined using the bespoke ImageJ method and is listed in Figure 6.28. The red dashed line denotes the central axis of the unit cell. A range of 5.86% localised cover factor as a result of location of axial tow placement was determined from these images.

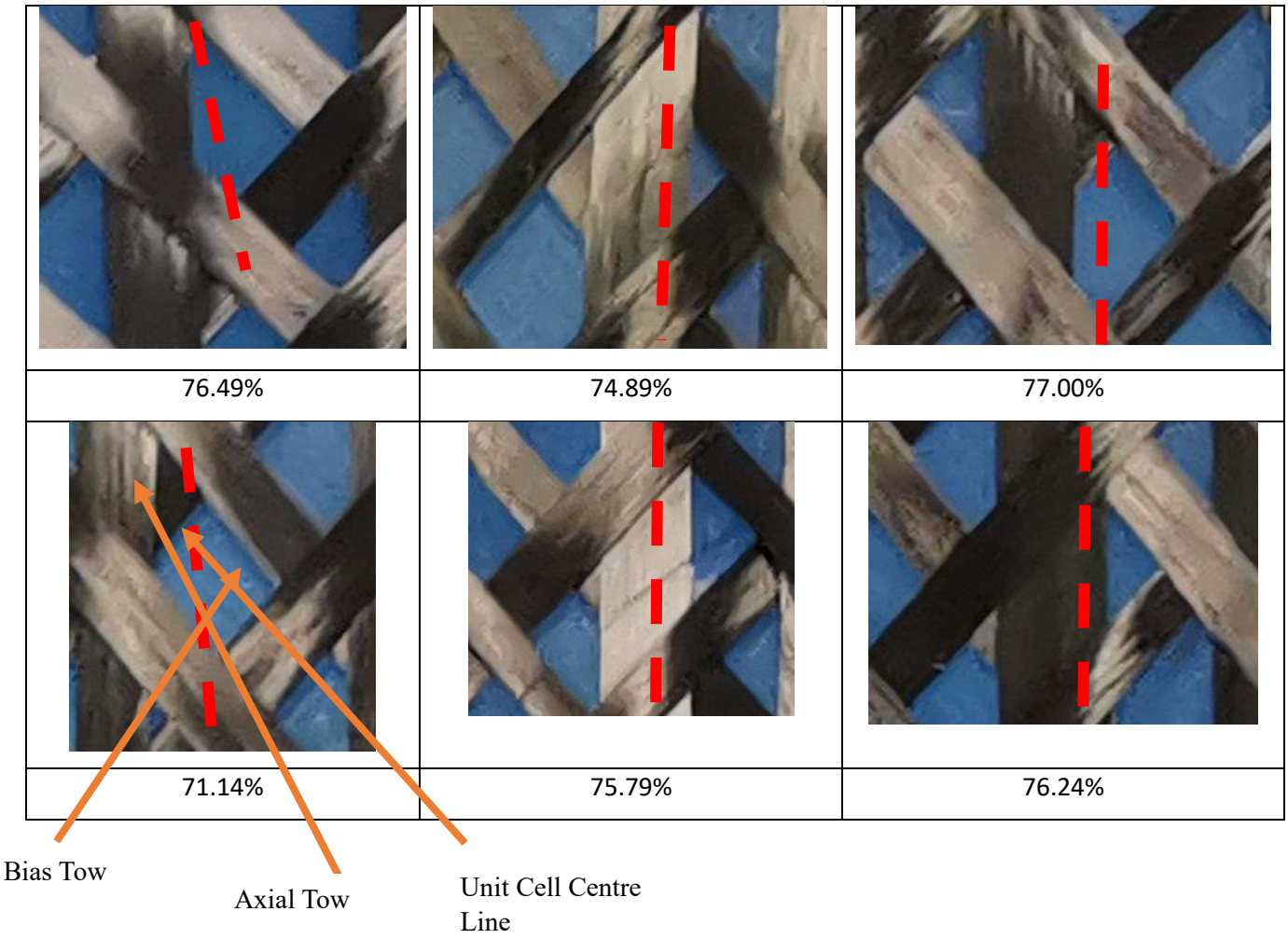


Figure 6.28 Images of Triaxial Braided Preforms and Calculated Cover Factor Using ImageJ

Figure 6.29 demonstrates the varying locations that an axial tow end in the braided unit cell. Heieck provides a generalised method for calculating the triaxial cover factor of a braid [34]. A biaxial tow width of 2.355mm and an axial tow width of 3.11mm is used for the purpose of this calculation. An analytical coverage of 73.7% is calculated. Textile fabrics comprise of multiple unit cells which are defined as the smallest section of the braid that represents the entirety of the architecture [3], like Figure 6.29. The coverage of the larger fabric region is analysed in ImageJ. Thirty measurements have been taken. The image clearly highlights the variable position of the axial tows within the unit cell caused by the serpentine motion of the braid carriers.

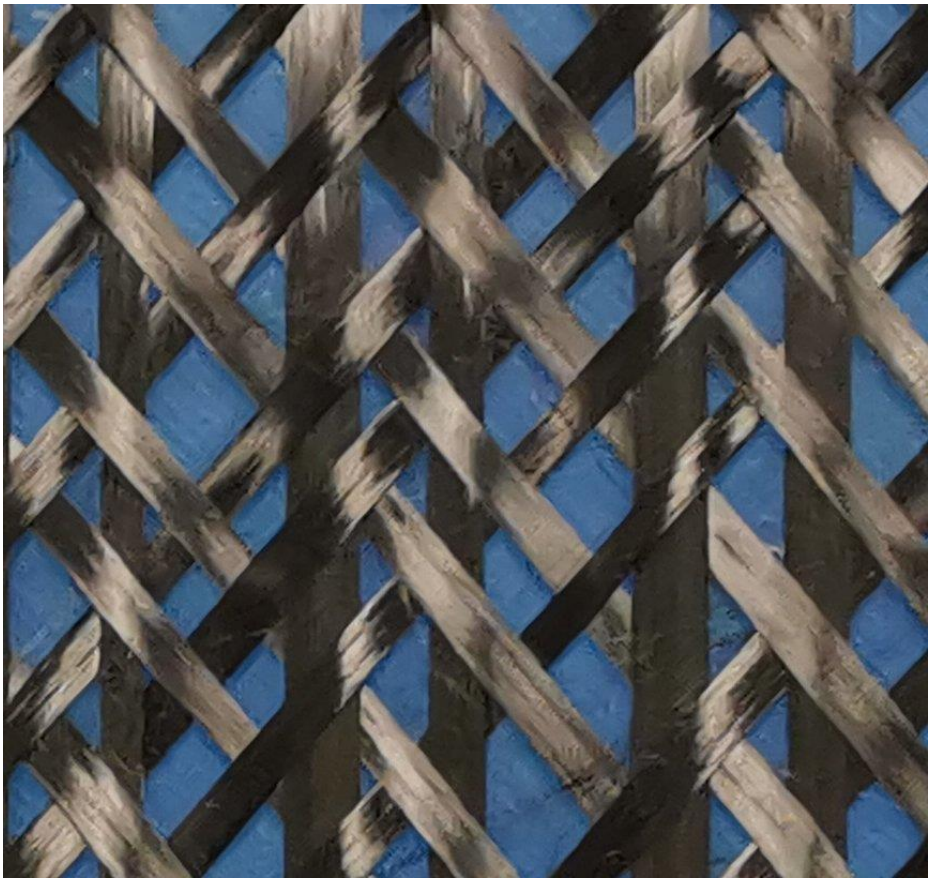


Figure 6.29 Triaxial Braided Preform

The average cover factor determined in ImageJ was 77.01% ±0.98%. The range of measured cover factors was 2.85% this is much lower than the 5.86% variation found among the individual unit cells. This is higher than the analytically calculated value due to an increased tendency of the braiding tows to spread due to the low coverage. However, it is still within the range of coverage values calculated in the individual unit cells in . This confirms the high variability in axial tow placement suggested by Heieck.

6.6.2 Summary of Conclusions for a Triaxial Preform

Comparing the bias fibres of both biaxial and triaxial braids, no significant difference was found between the tow width of the bias fibres. However, a significant difference was noted between the axial fibres which were untwisted and untwisted bias fibres of the same HTS45 12K carbon fibre. Image analysis of the triaxial preforms found a variation is axial tow location as result. This leads to deviation in localised cover factor.

6.7 Conclusions

At the start of the Chapter, the aim of developing a set of tow geometry approximations for cylinders were established. ImageJ has been determined to show an acceptable level repeatability and reproducibility as a measurement method for the key process variables of the cover factor, braid angle and tow width of a braided preform. This confirms work by Carey [3] that suggests ImageJ as a suitable measurement tool.

Guide rings had a significant influence on the stabilisation length of the preform as shown by Ebel [44], however this work was completed using a rectangular mandrel with a single size of cylindrical guide ring. This work built on this statement by looking at the level of impact of increase guide ring size on braid architecture. The larger guide rings resulted in a longer stabilisation length. Once the desired braid angle has been reached no difference in variability was noted as a result of different guide ring sizes. However, an increase in guide ring diameter results in an increase in tow width variability. Larger guide ring sizes caused greater difficulties with preforms conforming to the mandrel. Varying guide ring sizes had no impact on the global cover factor, however larger guide ring sizes resulted in more frequent localised deviations in cover factor. This is important when developing manufacturing set-ups in order to reduce run-in lengths and consequent material wastage.

It has been well accepted in literature by Ebel [48] and Kyosev [29] among others that rewinding is a critical component of the braiding process. With Torun [17] and Eurocarbon [16] suggesting that the introduction of rewinding twist can be beneficial for tow processability. However, this work develops this by determining the impact of this rewinding twist on the tow geometry and braid architecture of a braided preform. The addition of twist during the rewinding process results in changes in tow geometry. Optical microscopy images showed a change in tow cross-sectional shape with untwisted tows being more lenticular in comparison to twisted tows with an elliptical cross-section. This confirms work by Thompson [79] where the braided tow shape is acknowledged to vary. However, this builds on the literature by identified rewinding twist as a potential reason for this change in shape. Increasing the number

of rewinding twists reduces the tow width, quantification of tow geometry measurements is not currently available in the literature. For a 12K carbon fibre tow an increase from 0 to 5 Tpm results in a 28% tow width reduction. Tow thickness saw an increase with an increasing level of twist. These differences were found to be statistically significant. The changes in tow geometry because of the inclusion of rewinding twist had a significant impact on cover factor, for a preform manufactured with 12K carbon fibre the inclusion of fibre with 10 Tpm was found to reduce the cover factor by 28% compared to a preform manufactured with untwisted fibres. Understanding of this is critical when designing braided preforms in order to achieve the desired component properties and is something that has neither been identified or quantified by existing literature.

The tow geometry approximations identified at a single layer level were proven to be valid at a multilayer level. There was no statistically significant difference in tow width or braid angle between initial and subsequent layers of a multilayer braided preform irrespective of the level of rewinding twist added to fibres. A greater level of nesting was observed for the twisted preforms, 54% in comparison to the 0 Tpm preforms 46%. However, the thickness of a twisted preform is still greater due to a thicker tow bundle. The understanding of preform thickness variations as a result of twist has not previously been addressed but has potential impacts on part design and manufacture as braid thickness is a key process variable.

Machine size was not found to influence the key process variables of a braided preform, this comparison is novel and has not been done explicitly in the literature. It provides the potential for generating generalised yarn approximations that are valid for any braiding machine. The braiding process was determined to be scalable as preforms typically stabilised at 2x mandrel diameter. Twisting was found to reduce the stabilisation length of preforms. The influence of twisting on stabilisation length is something that has not been identified in the literature and offers potential for reduced manufacturing wastage.

It is understood in literature that axial yarns do not behave the same as the bias fibres in a triaxially braided preform. Heieck [34] has done some previous to calculate the triaxial cover factor. However, this work has built on this concept by quantifying the differences if any between biaxial fibres without twist and axial fibres to try to

determine a yarn approximation. Analysis of triaxial preforms demonstrated that there was no statistical difference in the bias fibres in biaxial or triaxial preforms. However, a difference in tow width between untwisted 12 K axial fibres and untwisted biaxial 12K fibres was recorded. This is due to the tensioning mechanisms of the fibres. Image analysis demonstrated variation of axial placement within triaxial unit cells demonstrating that cover factor measurement of a triaxial preforms improves by measuring a large section area. This confirms the work by Heieck.

Overall, this chapter highlights the causes of tow geometry variability within braiding on cylindrical mandrel with constant cross section and how the rewinding process parameters are intrinsically linked to this. This is vital information from a braid design perspective and coupled with the fibre processability and mechanical testing information in Chapter 5 offers potential improvements to manufacturing.

7 Effect of Rewinding Twist on Axisymmetric Non-Prismatic Geometries

7.1 Background and Aim

In practice, braided components will not necessarily have a constant cross section. Changes in cross section are likely to introduce a level of instability into the braided preform. This chapter aims to consider the effects of braiding on a non-prismatic, frusto-conical cross-section by analysing the key process metrics of tow width, braid angle and braid thickness.

The initial focus is on the influence of a part gradient variability on the braid architecture. It is understood that introducing a geometrical change in mandrel geometry poses manufacturing difficulties for achieving consistent architecture in a braided preform. Previous work has outlined differences in braid architecture when braiding on a diverging or converging cross-section at different part gradients. In a part with a tapered cross-section, the variability of the braid architecture was reduced by braiding on a converging cross-section [39]. This chapter starts by assessing the principles of part gradient and mandrel orientation before building on the work of Du and Popper by analysing the influence of twist on the braid architecture for diverging and converging cross-sectional geometrical changes. As described in Chapter 4 this is addressed for both small and large- scale conical sections along with examining the manufacturing limits of braiding analysed on the 'Oscar' geometry. The variability of the key process variables of braid angle and cover factor are compared for a cylindrical to conical section in both converging and diverging orientation.

7.2 Effects of Part Gradient on Braid Architecture Variability

A summary of the key data from the investigation into the effect of part gradient on the behaviour of the braid architecture of a braided preform are summarised below. Results are discussed in relation to the influence of the part gradient on the key process variables of braid angle, tow width and layer thickness. The influence of the inclusion of twist is also summarised.

7.2.1 Effect of part gradient on braid angle in single layer preforms

Table 7.1 summarises the tests conducted on the small cone mandrel at the UoN as explained in Chapter 4.

Table 7.1 Summary of the Tests Conducted on the Small Cone at UoN

Test ID	Transition Section Angle, °	Transition Section Orientation	Rewinding Twist, Tpm
1	5.4°	Diverging	0
2	5.4°	Diverging	5
3	5.4°	Converging	0
4	5.4°	Converging	5
5	10.6°	Diverging	0
6	10.6°	Diverging	5
7	10.6°	Converging	0
8	10.6°	Converging	5

Braiders are programmed using the respective part diameters at specific axial distances along the part. These spacing between these locations are determined by the operator. This produces a program with a set of speeds at these points but does not account for a transient speed change as the cross-section change.

Figure 7.1 shows a comparison between the average deviation from a predicted braid angle of 45° for mandrels of different part gradients braided in different orientations as described in Table 7.1 as Test 1,3,5 and 7. Thirty braid angle measurements were recorded from the respective transition regions of 5.4°, 10.6° and compared with the cylindrical mandrel data. All preforms in the comparison were manufactured with T700s 12K carbon fibre rewound with 0 Tpm.

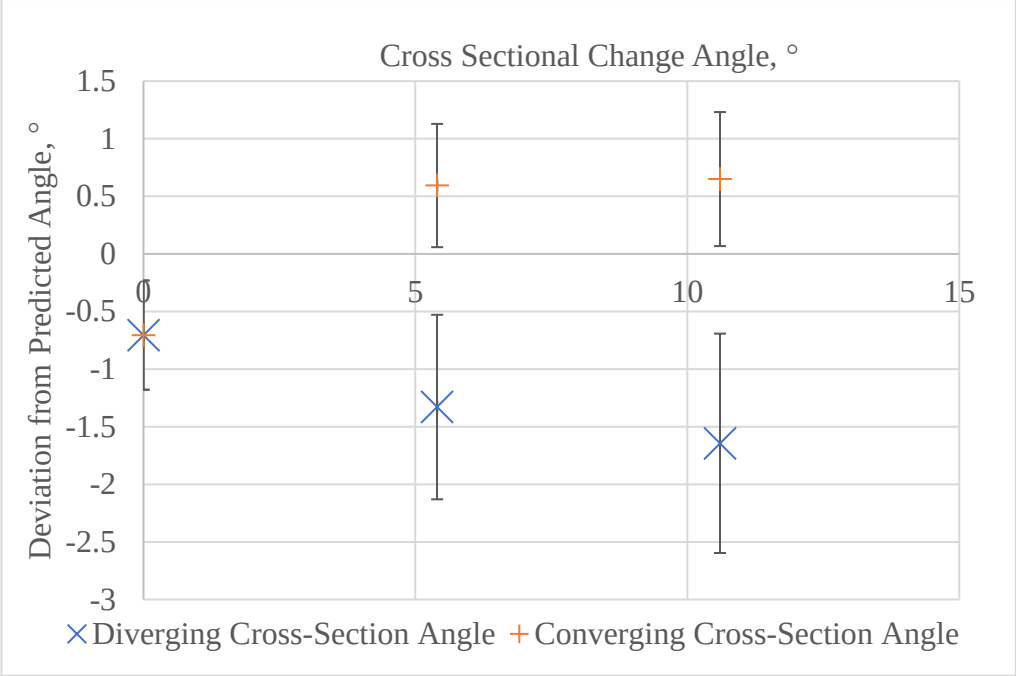


Figure 7.1 Deviation in predicted braid angle for different part gradients in both converging and diverging section orientations for 0 Tpm preforms in comparison to a cylindrical geometry.

An increase in deviation from the predicted braid angle was recorded as the angle of the cross-section change increased. Using a Pearson correlation analysis, a strong negative correlation of -0.984 was determined between the two variables. A visible increase in variability can also be seen as the part gradient increases which supports the work of Du and Popper which indicates steeper section gradients resulting in greater deviation from the braid program. An ANOVA test conducted in Minitab highlights that the difference in angle deviation was statistically significant.

In contrast to the diverging cross-section dataset, the braid angle on the converging cross-section exceeded the predicted braid angle. An ANOVA analysis in Minitab determined a statistically significant difference between deviation from predicted angle in the cylinder and both Test 3 and Test 7 in Table 4.2. However, any difference in Test 3 and Test 7 was not statistically significant. Therefore, it can be concluded that the angle of the cross-section is less influential in braid architecture for preforms of converging cross-section. The level of variability is consistent across the cylinder, Test 3 and Test 7. This contrasts to the corresponding data for the diverging cross-section where a steeper slope resulted in increased variability levels.

Figure 7.3 compares the deviation of the braid angle braid angle of 45° along the transition length for Tests 1,3,5 and 7 as defined in Table 4.2. This is displayed as a proportion of axial length as the transition length varies between the 5.4° and 10.6° transition. The proportion of axial length is defined from the starting point of the cross-sectional change as it moves from the braiding machine, this is 0 and the end of the cross-section change is 1. This is represented in Figure 7.2.

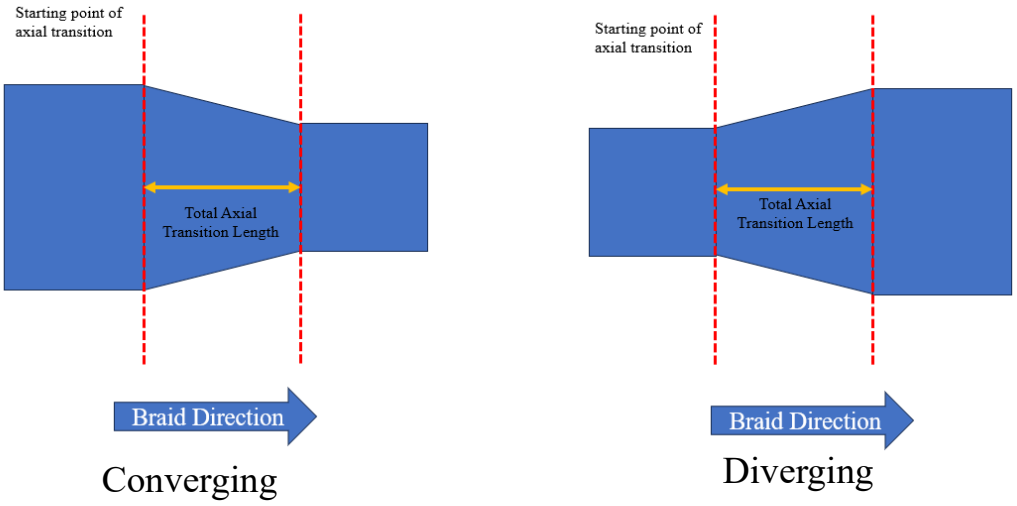


Figure 7.2 Description of Proportion of Axial Length for Converging and Diverging Conical Sections

The braid angle measured at each distance along the transition is an average of the three different repetitions of these trials completed with same braid program. The braid program defines a specific start location in relating the location of the mandrel in the machine.

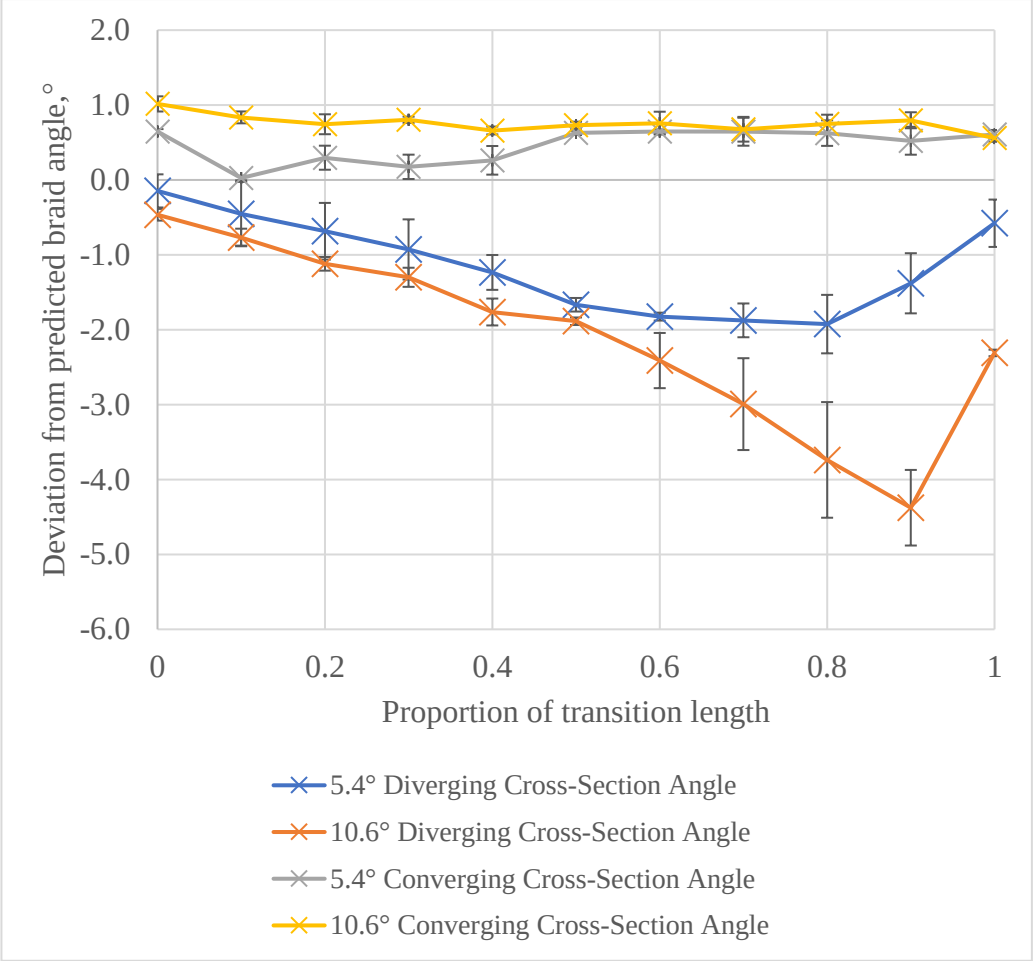


Figure 7.3 Deviation in predicted braid angle along the axial length of preforms of different part gradients manufactured in a diverging and converging orientation for 0 Tpm fibres.

A greater discrepancy between predicted and measured braid angle was seen consistently along the transition length of the steeper cone. The cross-sectional diameter changes over a shorter axial length, this results in a faster change in machine speeds. The difference from predicted angle continued to increase until approximately 0.8-0.9 of the transition length when the preform settled and the respective braid angle began to increase once more. This was still less than the predicted braid angle. It is evident that braiding on more extreme cross-sectional changes pose difficulties when maintaining a stable preform. The increase in measured braid angle deviation from the predicted angle is a result of the increasing cross-sectional diameter effectively reducing the stabilisation length of the braid as the mandrel moves through the machine. The braid angle of the preform with steeper section gradient has a larger deviation from predicted braid angle, -4.2° at peak,

compared to the shallower preform (-1.75°) as the cross-sectional diameter is changing more rapidly.

For converging preforms the magnitude of deviation from predicted braid angle and variability was much smaller than the diverging preforms. This corresponds to literature by suggesting that a more repeatable preform can be produced on a converging cross-section change. For converging cross-sectional changes, a greater deviation in predicted angle was measured with the more extreme 10.6° cross-sectional change. However, in comparison to the respective tests for the diverging cross-section change this deviation was much smaller at a maximum average of 1.2° across the preform length.

For both the 5.4° and 10.6° converging cross-sectional changes, the braid angle was within ±1° average braid angle. This contrasts with the diverging cross-sectional change preforms where larger angle deviations were seen of ±2° and ±4.5° for the 5.4° and 10.6° taper mandrels respectively. With a preform of converging cross-section, the effective stabilisation length of the braid is increasing as the section diameter decreases. There was no significant difference between the measured average braid angle for preforms manufactured in a converging orientation with part gradients of 5.4° and 10.6°.

7.2.2 Effect of part gradient on tow width in single layer preforms

This section assesses the influence of the geometrical change on tow width. Thirty tow width measurements were recorded from the respective transition regions of conical preforms in both diverging and converging orientations Figure 7.4 compares the measured tow width values with those on the cylindrical mandrel.

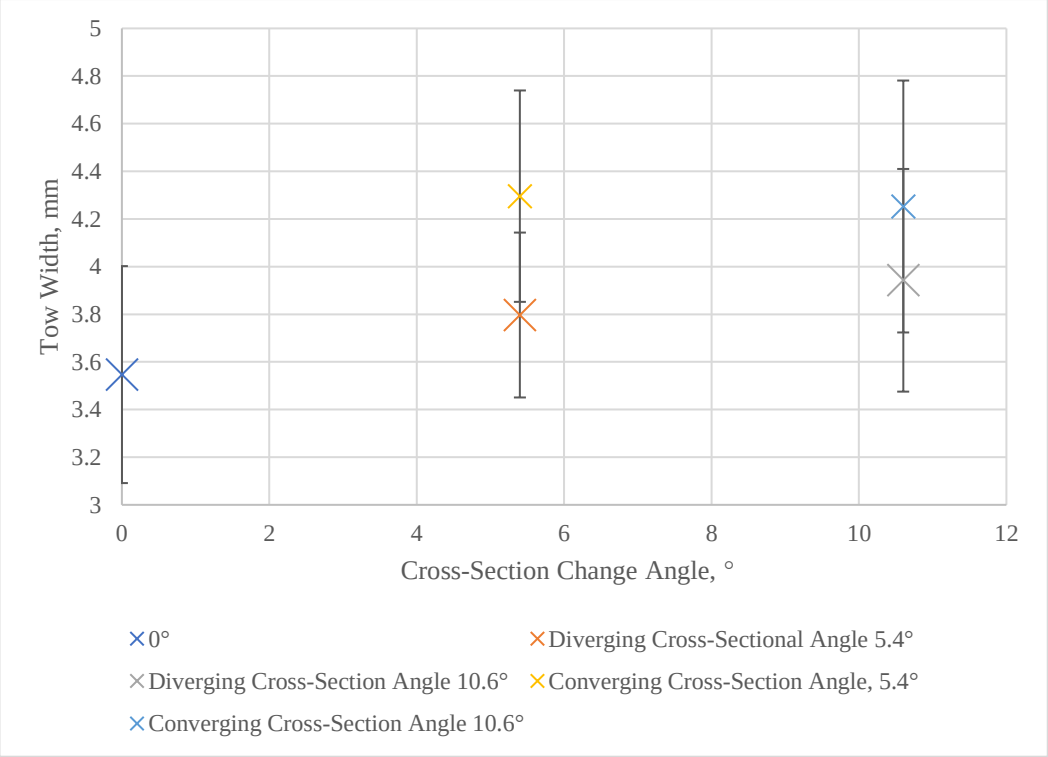


Figure 7.4 Comparison of measured tow width for cylindrical, diverging and converging mandrels

Both diverging and converging cross-sectional changes result in an increase in tow width compared to preforms manufactured on a geometry. There is no statistical difference in average tow width between converging and diverging cross-sections of the same part gradient. As the angle of the cross-section change increases the magnitude of the tow width increases. However, the overlap in standard deviation demonstrates there is no statistical significance attributed to the difference between tow widths because of part gradients. However, Tukey pairwise comparisons at a 95% significance level highlight that the increase in tow width on a cross-section change compared to a cylinder is statistically significant on a mandrel with changing cross section with untwisted carbon fibres.

7.2.3 Effect of Part Gradient on the layer thickness in a single layer preform.

The Apodius Vision System (AVS) 3D by Hexagon was used to measure the layer thickness of the preform. The layer thickness was recorded as an average of thickness around the circumference at multiple positions along the braid. Measurements were taken at 10mm locations along the preform, at each location thickness measurements were taken every 15°. For each circumferential point the thickness value is then

averaged. This is compared with a scan of the surface of the mandrel to calculate the layer thickness. Figure 7.5 presents the thickness of the preform along its length, this is represented as the mean thickness and associated standard deviation around the perimeter of the part at each discrete measurement location. This was completed for a cylindrical mandrel and diverging cross-sectional changes of 5.4° and 10.6°.

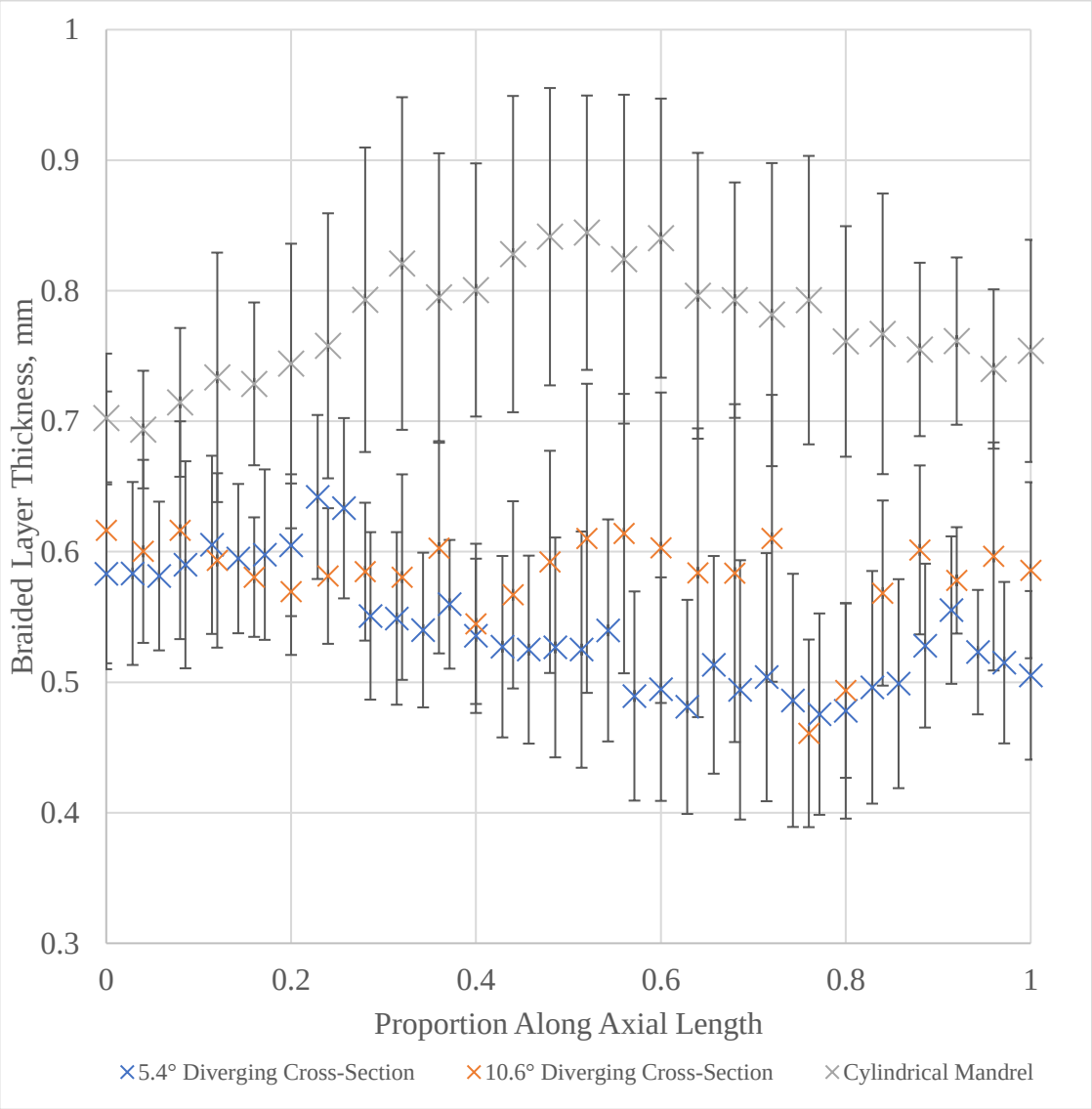


Figure 7.5 Preform thickness along the preform length for diverging preforms of different part gradients manufactured with 0 Tpm Fibres

The cylindrical mandrel was thicker than preforms braided on a diverging cross-section irrespective of the gradient of the part, with an average thickness of approximately 0.75mm. The introduction of a part gradient causes the tow to spread reducing the thickness. There was no statistically significant difference between the

braid thickness of the preforms with part gradients of 5.4° and 10.6°. This can be related to findings in Chapter 6 to the data for tow width which for untwisted fibres was not influenced by the magnitude of the section gradient, it follows that as tow width is proportional to tow thickness the layer thickness is not influenced by part gradient. An approximate preform thickness range of 0.475-0.6mm was recorded for both diverging preforms.

Figure 7.6 compares the preform thickness of the cylindrical preform manufactured with untwisted preforms with the preform thickness of the converging preforms with part gradients of 5.4° and 10.6°.

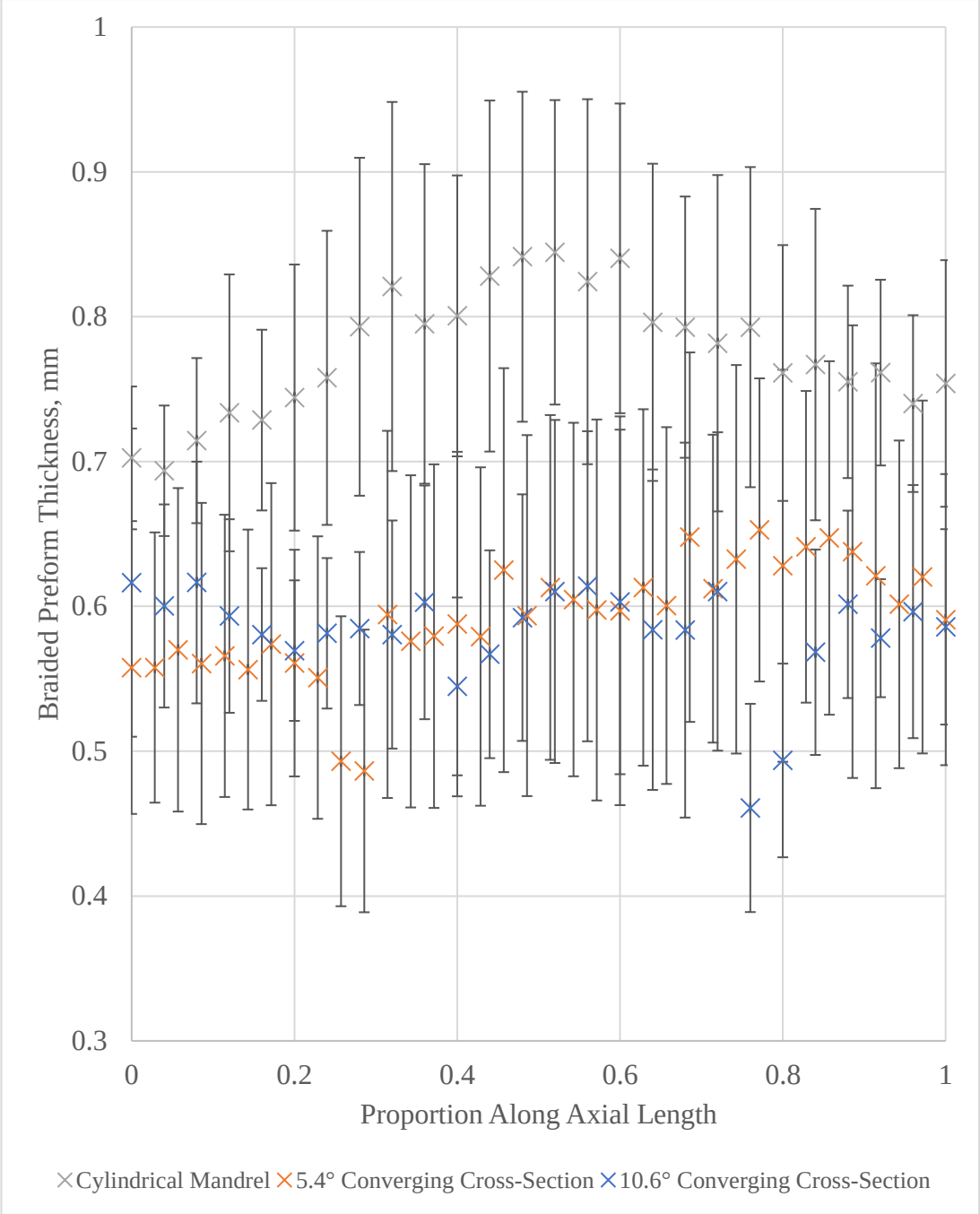


Figure 7.6 Preform thickness along preform length for converging preforms of different part gradients manufactured with 0 Tpm Fibres

The mean thickness of the braid on the cylindrical mandrel is greater than that of the converging cross-section. This corresponds to the observation that the tow spreads as the cross-section changes which corresponds to a reduction in preform thickness. There is less tow spread on the cylindrical preform therefore the preform is thicker. There is no statistically significant difference between the measured thicknesses of the 5.4° and 10.6° cross-section changes. This corresponds to Figure 7.4 which

demonstrated that the tow width did not change because of section gradient. Therefore, changes in tow cross-section are as a result of a section change, irrespective of the part gradient. A thickness in the range 0.475-0.65mm was measured. There is overlap between all three test cases despite significantly higher mean for the cylindrical preform value.

7.3 Influence of Twist on Braid Architecture Variability for Complex Preforms of different part gradients.

Section 5.2.3 assesses the impact of this additional twist on tow geometry with the introduction of cross-sectional change of different gradients. These tests are outlined in Table 7.1 with reference to mandrels in Figure 4.7 and Figure 4.8 for cross-sectional changes of 5.4° and 10.6°. Section 5.2.3 looks to compare Tests 1,3,5,7 for T700s 12K material rewound with 0 Tpm with their respective counterparts Test 2,4,6,8 rewound with 5 Tpm to determine the influence on braid architecture variability. The following section analyses Tests 2,4,6,8 to determine the influence of twist on the resulting braid architecture of a preform for complex geometries with different part gradients.

7.3.1 Influence of Rewinding Twist on the Braid Angle of Components With Different Part Gradients

The test procedure for the 0 Tpm preforms was replicated with fibre rewound with an additional twist of 5 Tpm. Figure 7.7 shows deviation from a predicted braid angle of 45° for conical sections of different part gradients braided in both diverging and converging orientations, outlined in Table 4.2.

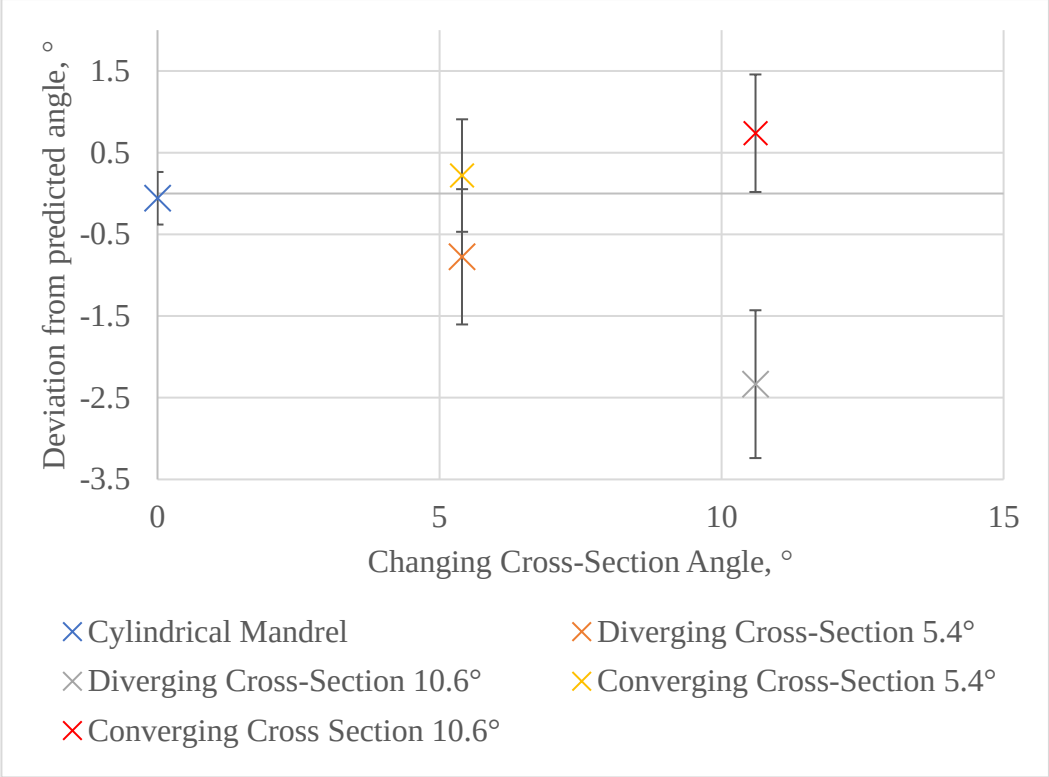


Figure 7.7 Deviation from predicted braid angle due to different part gradients for components in both converging and diverging orientations with twisted fibres

A greater increase in deviation in predicted braid angle was found as the magnitude of the diverging cross-section angle increases. Statistical analysis using an ANOVA in Minitab determined that this difference was statistically significant. A similar response was seen braiding on a converging diameter with the 5 Tpm fibres in comparison to the 0 Tpm fibres. The braid angle remained within ±1° of the predicted braid angle irrespective of the section gradient. This is due to the converging cross-section increasing the effective stabilisation length of the preform along the axial length of the component as the part diameter decreases. This deviation is similar in magnitude to the braid angle deviation shown in Figure 7.1 for untwisted fibres. A statistical analysis using an ANOVA in Minitab determined that there was no significant difference in the mean measured braid angle as a result of part gradient for converging cross-section changes. The inclusion of a rewinding twist did not have an influence on measured braid angle or stability.

Figure 7.8 demonstrates the measured braid angle along the length of each preform for mandrels in both diverging and converging orientations of different part gradients. All preforms were braided with twisted fibres. Three repetitions of each test were

conducted. The length is represented as a proportion along the length of the cross-sectional change due to the differences in section length. The deviation from the predicted braid angle of 45° was much more significant in the diverging preforms in comparison to the converging preforms.

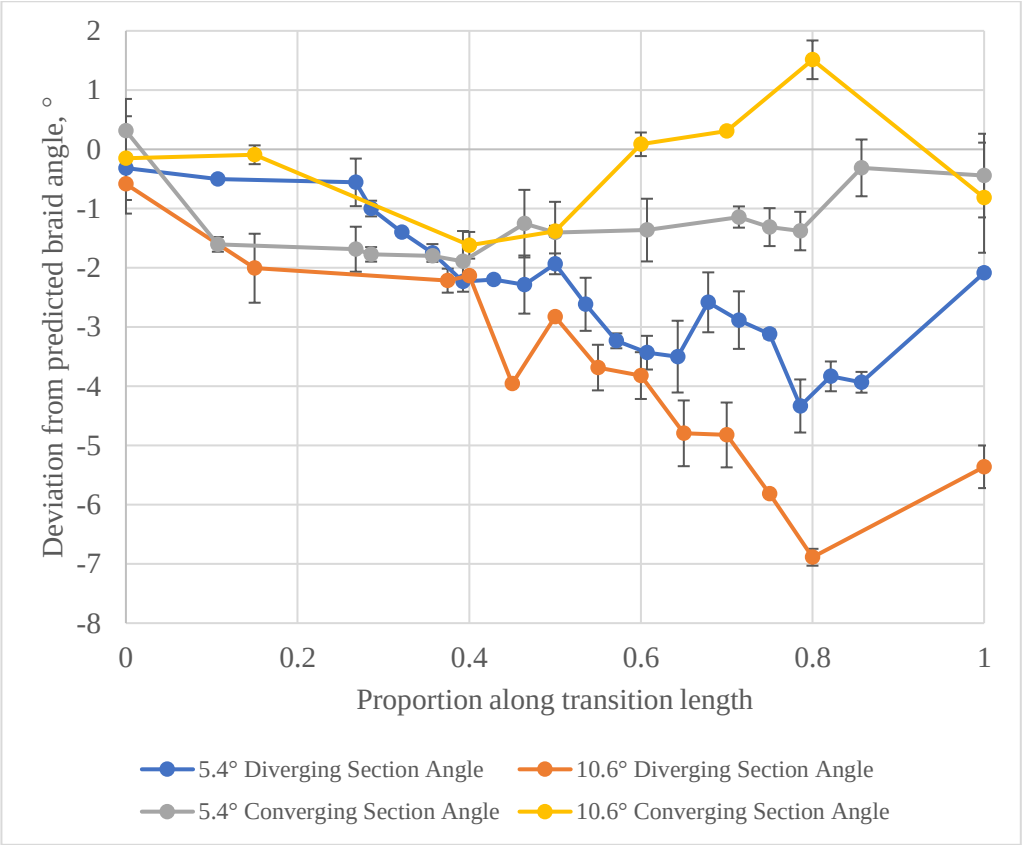


Figure 7.8 Deviation from predicted braid angle along the preform length for both diverging and converging mandrel orientations, of different part gradients braided with twisted fibres.

For diverging preforms, part gradient was found to influence the deviation from predicted braid angle. The 10.6° gradient conical section saw a maximum deviation of 7° in comparison to a 4° seen in the 5.4° gradient preform. This strengthens the idea that with a diverging cross-section the effective stabilisation length is shortened as the length of the fibres in the braid cone is reduced as the part diameter continues to increase. As a result, the angle does not stabilise as intended on mandrel as the braid is still in the transition phase.

For preforms braided in converging orientation, there is braid angle variability in both preforms, this differs from the measured data for the untwisted fibres and the

deviation on balance is at its maximum at ±1.5° for both 5.4° and 10.6°. This is significantly lower than the braid angle deviation for diverging preforms. This supports the proposal that converging cross-section changes provide an increase in effective stabilisation length reducing the braid angle deviation.

Overall, the data for Test 2,4,6 and 8 confirm that braiding on a cross-sectional change with converging diameter orientation reduces deviation from predicted braid angle as the effective stabilisation length is increased. The inclusion of an additional twist to fibres did not have a significant influence on the braid angle.

7.3.2 Influence of rewinding twist on the tow width of components with different part gradients

Figure 7.9 shows the average measured tow width for converging and diverging cross-sections of 5.4° and 10.6° compared to a cylinder. The converging cross-sections are represented as a negative angle.

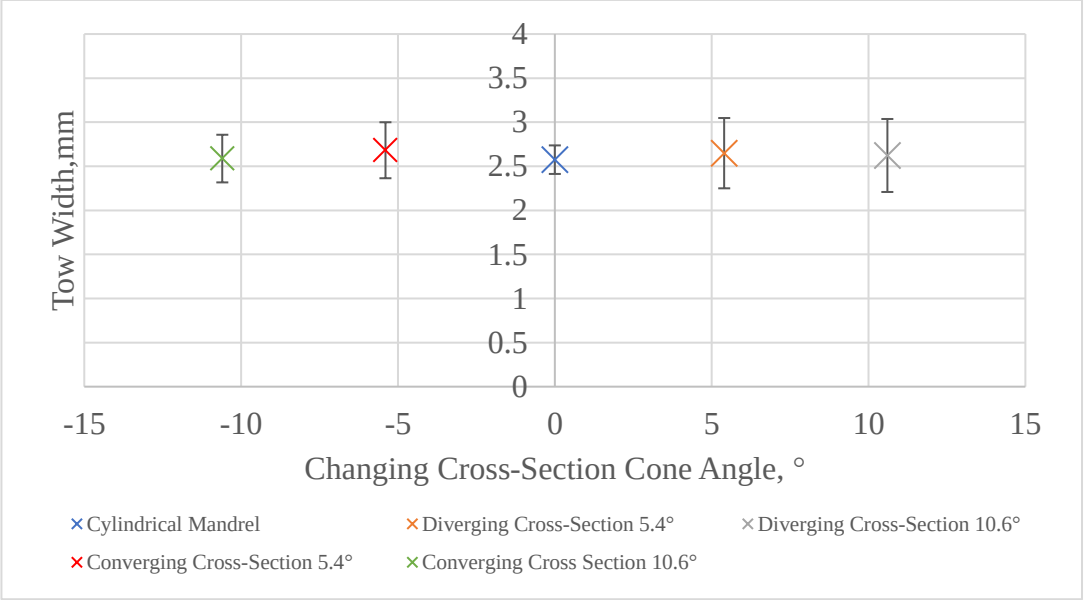


Figure 7.9 Measured tow width for converging and diverging preforms of different part gradientst when braided with twisted fibres

A tow width of approximately 2.6mm was measured for each mandrel, this was irrespective of section gradient. Although, the variability did increase with the inclusion of a part gradient but no difference in variability was seen due to part gradient magnitude. This is to be expected with a geometrical change as the tow resists slip creating tow spread. However, the variability was much less than the

corresponding tests with 0 Tpm. A statistical ANOVA in Minitab demonstrates that there is no statistically significant difference between the measured tow widths on the cylinder, 5.4° and 10.6°. This was confirmed through Tukey pairwise comparisons and indicates that the addition of twist to fibres during rewinding reduces tow spread and tow width variability on conical geometries. This results in downstream effects of reducing localised deviation in cover factor.

An ANOVA determines using Tukey pairwise comparisons at 95% significance that there is no significant difference between the measured tow width for the cylinder, 5.4° and 10.6°. Adding twist to fibres produces a more compact and constrained tow bundle which limits the tow spread of the fibres. There was no significant difference between the preforms manufactured with different part gradients. This confirms that the tow width of preforms manufactured with twisted fibres is not impacted by part gradient.

Overall, the influence of adding twist to fibres during the rewinding step caused a reduction in tow width, this is in line with the data presented in Chapter 6. However, in contrast to the untwisted fibres, where an increase in tow spread was found when braiding on a part gradient, no deviation in tow width as a result of part gradient was found. This suggests that braiding with twisted fibres can provide a more predictable tow width which enables greater cover factor control. This is a key design parameter.

7.3.3 Influence of rewinding twist on the layer thickness of components with different part gradients

The AVS is used to measure the thickness of the preforms manufactured with twisted fibres. Figure 7.10 compares the braided layer thickness measured using the AVS for a cylindrical preform and conical mandrels of 5.4° and 10.6° braided in a diverging orientation. There is an indication that braiding on a mandrel of constant cross-section produces thicker braid, however there is significant overlap between the mandrel of constant cross-section and the conical mandrels. The conical preform thickness ranged from 0.5-0.7mm and the cylindrical mandrel thickness ranged from 0.7-0.82mm. Significant overlap was seen between the standard deviation bars of all three mandrels.

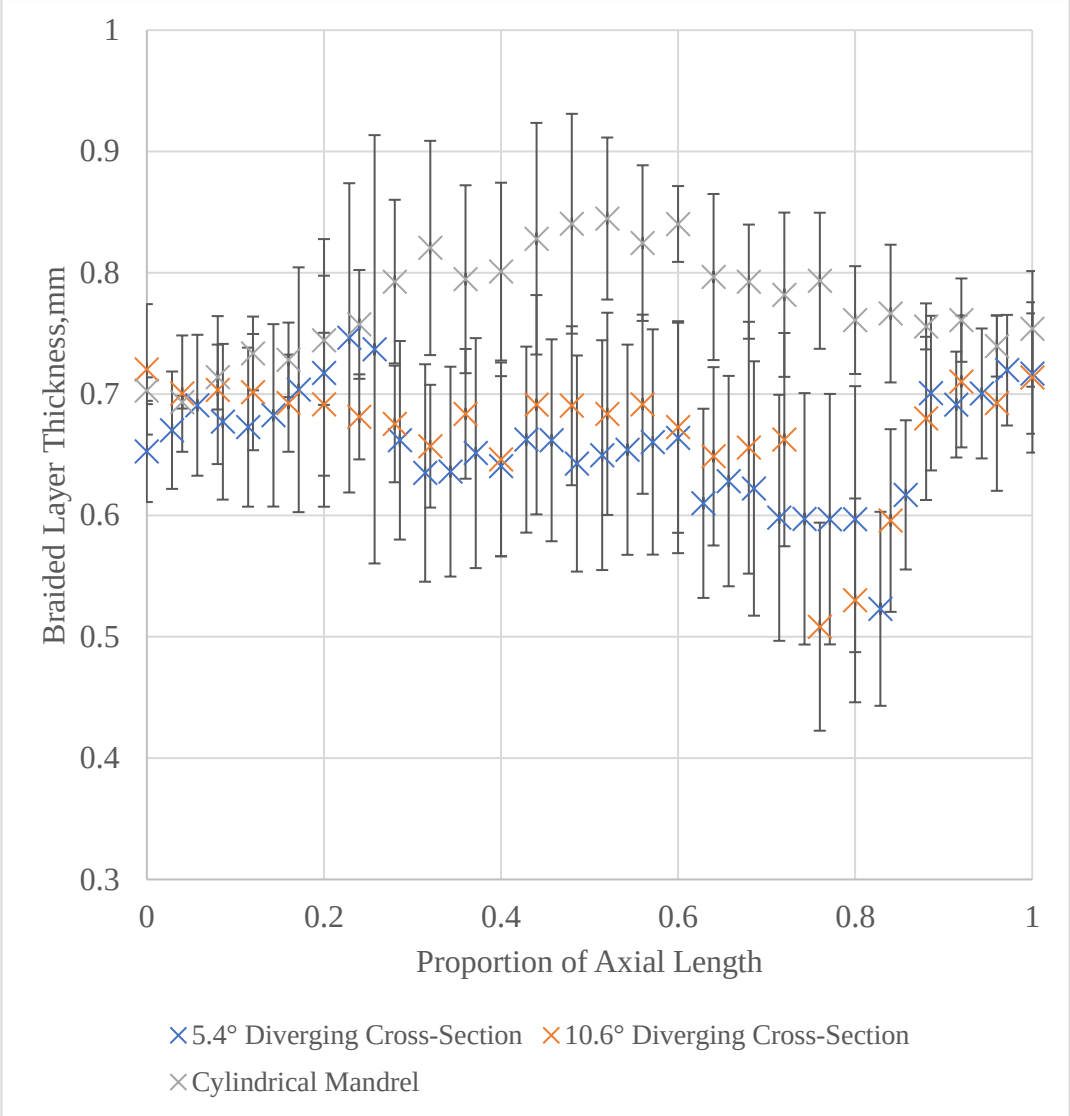


Figure 7.10 Preform thickness along the length for diverging cross-sections of different part gradients with twisted fibres.

Figure 7.11 compares the measured braided layer thickness using the AVS for a cylindrical preform and conical preforms braided in a converging cross-section orientation braided with fibres with 5 Tpm.

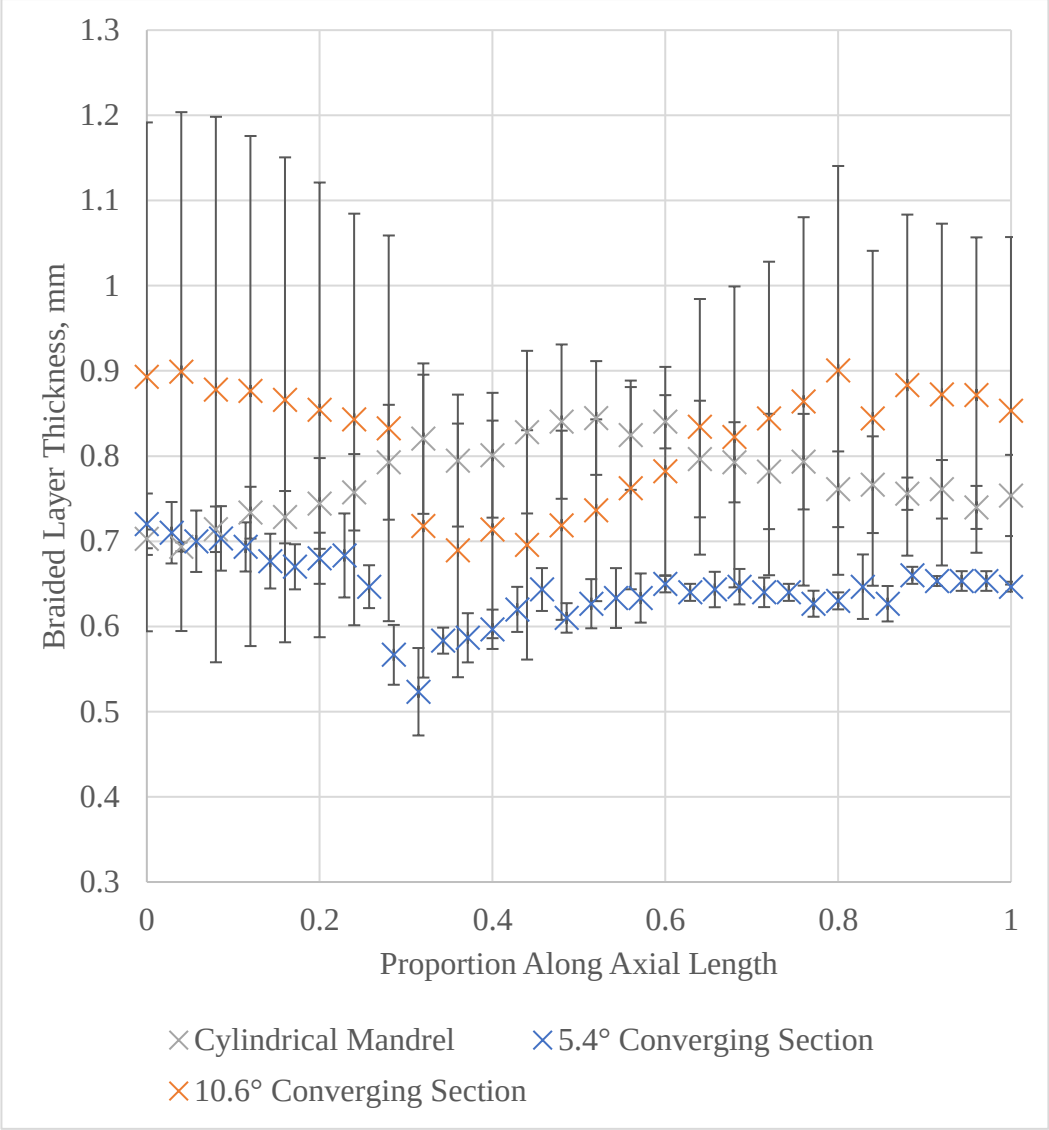


Figure 7.11 Preform thickness along the length for converging cross-sections of different part gradients with twisted fibres

There are indications that there is a slight reduction in layer thickness when braiding on a cross-section change however, this is minimised by braiding with twisted fibres. Similarly, to data for diverging cross-sections, there is overlap between all three datasets. The braided layer thickness of a cylindrical mandrel ranged from 0.68-0.82mm and the conical mandrels, 0.63-0.8mm. This indicates that the difference in layer thickness is not statistically significant. This is once again in contrast to the data for untwisted fibres demonstrating that adding twist to fibres during rewinding aids in reducing tow spread. An approximate thickness range of 0.6-0.8mm is recorded which is consistent with the preforms on diverging conical sections, suggesting that braid direction does not influence braid thickness.

Overall, braided layer thickness was found to increase due to the inclusion of an additional twist added to fibres during rewinding. However, in contrast to the untwisted fibres, the layer thickness did not change with the inclusion of a cross-sectional change in the mandrel geometry and the twist provided a more stable tow geometry.

7.4 Summary of the Effect of Part Gradient on Braid Architecture

This work confirms the work of Du and Popper [39], braiding a mandrel loaded so that the cross-section change is in a converging orientation provides a most consistent braid angle along the length of the cross-section change with a deviation of approximately 1° from the predicted braid angle in contrast to 5° for a mandrel in a diverging orientation of the same section gradient. This is due to the effective stabilisation length increasing when braiding on a converging cross-section. An increase in mandrel gradient results in a larger braid angle deviation for preforms braided in a diverging cross-section orientation as the more rapid cross-section changes leads to the braid stabilisation length being reduced more quickly leading to greater instability. This results in a larger deviation from predicted braid angle. An increase in mandrel gradient did not influence the deviation from predicted braid angle for mandrels orientated with the cross-section change in a converging alignment. The effective length of the fibre in the braid cone before it interacts with the mandrel increases as the part diameter increases. Thus, acting to increase the effective stabilisation length. These conclusions were reflected for preforms braided with twisted fibres.

For untwisted fibres a statistically significant increase in tow width was found for preforms manufactured on mandrels in both converging and diverging orientations. It was observed that braiding on a mandrel with non-constant cross section results more tow spread in untwisted fibres as they interact with the mandrel surface to resist slip. However, there was no significant difference in the tow width values because of part gradient. The increase in tow width was due to the inclusion of a change in cross-section as opposed to the magnitude of Rewinding Twist. For twisted fibres there was no statistically significant difference in measured tow width irrespective of part gradient and mandrel orientation. This suggests that the inclusion of twist can provide resistance to tow spread. As a result, cover factor is more predictable. There was no difference in tow width in comparison to the cylindrical mandrel geometry.

In summary, braiding on a mandrel with a cross-section change can cause instability in the braid architecture. This can be mitigated if the mandrel is with the cross-section change in a converging orientation if possible. The addition of braiding with twisted fibres can also reduce tow spread enabling cover factor to be predicted with a greater reliability. Braiding on any cross-section change with untwisted fibres results in tow spread which can lead to localised cover factor deviations.

7.5 Influence of Twist on Braid Architecture Variability for Complex Preforms for Different Part Acales

7.5.1 Effect of Converging and Diverging Frusto-Conical Sections on Braid Architecture for a Large Scale Preform

A summary of the tests completed on the large conical mandrel are summarised in Table 7.2.

Table 7.2 Summary of tests on large conical mandrel

Test ID	Mandrel Size	Transition Section Orientation	Rewinding Twist, Tpm
2.1	Large	Converging	0
2.2	Large	Converging	7
2.3	Large	Diverging	0
2.4	Large	Diverging	7

The deviation from predicted braid angle for the tests summarised in Table 7.2 braided with 0 Tpm and 7 Tpm fibres are shown in Figure 7.12, this is compared with the deviation along a mandrel of cylindrical cross-section. As expected, no difference between the straight section and the converging cross-section was seen this was irrespective of the level of rewinding twist to fibres, deviation from predicted angle remained within ±1° of the predicted angle. For a diverging cross-section, the braid

angle reached maximum deviation of -4°, this was irrespective of the rewinding twist added to fibres.

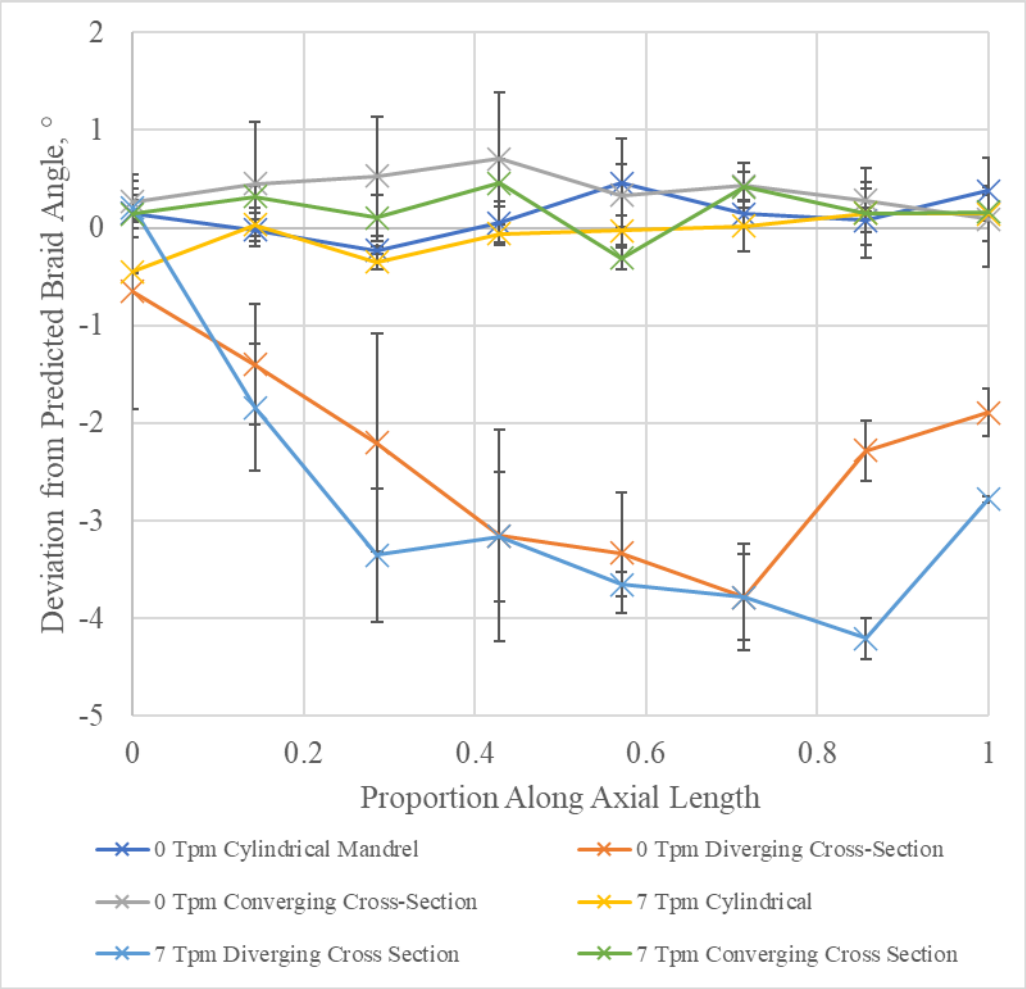


Figure 7.12 Recorded braid angle deviation along the axial length of preform for cylindrical, diverging and converging

An increase in variability was seen in the braid angle measurements for both converging and diverging cross-section changes. The constant change in section diameter results in a change in length of tow in the braid leading to a constantly stabilisation length. This results in an increase in angle variability compared to a straight section.

Figure 7.13 demonstrates the average measured tow width in straight, converging and diverging cross-sections for tests summarised in Table 7.2 manufactured on large mandrels at the NCC. Thirty tow width measurements were taken using ImageJ in each of the straight, converging and diverging preforms. The untwisted fibres increased in tow width section with geometrical change from approximately 3.4mm

to 3.6mm. According to an ANOVA conducted in Minitab, at a significance level of 0.95 this difference in tow width is statistically significant. The tow width remained consistent across all cross-section types at approximately 2.1mm. The twist appeared to aid in reducing tow spread on the changing cross-sections. This would reduce localised cover factor deviations. An ANOVA determined there was no statistically significant difference between the average tow width values.

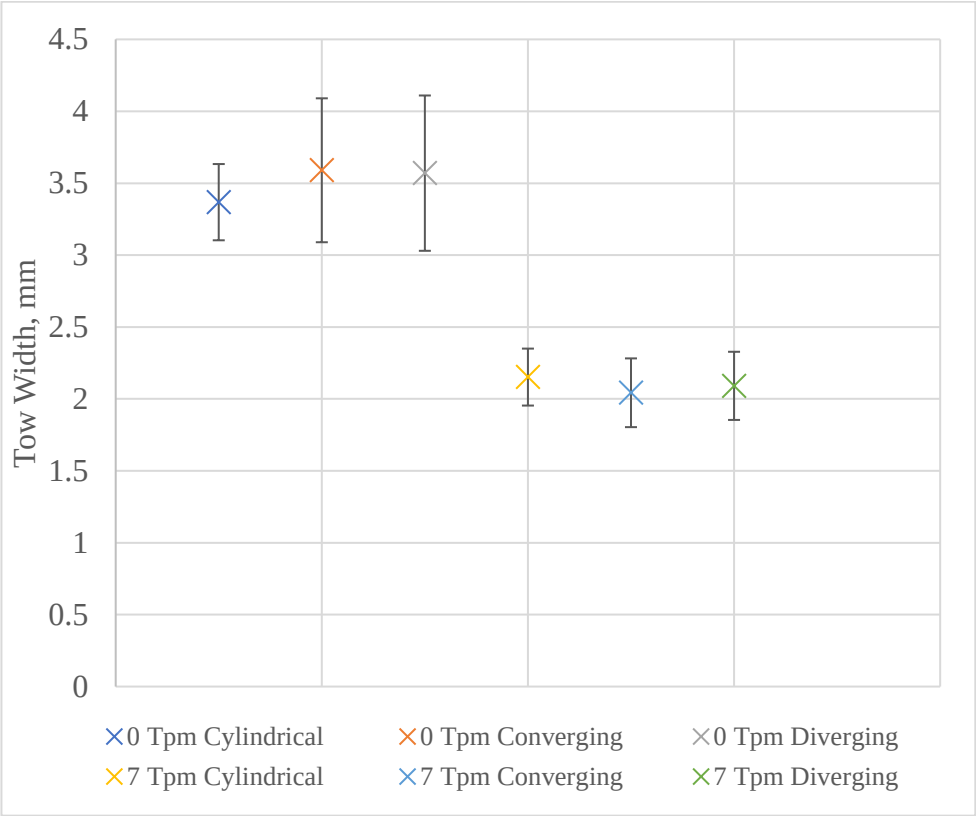


Figure 7.13 Measured tow width for cylindrical, converging and diverging preforms with different levels of twist

In summary, for Test 2.1 and Test 2.3 (Table 7.2) using untwisted fibres at a larger scale the differences outlined by Du and Popper [39] are validated. Braiding with a mandrel orientated so the cross-section is converging results in less deviation from predicted braid angle. Tow width increased significantly when braiding with untwisted fibres on a cross-section change. The calculated standard deviation was larger for the fibres braided on a conical cross-section suggesting that a section change introduces some level of instability. However, for twisted fibres, no difference in either variability or magnitude was seen between the converging and diverging cross-sections. Suggesting that adding twist to fibres can limit tow spread on

mandrels with a cross-section change resulting in fewer localised cover factor deviations.

7.5.2 Comparison of the Braid Architecture for Scaled Preforms Using Small and Large Machinery

Figure 7.14 summarises Test 5 and 7 in Table 7.1 and Test 2.1 and Test 2.3 in Table 7.2 which compares the data on a conical section with a 10.6° part gradient braided with T700s fibred rewound with 0 Tpm. The mandrel was loaded with the cross-section in both converging and diverging orientations. Braiding on a diverging cross-section was seen to result in a larger deviation from predicted angle irrespective of machine scale. The maximum angle deviation for a preform manufactured in a diverging cross-section reaches approximately -4.5° for both machine sizes. Both the small and large cone converging sections showed less deviation from predicted braid angle fluctuating within ±1°.

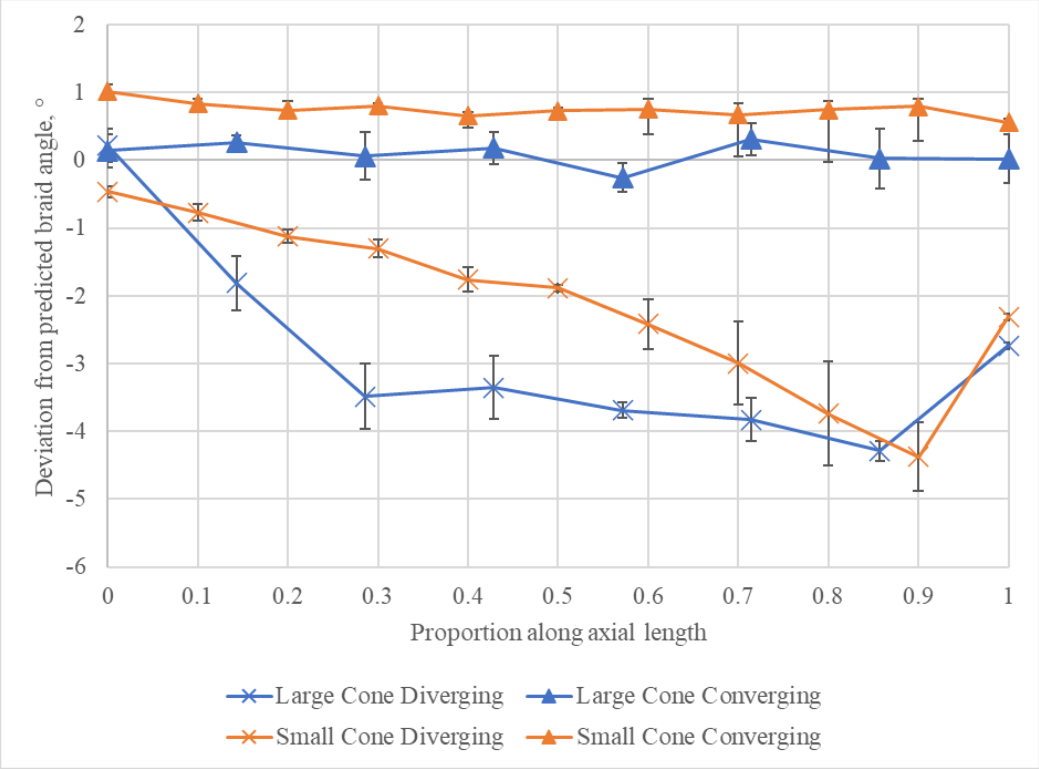


Figure 7.14 Comparison of braid angle deviation for conical sections on 48-carrier and 192-carrier braiders

For the converging cross-section, the large cone remained closer to the predicted braid angle. A difference was seen as there was no overlap in standard deviation bars between the large and small cones. This suggests that braiding sensitivity is greater

when braiding small geometries with a cross-sectional change. This contrasted for diverging cross-sections when larger deviation was seen for the large cone. This results from the effective increase in stabilisation length as the cross-section reduces. The final magnitude of deviation is not significantly different which suggests that instability is introduced into the braid angle through braiding on a diverging cross-section change. Overlap can be observed between the trendlines for the diverging cross-section deviation.

Figure 7.15 demonstrates the measured tow widths on a conical section of 10.6° in both diverging and converging orientations for the small and large mandrels. This is compared with the measured tow width on a cylindrical section of the frusto-conical mandrel.

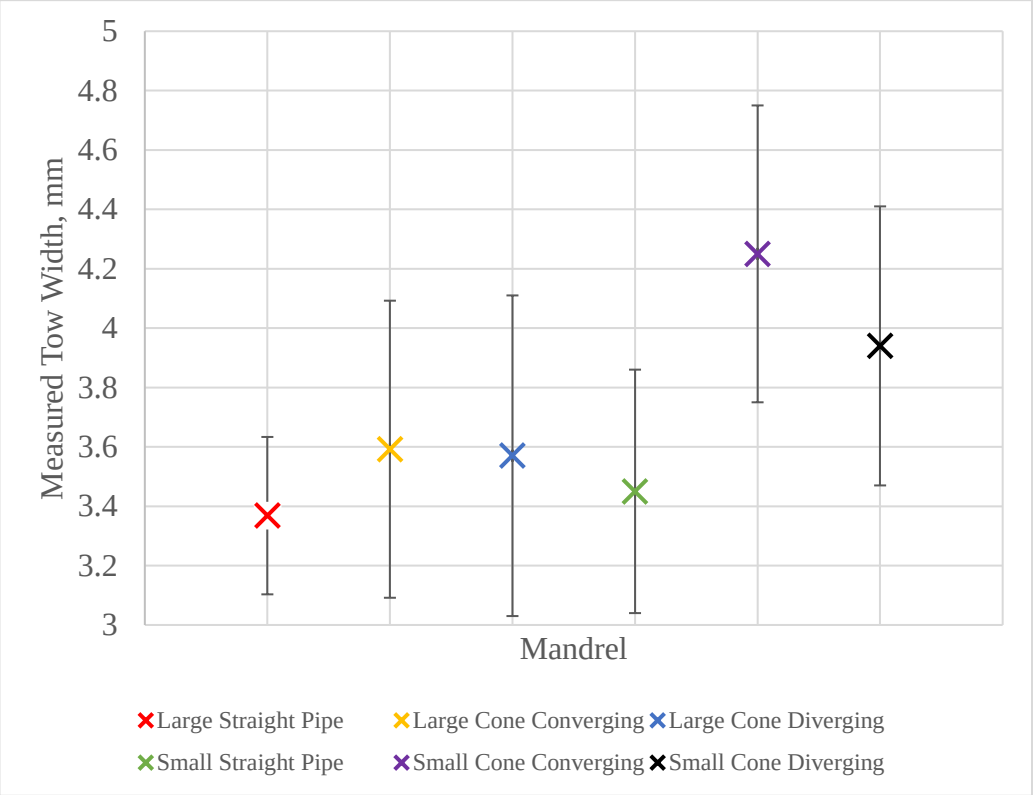


Figure 7.15 Comparison of tow width measurements for 48-carrier and 192-carrier braiders, with both conical and straight sections

The difference between the tow width in the constant cross-section regions in the small and large cylindrical mandrels was not statistically significant at 3.4mm and 3.45mm respectively shown by the overlap of standard deviation bars. Both small and large conical sections saw a statistically significant increase in tow width

irrespective of cross section orientation. As previously discussed, a cross-sectional change results in tow spread when braiding with untwisted fibres. The increase in tow width was more notable with the small cone this is due to a reduced number of picks along the axial length and therefore proportionally a more rapid change in cross-section causing greater instability in the braided preform. This difference between tow width for small and large cones was statistically significant.

In summary, the behaviour of both diverging and converging conical cross-sections was reflected in both small and large conical mandrels. More significant deviation from predicted braid angle was noted with a mandrel orientated in a diverging orientation due to an effective reduction in stabilisation length whereas mandrels orientated in converging orientation provided a more consistent braid angle. However, maximum angle deviation and an increase in tow spread was noted on the small mandrels.

7.5.3 Process Simulation of Frusto-Conical Structure

Kinematic process simulation software Composites Braiding Modeler (CBX) is used to simulate the braiding of the large frusto-conical section. The materials catalogue was updated to reflect the T700s carbon fibre used in the manufacturing with 0 Tpm. Yarn approximations defined the tow width as 3.661mm and 2.355mm. A guide ring diameter of 400mm was inputted which directly mirrored the guide ring used in the manufacturing process and the carrier number was specified as 192. The settings were defined so that a constant braid angle of 45° would be produced along the length of the preform based on the calculation modules in CBX.

Figure 7.16 and Figure 7.17 depict the CBX output for clockwise braid angle from the CBX user platform. The colour banding highlights that for braiding with the cross-section in a diverging orientation the braid angle progressively increases, deviating further from the predicted angle along the axial length. This increase in deviation corresponds with the manufactured preforms where the deviation increased along the axial length. However, CBX overestimated the deviation with a maximum deviation of +11.6° in comparison to the -4.5° in the manufactured preform. There is a contrast in the magnitude of deviation from predicted angle between manufactured and simulated preforms. In the manufactured preform the negative deviation is due to a delay between the machine speed changes and this reaching braiding point.

Machine speeds are calculated using the measured part diameter at specific point locations. Using the required braid angle, a traverse speed is then calculated. This method does not allow for transient speeds between points to be determined. As a result, the speed at the braiding point is too fast leading to a reduction in braid angle. The effect of this can be mitigated through increasing the number of points in the braiding program so that the frequency of speed changes increases throughout the mandrel or introducing an angle correction factor based off trial preforms.

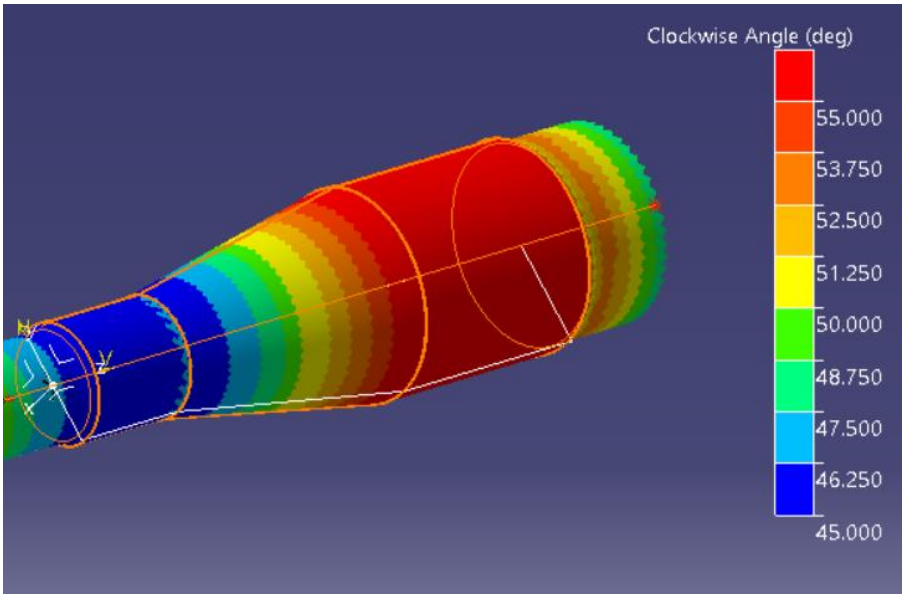


Figure 7.16 CBX Braid Angle Simulation in Diverging Orientation

Figure 7.17 demonstrates that similarly to the manufactured preform, in CBX the braid angle deviates from the predicted angle when braiding on a converging cross-section. However, significantly increased deviation is seen peaking at +8° in comparison to the manufacturing which saw a deviation of +1°. This level of deviation is consistent with the CBX diverging preform. Whereas, in the manufactured converging preform the deviation is considerably less than the deviation from the diverging preform.

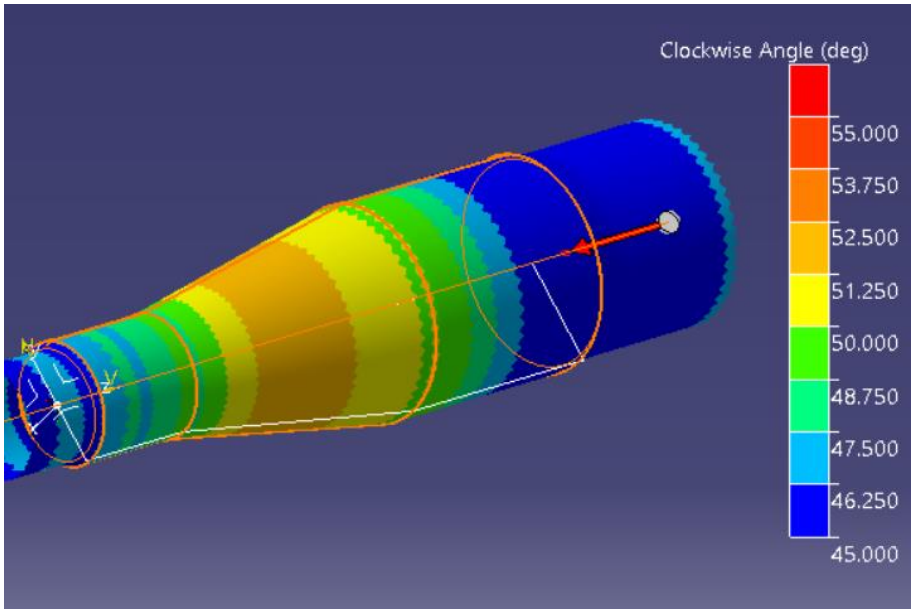


Figure 7.17 CBX Braid Angle Simulation in Converging Orientation

A comparison of the braid angle deviation along the axial length for both CBX and manufactured preforms is shown in Figure 7.18. It is evident that the process simulation software overestimated the braid angle of the preform irrespective of the orientation of the cross-section change.

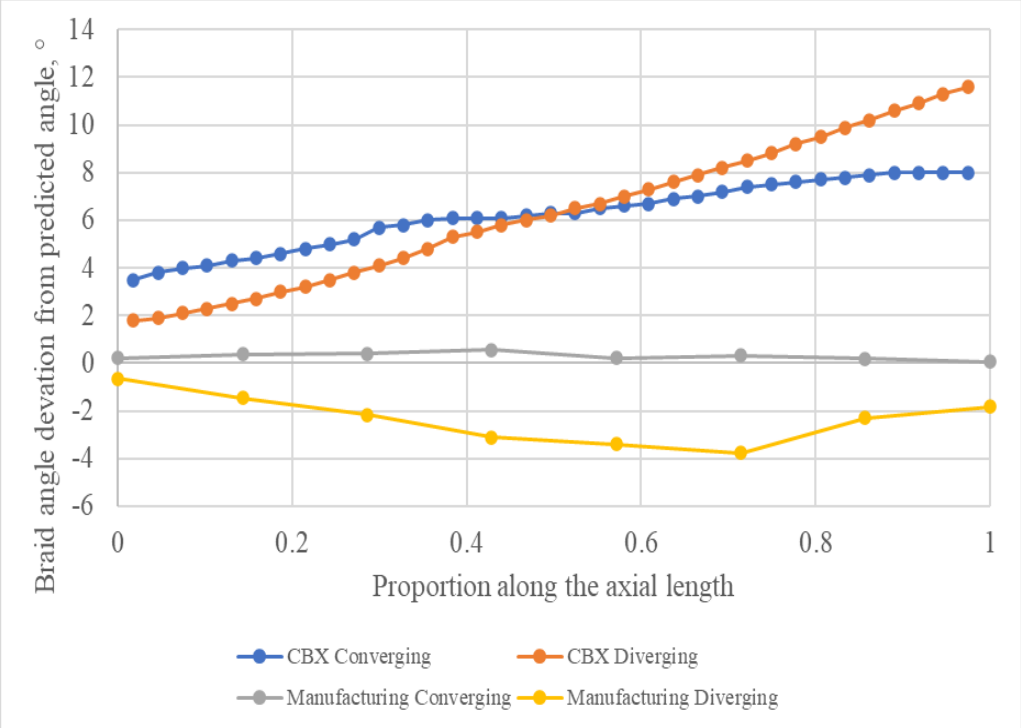


Figure 7.18 Comparison of the braid angle deviation for simulation and manufacturing

In summary, the introduction of a cross-section change resulted in deviation from the predicted braid angle. This was overestimated in comparison to the manufactured preform by a maximum of 8° for the converging preforms and 14° for the diverging preforms. This difference between manufacturing and simulation could be minimised through incorporating a correction factor to account for the changing stabilisation length. Using the knowledge developed that suggests a part braided in a converging orientation result in more minimal deviation from predicted angle, could be included in the process simulation to prevent such a discrepancy. For preforms manufactured in a diverging orientation incorporating a correction that is related to part gradient would minimise the discrepancy between designed and manufactured preforms.

7.5.4 Summary for large conical preforms

Section 7.5 discussed the braiding and simulation of a large frusto-conical section with a part gradient of 10.6°. Part orientation, the influence of rewinding twist, consistency with process simulation and comparison to small scale preforms were all analysed in this section and the conclusions are summarised. Part orientation has a significant impact on the deviation from predicted braid angle. Braiding with a mandrel with a cross-section change in a converging orientation produces a more stable braid angle with less deviation from the predicted angle, ±1° irrespective of mandrel size. With a mandrel in a diverging orientation, the large-scale mandrel saw the same magnitude of deviation from predicted angle (-4°) as a small-scale mandrel.

Process simulation overestimates the deviation along the axial length of the preform for both diverging and converging geometrical cross-section changes. For diverging cross-section changes a deviation of 11.6° in braid angle was observed whereas for manufactured preforms this was -4.5°. The negative braid deviation in manufactured preforms is due to a delay in changes in machine speed reaching the braiding point. The speed at the braiding point is consequently too fast leading to a reduction in braid angle. Preforms simulated in a converging cross-section orientation saw an increase in maximum deviation to 8° which was considerably less than preforms orientated in a diverging cross-section, approximately 12°.

7.6 Increasingly Complex Preforms- the 'Oscar' geometry

7.6.1 Influence of geometrical complexity of the 'Oscar' on braid angle

The 'Oscar' mandrel was programmed such that except for Section 6 the braid angle was 45°. Table 7.3 details the angles in the respective sections of the preforms.

Table 7.3 Measured Braid Angle on the Oscar Mandrel

Section Number	Section Gradient	Average Measured Braid Angle, °	Deviation from Predicted Braid Angle, °
1	0	45.7 ± 0.21	0.67
2	-1.67	43.2 ± 0.76	-1.73
3	1.40	34.4 ± 2.47	-10.63
4	0	44.0 ± 0.40	-0.98
5	-0.3	46.2 ± 0.31	1.23
6	0	N/A	N/A
7	0.67	40.5 ± 0.99	-4.46
8	0	45.0 ± 0.56	0

All areas of constant cross-section, sections 1,4 & 8, had less than 1° deviation from predicted braid angle. The introduction of a cross-section change in either direction introduced a higher level of variation, for a converging cross-section this was approximately ± 1.5°. For diverging cross-sections, the variation was statistically significantly higher peaking at -10.63°.

Figure 7.19 summarises the deviation in braid angle from the programmed braid angle in for each section number. The most significant deviation was noted in the diverging cross-sections with the greater the gradient of the diverging cross-section resulting in a larger deviation from predicted angle, Section 3 and 7. This peaked at -10.63° for the steepest diverging cross-section of a gradient of 1.4 (section 3). A similar gradient magnitude of -1.67 for the converging cross-section, section 2, resulted in a much lower deviation of -1.73° from predicted braid angle.

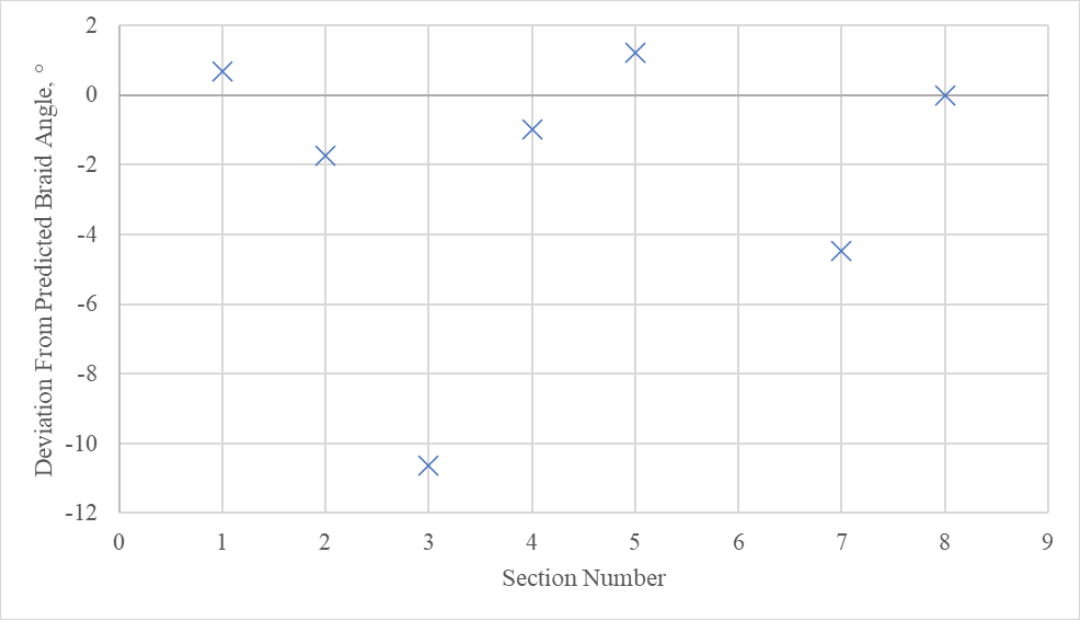


Figure 7.19 Magnitude of Braid Angle Deviation for Different Sections of the Oscar

A statistical analysis on the data set demonstrated a statistically significant difference between magnitude of deviation in braid angle for converging, diverging and constant cross-sections. This is in line with the previous work on the conical section where diverging cross-section saw a magnitude of maximum deviation of approximately 4° for a 10.6° incline and a 2.5° deviation for a 5.4°. This demonstrates that the steeper the gradient the larger the deviation from predicted braid angle. This is because the diameter is changing more rapidly in a part with steeper gradient shortening the stabilisation rate at a faster rate. A steeper section gradient does not impact the magnitude of deviation for converging cross-sections.

7.6.2 Influence of geometrical complexity of the 'Oscar' on tow width

Table 7.4 compares this stabilised tow width with the tow width measured in each section of the 'Oscar' mandrel.

Table 7.4 Measured Tow Width on the Oscar Mandrel

Section Number	Section Gradient	Average Measured Tow Width, mm	Deviation from Stabilised Tow Width 7 Tpm, mm
1	0	2.28 ± 0.12	0.003
2	-1.67	2.38 ± 0.04	0.1
3	1.40	2.21 ± 0.14	-0.07
4	0	2.23 ± 0.08	-0.05
5	-0.3	2.25 ± 0.22	-0.03
6	0	2.30 ± 0.09	0.02
7	0.67	2.32 ± 0.08	0.043
8	0	2.25 ± 0.06	-0.03

All average measured tow widths were with the standard deviation of the measured stabilised tow width of a 7 Tpm preform. This was irrespective of cross-section change type or magnitude. Maximum tow width variability was found to be less than 10% of the measured tow width value.

Figure 7.20 demonstrates the measured tow width in each section of the mandrel and associated variability and compares this to the measured value of a 12K carbon fibre tow rewound with 7 Tpm in a stabilised braid. There is overlap in the error bars for measured tow width in each section with the measured tow width of a stabilised 7 Tpm braid. This demonstrates that there is no significant difference in tow width introduced by a complex geometry when braiding with twisted fibres.

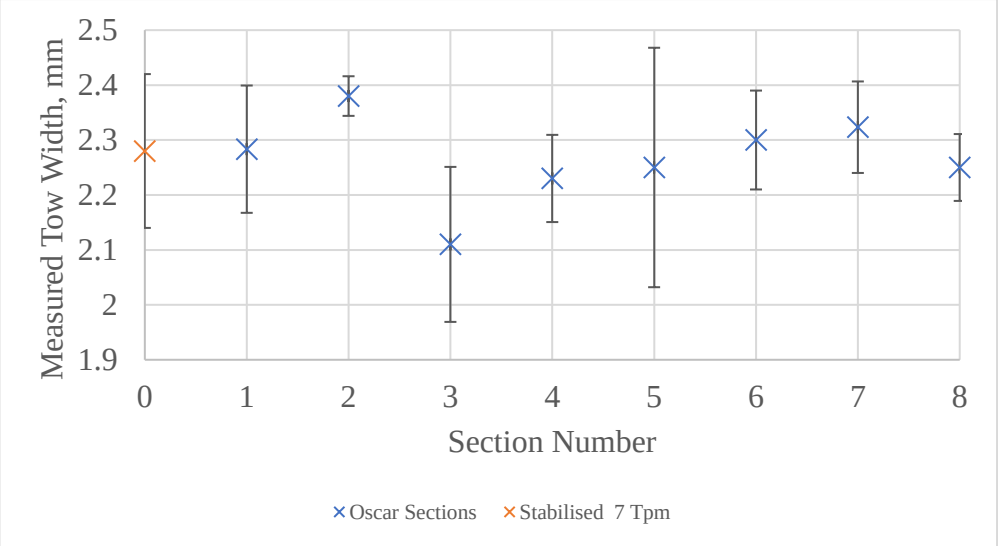


Figure 7.20 Measured tow width comparison to stabilised 7 Tpm braid

No correlation between the magnitude of variability and the magnitude or type of section gradient was seen. However, this does validate previous work on the conical mandrel which suggests that introducing a twist to fibres during the rewinding process can mitigate tow spread when braiding complex geometry.

7.6.3 Summary of the braiding of increasingly complex geometries such as the 'Oscar'

Behaviour of the deviation in braid angle from predicted is as detailed by Du and Popper [39] and shown in previous work in this chapter. Braiding on a diverging cross-section result in a larger deviation from predicted braid angle as the effective stabilisation length is shortening. The sequential nature of the cross-section changes did not appear to influence this behaviour. For diverging cross-sections, a steeper gradient saw larger deviation from predicted braid angle as the effective stabilisation length was reducing more rapidly. When braiding with twisted fibres, no difference in tow width was recorded irrespective of geometry cross-section type or magnitude.

Manual intervention is often required when braiding concave sections for the braiding tows to deposit onto the mandrel surface and prevent bridging. Convex curvatures result in yarn slippage which leads to inconsistent braid angle and preform defects due to tension changes in tow as slippage occurs.

7.7 Conclusions

The aim of determining if the braid architecture and tow geometry assumptions for cylindrical geometries made in Chapter 6 were valid for complex geometry. Literature suggests that braiding complex geometries introduces variability to both braid angle and tow width [39] [43], with greater deviation in braid angle noted for diverging cross-sections. The study into the braiding of complex geometries was broken down to account for numerous factors.

Previous work by Van Ravenhorst [43] has looked at the influence of cross-section change on the stability of braid angle using a 48-carrier braider. This work confirms the conclusions made in this work using the 48-carrier braider, but goes further by identifying the impact of the magnitude of the section change for both braid angle and tow width. The first stage analysed the influence of part gradient on the braid architecture of a preform when braided with untwisted fibres. Two 3D printed mandrels were manufactured with a 5.4° and 10.6° gradient for braiding at the UoN on the 48-carrier axial braider. Findings corresponded with literature with a diverging gradient resulting in a larger deviation from predicted braid angle that the corresponding converging cross-section as shown in Du and Popper [39] . However, this work develops those conclusions by looking at the influence of the magnitude of section gradient across two different machine sizes. The increase in diameter was found to reduce the effective stabilisation length of the preform resulting in instability. It was also identified that for a steeper gradient, where the diameter increases more quickly, a greater deviation in braid angle was found for a diverging orientation as the effective stabilisation length is reducing at a faster rate. No difference due to part gradient was determined for mandrels orientated with a cross-section change in a converging alignment. With regards to tow width, the introduction of a change in cross-section increased the tow width magnitude and the tow was allowed to spread. This was irrespective of the direction of the section change. An increase of approximately 0.2mm was seen in the tow width for both diverging and converging preforms. The magnitude of the gradient also did not have a statistically significant effect with the two gradients used in this study. Neither direction or magnitude of cross-section change influenced the braid thickness, however the level of variability of braid thickness was notable in all preforms.

Chapter 6 suggests the influence of twist on the braid architecture indicating its potential for producing a preform with a more uniform braid architecture. The next stage was to use the same 3D printed mandrels but braid them with 12K carbon fibre rewound with 7 Tpm. There is no existing work that explicitly states the inclusion of a rewinding twist and determines it's influence on the braid architecture. In terms of braid angle, the addition of a twist to fibres during the rewinding stage of the process had no impact on variability. Preforms braided in a diverging orientation were still found to have a larger variability than their converging equivalents with both levels of variation equivalent to the corresponding values for untwisted fibres. However, the introduction of twist did influence tow geometry. No statistically significant difference in tow geometry was measured in either diverging or converging preforms irrespective of section gradient. This suggests that the addition of twist to fibres can reduce tow spread improving the consistency and predictability of a braided preform. This also reduces the likelihood of surface defects. Once again, with thickness there was no evidence of a difference in braid thickness due to the orientation or gradient of the mandrel. However, the general thickness of the preform did increase because of the additional twist.

Further work was completed using the steeper gradient section, 10.6° mandrel, at the NCC. This builds on the work by Du and Popper [39] which had previously confirmed an improvement in braid consistency with converging geometries but only on a small 72-carrier braider. This work develops this by braiding with both twisted and untwisted fibres in diverging and converging cross-sectional orientations. The braid angle behaviour seen in braiding the small mandrels was reflected on the larger conical section, with greater deviation from predicted braid angle demonstrated in the diverging cross-section whereas braiding in a converging orientation produced a braid much closer to the desired program. Similarly, for tow width, the introduction of twist reduced the tow spread on the preform for both converging and diverging cross-sections. The influence of a cross-sectional change on tow width is something that has not been studied previously. This work was then repeated in kinematic simulation software CBX. It was found that the inclusion of a cross-section change did introduce variation from the programmed braid angle however this was overestimated in comparison to the manufacturing set-up.

Finally, the ‘Oscar’ mandrel was utilised to demonstrate the limits of the braiding process along with the introduction of multiple different types of sequential features. This builds on work by Kessels and Akkerman [6], which used a small 72-carrier braider to look at mandrels with drastically varying cross-sections. However, this work only looked at braid angle. This work extends this by looking at tow width variability. The principals identified in the braiding of the conical sections were found in the ‘Oscar’ with all diverging cross-sections showing the most significant variation from predicted braid angle. The inclusion of the twist to fibres during rewinding however did prevent significant tow spread with the maximum standard deviation less than 10% of the stabilised measured tow width. The braiding of this mandrel did highlight some concerns with braiding extremely complex geometry which would lead to suggestions of future work.

8 Conclusions

8.1 Final Remarks

Braiding as a manufacturing process offers great potential in many applications. The braiding process can produce near-net-shaped preforms which results in low material wastage. The high material deposition rate lends itself to automotive and aerospace applications. Machine parameters offer the ability to tailor preforms with specific angles. However, the application of braiding as an industrial manufacturing process poses certain challenges. The challenge in predicting the properties of braided composites is one of the primary concerns which limits the application of braiding in composites manufacturing. Understanding the behaviour of braid architecture on complex geometries is key to the increase industrial application.

This work aims to address these challenges by investigating the influence of rewinding parameters on the quality of braiding and braid architecture parameters. Industrial braid manufacturers have varying opinions on the inclusion of a twist to fibres during rewinding, with some including it as standard procedure and others not adding twist during rewinding. At the time of writing there are no publications on the inclusion of a rewinding twist and its impact on the braid architecture outside of this body of work. Therefore, to develop consistency in the braiding process across manufacturers an understanding of twist on both braid architecture and mechanical properties is required. Tow geometry assumptions are presented in this work. Twisting was also demonstrated to show improve in tow geometry when braiding on complex geometries which lends itself to more consistent cover factors, although complex geometries have been studied for braiding the influence of braiding with twisted fibres has not.

The combination of both academic and industrial approaches has proven beneficial to maximise the understanding of this technology. In this research, the access to two braiding machines of different scales at the UoN and NCC has been taken advantage of to develop tow geometry assumptions that are valid independent of braider size. The majority of braiding work has been completed on smaller machinery, this work goes further through validating the assumptions produced on the smaller machine for the larger machine at the NCC. The academic interaction has enabled multiple proof of concept studies to take place for rewinding twist levels and variations in part

geometry, which then have been validated using the industrial scale machine at the NCC. Access to both institutions has maximised potential measurement methods along with testing facilities that have enabled the production of comprehensive piece of work with a large dataset. With a good degree of confidence in the tow geometry approximations suggested.

In summary, this work has provided an extensive insight into the influence of rewinding twist on mechanical properties and braid architectures for simple and complex geometries. It is accepted that further work is required to continue to validate these approximations and develop wider process knowledge on overbraiding. Some of this work is outlined at the end of this Chapter with some proposed next steps to increase process application.

8.2 Contributions to wider research community

The aim of this work was to determine the influence of the addition of twist added to fibres during the rewinding stage of the process on the mechanical properties and braid architecture of braided composites. A series of objectives were defined to address this aim.

- Characterisation of the influence of rewinding twist on the tow geometry of a braided preform.
- Understanding the influence of additional rewinding twist on the mechanical properties of a braided composite
- Characterisation of braid architecture behaviour on a geometry of non-prismatic cross-section
- Understanding of the differences in braiding on small and large machinery.

These objectives have been completed through a vast experimentation program comparing a range of process parameters including part geometry, number of rewinding twists, braid type and machine size. Tow geometry assumptions have been developed for both cylindrical and complex geometries for different levels of rewinding twist. Tensile testing of braided coupons of different levels of rewinding twist has identified the variation in mechanical properties as a result of rewinding twist. Multiple studies have been completed on both the small and large machines to enable identification of the similarities and differences.

At present, the general academic picture of braiding is still under development as not all facets of the process have been explored. As a result, the current literature provides a somewhat fragmented picture of the process. The present work provides context for current areas of recent developments in the braiding process, along with addressing potential research needs to further the application of braiding as an industrial manufacturing process.

8.2.1 Conclusions of the Influence of twist of mechanical properties of braided composites

Twisting is exploited by some braid manufacturers to improve processibility benefits. However, little is known about the influence of twist on mechanical properties. This work compares the mechanical performance of braided test coupons for both twisted and untwisted fibres which is something not present in current literature. Chapter 5 highlights that although the addition of twist reduces the average UTS, however it significantly reduces the variability. This results in an A-basis allowable that is higher for twisted fibres. Failure behaviour of braided coupons has been discussed by Wehrkamp-Richter et al [59] but the application of this idea to the inclusion of rewinding twist is something that has not been previously identified. Differences in failure behaviour are apparent with untwisted fibres failing m a more brittle manner with instantaneous failure. Whereas twisted fibres saw a progressive failure which resulted in delamination of the coupon and increased energy absorption. A visible difference in stress-strain behaviour for samples tested in tension was reported. Untwisted coupons failed instantaneously with a brittle failure. Whereas twist coupons have an initial failure point and then continue to fail progressively until final failure. As each ply failed, it offloaded into adjacent plies which then subsequently failed until total failure. The progressive failure resulted in delamination in the coupons. Failure strength in twisted coupons was lower in comparison to untwisted coupons. However, a higher level of variability in the untwisted samples resulted in a lower A-basis design allowable. This suggests mechanical properties are more predictable with twisted coupons. Understanding of this behaviour difference with twisted and untwisted fibres may result in different load case applications. The reduction in variability in twisted coupons offers the potential to improve design processes as the failure is more predictable. Some suggestions about further testing

work in compression would help complete the picture on the influence of twist on mechanical properties of braided composites.

Twisted fibres saw a significant improvement in fibre processibility, a combination of fibre damage test methods was utilised to compare both untwisted and twisted fibres and concurred that braiding with untwisted fibres results in a higher level of fibre damage. The work builds on existing work through relating existing fibre damage testing methods and evolution of fibre damage throughout the braiding process to twisted fibres. Observations during manufacturing demonstrated that fibre damage accumulates at each stage of the manufacturing process, rewinding and then braiding. This manifests itself as filamentisation, partial tow snagging and tow breakages. This damage as a cumulative effect with a single filament damage escalating to an entangled braid cone causing process interruptions. Fibre damage was more severe with untwisted fibres, as the addition of twist helps to provide a more compact tow bundle, a greater number of tow breakages occurred when manufacturing with untwisted fibres. A gravimetric test for fibre damage evaluation showed good correlation with a visual inspection study, both methods are qualitative and require destruction of the preform. Further work to develop a machine learning fibre damage inspection would be a useful tool for industrial application to quantify the level of fibre damage within a part.

The work also consisted of method development for manufacture of braided panels in line with typical industry standard methodology. The discussion of infusion variability as a result of the inclusion of twist has not been discussed in literature. The method used a cylindrical mandrel to manufacture the preform which was then flattened to produce a panel. The data analysis validates that the flattening of cylindrical preforms to form panels shown no discernible impact on braid architecture parameters.

Cured ply thickness was found to be much thicker for twisted preforms due to the more rounded tow shape. The addition of twist to fibres altered the shape of the resin flow front during infusion. The more compacted tow bundles had a reduced permeability, reducing flow in the axial direction. As a result, the flow front for twisted preforms was more angular. However, this had no significant increase in infusion time.

8.2.2 Conclusions on the manufacture of cylindrical braided preforms.

Braiding provides a reliable production method of producing a preform with an angle tolerance of $\pm 1^{\circ}$ which was unaffected by altering the ratio of machine parameters of carrier speed and take-up speed.

The application of an appropriately sized guide ring was found to reduce the transient length of the preform however, there was no difference in braid angle variability once the stabilisation point had been reached. The addition of twist to fibres during rewinding did not significantly influence the braid angle of the preform. Varying the guide ring size did not have an impact on the cover factor, however localised variations in cover factor were much more common with preforms manufactured with a larger guide ring size. This indicates the potential for braid defects caused by instability.

The influence of twist on braid architecture values such as tow width is quantified for different levels of rewinding twist, this has not been discussed in literature prior to this work. The significant difference in tow width due to twist highlights the importance of understanding this rewinding parameter so that the designed preforms corresponds to the manufactured output. A reduce in both tow width and tow width variability was seen when adding twist to fibres during rewinding. This was shown in optical microscopy to correspond to the tow cross-section becoming less lenticular and more rounded in shape. For a 12K carbon fibre tow, a reduction of 28% tow width was measured through adding 5 Tpm during the rewinding stage. This improves the understanding of tow geometry enabling greater predictive capabilities. Optical microscopy determined a change in tow shape because of the addition of twist during rewinding. Untwisted tows were more lenticular in shape due to tow spread whereas twisted fibres were more compact and rounded.

The tow geometry approximations identified at a single layer level were proven to be valid at a multilayer level. There was no statistically significant difference in tow width or braid angle between initial and subsequent layers of a multilayer braided preform irrespective of the level of rewinding twist added to fibres. The maximum layer thickness measured using the AVS demonstrated that the thickness addition for subsequent layers of a braided preform is linear however this addition is less than the initial layer thickness due to nesting. A comparison between analytical and

experimental cover factor demonstrates that twisted fibres produced a more repeatable cover factor with good agreement between the analytical and experimental data. The analytical data overestimated the cover factor for untwisted fibres due to a greater number of localised deviations in cover factor in the preform. This is indicative of a greater amount of surface defects and fibre damage.

Machine size was not found to influence the key process variable of a braided preform. Preforms typically stabilised at 2x mandrel diameter irrespective of mandrel or machine size. Comparisons of different machine sizes is limited in literature.

Analysis of triaxial preforms demonstrated that there was no statistical difference in the bias fibres in biaxial or triaxial preforms. However, a difference in tow width between untwisted 12 K axial fibres and untwisted biaxial 12K fibres was recorded. This is due to the tensioning mechanisms of the fibres. Image analysis demonstrated variation of axial placement within triaxial unit cells demonstrating that cover factor measurement of a triaxial preforms improves by measuring a large section area. This work validates existing analytical approximations by Heieck [34] but develops it by relating the axial tow geometry to the untwisted biaxial tow geometry, acknowledging the difference in geometry is due to the tensioning mechanism.

8.2.3 Conclusions on the manufacture of axisymmetric non-prismatic geometries

It was demonstrated that braiding axisymmetric cylindrical and frusto-conical mandrels in a diverging cross-section orientation resulted in greater braid instability due to the effective shortening of the stabilisation length. This extends work by Du and Popper by analysing the stability of braid architecture at different magnitudes of section gradient [39]. An increase in mandrel gradient results in a larger braid angle deviation for preforms braided in a diverging cross-section as the more rapid cross-section change leads to the effect stabilisation length shortening more quickly. An increase in mandrel gradient did not influence the deviation from predicted braid angle for mandrel orientated with the cross-section change in converging alignment, as the effective stabilisation length increases as the part diameter decreases. This is useful manufacturing knowledge for industry where mandrels can be manipulated to be braided in a converging orientation thus providing a more stable braid architecture. Previous work has only focused on braid angle deviation, this work extends this by investigating the influence of complex geometry on tow width. A significant increase

in tow width was found for both converging and diverging orientations indicating that the introduction of a geometrical change results in tow spread. Previous work has demonstrated that tow width is inversely proportional to tow thickness, therefore as expected as tow spread results in a wider tow so the resulting preform is thinner. This work provides the novel information of the influence of rewinding twist on both braid angle and tow geometry of complex geometries, this has not been previously addressed in the literature. The inclusion of rewinding twist to fibres when braiding a complex geometry was found to have no impact on the braid angle, however twisted fibres were found to reduce tow spread irrespective of the cross-sectional change orientation. For twisted fibres there was no statistically significant difference in tow width irrespective of part gradient and mandrel orientation. This contrasts to the results for untwisted fibres. As a result, cover factor is more predictable on complex geometries braiding with twisted fibres. There was no statistically significant difference in layer thickness between the cylindrical and complex preforms.

A large frusto-conical mandrel with a 10.6°part gradient was compared to the small-scale part manufacture, this extends previous work on complex geometries in the literature by comparing two different scales of geometry. Similar results were found. Braiding with the preform in a converging orientation produces a more stable braid angle with less deviation from predicted braid angle. The same magnitude of deviation was seen in both small and large geometries. A statistically significant increase in tow width magnitude was measured for the untwisted fibres irrespective of direction of cross-section change. Any change in tow width for twisted fibres was not found to be statistically significant, suggesting that twist can reduce tow spread. The preforms manufactured on the large frusto-conical mandrel were replicated in a kinematic processing software from CATIA. Process simulation was found to overestimate the deviation along the axial length of the preform for both diverging and converging cross-section. The change in stabilisation length is not accounted for due to the neglection of interyarn friction by the model which results in the difference between manufacturing and simulation.

The ‘Oscar’ mandrel highlighted the limits of the braiding process consisting of a series of sequential cross-section changes. Van Ravenhorst has previously looked at variability of braid angle across an increasingly complex geometry, however this work develops this by including the addition of a rewinding twist. The increased

deviation in braid angle was found on all diverging cross-sections, however the inclusion of twist to fibres did significantly reduce the tow spread. However, the braiding of the 'Oscar' did highlight some concerns of braiding complex geometries which should be investigated in future work. From a manufacturing perspective, manual intervention is often required when braiding concave sections for the braiding tows to deposit onto the mandrel surface and prevent bridging. Convex curvatures result in yarn slippage which leads to inconsistent braid angle and preform defects due to tension changes in tow as slippage occurs. For parts of significantly varying diameter an adaptable guide ring would offer a novel but potential solution. These are not yet commonplace in manufacturing set-ups but would enable better control of the braid architecture for consistently changing preforms.

8.3 Further Work

The current research is by no means exhaustive of the potential of the braiding process and further work is required to develop understanding. Initial mechanical testing trials indicated that there were some potential design benefits to braiding with twisted fibres including a reduced variability resulting in a high A-basis allowable. However, further testing in compression is required to fully determine any potential benefits. It is also worth noting that coupon level testing has only been done to date, further work would focus on scaling up the testing program to part level testing. This would provide a better understanding of the impact of including twist on braided components.

This work solely utilises axial braiders to manufacture preforms for analysis. It is documented that radial braiders offer a potential reduction in fibre damage due to the different carrier mechanism. This could reduce the necessity for adding twist to fibres. Therefore, a useful exercise would be replicating a twist study on a radial machine of a similar size to one used in this work. This would determine firstly if adding twist during rewinding is only a necessary pre-process step on axial machine but secondly if the tow geometry approximations developed are valid globally across braiding machines.

In Chapter 7 extensive focus is placed on the braiding of a conical section at different part gradients and orientations. Further work would ideally study different geometrical features such as curved or double curved surfaces and whether the idea

that adding twist to fibres reduces tow spread on a cross-sectional change is transferable. Isolation of individual geometric features would increase the potential industrial applications for braiding. Furthermore, development of the CBX software for suitability to complex geometries would help improve consistency between simulation and manufacturing. This would provide a more direct processing route for braided components.

In-process monitoring has been loosely touched on throughout this thesis with the difficulties of measuring braided layer thickness non-destructively and with minimal machine noise being identified. The development of a system that could provide instantaneous thickness measurements without the machine noise would be able to feed into the analytical tool to redefine the layer thickness assumptions. This would not only provide the operator with real-time thickness data but also improve the predictive capabilities. Similarly, an in-process monitoring system capable of determining the cover factor of a braid would enable real-time data to be passed to the operator and monitor if the preform corresponds to both predictive tool and simulation.

Appendix A:

Figure 0.1 shows the individual data plots for the twisted samples for each coupon from the three panels tested.

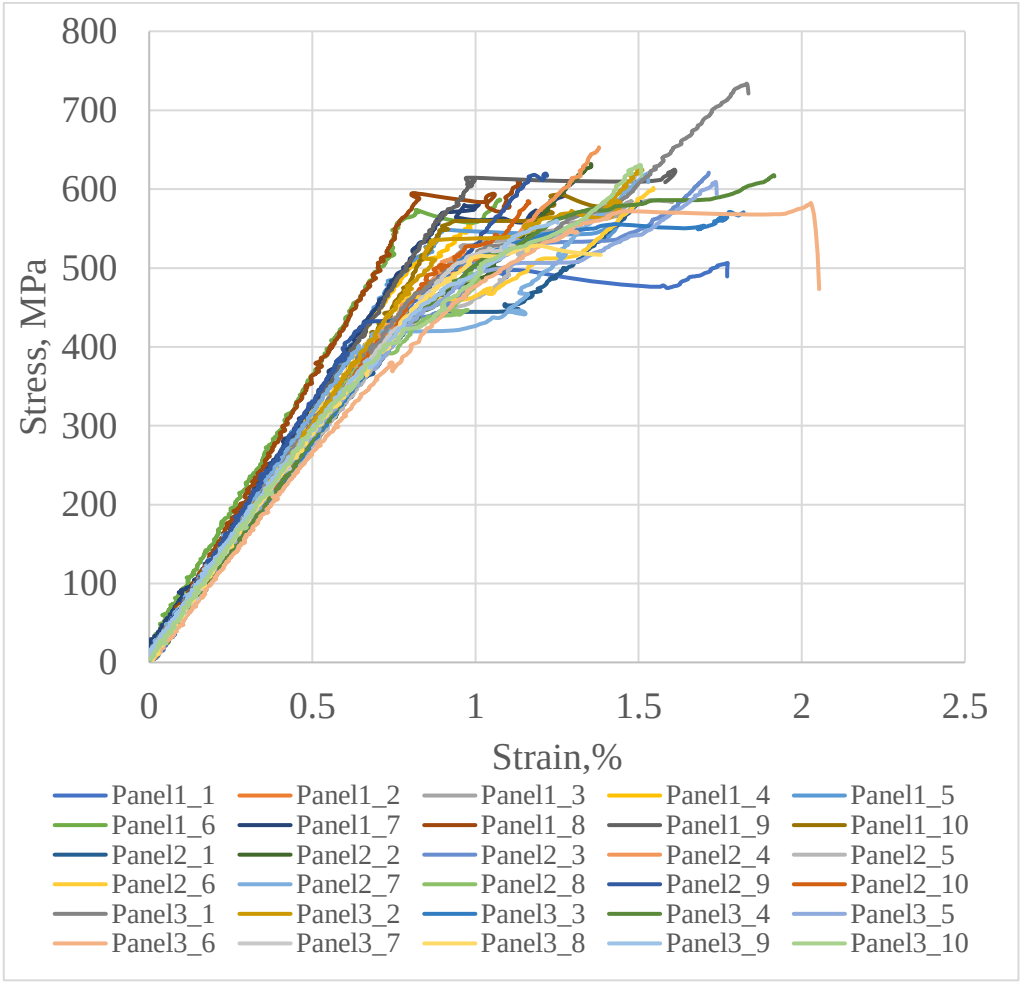


Figure 0.1 Twisted Sample Data

A summary of the data for each coupon tested for the twisted coupons is displayed in Table 0.1.

Table 0.1 Data Summary for Twisted Coupons

	Failure Strength, MPa	0° Tensile Strength, MPa	0° Tensile Modulus, GPa	0° Strain at Failure,%	Failure Type
Panel1_1	430	507.72	57.20	1.76	AGM
Panel1_2	478	537.74	56.26	1.22	AGT
Panel1_3	528	587.09	54.79	1.59	AGT
Panel1_4	510	559.25	57.39	0.99	LGB
Panel1_5	464	565.93	58.80	1.48	D/LGT
Panel1_6	516	595.29	58.22	1.07	D/LGT
Panel1_7	546	616.56	55.10	1.31	LGT
Panel1_8	581	611.33	59.70	1.13	LGT
Panel1_9	578	641.51	59.70	1.79	LGT
Panel1_10	548	595.26	59.34	1.28	LGT
Panel2_1	428	586.70	53.23	1.48	LGV
Panel2_2	443	634.41	56.02	1.36	LGT
Panel2_3	419	623.73	55.14	1.73	LGM
Panel2_4	463	655.74	54.52	1.39	LGV
Panel2_5	424	627.27	54.63	1.51	LGM
Panel2_6	463	603.52	57.00	1.55	LGV
Panel2_7	407	622.11	56.99	1.59	LGT
Panel2_8	390	495.77	56.67	0.99	LGT
Panel2_9	391	621.21	57.37	1.22	LGT
Panel2_10	399	586.33	56.68	1.16	LGV
Panel3_1	463	736.57	57.98	1.84	LGM
Panel3_2	533	627.81	54.93	1.51	LGM
Panel3_3	514	574.41	58.83	1.84	LGM
Panel3_4	505	620.28	61.63	1.93	LGB
Panel3_5	611.11	56.50	1.75	LGB	
Panel3_6	437	583.42	56.07	2.03	AGT
Panel3_7	477	530.58	53.71	1.11	AGT
Panel3_8	424	529.95	54.12	1.16	AGT
Panel3_9	380	562.11	56.07	1.23	LGB
Panel3_10	423	632.27	53.13	1.50	AGT

Figure 0.2 shows the individual data plots for the untwisted samples for each coupon in the three panels tested.

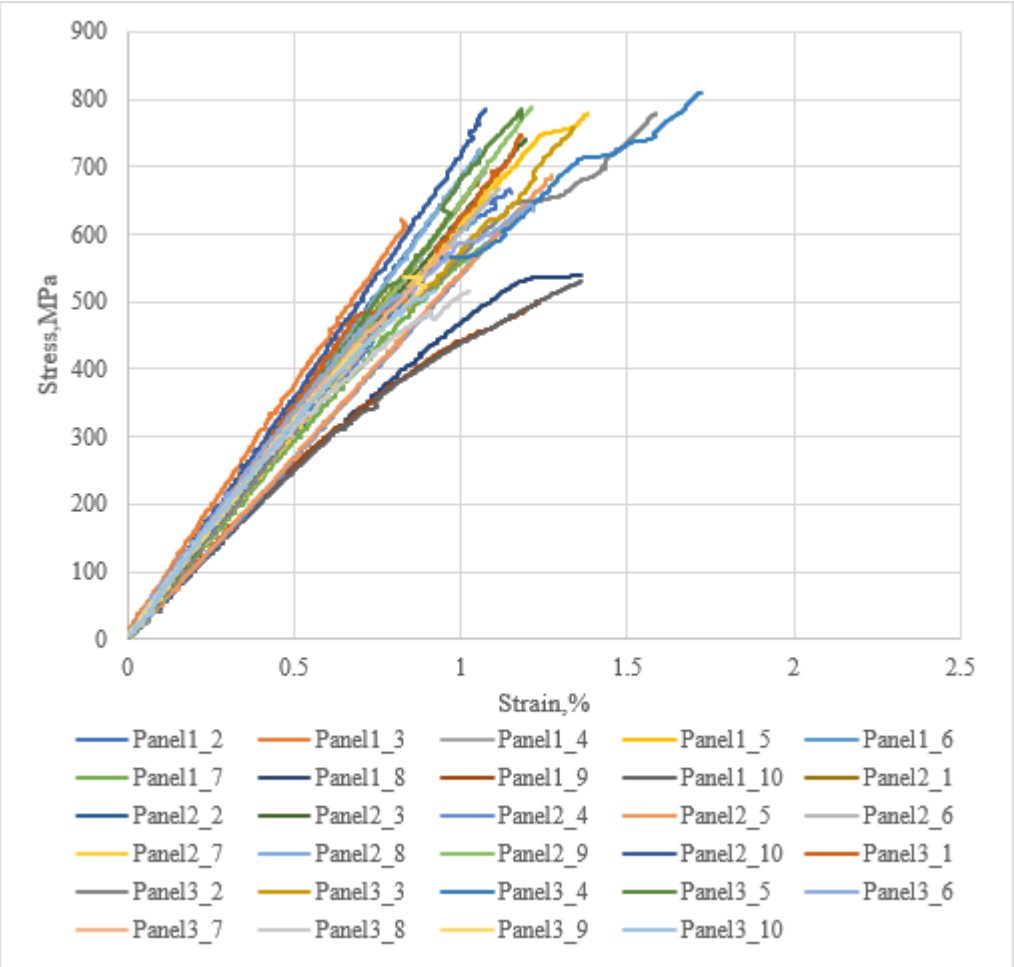


Figure 0.2 Untwisted samples

A summary of the data for each coupon tested for the untwisted data set is shown in Table 0.2.

Table 0.2 Summary of the data for the untwisted coupons

	Failure Strength, MPa	0° Tensile Strength, MPa	0° Tensile Modulus, GPa	0° Strain at Failure,%	Failure Type
Panel1_2	463	669.47	54.95	1.15	LGV
Panel1_3	603	624.65	57.36	0.83	LGT
Panel1_4	691	697.81	53.71	1.08	LGV
Panel1_5	298	781.06	59.37	1.39	LGV
Panel1_6	384	624.08	58.60	1.05	LGT
Panel1_7	459	593.61	53.52	1.09	LGB
Panel1_8	512	541.94	49.15	1.24	LGB
Panel1_9	320	533.08	47.08	1.38	LGM
Panel1_10	342	747.88	57.32	1.18	LGM
Panel2_1	672	679.72	55.12	1.05	LGT
Panel2_2	709	717.95	52.33	1.06	LGT
Panel2_3	689	742.69	52.68	1.20	LGV
Panel2_4	493	639.36	49.43	1.19	LGB
Panel2_5	668	690.69	52.17	1.27	LGB
Panel2_6	465	671.61	56.36	1.12	LGB
Panel2_7	419	694.20	52.19	1.14	LGV
Panel2_8	563	729.23	53.35	1.6	LGB
Panel2_9	545	791.53	55.04	1.22	LGB
Panel2_10	499	788.85	54.72	1.07	LGM
Panel3_1	471	748.35	64.77	1.19	LGT
Panel3_2	504	782.23	61.62	1.59	LGT
Panel3_3	441	761.64	61.62	1.35	LGV
Panel3_4	526	813.31	59.92	1.73	LGV
Panel3_5	474	787.81	58.98	1.19	LGB
Panel3_6	455	643.56	55.45	1.21	LGT
Panel3_7	364	583.68	54.85	0.98	LGT
Panel3_8	435	519.45	54.38	1.04	AGB
Panel3_9	488	538.16	52.39	0.83	AGT
Panel3_10	546	518.09	60.16	0.93	AGB

Tensile Modulus data was obtained as per the test standard calculated between 500-2500 usn. The test standard this can be calculated through chord modulus or linear regression. The Shimadzu test machine use for this work calculates the tensile modulus as shown in Figure 0.3.

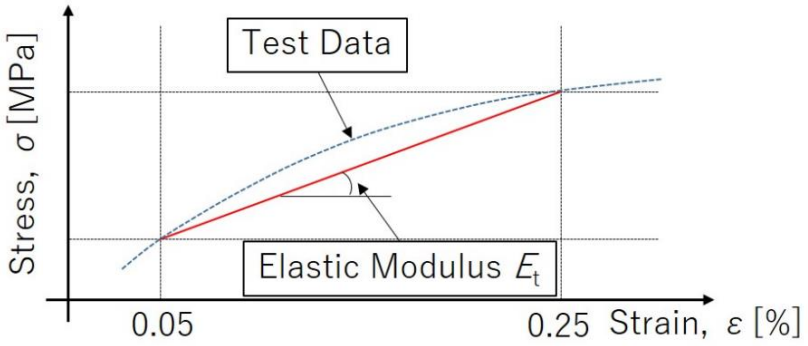


Figure 0.3 Method of Modulus Calculation

The raw data samples had large amounts of noise which limits the accuracy of the modulus calculations resulting in variability depending on the method used for calculation. The same testing machine and conditions were used for both untwisted and twisted samples.

A comparison of the tensile modulus calculated using the test standard and calculated through graphical analysis is summarised in Table 0.3.

Table 0.3 Summary of tensile modulus from test standard and graphical analysis

	Sample ID	**CTE Modulus Value, GPa**	**Calculated Modulus, GPa**
Twisted	Panel1_1	57.20	58.70
Twisted	Panel1_2	56.26	57.50
Twisted	Panel1_3	54.79	53.80
Twisted	Panel1_4	57.39	55.70
Twisted	Panel1_5	58.80	56.2
Twisted	Panel 1_6	58.22	60.20
Twisted	Panel1_7	55.10	53.5
Twisted	Panel1_8	59.07	63.21
Twisted	Panel1_9	59.70	54.4

Twisted	Panel1_10	59.34	60.1
Twisted	Panel2_1	53.23	52.6
Twisted	Panel2_2	56.02	53.5
Twisted	Panel2_3	55.14	51.5
Twisted	Panel2_4	54.52	54.72
Twisted	Panel2_5	54.63	56.31
Twisted	Panel 2_6	57.00	55.97
Twisted	Panel2_7	56.99	56.17
Twisted	Panel2_8	56.67	57.22
Twisted	Panel2_9	57.37	54.59
Twisted	Panel2_10	56.68	55.38
Twisted	Panel3_1	57.98	60.45
Twisted	Panel3_2	54.93	55.9
Twisted	Panel3_3	58.83	56.3
Twisted	Panel3_4	61.63	58.38
Twisted	Panel3_5	56.50	56.01
Twisted	Panel 3_6	56.07	55.10
Twisted	Panel3_7	53.71	56.12
Twisted	Panel3_8	54.12	57.84
Twisted	Panel3_9	56.07	57.2
Twisted	Panel3_10	53.13	53.78
Twisted	Panel3_11	54.72	56.7
Twisted	Panel3_12	60.37	63.59
	Sample ID	**CTE Modulus Value, GPa**	**Calculated Modulus, GPa**
Untwisted	Panel1_2	54.95	58.24
Untwisted	Panel1_3	57.36	61.40
Untwisted	Panel1_4	53.71	58.62
Untwisted	Panel1_5	59.37	60.95
Untwisted	Panel 1_6	58.60	61.57
Untwisted	Panel1_7	53.52	56.98
Untwisted	Panel1_8	49.15	49.71

Untwisted	Panel1_9	46.05	43.49
Untwisted	Panel1_10	47.08	50.78
Untwisted	Panel2_1	57.32	56.60
Untwisted	Panel2_2	55.12	53.08
Untwisted	Panel2_3	52.33	57.44
Untwisted	Panel2_4	52.68	48.28
Untwisted	Panel2_5	49.43	49.85
Untwisted	Panel 2_6	52.17	54.6
Untwisted	Panel2_7	56.36	60.29
Untwisted	Panel2_8	52.19	57.88
Untwisted	Panel2_9	53.35	49.60
Untwisted	Panel2_10	55.04	57.85
Untwisted	Panel2_11	54.72	57.99
Untwisted	Panel3_1	64.77	60.55
Untwisted	Panel3_2	61.62	65.19
Untwisted	Panel3_3	56.72	61.30
Untwisted	Panel3_4	59.92	65.26
Untwisted	Panel3_5	58.98	63.37
Untwisted	Panel 3_6	55.45	59.85
Untwisted	Panel3_7	54.85	59.01
Untwisted	Panel3_8	54.38	56.25
Untwisted	Panel3_9	52.39	57.35
Untwisted	Panel3_10	60.16	59.80
Untwisted	Panel3_11	63.72	61.55

Bibliography

[1] S. S. Roy and P. Potluri, “Braiding and Filament Winding,” in *Design and Manufacture of Structural Composites*, Elsevier, 2023, pp. 145-187.

[2] Y.Kyosev, Braiding Technology for Textiles, Woohead Publishing, 2015.

[3] J. Carey, Handbook of Advances in Braided Composite Materials, Woodhead Publishing, 2017.

[4] S. S. Roy and P. Potluri, “Braiding: from Cordage to Composites,” in *Textile Research Conference*, Dhaka, 2016.

[5] A & P Technology, “Megabraiders,” 2023. [Online]. Available: https://www.braider.com/About/Megabraiders.aspx. [Accessed 20 May 2023].

[6] J. Kessels and R. Akkerman, “Prediction of the yarn trajectories on complex braided preforms,” *Composites:Part A,* vol. 33, pp. 1073-1081, 2000.

[7] Y. Kyosev, “Braiding Machine Components,” in *Braiding Technology for Textiles*, Woodhead Publishing Series.

[8] P. Potluri, A. Rawal, M. Rivaldi and I. Porat, “Geometrical modelling and control of a triaxial braiding machine for producing 3D preforms,” *Composites Part A: Applied Science and Manufacturing,* vol. 34, pp. 481-492, 2003.

[9] R. Akkerman and B. H. Villa Rodriguez, “Braiding Simulation for RTM Preforms,” 2006.

[10] xComposites, “Modelling procedure of braided composites,” 2023. [Online]. Available: https://www.xcomposites.com/braided.html. [Accessed 20 May 2023].

[11] D. Branscomb, D. Beale and R. Broughton, “New directions in Braiding,” *Journal of Engineered Fibers and Fabrics,* vol. 8, no. 2, pp. 11-24, 2013.

[12] Steeger USA, “Medical Braiders,” 2023. [Online]. Available: https://steegerusa.com/product/medical-braiders/. [Accessed 20 May 2023].

[13] Herzog, “Radial Braiding Machines,” 2023. [Online]. Available: https://herzog-online.com/radial-braiding-machines/. [Accessed 20 May 2023].

[14] Eurocarbon BV, “Overbraiding and Turn-key Solutions,” 2023. [Online]. Available: https://www.eurocarbon.com/composite-reinforcement/overbraiding-and-turn-key-solutions/. [Accessed 20 May 2023].

[15] TextileBlog, “What is Yarn Twist, Twist Direction, Twist Level,” [Online]. Available: https://www.textileblog.com/what-is-yarn-twist/?utm_content=cmp-true. [Accessed 20 May 2023].

[16] Eurocarbon BV, Interviewee, *Rewinding Discussion.* [Interview]. October 2018.

[17] A. R. Torun, G. Hoffman, A. Mountasir and C. Cherif, "Effect of twisting on mechanical properties of GF/PP commingled hybrid yarns and UD-composites," *Journal of Applied Polymer Science,* vol. 123, no. 1, 2011.

[18] R. Alagirusamy and V. Ogale, "Commingled and Air Jet-Textured Hybrid Yarns for Thermoplastic Composites," *Journal of Industrial Textiles,* no. 33, pp. 223-243, 2004.

[19] U. Bunzel, B. Lauke and K. Schneider, "Air Textured Hybrid Yarn Structures and Their Influence on the Properties of Long Fibre Reinforced Thermoplastic Composites," *Technische Textilien,* no. 42, 1999.

[20] M. Lefebvre, F. Boussu and D. Coutellier, "Influence of High Performance Yarns Degradation Inside Three- Dimensional Warp Interlock Fabric," *Journal of Industrial Textiles,* no. 42, pp. 475-488, 2013.

[21] S. El-Ghezal Jeguirim, S. Fontaine, C. Wagner-Kocher and D. Durville, "Transverse Compression Behaviour of Polyamide 6.6 Rovings:Experimental Study," *Textile Research Journal,* no. 82, pp. 77-87, 2012.

[22] Herzog, "Bobbin Winding Machines," Herzog, 2023. [Online]. Available: https://herzog-online.com/bobbin-winding-machines/. [Accessed 2023 May 20].

[23] CEZOMA, "CEZOMA CE-1187," CEZOMA, 2023. [Online]. Available: https://cezoma.com/winding-systems/ce-1187/. [Accessed 2023 May 20].

[24] J. Calba, D. Soulat, X. Legrand and S. Renauld, "Damage Investigation on Carbon Tows during rewinding and braiding processes," *FIbres,* vol. 11, no. 30, 2023.

[25] RATERA, "2PVLU/220," Ratera, 2023. [Online]. Available: https://ratera.com/en/productos/2pvlu-220/. [Accessed 20 May 2023].

[26] Eurocarbon, "Twisting Machine NCC," 2018.

[27] CompositesWorld, "An impec-able bike frame: Handmade by machine," [Online]. Available: httpa://www.compositesworld.com/articles/an-impec-able-bike-frame-handmade-by-machine. [Accessed June 2019].

[28] CompositesWorld, "Airbus A350 Update:BRaF&amp, FPP: Composites World," [Online]. Available: https://www.compositesworld.com/articles/airbus-a350-update-braf-fpp. [Accessed June 2019].

[29] Y.Kyosev, Advances in Braiding Technology, Woodhead Publishing, 2016.

[30] H. Mason, "A&P Technology launches 864-carrier braiding machine," *Composites World,* 19 September 2019.

[31] Porsche, “Porsche AG: Braided carbon wheels for the Porsche 911 Turbo S Exclusive Series- Porsche Greater Britain,” [Online]. Available: https://www.porsche.com/uk/about porsche/pressreleases. [Accessed June 2019].

[32] CompositesWorld, “Porsche and the braided carbon fiber wheel,” [Online]. Available: http://www.compositesworld.com/blog/post/porsche-and-the-braided-carbon-fiber-wheel. [Accessed 2019].

[33] ISO, “ISO 10122:2014,” [Online]. Available: https://www.iso.org/standard/59254.html. [Accessed 20 May 2023].

[34] F. Heieck, F. Herman, P. Middendorf and K. Schladitz, “Influence of the cover factor of 2D biaxial and triaxial braided carbon composites on their in-plane mechanical properties,” *Composites Structures,* vol. 163, pp. 114-122, 2016.

[35] D. Griffin, “Enabling data-driven research and development in composite product engineering: An over-braiding case study,” University of Bristol, 2021.

[36] R. Schmitt, A. Orth and C. Niggemann, “A method for edge detection of textile preforms using a light-section sensor for the automated manufacturing of fibre reinfored plastics,” in *SPIE*, Munich, 2007.

[37] M. Thompson, “Geometrical Modelling of Braided Textiles,” University of Nottingham, 2023.

[38] “Apodius delivers dedicated carbon-fibre analysis for Romer absolute arm,” Composites World, [Online]. Available: https://www.composites.media/apodius-delivers-dedicated-carbon-fibre-analysis-romer-absolute-arm.

[39] G. D and P. Popper, “Analysis of circular braiding process for complex shapes,” *Journal of the Textile Institute,* no. 85, 1994.

[40] G. Guyader, A. Gabor and P. Hamelin, “Analysis of 2D and 3D circular braiding process: Modelling the interaction between the process parameters abd the pre-form architecture,” *Mechanism and Machine Theory,* vol. 69, pp. 90-104, 2013.

[41] A. Fouladi and R. J. Nedoushan, “Prediction and optimisation of yarn path in braiding of mandrels with flat faces,” *American Society of Composites,* vol. 52, no. 5.

[42] A. Fouladi, R. J. Nedoushan, J. Hajrasouliha, M. Sheikhzadeh, Y. Kim, W. Na and W.-R. Yu, “Control of Braid Pattern on Every Side of a Braided Composite Part Produced by Asymmetrical Braiding Process,” *Applied Composite Materials,* pp. 479-492, 2018.

[43] Van Ravenhorst, “Design Tools for Overbraiding of Complex Mandrels,” 2018.

[44] C. Ebel and H. Thorsten, “Interaction of braiding ring geometry and fiber lay-up in the braiding process,” in *Symposium on the occasion of the 5th anniversary of the Institute for Carbon Composites*, 2014.

[45] H. Nishimoto, A. Ohtani, A. Nakai and H. Hamada, “Generation and prediction methods for circumferential distribution changes in the braiding angle on a cylindrical braided fabric,” *Institution of Mechanical Engineers Part L Journal of Materials Design and Applications,* vol. 224, no. 2, 2010.

[46] W.-J. Na, H. Ahn, S.-Y. Jeon, J. Lee and H.-M. Kang, “Prediction of the braid pattern on arbitary-shaped mandrels using the minimum path condition,” *Composites Science and Technology,* vol. 91, no. 31, 2014.

[47] T. Buns, M. Scott, B. Grimes and P. Giddings, “Large Braided Hydrofoil Development Approach,” in *SAMPE Europe*, Nantes, 2018.

[48] C. Ebel, “Effects of fiber damage on the efficiency of the braiding process,” 2013.

[49] P. Falzon and I. Herszberg, “Mechanical performance of 2D braided carbon/epoxy composites,” *Composites Science and Technology,* vol. 58, pp. 253-265, 1998.

[50] L. Dandy, G. Oliveux, J. Wood, M. Jenkins and G. Leeke, “Counting carbon fibres by electrical resistance measurement,” *Composites: Part A,* vol. 68, pp. 276-281, 2014.

[51] M. Charlebois, R. Boukhili and A. Gasmi, “Evaluation of the physical and mechanical properties of braided fabrics and their composites,” *Reinforced Plastics and Composites,* vol. 24, no. 14, 2005.

[52] E. Swery, T. Hans, M. Bultez, W. Wijaya, P. Kelly, R. Hinterholzl and S. Bickerton, “Complete simulation process chain for the manufacturing of braided composite parts,” *Composites: Part A,* vol. 102, pp. 378-390, 2017.

[53] J. Starke, “Carbon composites in automative structural applications,” in *Composites Sustainability*, Brussels, 2016.

[54] X. Xiao, H. Kia and X. Gong, “Strength prediction of triaxially braided composites,” *Composites: Part A,* vol. 42, pp. 1000-1006, 2010.

[55] A. Long, “Process modelling for liquid moulding for braided preforms,” *Composites: Part A,* vol. 32, pp. 941-953, 2001.

[56] A. Aggarwal, S. Ramakrishna and V. Ganesh, “Predicting the strength of diamond braided composites,” *Composites Materials,* vol. 36, pp. 625-643, 2002.

[57] G. D. Roberts, R. K. Goldberg, W. K. Binienda, W. A. Arnold, J. Littell and L. Kohlman, “Characterisation of Triaxial Braided Composite Material Properties for Impact Simulation,” NASA, 2009.

[58] G. Roberts and J. Salem, “Approaches for Tensile Testing of Braided Composites,” in *CompTest*, Lausanne, 2011.

[59] T. Wehrkamp-Richter, R. HInterholzl and S. Pinho, “Damage and failure of triaxial braided composites under multi-axial stress states,” *Composites Science and Technology,* 2017.

[60] A. Ohtani and A. Nakai, “Effect of internal structure on mechanical properties of braided composite tubes,” in *Internation Conference on Composite Materials*, 2007.

[61] A. &. P. Technologies, “A&P guidelines for testing QISO braided fabric,” A&P.

[62] A. Harte and N. Fleck, “Deformation and failure mechanisms of braided composite tubes in compression and torsion,” *Acta Materialia,* vol. 48, no. 6, pp. 1259-1271, 2000.

[63] O. Calme, D. Bigaud and P. Hamelin, “3D braided composite rings under lateral compression,” *Composites Science and Technology,* 2004.

[64] C. Ayranci and J. Carey, “Effect of diameter in predicting the elastic properties of 2D braided tubular composites,” *Composite Materials ,* 2010.

[65] C. Ayranci and J. Carey, “2D braided composites: A review for stiffness critical applications,” *Composite Structures,* vol. 85, pp. 43-58, 2007.

[66] B. Dauda, S. Oyadiji and P. Potluri, “Characterising Mechanical Properties of Braided and Woven Textile Composite Beams,” *Applied Composite Materials,* vol. 16, pp. 15-31, 2009.

[67] J. Masters and R. Foye, “Mechanical Properties of Triaxially Braided Composites: Experimental and Analytical Results,” NASA, 1992.

[68] G. Melenka and J. P. Carey, “Development of a generalised analytical model for tubular braided-architecture composites,” *Journal of Composite Materials,* vol. 51, no. 28, pp. 3861-3875, 2017.

[69] T. Alpyildiz, “3D geometrical modelling of tubular braids,” *Textile Research Journal,* vol. 83, no. 5, pp. 443-453, 2012.

[70] G. Melenka and J. P. Carey, “Braid CAM: Braided composite analytical model,” *SoftwareX,* vol. 7, pp. 23-27, 2017.

[71] G. Du and F. Ko, “Analysis and Design of 2D Braided Preforms for Composite Reinforcement,” 1993.

[72] J. H. Van Ravenhorst and R. Akkerman, “A yarn interaction model for circular braiding,” *Composites: Part A,* vol. 81, pp. 254-263, 2015.

[73] J. H. Van Ravenhorst and R. Akkerman, “Circular braiding take-up speed generation using inverse kinematics,” *Composites: Part A,* vol. 64, pp. 147-58, 2013.

[74] Dassault Systemes, “3DExperience,” [Online]. Available: https://my.3dexperience.3ds.com/welcome/compass-world/rootroles/composites-braiding-and-forming-engineer.

[75] A. K. Pickett, A. Erber, T. Von Reden and K. Dreschler, “Comparison of analytical and finite element simulation of 2D braiding,” *Plastic Rubber and Compostes,* vol. 38, pp. 387-95, 2009.

[76] A. Treviso, L. Thadani, D. Ivanov, L. Kawashita and X. Sun, “Braiding process simulation: comparison of kinematic and finite element models for large scale components,” Vancouver , 2019.

[77] P. Potluri and A. Manan, “Mechanics of non-orthogonally interlaced textile composites,” *Composites: Part A,* pp. 1216-1226, 2007.

[78] L. Brown, “Texgen,” in *Advanced Weaving Technology* , Woodhead, 2022.

[79] M. Thompson, L. Brown, K. Rengaraj and N. Warrior, “TexGen- Geometrical Modelling of Biaxial Braided Fabrics,” in *European Conference on Composite Materials*, Lausanne, 2022.

[80] Q. Zhang, D. Beale and R. M. Broughton, “Analysis of Circular Braiding Process, Part 1:Theoretical Investigation of Kinematics of the Circular Braiding Process,” 1999.

[81] R. Akkerman and B. Villa-Rodriguex, “Braiding SImulation and Slip Evaluation for Arbitary Mandrels,” in *10th Esaform Conference on Material Forming*, Zaragoza, Spain , 2006.

[82] F. Ning, P. Potluri and J. Hearle, “Geometrical modelling of tubular braided structures using generalised rose curves,” *Textile Research Journal,* vol. 87, no. 4, 2016.

[83] T. Zheng, J. Wei and Z. L. Shi, “An overview of modeling yarns 3D geometric configuration,” *Textile Science and Technology,* 2015.

[84] T. Buns, “NCC Large Overbraider Literature Review,” 2018.

[85] R. Gonzalez and R. Woods, Digital Image Processing 2nd edition, Prentice Hall , 2002.

[86] SPC for Excel, “Acceptance Criteria for Measurement Systems Analysis,” [Online]. Available: https://www.spcforexcel.com/knowledge/measurement-systems-analysis/acceptance-criteria-for-msa/#:~:text=You%20look%20at%20the%20acceptance,be%20acceptable%20for%20some%20applications..

[87] B. Grimes, M. Thompson and N. Warrior, “Effect of twist on braid architecture and stability,” in *SAMPE Europe*, 2021.

[88] Teijin, “Tenax FIlament Yarn,” [Online]. Available: https://www.teijincarbon.com/fileadmin/user_upload/Datenbl%C3%A4tter/Filament_Yarn/Product_Data_Sheet_TSG01en__EU_Filament_.pdf.

[89] Statology, “The minimum sample size for a t-test: Explanation and Example,” [Online]. Available: https://www.statology.org/minimum-sample-size-for-t-test/. [Accessed January 2023].

[90] “Central Limit Theorem: Definition and Key Characteristics,” [Online]. Available: https://www.investopedia.com/terms/c/central_limit_theorem.asp#:~:text=Key%20Takeaways-,The%20central%20limit%20theorem%20(CLT)%20states%20that%20the%20distribution%20of,for%20the%20CLT%20to%20hold.. [Accessed January 2023].

[91] Minitab, “What is ANOVA?,” [Online]. Available: https://support.minitab.com/en-us/minitab/21/help-and-how-to/statistical-modeling/anova/supporting-topics/basics/what-is-anova/. [Accessed January 2023].

[92] Minitab, “Interpret the key results for correlation,” [Online]. Available: https://support.minitab.com/en-us/minitab/21/help-and-how-to/statistics/basic-statistics/how-to/correlation/interpret-the-results/key-results/. [Accessed January 2023].

[93] A. Nettles, “Allowables for Structural Composites,” [Online]. Available: https://ntrs.nasa.gov/api/citations/20040111395/downloads/20040111395.pdf.

[94] Department of Defence, USA, Composite Materials Handbook Volume 1 Polymer Matrix Composites Guidelines for Characterisation of Structural Materials, 2002.

[95] Minitab, “Using P-value for goodness of fit test,” [Online]. Available: https://support.minitab.com/en-us/minitab/21/help-and-how-to/quality-and-process-improvement/capability-analysis/supporting-topics/distributions-and-transformations-for-nonnormal-data/p-value-for-a-goodness-of-fit-test/#:~:text=Minitab%20performs%20goodne. [Accessed January 2023].

[96] BMJ, “Mean and Standard Deviation,” [Online]. Available: https://www.bmj.com/about-bmj/resources-readers/publications/statistics-square-one/2-mean-and-standard-deviation. [Accessed January 2023].

[97] C. Ebel, “Effects of Fiber Damage on the Efficiency of the Braiding Process,” in *TEXCOMP-11*, Leuven, 2013.

[98] M. Amini and A. Khavandi, “Degradation of poylmer-based composites in corrosive media:experimental attempts towards underlying mechanisms,” *Mechanics of Time Dependent Materials,* 2019.

[99] GeneralPlastics, “Why use polyeurethane foam,” 2019. [Online]. Available: www.generalplastics.com/why_polyeurethane.

[100] S. Holdings, “Smart Tooling- A Division of Spintech Holdings,” [Online]. Available: https://smarttooling.com/.

[101] *Composite Mandrel inlet Duct Demonstration- Smart Tooling Process.* [Film]. Smart Tooling , 2020.

[102] H. Mason, “Braided Preforms meet phase-change tooling,” *Composites World ,* 29 October 2020.

[103] KTMTechnologies, “The Cavus Project,” 2018. [Online]. Available: www.ktm-technologies.com/projekte/cavus/?lang=en.

[104] AeroConsultants, “CavusCore Water Soluble Mandrels for High Volume Production,” 2018. [Online]. Available: www.aero-consultants.ch/view/data.

[105] Stratasys, “FDM Sacrificial Cores and Mandrels for Composite Layups,” [Online]. Available: https://www.stratasys.com/siteassets/3dlc/higher-education/tag_fdm_solublecores_en_0915_web.pdf?v=48f56f.

[106] S. Voskamp, “Advances in automated composite preforming by overbraiding technology,” in *SAMPE*, 2016.

[107] Herzog, “Braiding and winding machines from the market leader,” Herzog, [Online]. Available: http://herzog-online.com/en/home. [Accessed June 2018].

[108] A. Kumar, “Computer vision based fabric defect detection: a survey,” *Industrial Electronics,* 2008.

[109] L. Smith and S. Swanson, “Strength Design with 2-D Triaxial Braid Textile Composites,” *Composites Science and Technology,* vol. 56, pp. 359-365, 1996.

[110] C. Bowman, G. Roberts, M. Braley, M. Xie and M. Booker, “Mechanical Properties of Triaxial Braided Carbon/Epoxy Composites,” NASA.

[111] X. Yu and J. Cui, “The prediction on mechanical properties of 4-step braided composites via two-scale method,” *Composites Science and Technology,* vol. 67, no. 3-4, pp. 471-480, 2007.

[112] J. Hajrasouliha, R. Nedoushan and Y. Woong-Ryeol, “Theoretical and experimental study of braid pattern in mandrels with arbitary cross-sections,” *Composite Materials,* vol. 52, no. 29, 2018.

[113] K. Birkefeld, M. Roder, T. von Reden and M. Bulat, “Characterisation of Biaxial and Triaxial: Fiber Architecture and Mechanical Properties,” *Applied Composite Materials,* vol. 19, no. 3-4, pp. 1-15, 2012.

[114] A. Harte and N. Fleck, “On the mechanics of braided composites in tension,” *European Journal of Mechanics- ,* vol. 19, no. 2, pp. 259-275, 2000.

[115] S. Beard and F. Change, “Energy Absorption of Braided Composites Tubes,” *International Journal of Crashworthiness,* vol. 7, no. 2, 2002.

[116] H. Cao and H. Chen, “Influence of braided angles on mechanical properties of three-dimensional full five-direction braided composites,” *Textile Engineering & Fashion Technology,* 2017.

[117] J. Tate, A. Kelkar and J. Whitcomb, “Effect of braid angle on fatigue performance of biaxial braided composites,” *International Journal of Fatigue,* vol. 28, no. 10, pp. 1239-1247, 2006.

[118] J. Yang, C. Ma and T.-W. Chou, “Elastic Stiffness of Biaxial and Triaxial Woven Fabric Composites,” in *National SAMPE Symposium and Exhibition* , 1984.

[119] M. Yang, C.-L. Ma and T.-W. Chou, “Fiber inclination model of three dimensional textile structural composites,” *Composite Materials,* vol. 20, no. 5, pp. 472-84, 1986.

[120] D. Whyte, “On the structue and properties of 3D braid reinforced composistes, PhD Thesis,” Drexel University, 1986.

[121] P. Falzon, I. Herszberg and A. Baker, “Stiffness analysis of textile composites,” in *National Conference Publication- Institute of Engineers*, Austrailia, 1996.

[122] S. Quek, A. Waas, W. Shahwan and V. Agaram, “Analysis of 2D triaxial flat braided textile composites,” *Mechanical Sciences ,* pp. 1077-1096, 2003.

[123] J. Carey, M. Munro and A. Fahim, “Longitudinal elastic modulus prediction of a 2D braided fibre composites,” *Reinforced Plastic Composites,* vol. 22, no. 9, pp. 813-31, 2003.

[124] J. Carey, M. Munro and A. Fahim, “Regression-based model for elastic constants of 2D braided/woven open mesh angle play composites,” *Polymer Composites,* vol. 26, pp. 152-64, 2005.

[125] J. Carey and G. Melenka, “Experimental analysis of diamond and regular tubular braided composites using three-dimensional digitial image correlation,” *Composite Materials,* vol. 51, no. 28, pp. 3887-3907, 2017.

[126] S. Song, A. Waas, K. Shahwan, X. Xiao and O. Faruque, “Braided textile composites under compressive loads: Modeling the response, strength and degradation,” *Composites Science and Technology,* vol. 67, pp. 3059-3070, 2007.

[127] HP, “HP 3D Scan, Structured Light Scanner Pro S3”.

[128] I. Standards, *ISO 527-4: Plastics determination of tensile properties Part 4: Test conditions for isotropic and orthotropic fibre reinforced plastic composites,* ISO, 2021.

[129] I. International, “Composite Winders, Izumi International,” [Online]. Available: https://www.izumiinternational.com/product-category/winders/.

[130] B. Grimes, P. Giddings and N. Warrior, “The influence of guide ring size on braid architecture,” in *ICMAC*, 2021.

[131] D. Li, J. Li, L. Chen and Z. Lu, “Finite Element Analysis of Mechanical Properties of 3D Four Directional Rectangular Braided Composites Part 1: Microgeometry and 3D Finite Element Model,” *Applied Composites Materials,* 2010.

[132] W. Na, “Prediction of the braid pattern on arbitary-shaped mandrels,” *Composites Science and Technology,* vol. 91, pp. 30-37, 2013.

[133] A. Miller, N. Dodds, J. Hale and A. Gibson, “High speed pultrusion of thermoplastic matrix composite,” *Composites Part A: Applied Science and Manufacturing,* no. 29, 1998.

[134] R. Algirusamy, R. Fangueiro, V. Ogale and N. Padaki, “Hybrid yarns and textile preforming for thermoplastic composites,” *Textile Progress,* no. 38, 2006.

[135] Eurocarbon BV, “Overbraiding,” [Online]. Available: http://eurobraider.com/index.php/overbraiding. [Accessed 2018].

[136] A & P Technology, “The Reinforcement of Choice,” A&P Technology, [Online]. Available: http://braider.com. [Accessed June 2019].

[137] C. K. Leung, G. W. Melenka, D. S. Nobes and J. P. Carey, “The effect on elastic modulus of rigid-matrix tubular composite braid radius and braid angle change under tensile loading,” *Composite Structures,* vol. 100, 2013.

[138] M. Frost, “Braided Impact Structures,” in *SAMPE Europe*, 2004.

[139] A. K. Pickett, J. Sirtautas and A. Erber, “Braiding SImulation and prediction of mechanical properties,” *Applied Composite Materials,* vol. 16, pp. 345-64, 2009.

[140] T. Hans, J. Cichosz, M. Brand and R. Hinterholzl, “Finite element simulation of the braiding process for arbitary mandrel shapes,” *Composites: Part A,* vol. 77, pp. 124-132, 2015.